

A Study of Predictive Control Strategies
for Optimally Designed Solar Homes

José Agustín Candanedo Ibarra

A Thesis
In the Department
of
Building, Civil and Environmental Engineering

Presented in Partial Fulfillment of the Requirements
For the Degree of
Doctor of Philosophy (Building Engineering) at
Concordia University
Montréal, Québec, Canada

May 2011

©José Agustín Candanedo Ibarra, 2011

Abstract

A Study of Predictive Control Strategies for Optimally Designed Solar Homes

José Agustín Candanedo Ibarra, Ph.D.

Concordia University, 2011

This thesis investigates the development of predictive control strategies for optimally or near-optimally designed solar homes. Optimal design refers to the integration of renewable energy technologies (mainly active and passive solar) with a high-quality building envelope as well as efficiency and conservation measures to achieve substantial reductions in energy consumption and peak demand. Effective implementation of these technologies requires an integrated design approach, which considers their interactions with the building and its services. Furthermore, control strategies must be an essential part of the integrated design of a building to improve energy performance and ensure occupant comfort. In optimally designed solar homes, control strategies should incorporate the collection, storage and delivery of solar energy. Weather forecasts along with an understanding of the building's thermal dynamics (e.g., time delays due to thermal mass) enable predicting and managing loads and solar energy availability.

Design and operation strategies of a case study, the Alstonvale House, are presented. Features of this house include passive solar design, a building-integrated photovoltaic/thermal (BIPV/T) system coupled with a solar-assisted heat pump, a thermal energy storage tank and a radiant floor heating system in a thermally massive concrete slab. Design and control approaches developed for the Alstonvale House provided the basis for generalized control strategies applicable to optimally designed solar homes.

Simplified building models, which can be derived from more detailed models or on-site measurements, can facilitate the implementation of predictive control techniques. In this investigation, model-based predictive control was applied to a radiant floor heating system and the position of roller blinds in a room with high solar gains.

Predictive control can also be applied to optimize the operation of renewable energy systems. In this study, forecasts of heating loads and solar radiation were used in a dynamic programming algorithm to select a near-optimal set-point trajectory for an energy storage tank heated with a heat pump assisted by a BIPV/T system.

Acknowledgements

I want to thank my supervisor, Dr. Andreas K. Athienitis, for his guidance, support and for the opportunity to pursue my doctoral studies in the Solar Laboratory at Concordia. Thank you for your trust in my abilities. Thank you for allowing me to work within the IEA activities and for allowing me to attend relevant conferences and other events in this field during the course of my doctoral studies. Ευχαριστίες!

Sevag Pogharian deserves a special mention for giving me the opportunity to join the Alstonvale Net Zero House team, and for his example of courage, fortitude and perseverance. Your labour was not in vain! I would also like to thank Josef Ayoub, Yves Poissant and Dave Turcotte (NRCan); Jocelyn Harel (Régulvar); Vasile Minea (Hydro-Québec); Peter Kettenbeil (SPD); and numerous others involved in the Alstonvale project.

I am very grateful for the financial support provided by NSERC through a CGS D2 Alexander Graham Bell Scholarship. I also wish to thank Concordia University, the Solar Buildings Research Network, France and André Desmarais and Professor Hugh McQueen for their scholarships, which have been a great encouragement.

I would like to say thank you to Lewis Poulin and Sophie Pelland for their collaboration with weather forecasts. Lyne Dee, project coordinator of SBRN, deserves a special note for all her work and patience in the network. I would also like to thank Jacques Payer, Olga Soares, Debbie Reynolds, Linda Swinden, Jenny Drapeau, Luc Demers, Joe Hrib, Sylvain Bélanger and all the personnel in the BCEE Department.

I want to thank SBRN and its member institutions, all the professors and graduate students with whom I had the pleasure of discussing ideas during these years.

A special thank you to my brother Luis (the younger and wiser of the two), for his continuous advice, support, sense of humour and his witty turns of phrase (e.g., “V.V.!”). I would also like to say thank you to the rest of my brothers and my sisters of the Solar Laboratory and the neighbouring labs on the 15th and 16th floors. You have all made the long and winding road of my doctoral studies an enjoyable and rewarding journey. I have learned a great deal, both professionally and personally, from this fascinating, multicultural group of highly motivated people, who work tenaciously in the pursuit of a better future. Thank you for your support in hard times and for sharing the good ones. Even on the rare occasions when we have disagreed, I have always maintained a great deal of respect, admiration and appreciation for you all. The conversations in the lab, the exchange of ideas over coffee or tea, (not to mention the fun times at McKibbin’s and elsewhere) will be missed. I hope we can keep in touch and collaborate in the future.

I would like to thank all my other friends, near and far, for their help and support. In particular, I would like to thank my friends Julio and Ruth in Montréal for their continuous support and friendship and the Uruguayan *asados*. I would like to express my gratitude to Professor B. Rabi Baliga, from McGill University, for his enduring friendship and advice.

I would like to thank my mom Rosalina and my dad José for their help and support, as well as the rest of my relatives in Panama. And of course, I thank my wife Stephanie for her unwavering support, understanding, patience and love along the way.

The supreme goal of all theory is to make the irreducible basic elements as simple and as few as possible without having to surrender the adequate representation.

Albert Einstein

*On fait la science avec des faits, comme on fait une maison avec des pierres : mais une accumulation de faits n'est pas plus une science qu'un tas de pierres n'est une maison.**

Henri Poincaré

Only primitives and barbarians lack knowledge of houses turned to face the winter sun.

Aeschylus, 500 B.C.

Essentially, all models are wrong, but some are useful.

George E.P. Box

* Science is made of facts, the same way a house is made of stones: but an accumulation of facts is no more a science than a pile of stones is a house.

Table of Contents

List of Figures	xi
List of Tables	xviii
Nomenclature	xx
1. Introduction.....	1
1.1 Motivation.....	1
1.1.1 Problem Statement	1
1.1.2 Concept of Optimally Designed Solar House	7
1.2 Implications of this Thesis.....	7
1.2.1 Net-Zero Energy Homes	7
1.2.2 Load Management and Interaction with the Electric Grid.....	9
1.2.3 Electric Vehicles and Other Peripheral Systems.....	13
1.4 Objectives and Scope	14
1.4.1 Main Objective.....	14
1.4.2 Specific Objectives.....	15
1.4.3 Scope.....	15
1.3 Thesis Overview	16
2. Literature and Technology Review.....	18
2.1 Introduction.....	18
2.2 Model-Based Building Control	20
2.2.1 Early Work on Dynamic Control of Buildings	20
2.2.2 Optimal Control for Management of Active and Passive TES	22
2.2.3 Model-Based Predictive Control of Solar Buildings.....	28
2.2.4 Recent Developments in Model-Based Predictive Control.....	33
2.3 Artificial Intelligence Techniques for Building Control.....	38
2.4 Relevant Technologies and Tools for Solar Homes	40
2.4.1 Passive Solar Design.....	40
2.4.2 BIPV and BIPV/T Systems	41
2.4.3 Solar Thermal Collectors	44

2.4.4 Heat Pumps	46
2.4.5 Thermal Energy Storage	47
2.4.6 Advanced Fenestration.....	51
2.4.7 Technology Trends in Building Controls.....	56
2.4.8 Building Simulation Methodologies and Tools	58
2.4.9 Advanced Solar Homes in Canada: a Brief Overview	62
3. Theoretical Considerations	67
3.1 Research Needs in Control of Solar-Optimized Homes	67
3.2 Thermal Networks for Building Energy Modeling.....	69
3.2.1 Analytical Methods and Conduction Transfer Functions.....	69
3.2.2 Control Volume Finite Difference (CVFD) Method.....	73
3.2.3 Thermal Network Analysis and Transfer Functions	75
3.2.4 Discrete-Time Transfer Functions Using z-Transforms.....	79
3.3 Predictive Control Methodology for Solar-Homes	83
3.3.1 System Identification of Simplified Models	83
3.3.2 Model Predictive Control (MPC) of Radiant Floor Heating.....	90
3.3.3 Optimal Set-point Sequence for Solar-Heated TES Tank.....	93
4. Design and Control of a Solar House.....	97
4.1 The Alstonvale Net Zero House.....	97
4.2 Design Procedure and Building Simulation	98
4.2.1 Preliminary Simulations.....	99
4.2.2 Dynamic Simulation of Thermal Phenomena	109
4.2.3 Addition of Electric Vehicle and Roof Design Modifications	113
4.3 Heating System.....	115
4.3.1 BIPV/T Roof.....	115
4.3.2 Solar-Assisted Heat Pump System and TES Tank.....	122
4.4 Final Schematic and Control Sequences.....	134
4.5 Design Suggestions for Other Cases: the ÉcoTerra House	137
5. Predictive Control Strategies.....	142
5.1 Introduction.....	142
5.2 Experimental Work at the Concordia Solar House.....	142

5.3 Rule-Based Predictive Control	150
5.3.1 Simple Weather Scenarios for Building Control Prototyping.....	151
5.3.2 Comparison of Heuristic Control Strategies	152
5.3.3 Set-point modification based on forecast	156
5.4 System Identification of Simplified Model	165
5.5 MPC for Radiant Floor Heating (RFH).....	170
5.6 MPC for RFH and Blind Position	173
5.7 Optimal Control of TES Tank Set-point	178
5.7.1 System Description	178
5.7.2 Dynamic Programming Algorithm.....	180
5.7.3 Cost of Switching from State to State	186
5.7.4 Results of Dynamic Programming Algorithm	191
6. Conclusions.....	196
6.1 Summary.....	196
6.2 Research Contributions.....	200
6.3 Lessons Learned.....	201
6.4 Recommendations for Future Research Work	204
References.....	206
Appendices.....	229
A. Alstonvale Net Zero House Schematics.....	229
B. Equipment Technical Specification Sheets.....	233
C. MATLAB M-FILE Model.....	242
D. Overview of Simulink Model	258
E. BIPV/T Model and Heat Pumps	266
F. System Identification and MPC Implementation	274
G. Cost Function and Dynamic Programming.....	277
H. Perez Model	284

List of Figures

Figure 1.1. Secondary energy use (left) and GHG emissions (right) by sector in Canada, 2007 (NRCan-OEE, 2010a).....	2
Figure 1.2. Design techniques and technologies that may be used in a solar house: (1) south-facing fenestration; (2) significant thermal mass; (3) sunscreens and overhangs; (4) solar thermal collectors; (5) thermal energy storage tank; (6) domestic hot water tank; (7) solar-assisted heat pump; (8) radiant floor heating (RFH) system.....	3
Figure 1.3. Typical response of a passive solar house in the case of two sunny days followed by two cloudy days (adapted from (Athienitis, 1994)). $T_{o,p}$ and Rad_p are respectively the simulated outdoor temperature and the solar radiation on a 45° surface for a time step p . $T_{i,p}$ is the resulting indoor air temperature.....	5
Figure 1.4. Primary source of energy for domestic space heating in Canada(NRCan-OEE, 2010b). In Québec, 76% of households use electricity as the main source of heating (36% in Canada).....	10
Figure 1.5. Newspaper article on peak loads (Anonymous, 2011).	10
Figure 1.6. Load duration curve for the province of Ontario in 2006 (OCA, 2007).....	12
Figure 2.1. Classification of advanced building control methodologies, adapted from Wang and Ma (2008).	20
Figure 2.2. Set-points, simulation results and experimental results for night setback and optimal energy control, from Morris <i>et al.</i> (1994). (a) Set-points for night set-back and optimal energy consumption. (b) Simulation results of cooling load for the same conditions. (c) Experimental results for the cooling load with night setback and optimal control.	24
Figure 2.3. Schematic of a TES system, adapted from ASHRAE (2007). The chiller can provide cooling (i.e., remove heat from) the ice storage system or the building itself.....	26
Figure 2.4. Office building control system (Lute & Paassen, 1989; Paassen, 1989).....	32
Figure 2.5. Approach of the <i>OptiControl</i> project (a). Simplified model (b). Adapted from (Gyalistras & OptiControlTeam, 2010).	35
Figure 2.6. Progression of PV price over the last decade (Solarbuzz, 2011).....	43

Figure 2.7. Comparison of the performance of different kinds of solar collectors (SunEarth Inc., 2005).....	45
Figure 2.8. Comparison of different TES systems (Hauer, 2010).....	51
Figure 2.9. Cooling load curves for a hot summer day under different control conditions of lighting, as well as venetian and roller blind control (Tzempelikos, 2005).....	56
Figure 2.10. The ÉcoTerra House (photo: YuXiang Chen).	64
Figure 3.1. Two-port network model for a wall, adapted from (Athienitis, 1985).	69
Figure 3.2. Norton equivalent for a wall with an exterior insulating layer of negligible thermal mass. Adapted from Athienitis & Santamouris (2002).....	71
Figure 3.3. Control volume discretization.....	74
Figure 3.4. Thermal network representation of a single-zone room (radiative exchange between the internal surfaces is not shown). Each part of the building envelope is exposed to sol-air temperatures (T_{SA}) and to solar radiation hitting its internal surface.....	76
Figure 3.5. Building control diagram based on transfer functions. Adapted from Athienitis <i>et al.</i> (1990).....	78
Figure 3.6. Numerical determination of a transfer function for a sample building (Athienitis <i>et al.</i> , 1990). This figure shows the Bode diagram of exact discrete responses found with a computer program (BEEP, see Athienitis <i>et al.</i> (1990) for details) and a curve-fitted third-order transfer function.	79
Figure 3.7. Superposition principle applied to a simplified model, with three inputs used: solar gains, outdoor temperature and heat delivered by a RFH system.....	86
Figure 3.8. Receding horizon control, as presented by Bemporad <i>et al.</i> (2010).....	92
Figure 3.9. Principle of optimality: if the optimal path includes \mathbf{x}_1^a , then <i>it has to contain</i> the optimal path from \mathbf{x}_1^a until the end.....	95
Figure 4.1. Alstonvale Net Zero House (January 2010).	98
Figure 4.2. Scoring system in the energy category as a function of ERS rating. Adapted from (CMHC, 2006a).	105
Figure 4.3. First roof configuration (PV panels in grey, glass panels in white).....	108

Figure 4.4. Energy output for Montréal of a 5.6 kW PV system.	109
Figure 4.5. Thermal network used in the preliminary dynamic simulations of the Alstonvale Net Zero House. Resistances corresponding to radiation exchange between the surfaces are not shown.	110
Figure 4.6. Typical results obtained with the Mathcad model.	111
Figure 4.7. Typical node equation in a Simulink representation.	112
Figure 4.8. Second roof configuration (8 additional PV modules).	114
Figure 4.9. Final roof configuration with 48 PV modules.	114
Figure 4.10. BIPV/T roof of the ANZH.	115
Figure 4.11. Principle of operation of the BIPV/T Roof.	116
Figure 4.12. Low-emissivity absorber plate (TiNOX).	117
Figure 4.13. Conceptual representation of the code used for the BIPV/T system.	117
Figure 4.14. Modeling of the BIPV/T roof.	118
Figure 4.15. Temperature change as a function of distance from inlet in the Alstonvale BIPV/T roof for different wind speeds. Irradiance = 900 W/m ² , Outdoor temperature = -10°C, air flow rate = 1300 CFM, attic temp. = 10 °C.	121
Figure 4.16. Outdoor dry-bulb temperature and BIPV/T exit temperatures for different flow rates. Montréal TMY2 weather file.	121
Figure 4.17. TES Tank.	123
Figure 4.18. Left: ducting system used to bring hot air to the heat exchanger (drawing courtesy of Kwang-Wook Park). Right: air-to-water heat exchanger.	124
Figure 4.19. The four charging modes for the TES tank.	125
Figure 4.20. Heat exchanger-heat pump-TES tank group.	126
Figure 4.21. Schematic of the function used to model the heat pump operation.	128
Figure 4.22. Heat delivered to the TES tank in mode B (two heat pumps operating in parallel). $T_{bot_tank} = 33$ °C. pumps used: Genesis GSW036.	129
Figure 4.23. COP in mode B (two heat pumps in parallel). $T_{bot_tank} = 33$ °C. Heat pumps GSW036.	129

Figure 4.24. Stratification in TES tank modeled with 4 nodes, as per Duffie and Beckman (2006a).....	131
Figure 4.25. Pressure drop in BIPV/T ducting system.....	132
Figure 4.26. Static pressure/flow rate curve for the fan used in the Alstonvale House (NYB, 2007).....	133
Figure 4.27. Measured flow rate vs. fan speed (Allard <i>et al.</i> , 2010).....	134
Figure 4.28. Near-final control schematic of the Alstonvale House. Adapted from Candanedo <i>et al.</i> , (2010).....	136
Figure 4.29. BIPV/T roof of the ÉcoTerra House.....	137
Figure 4.30. Mechanical system of the ÉcoTerra House (Chen, 2009).	138
Figure 4.31. COP of the BIPV/T assisted heat pump. ÉcoTerra BIPV/T roof with an air flow rate of 800 CFM.....	139
Figure 5.1. <i>Northern Light</i> (a.k.a. Concordia Solar House) at the Loyola campus.....	142
Figure 5.2. Passive thermal response of the Concordia Solar House for February 2007. Pyranometer used for irradiance measurements, temperatures measured with type T thermocouples. Measurements every 200 s. Adapted from Candanedo <i>et al.</i> (2007a).....	143
Figure 5.3. Simplified thermal circuit used to model the Concordia Solar House (Candanedo <i>et al.</i> , 2007a).	144
Figure 5.4. The four curves used to represent solar radiation conditions: Soc (overcast day), Spc (partially cloudy), Sps (partially sunny), Scs (clear sunny).....	148
Figure 5.5. Temperature fluctuation modeled and predicted, March 29 th , 2007 (note: initial measured temperature at 0:00 was “fed-in” into the program).	150
Figure 5.6. Global horizontal radiation according to scenarios designed for testing control strategies. (Candanedo & Athienitis, 2008a).	152
Figure 5.7. Summary of rule-based algorithm for adjusting set-points based on expected solar radiation (RAD_TODAY and RAD_TOM are given in MJ/m ²).	157
Figure 5.8. Algorithm for selecting the mode of operation for the BIPV/T-heat pump group. ...	159
Figure 5.9. Set-point adjustments with blinds fully open.	161

Figure 5.10. Position of blinds adjusted based on the expected radiation.....	162
Figure 5.11. Power generated by PV and used by heat pumps.	163
Figure 5.12. System’s performance over 10 days in January (TMY2 file).....	164
Figure 5.13. System’s performance over 10 days in January (TMY2 file). Note the set-point change when a cloudy day follows a sunny day.	164
Figure 5.14. Methodology for system identification and model-based predictive control implementation.	166
Figure 5.15. Geometry of the shed used for system identification and modeling of MPC strategies.	166
Figure 5.16. Input signals (forcing functions) used to study the response of a simple building to weather variables and heat from a radiant floor heating system. (Candanedo & Athienitis, 2011).	168
Figure 5.17. Comparison between EnergyPlus and TF model (Candanedo & Athienitis, 2011).	170
Figure 5.18. MPC in MATLAB/Simulink (Candanedo et al., 2011a).	171
Figure 5.19. Results obtained with the MPC controller for Montréal weather.	173
Figure 5.20. Multiplication of solar gains by and adjustment factor (“equivalent transmittance”) to account for the presence of a roller blind or similar device.....	174
Figure 5.21. Linearized equivalent of system shown in Figure 5.20.	175
Figure 5.22. Simulink model with an MPC block generating two controlled variables (RFH heat output and blind position).	176
Figure 5.23. RFH heat delivery rate and room temperature without blind control.....	177
Figure 5.24. RFH heat delivery rate, adjusting factor and room temperature with blind control.	177
Figure 5.25. BIPV/T assisted heat pump used to heat a TES water tank.....	178
Figure 5.26. Two possible set-point trajectories for the TES tank set-point.....	182
Figure 5.27. Nomenclature used and two sample points.	183
Figure 5.28. Algorithm used to calculate the cost of moving from set-point A to set-point B...	190

Figure 5.29. Comparison of an optimal set-point trajectory and an arbitrary trajectory for the TES tank.....	191
Figure 5.30. Weather conditions and RFH heat output calculated by MPC algorithm (Jan. 10 th - 12 th).....	192
Figure 5.31. Optimal TES set-point trajectory (Jan. 10 th to 12th).....	193
Figure 5.32. Weather conditions and RFH heat output calculated by MPC algorithm (Jan. 24 th - 26 th).....	194
Figure 5.33. Optimal TES set-point trajectory (Dec 11 to Dec 13).	194

Figures in Appendices

Figure A.1. Main floor plan.	229
Figure A.2. Upper floor plan.....	229
Figure A.3. Radiant floor heating zones, main floor.....	230
Figure A.4. Radiant floor heating zones, upper floor.	230
Figure A.5. South elevation view (Pogharian, 2007).....	231
Figure A.6. East elevation view (Pogharian, 2007)	231
Figure A.7. West elevation view (Pogharian, 2007).....	232
Figure A.8. North elevation view (Pogharian, 2007).....	232
Figure B.1. Window details from manufacturer.	233
Figure B.2. Day-4 PV panels used on the Alstonvale Net Zero House.	234
Figure B.3. Air-to-water heat exchanger.....	235
Figure B.4. Heat pump Genesis GSW036 (ClimateMaster).....	236
Figure B.5. Heat Pump EW020 (Waterfurnace).	237
Figure B.6. Performance curves of NIBE F2025-6.....	238
Figure B.7. Technical specifications, NIBE F2025-6.....	239
Figure B.8. Details of BIPV/T fan used in the Alstonvale Net Zero House.	240

Figure B.9. Curve of BIPV/T fan used in the Alstonvale Net Zero House.....	241
Figure D.1. Summary of Simulink Model.	258
Figure D.2. House Thermal Model (Partial View).	259
Figure D.3. Model for Node 1 (out of 22 nodes) within “House Thermal Model”.	260
Figure D.4. Close-up of selection between modes of operation (higher level of several nested blocks).....	261
Figure D.5. Selection between modes B, C and D.....	262
Figure D.6. Graphical implementation of a MATLAB M-function of multiple variables.	263
Figure D.7. Partial view of the TES tank model (4 nodes).	264
Figure D.8. Close-up: predictive control for set-point adjustments in the house and the TES tank.	265

List of Tables

Table 2.1. Installed area (m ²) of several types of solar collectors in some IEA member countries in 2000 (Weiss & Faninger, 2002).....	46
Table 4.1. Degree-days and design temperatures corresponding to Montréal used by HOT2000 (HOT2000, 2003).....	100
Table 4.2. Weather parameters corresponding to Montréal used by HOT2000 (monthly values) (HOT2000, 2003).....	101
Table 4.3. Parameters used by HOT2000 as standard operating conditions (CMHC, 2006a) ...	102
Table 4.4. Space heating and DHW loads, and corresponding ERS Rating. Basic HOT2000 default values applied without renewable energy systems.	102
Table 4.5. Relevant parameters of the house layout and building envelope.	103
Table 4.6. Energy use of major appliances. Adapted from Pogharian (2007).	106
Table 4.7. Energy use of minor appliances. Adapted from Pogharian (2007).	106
Table 4.8. Estimated annual electric energy consumption (kWh).....	108
Table 4.9. Comparison between the Simulink and HOT200 models, heating energy from December through March (Candanedo & Athienitis, 2010a).	112
Table 4.10. Parameters of BIPV/T roof in the ANZH.	115
Table 4.11. Heat capacity rates, temperature rises and heat removed for different flow rate conditions at noon, Feb. 5 th (35 th day of the year).....	122
Table 4.12. Heating energy and power consumption. Simulations for a BIPV/T-assisted heat pump at the ÉcoTerra house.	140
Table 5.1. Temperature swing in °C as a function of blind position and radiation. Adapted from (Candanedo <i>et al.</i> , 2007a).	149
Table 5.2. Measured and expected temperature swings. Adapted from Candanedo <i>et al.</i> (2007a).	149

Table 5.3. Summary of control strategies (relevant features of each strategy are highlighted). T_{exit} is the exit temperature of the BIPV/T air, and T_{bot_tank} is the temperature of the bottom of the TES tank. The green shading indicates the change with respect to the previous strategy. 154

Table 5.4. Heat delivery and heat pump power consumption for the six control strategies (kWh), corresponding to the month of February (TMY2 file). 155

Table 5.5. Adjustment values for the tank set-point and the house set-point according to the solar radiation expected on the roof over the next two days..... 157

Table 5.6. Heating capacity (HC) and electric power consumption of the NIBE F2025-6 used in this example as a function of the air-source temperature and the temperature of the water supplied to the reservoir. 179

Nomenclature

Symbols

A	Surface area; Two-port network parameter
A_w	Window area (Eq. 5.11)
$A(q)$	Polynomial in terms of q^{-1} (Eq. 3.34)
B	Two-port network parameter
$B(q)$	Polynomial in terms of q^{-1} (Eq. 3.34)
C	Two-port network parameter
C_{air}	Heat carrying capacity of air flow [W/K] (Eq. 4.13)
C_{wg}	Heat carrying capacity of water-glycol mixture (Eq. 4.14)
C_{AB}	Cost of going from state A to state B (Fig. 5.28)
C_r	Ratio of heat carrying capacities $C_r = \min(C_{air}, C_{wg}) / \max(C_{air}, C_{wg})$
$C(\mathbf{x}_k, \mathbf{u}_k, \mathbf{w}_k)$	Cost as a function of states, inputs and disturbances (Eq. 3.42)
$C(q)$	Polynomial in terms of q^{-1} (Eq. 3.35)
C_i	Thermal capacitance of node i
c_{p_air}	Specific heat of air
c_{pw}	Specific heat of water
D	Two-port network parameter
D_{ET}, D_{SR}, D_{RFH}	Denominators of transfer functions (Figure 3.7)
$E_{del,AB}$	Energy required for heating between points A and B (Eq. 5.43)
$E_{req,AB}$	Energy required for the set-point change from A to B (Eq. 5.44)
EE_{AB}	Electric energy use between A and B
G	Solar irradiance; solar gains (Fig. 5.3)
$G(\omega)$	Solar gains, frequency domain (Fig. 5.3)

G_{roof}	Irradiance on roof (Eq. 5.16)
G_{ET}, G_{SR}, G_{RFH}	Transfer functions (Figure 3.7)
$\tilde{G}_{SG}, \tilde{G}_{EXT}, \tilde{G}_{RFH}$	Approximate value of transfer functions (Eq. 5.20-5.22)
$H_{HP, AB}$	Available heat from BIPV/T-heat pump system, between states A and B
h_{ct}	Convective HT coefficient at top surface of BIPV/T channel (Fig. 4.14)
h_{cb}	Convective HT coeff. at bottom surface of BIPV/T channel (Fig. 4.14)
h_o	Exterior convective heat transfer coefficient
h_r	Exterior radiative heat transfer coefficient (Fig. 4.14)
i	Sub-index, time step counter
$J_{i,j}$	Minimum cost of going from state $S_{i,j}$ to the final state (Eq. 5.33)
J_0	Objective function (Eq. 3.42)
J_0^*	Optimal value of objective function (Eq. 3.43)
JG_i	Global minimum of going from time step i to the end
K	Transfer function gain (e.g., Equation 3.32)
K_T	Daily clearness index
k	Thermal conductivity
k_T	Hourly clearness index
L	Thickness of a material (Equation 3.3)
L_{CV}	Length of control volume in BIPV/T roof
LWT	Leaving water temperature in heat pump (Eq. 4.13)
\dot{m}_{air}	Air mass flow rate
N_{ET}, N_{SR}, N_{RFH}	Numerators of transfer functions (Figure 3.7)
OS_i	Optimum sequence of set-points from time step i to the end
P_{elect}	Electrical power per unit area
$q_1; q_2$	Heat transfer rates in a two-port network

Q_{rem}	Heat removed by the heat exchanger
q_{rem}	Heat removed by the air in the BIPV/T control volume (Fig. 4.14)
P_{elec}	Electric power generated by the PV within the control volume (Fig. 4.14)
P_{HP}	Power consumed by the heat pump (Eq. 5.29)
Q_N	Norton equivalent
Q_i	Heat entering node i (Eq. 3.10)
q_{sky}	Radiative heat loss to the sky per unit area
q_{rec}	Heat recovered in the control volume per unit area
RAD_{TODAY}	Total radiation per m^2 on the roof expected for today (Eq. 5.16)
RAD_{TOM}	Total radiation per m^2 on the roof expected for tomorrow (Eq. 5.16)
Rad_p	Radiation on a 45° south-facing surface (Fig. 1.1)
R_{ins}	Resistance of insulation (e.g. roof insulation, as in Fig. 4.14)
r_{k+i}	Reference (set-point) at time step $k + i$ (Eq. 3.41)
$S(t)$	Solar irradiance (Eq. 5.7)
$\hat{S}(n)$	Solar irradiance for harmonic n , frequency domain (Eq. 5.7)
$S_{i,j}$	State corresponding to time step i and set-point value j (Fig. 5.27)
S_k	Sum of square deviations (output – set-point), at time step k (Eq. 3.41)
S_{max}	Maximum solar radiation used in different profiles (Eq. 5.14)
s	Parameter in Laplace transform ($j\omega$)
T	Temperature; Sampling time (Eq. 3.20)
T_a	Ambient (outdoor) dry-bulb air temperature
T_{air}	Air temperature (room air, BIPV/T, etc. according to context)
$T_{air_avg,AB}$	Time-average BIPV/T temperature between t_A and t_B
T_{exit}	Temperature of BIPV/T air (Fig. 4.21)
$T_{BIPV/Tair}$	Temperature of BIPV/T air (Fig. 5.8)

T_{ai}, T_{af}	Temperature of air entering and leaving a control volume (Eq. 4.6)
T_{attic}	Temperature of attic under the BIPV/T roof (Fig. 4.13)
T_{bot}	Temperature of the bottom surface of BIPV/T channel (Fig. 4.14)
T_{bot_tank}	Temperature of the bottom of the TES tank (Eq. 4.12)
T_{eo}	Sol-air temperature
T_i	Temperature of node i
T_i^p	Temperature of node i at time step p (Eq. 3.11)
T_{in}	Temperature of air entering the BIPV/T roof (Fig. 4.13)
T_{ma}	Average air temperature in control volume (Fig. 4.14)
T_o, T_{ext}	Outdoor temperature
$T_{out}, T_{air-out}$	Temperature of air leaving the BIPV/T roof (Fig. 4.13)
T_{PV}	Temperature of PV panel within the control volume (Fig. 4.14)
T_R	Room air temperature (Fig. 5.3)
$\hat{T}_R(n)$	Room temperature component for the n^{th} harmonic (Eq. 5.13)
T_{ret}	Water return temperature (Fig. 5.25)
T_{sup}	Water supply temperature (Fig. 5.25)
$T_{sup,AB}$	Water supply temperature between states A and B (Eq. 5.49)
T_S	Temperature of internal surfaces (Fig. 5.3)
T_{STC}	Standard test conditions temperature for PV (25 °C)
T_{Tank_top}	Temperature of top of the TES tank (Eq. 5.19)
$T_{1,p}$	Temperature of node 1 at time step p (Figure 1.1)
T_1, T_2	Two-port network temperatures
$T_1(\omega); T_2(\omega)$	Temperature components in the frequency domain (Eq. 5.1 and 5.2)
T_d	Time delay (Eq. 3.32)
T_{p1}, T_{p2}, T_{p3}	Times corresponding to poles (Eq. 3.32)

Tsp_A, Tsp_B	Temperature set-points A and B , between consecutive time steps
t_A, t_B	Time corresponding to state A ; Time corresponding to state B
$t; t_i$	Time, time at step i
U	Thermal conductance (W/K)
U_o	Heat conductance between room air and outdoor air (Fig. 5.3)
U_S	Heat conductance between room air and internal surfaces (Fig. 5.3)
U_{ij}	Thermal conductance between nodes i and j
u_i	Input value at time t_i
$u(n); U(z)$	Sequence and corresponding z-transform (Equation 3.18)
V_{tank}	Volume of TES tank
$\dot{V}; \dot{V}_{\text{air}}$	Volumetric air flow rate (Fig. 4.13)
$\dot{V}_{\text{w_source}}$	Volumetric flow rate of liquid, source side of heat pump (Fig. 4.21)
$\dot{V}_{\text{w_sink}}$	Volumetric flow rate of liquid, sink side of the heat pump (Fig. 4.21)
v_{wind}	Wind speed
w_{PV}	Width of the control volume in BIPV/T system
w	Weighting factor (Eq. 3.41)
x_i	Set-point value at time step i
Y	Thermal admittance
Y _{Eq}	Equivalent admittance
Y _S	Self admittance
Y _T	Transfer admittance
$y(t); Y(s)$	Output variable; corresponding Laplace transform
$y(n)$	Measured output value
$\hat{y}(n)$	Output value calculated by the model

$\bar{y}(t)$	Arithmetic mean of the output
y_{k+i}	Measured output at time step $k + i$ (Eq. 3.41)
Z	Thermal impedance
$Z_{i,j}$	Thermal impedance between nodes i and j
z	z-transform operator

Greek Letters

α	Thermal diffusivity; absorptance
α_{AB}	Absorptance of absorber plate under the glazing (Eq. 4.5)
γ	Variable used in Equation 3.4
ΔT	Temperature change
ΔU_{AB}	Change of internal energy in the tank (Eq. 5.42)
Δt	Time step
ϵ_{HX}	Heat exchanger effectiveness (Eq. 4.13)
η_e	Electric efficiency of the PV panel
ρ_w	Density of water
σ	Stefan-Boltzmann constant ($5.67 \times 10^{-8} \text{ W m}^{-2} \text{ K}^{-4}$)
τ_{eq}	Equivalent transmittance of group blind-window (Eq. 5.15)
τ_{closed}	Transmittance of group window-blind, blind fully closed (Eq. 5.15)
τ_{open}	Transmittance of group window-blind, blind fully open (Eq. 5.15)
τ_g	Glass transmittance in BIPV/T glazing section (Eq. 4.5)
τ_w	Window transmittance (Eq. 5.11)
ω	Frequency (rad/s)
ω_n	Frequency for harmonic n

Abbreviations and Acronyms

ARX	Autoregressive model with exogenous input
ARMAX	Autoregressive moving average model with exogenous input
ASHRAE	American Soc. of Heating, Refrigerating and Air-Conditioning Engineers
BIPV	Building Integrated Photovoltaic
BIPV/T	Building Integrated Photovoltaic/Thermal
CFM	Cubic feet per minute
CMHC	Canada Mortgage and Housing Corporation
COP	Coefficient of performance
CTF	Conduction Transfer Function Factors
DHW	Domestic Hot Water
DP	Dynamic programming
DST	Daylight saving time
ECBCS	Energy Conservation in Buildings and Community Systems
EGH	EnerGuide Rating for Houses
EMS	Energy management systems
EMCS	Energy management and control systems
EP	Electric power consumed by heat pump (Fig. 4.21)
ERS	EnerGuide Rating for Houses (<i>new acronym</i>)
ESP-r	Energy systems performance-research program
EWT	Entering water temperature in heat pump (Eq. 4.12)
GHG	Greenhouse gas
HD	Heat delivered by the heat pump (Fig. 4.21)
HP	Heat pump; Horsepower (756 W)
IEA	International Energy Agency

MACS	Multi-agent control systems
MPP	Maximum power point
HBM	Heat Balance Method
HC	Heating capacity of the heat pump (Eq. 5.28)
HVAC	Heating, Ventilating and Air Conditioning
NTU	Number of heat transfer units (Eq. 4.15)
NZEB	Net Zero Energy Building
PMV	Predicted mean vote
PRF	Periodic response factors
PSV	Possible set-point values
PV	Photovoltaics
RTSM	Radiant time series method
SCCCC	Sequence of one sunny day, followed by four cloudy days (Fig. 5.6)
SI	System identification
TABS	Thermally-activated building systems
TES	Thermal energy storage
TF	Transfer function
TMY2	Typical meteorological year weather file, v.2
TOU	Time-of-use
TRNSYS	TRaNsient SYstems Simulation program

1. Introduction

1.1 Motivation

1.1.1 Problem Statement

It can be easily shown that our planet receives from the sun in one hour an amount of radiative energy exceeding the needs of humanity for one year (Rogner, 2000; Lewis & Nocera, 2006; World Energy Council, 2007). This is a compelling argument for considering solar energy and other sun-driven renewable sources the most promising alternative to fossil fuels, which presently supply most of our needs. Serious environmental concerns, of which climate change is the most prominent (IPCC, 2007), together with the inexorable depletion of petroleum and other fossil fuels (IEA, 2010; Owen *et al.*, 2010) and the resulting economic and geopolitical pressures (Hirsch *et al.*, 2005; Hirsch, 2008), urgently call for the use of the vast solar resource to gradually replace non-renewable energy sources.

Buildings (commercial, institutional and residential) consume about 31% of the secondary energy used in Canada and about 50% of the electric energy used in the country (NRCan-OEE, 2010a). Residential buildings (houses, apartments and other dwelling units) account for 17% of the total (Figure 1.1). A similar portion of the Canadian greenhouse gas (GHG) emissions can be attributed to the building sector (NRCan-OEE, 2010a). It is evident that energy conservation and distributed generation in buildings can play a significant role in reducing our global energy use and GHG emissions.

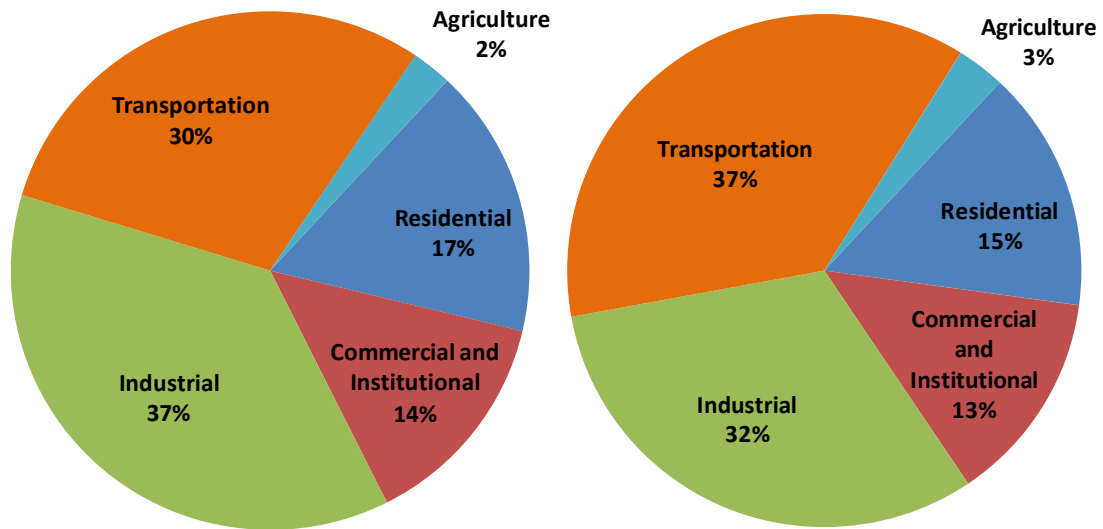


Figure 1.1. Secondary energy use (left) and GHG emissions (right) by sector in Canada, 2007 (NRCan-OEE, 2010a).

Fortunately, improved design techniques and new technologies facilitate a more effective use of solar radiation to satisfy the needs of the buildings' occupants, and could ultimately have a large impact if their use becomes more prevalent. Some of the most relevant trends are:

- Passive solar design (Athienitis & Santamouris, 2002).
- Increasingly accurate, informative and longer-term weather forecasts (Wittchen *et al.*, 2005; Poulin, 2006; Poulin *et al.*, 2006).
- Fenestration technologies, such as low emissivity coatings, argon-filled windows and triple-glazed windows.
- Dynamic façades with controllable blinds (Tzempelikos & Athienitis, 2003, 2005) and active windows (Assimakopoulos *et al.*, 2004), such as electrochromic, thermochromic and gasochromic technologies, that may be used for the control of solar heat gains and daylighting.
- Active thermal storage systems (Dincer, 2002).

- Building-integrated photovoltaic (BIPV) or BIPV/Thermal (BIPV/T) installations (Østergaard, 2003).
- Solar collectors (Duffie & Beckman, 2006).
- Ground source heat pumps (Biaou *et al.*, 2004).

An example of a house incorporating some of these features is shown in Figure 1.2.

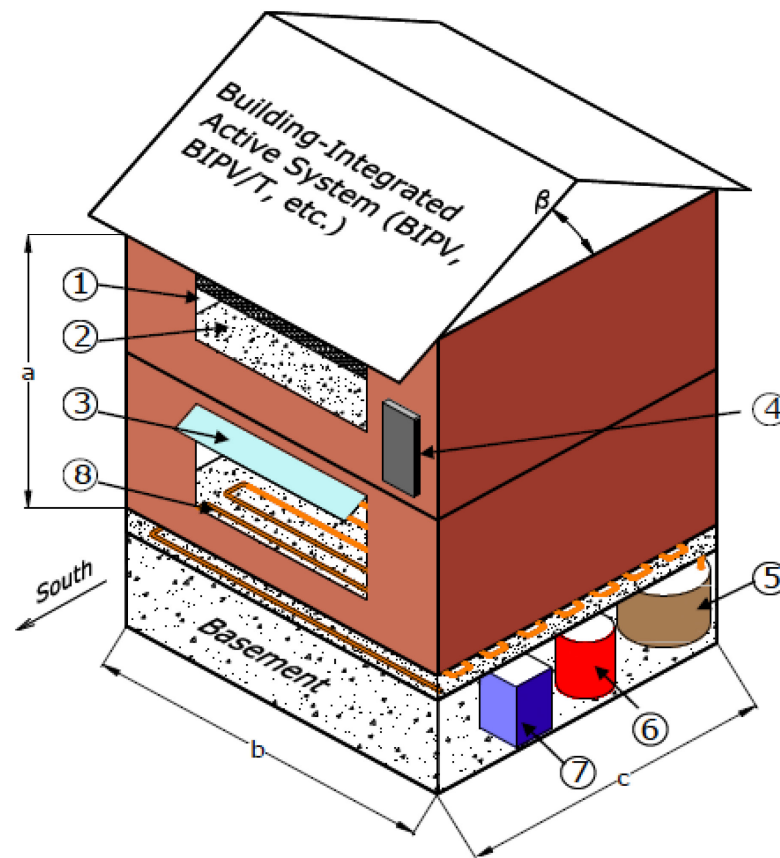


Figure 1.2. Design techniques and technologies that may be used in a solar house: (1) south-facing fenestration; (2) significant thermal mass; (3) sunscreens and overhangs; (4) solar thermal collectors; (5) thermal energy storage tank; (6) domestic hot water tank; (7) solar-assisted heat pump; (8) radiant floor heating (RFH) system.

The aforementioned design techniques and technologies open up new possibilities for the utilization of solar energy in buildings. Although solar energy is very abundant, like most renewable energy sources, it is highly variable. Therefore, storage and energy

management are essential conditions for the success of any solar house design. Strategies to plan the **collection, storage and delivery** of solar energy are necessary.

Electric or **thermal** energy supplied by the sun can be stored in several ways. Batteries can provide some limited **electric energy storage** capacity in off-grid systems or as a backup system for emergencies. **Grid-tied** installations can mimic “electric energy storage” (strictly speaking, the grid has no storage capacity). In this scheme, if the electricity generated at a given time by photovoltaic (PV) panels exceeds the needs of the house, the surplus can be delivered to the local utility grid. Conversely, if the power generated by the PV panels is insufficient for the needs of the house, then the utility grid supplies the difference. Grid-tied installations can therefore replace batteries. Although electric utility grids can currently handle domestic grid-tied installations rather easily, higher PV penetration rates will prove more challenging.

In a building, passive and active **thermal energy storage** (TES) can be used. **Passive (or distributed)** thermal energy storage refers to the capacity of the building materials to receive and gradually release energy to the indoor space. Materials with relatively high density and specific heat, such as concrete, stone and masonry can store significant amounts of heat. When these materials—which usually cover the internal surfaces of the building—are exposed to the solar gains entering the space through the fenestration (i.e. windows and transparent components of the building envelope), they can store a significant portion of this energy. The release of the thermal energy is thus delayed. This phenomenon allows the collected heat to be used during the night and cloudy periods, and helps mitigate indoor temperature fluctuations, which could affect thermal comfort.

Advanced technologies such as phase change materials (PCMs) can effectively increase the thermal mass of the building.

As Figure 1.3 illustrates, comfortable temperatures can be maintained in a solar house for a period of 18-24 hours by using passive thermal energy storage only.

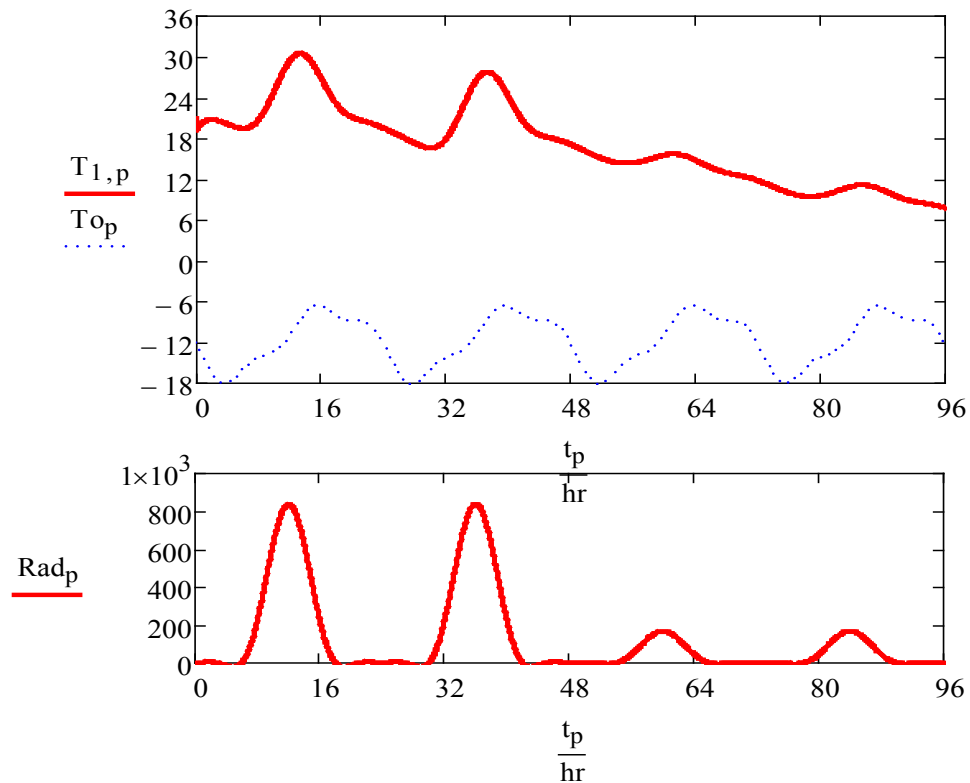


Figure 1.3. Typical response of a passive solar house in the case of two sunny days followed by two cloudy days (adapted from (Athienitis, 1994)). $T_{o,p}$ and Rad_p are respectively the simulated outdoor temperature and the solar radiation on a 45° surface for a time step p . $T_{1,p}$ is the resulting indoor air temperature.

Active (or isolated) thermal energy storage refers to devices such as hot or cold water reservoirs, ice storage devices, thermo-chemical systems and PCM tanks, whose state of charge can be modified by some active intervention, such as using a solar thermal collector or a heat pump to change their temperature.

Strategies for controlling these passive and active thermal energy storage capabilities should be incorporated as early as possible in the design approach. Control strategies must be considered as an essential part of the design.

This thesis investigates the use of predictive control strategies at two different, but closely related, control levels: (a) the **supervisory control level**, which deals with the selection of set-point profiles for the house and active TES systems and (b) the **local-loop control level**, which regulates the operation of the actuators (valves, blinds, etc.) in order to track the desired set-points.

Both control levels present their own challenges. Supervisory control requires tackling an optimization problem that should consider the availability of energy (in the case of renewable energies), the capabilities and limitations of the HVAC system, as well as the constraints imposed by thermal comfort. Tracking the desired set-point can also be difficult when the time constants of the “plant” (the house or space to be controlled) are very long. For example, controlling a radiant floor heating (RFH) system when the pipes are installed deep in a thick concrete slab can be complicated, as the heat released can take a long time to have a noticeable effect on the indoor temperature. Furthermore, in the case of a house with large south-facing windows, the floor may be exposed to tens of kW of solar radiation at a given point. This factor complicates even more the control problem; if not properly managed, it may present the risk of overheating the space. On the other hand, it offers the opportunity of using the floor to store solar energy for future use. If clear sunny conditions are expected, anticipatory actions can be taken so that the temperature of the floor surface is lower when it starts receiving solar gains (typically, in the early hours of the morning).

1.1.2 Concept of Optimally Designed Solar House

It is important to explain the concept of “optimally designed solar house”. Although it is difficult to give a formal definition of this term, optimally designed solar house (which are also referred to here as “advanced solar homes”) share some common features:

- Use of multiple solar-based technologies and design techniques (e.g., passive solar design, PV panels, daylighting, solar thermal collectors).
- Incorporation of solar energy as an essential design principle from an early phase, not as an afterthought or addition without major impact. For example, a conventional house with a “token” 100 W of PV panels would not qualify.
- Integrated design. A coherent plan for the interaction of the different systems should exist. Systems may have more than one function.
- Controlled operation. Control strategies should be an essential part of the system’s design from the early stages.

1.2 Implications of this Thesis

1.2.1 Net-Zero Energy Homes

Net-zero energy buildings (NZEBS) can be defined as those that use renewable energy sources to generate as much energy as they consume when the balance is made over a one-year period. Different regions and countries employ different versions of this definition: for example, “net-zero cost”, “net-zero emissions”, “net-zero primary energy” and “net-zero life cycle”. In Canada, the most accepted definition for residential buildings is the one proposed by Canada Mortgage and Housing Corporation (CMHC) for its

Equilibrium Initiative (CMHC, 2008). This definition is based on the EnerGuide rating system (EGH), previously developed for the R-2000 program (NRCan, 2010). The EGH score is calculated by performing an energy balance at the point of measurement installed by the utility, and then comparing this balance with that obtained for a reference building. An EGH score of 100 is equivalent to a “net-zero secondary energy”.

However, beyond the nuances of each version of the NZEB definition, it is clear that the widespread adoption of this design approach can significantly reduce the energy consumed by the building sector. It is also clear that solar energy utilization offers a pathway (often the only practical one) towards the construction of net-zero energy homes. Two programs of the International Energy Agency (IEA), the Solar Heating and Cooling Program (SHC) and the Energy Conservation in Buildings and Community Systems Program (ECBCS), started a joint activity in 2009, the **IEA SHC Task40 - ECBCS Annex 52**, “Towards Net Zero Energy Solar Buildings” (IEA-SHC/ECBCS, 2008). The subprojects of Task40-Annex52, in which the author of this thesis has participated as one of the Canadian delegates, include:

- The development of a general framework for international definitions of NZEB (Subtask A),
- The identification and development of design methods and tools (Subtask B),
- The collection of case studies for different climates and solution methods (Subtask C),
- And the dissemination of findings (Subtask D).

1.2.2 Load Management and Interaction with the Electric Grid

The problem of peak electric loads is as important —maybe even more so— than the overall energy consumption. The main constraint for the operation of a system is usually its maximum power demand.

The problem of peak loads can be studied from the point of view of either the utility or the energy users. Utilities are naturally interested in load management, since peak demands impose the maximum burden on their capacity to generate, transmit and distribute electric power. Load management (Gellings & Talukdar, 1987) is an encompassing expression that refers to diverse strategies used by utilities, such as “peak shedding” and “load shifting”, aimed at creating a more even distribution of energy utilization over time.

Apart from the benefits to the grid, peak load reduction has other significant benefits from the perspective of the building operator. For example, oversizing of HVAC equipment is a common problem, which leads to unnecessary expenditures and inefficient part-load operation. Energy storage and predictive control may allow the size of the installed equipment to be reduced.

In the case of Québec, there is significant potential for reducing peak loads through advanced building design. More than three quarters of the homes in Québec use electricity as their main source of heating (NRCan-OEE, 2010b). Other Canadian regions (notably Atlantic Canada and British Columbia) also intensively use electricity for space heating (Figure 1.4). Low winter temperatures tend to have a significant impact on peak

electric loads. A record winter peak (38,200 MW) in Québec (recently registered on January 24th, 2011 at 7:38 a.m.) elicited public attention (Figure 1.5).

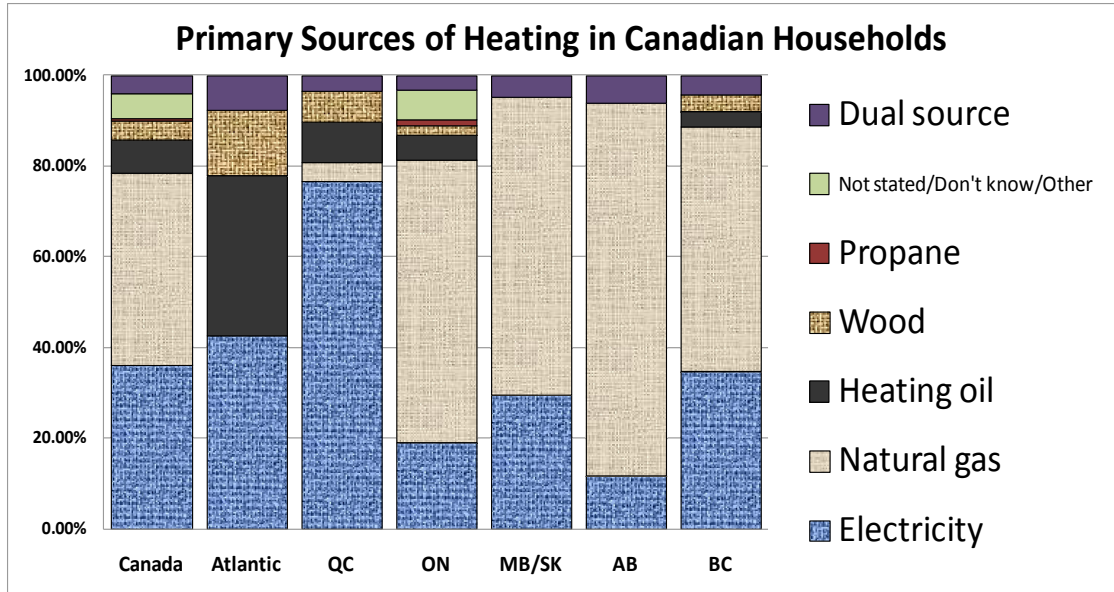


Figure 1.4. Primary source of energy for domestic space heating in Canada(NRCan-OEE, 2010b). In Québec, 76% of households use electricity as the main source of heating (36% in Canada).



Figure 1.5. Newspaper article on peak loads (Anonymous, 2011).

While the common approach to dealing with higher loads is to increase the power generated or to purchase it from neighbouring jurisdictions (in Québec, this means typically the U.S.), advanced building design and control strategies can also lead to peak

load reductions. To put in perspective the potential impact of load management measures in Québec homes, if each of the approximately 3 million dwelling units of the province reduced its load by 500 W, about 1,500 MW would be saved. This is equivalent to the generation capacity of a large hydro plant. Solar technologies and predictive control could contribute to peak shaving in houses, especially if TES systems (e.g., hot water tanks) are available and measures such as demand response in appliances are applied.

In contrast with Québec, peak loads in Ontario are mostly associated with cooling loads during the summer. Figure 1.6 shows a load duration curve for the province of Ontario in 2006. That year, the peak load (27,005 MW) occurred on August 1st, a hot summer day. The top 1% (i.e., 88 hours) had a demand exceeding 23,389 MW (OCA, 2007). In other words, 99% of the time the demand was below that number. This means that the grid (generation units, transmission and distribution lines) works at maximum capacity during quite a short time. It should also be noted that about 50% of the time the demand was below 17,000 MW. The installation of PV panels with the right orientation, for example towards the south-west (Pelland & Abboud, 2007) can be combined with strategies such as predictive control, demand response and thermal energy storage to reduce peak loads.

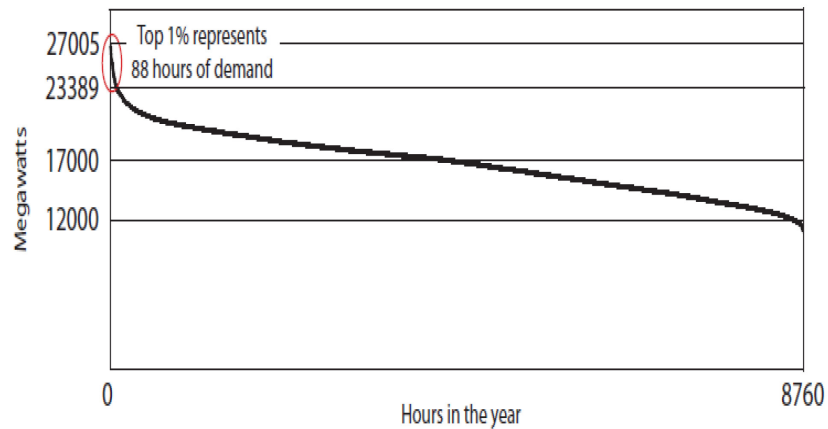


Figure 1.6. Load duration curve for the province of Ontario in 2006 (OCA, 2007).

Smart grid technologies have received considerable attention in recent years (Gellings, 2009). The term “demand response” is most commonly associated with the automatic control of domestic appliances as a reaction to signals from a smart grid. However, predictive control and energy storage capacity can also be used as demand-side management actions.

In the aforementioned Task40/Annex52, it has been recognized that the concept of NZEB, while being a desirable objective, is insufficient to describe the energy performance of a building. Even if the annual energy balance of a building is zero, the “mismatch” between its own power generation and demand could be significant, or even comparable to a conventional building. This “load mismatch” may occur at several time scales (e.g., daily, monthly, seasonal) because of the natural periodical patterns of energy availability and consumption. Since most NZEBs have a grid-tied configuration, the difference between the building’s generation and its own load will have an impact on the grid.

The impact of this “grid interaction” on the grid operation can be beneficial or detrimental, depending on the magnitude and timing of each event (Salom *et al.*, 2011). For example, PV electricity generation –or even a largely reduced load– during peak hours can decrease the need for additional power supplied by the utility. Conversely, if higher loads occur during peak hours, more generation capacity will be needed; even if the house is “net-zero” on a yearly basis, it may still add to the utility’s burden. Another important factor to be considered is the impact on voltage regulation of PV generation, especially for high PV penetration rates in a small distribution grid. Technological innovations can help in overvoltage prevention due to PV generation (Tonkoski *et al.*, 2010, 2011).

Local power generation also implies “fuel switching”, i.e. the replacement of an energy source with another. For example, electricity generated with coal at a thermal power station during peak hours could be replaced with power from a BIPV roof. Realizing the relevance of these three factors (“load matching”, “grid interaction” and “fuel switching”), the participants in Task40/Annex52 have decided to propose quantitative indicators describing load matching and grid interaction as part of a complete description of a NZEB (Voss *et al.*, 2010).

1.2.3 Electric Vehicles and Other Peripheral Systems

Another advantage of incorporating solar energy in buildings is that additional generation could supply power for electric vehicles. Presently, petroleum provides 98% of the energy used for transportation in Québec, in contrast with other sectors of the economy mostly supplied by hydroelectric power (RDVE, 2010). It is conceivable that a house with a BIPV roof be able to provide electricity for its own needs and for an electric

vehicle (Pogharian *et al.*, 2008), but this performance can only be attained if an integrated design approach, including energy conservation, passive solar design and advanced control, is applied.

To this end, the schemes known as V2H (vehicle to house) and V2G (vehicle to grid) are promising developments involving the use of the energy storage capacity of an electric or plug-in electric hybrid vehicle to exchange power with the house and the electric grid (Lund & Kempton, 2008). Additionally, in the case of high penetration rates of PV panels, electric cars could be used to store excessive power generation from PV panels, which the grid may not be able to handle. The use of the electric energy stored in the batteries could also result in peak load reduction at the early hours of the evening (mainly due to the use of appliances when the house occupants are at home). Finally, electric vehicles could also play a limited role as emergency supply devices (i.e., cover basic loads during a few hours) in case of an electric grid breakdown.

1.4 Objectives and Scope

1.4.1 Main Objective

The main objective of this thesis is to investigate the development of predictive control and design strategies for advanced solar homes. These strategies, which could also be applied to small commercial buildings, will focus on the use of passive and active TES capabilities to improve the utilization of the solar energy collected, reduce energy consumption and peak loads, and extend the energy autonomy of the building. These control strategies must incorporate the preservation of comfortable indoor conditions for the occupants as their first priority.

1.4.2 Specific Objectives

The specific objectives of this thesis are as follows:

1. To investigate supervisory control strategies for the coordinated management of:
 - (a) the thermal energy stored in the building's thermal mass (i.e. by controlling the building's dynamic response) and (b) active TES devices.
2. To investigate the implementation of predictive algorithms at the local-loop control level, in order to track the desired set-points.
3. To investigate the link between design and control in solar homes, the selection of appropriate modeling complexity levels for the development and testing of advanced control strategies, and the application of system identification tools to develop simplified models.
4. To investigate the impact of advanced control strategies on energy consumption and peak loads.

1.4.3 Scope

This thesis deals mainly with predictive control strategies for optimally designed *houses* (i.e., low-rise residential buildings). Optimal design refers to the use of a high-quality building envelope (high levels of insulation and air-tightness), passive solar design, energy efficiency and the use of renewable energy technologies (BIPV and BIPV/T systems), and generally having the features described in section 1.1.2.

The theoretical foundations of system identification techniques and model predictive control are not the subject of this investigation; however both techniques are applied as valuable tools for predictive control of a solar house.

While the scope of this work does not include high-rise commercial buildings, many of the techniques developed may be applied to small commercial buildings sharing the features of an advanced solar house.

This study does not address the problem of demand-side management strategies in domestic appliances. The impact of human behaviour on the building's energy performance, while being a significant factor deserving further research, is also beyond the scope of this investigation.

1.3 Thesis Overview

Chapter 1, the introductory chapter, includes a description of the problem, the main objectives and implications of this work, the scope of the investigation and a summary of the problems investigated.

Chapter 2 presents a literature and technology review on relevant subjects, including building traditional and advanced control strategies, and a brief overview of appropriate technologies for solar homes.

Chapter 3 consists of an overview of the theoretical concepts used throughout this investigation. The chapter begins with a summary of basic research needs on control of solar buildings. A brief description of the theoretical foundations of building simulation is presented, followed by the predictive control methodology used for this investigation. This chapter includes a brief discussion about the importance of selecting the right resolution model for the development of control strategies. Finally, the two main algorithms used for this research are presented: model predictive control, for local loop

control, and dynamic programming for the selection of set-points in a thermal energy storage system.

Chapter 4 presents a description of a case study, the Alstonvale Net Zero House, a project in which the author of this thesis played an active role, particularly on the energy simulations –both for the building and for its renewable energy systems– and the development of the control strategies. This case study provided significant insight on the design of a net-zero solar home, and provided ideas for the development of generalized control algorithms.

Chapter 5 presents a description of the predictive control strategies developed during this study. These strategies were applied to the case study building and to a building with a simplified geometry. Supervisory and local-loop control strategies are presented, based in rule-based approaches and in the application of optimal control and model-based predictive control.

Chapter 6 summarizes the contributions of this study, discusses recommendations for the design and control of advanced solar homes, and suggests future areas of research suggested by the findings of this investigation.

2. Literature and Technology Review

2.1 Introduction

Controls are critical for the success of high performance buildings (Torcellini *et al.*, 2004). Advanced building control includes a large diversity of systems and technologies in residential and commercial buildings. Smart building systems include access control, communication, IT systems, elevator control and fire protection (Wong *et al.*, 2005), integrated within what is commonly called a “building automation system” (BAS). There is a vast literature on advanced energy management systems (EMS) (a.k.a. energy management and control systems, EMCS) for buildings: significant progress continues to be achieved in terms of technological innovation, control algorithms and software implementation. This literature review is mainly concerned with the main energy systems: HVAC, lighting/daylighting, hot water and appliances. The review deals mainly with controls for residential low-rise buildings, in particular solar homes.

In general, research on advanced control has focused more on commercial buildings than houses, as home automation (also known as “domotics”) has not been widely adopted yet. Advanced control systems are still mainly used in the commercial sector, especially in large buildings (Braun, 2007a), although recent developments have enabled their installation in smaller commercial buildings. The energy requirements and control needs of commercial and residential buildings are often quite different. For example, in commercial buildings, cooling and lighting play major roles, while in houses, especially in cold climates, space heating and domestic hot water (DHW) heating are the dominant

factors in energy consumption. Despite these differences, control strategies can often be adapted from commercial to residential buildings, and vice versa.

A short overview of the research performed on building control over the last quarter of a century, as well as currently active topics, is presented below. Classifying building control technologies and strategies is a challenging task; boundaries between methodologies and systems are not clearly defined and there is significant overlap and hybridization between applications, algorithms and approaches. However, two trends have been followed in research on advanced building control: (a) methods based on physical models; and (b) model-free (or almost model-free) methods (Dounis & Caraiscos, 2009). In the first approach, a physical model of the system is used in optimal and predictive control algorithms. In the second, algorithms consist mostly of model-free techniques (e.g., reinforcement learning, expert systems) or black-box models (e.g., obtained with artificial neural networks, correlation techniques and polynomial curve fits).

Figure 2.1, adapted from Wang and Ma (2008), presents an overview of supervisory control methodologies. Again, there is no sharp separation between approaches: boundaries are blurry. Methods presented on the left of the graph are usually based on artificial intelligence (AI) techniques, while methods presented on the right tend to employ models of higher resolution with formal mathematical optimization algorithms (arrow included by the author of the thesis). The dashed line (also included by this author) indicates that a black-box model, while not giving much information on the system, may be used in a “model-based” strategy. Conversely, a purely physically based model can be used with an optimization algorithm based on AI techniques (e.g., genetic

algorithms). In “Grey-box” models, hypotheses are made on the configuration of a physical model (e.g., a thermal network); optimization techniques are then used to find the best fit for the value of the parameters (Kämpf & Robinson, 2007; McKinley & Alleyne, 2008).

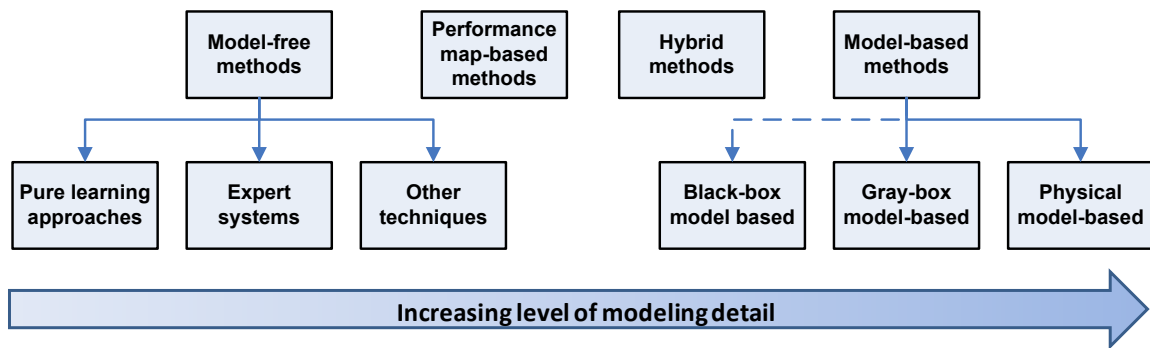


Figure 2.1. Classification of advanced building control methodologies, adapted from Wang and Ma (2008).

Each emergent technology (PCM, dynamic façades, renewable energy systems) opens up new challenges and possibilities to improve comfort and to reduce energy consumption and peak loads. A brief overview of technologies and software tools relevant for solar homes is also presented in this chapter.

2.2 Model-Based Building Control

2.2.1 Early Work on Dynamic Control of Buildings

The most basic supervisory control strategy consists of keeping a fixed temperature set-point. A slightly more sophisticated approach uses a lower set-point at night during the heating season (“night setback”), or a higher set-point at night during the cooling season (“night setup”, although the wording “night setback” is also sometimes used for this strategy). Different temperature set-point profiles have been proposed. For example,

a typical scheme of a programmable residential thermostat, attempting to follow the needs of the occupants, uses four set-points: a wake-up set-point (approximately from 06:00 to 08:00), a daytime set-point (08:00 to 17:00), evening set-point (17:00 to 22:00), and a night set-point (22:00 to 06:00).

There are several advantages to integrating the building thermal mass in a well-conceived control strategy: improved comfort because of higher mean radiant temperature, reduction of peak loads, and dampening of fluctuations due to sudden changes in solar radiation or exterior temperature. The ASHRAE Handbook of Applications (ASHRAE, 2007) mentions other benefits: (a) reduction in demand costs where demand charges apply; (b) the use of electricity when it is less expensive; (c) the use of exterior air at night for ventilation pre-cooling in the cooling season; and (d) the improved performance of the system because of better ambient conditions.

Traditionally, heating equipment has been selected for the worst case scenarios under static conditions (McQuiston *et al.*, 2005; ASHRAE, 2009). The ASHRAE Handbook of Fundamentals (ASHRAE, 2009), in Section 17.1, states: “*Heating calculations use simple worst-case assumptions: no solar or internal gains, and no heat storage (with all heat losses evaluated instantaneously).*” In Section 17.11, it is written: “*This leaves a simple steady-state heat loss calculation, with the only significant difficulty being surfaces adjacent to the grade.*” This approach is not suitable for solar homes with large thermal mass and glazing areas.

Dynamic control, a strategy incorporating the use of the building’s thermal mass into the HVAC control to reduce energy consumption, has been studied for decades, in particular for commercial buildings (Hartman, 1980, 1988). Dynamic control allows

smaller HVAC equipment, improved part-load operation and a more even distribution of the energy supply over time. Despite these opportunities, implementing dynamic control of the thermal mass can be challenging since the long time constants introduce significant delay between external stimuli (e.g., solar radiation, outdoor temperature) and their effects. Hartman discussed the potential of dynamic control for energy savings, describing basic features of this technique, including the use of weather forecasts to anticipate load conditions and the need for a supervisory control coordinating the actions of all the systems. Hartman mentions the need for collaboration among all the professionals involved in the design of a building, so that energy use is minimized.

The work by Borresen (1981) presented a basic approach to the mathematical modeling of a room and its use for control purposes. Borresen stated that a single capacitance for the air node might suffice for short-term control purposes. Modeling complexity becomes an issue for long term analysis. Borresen suggested a method for adjusting the time constants of the models with experimental data.

2.2.2 Optimal Control for Management of Active and Passive TES

Optimal control theory is the collective name given to the mathematical and numerical techniques focusing on the optimization of a performance parameter (e.g., cost or energy consumption) called the “objective function” over time. The optimization is subject to constraints (e.g., thermal comfort limits), and is performed based on estimations or forecasts of future loads. Chapter 41 of the HVAC Handbook of Applications provides an overview of optimal control strategies used in supervisory control of buildings (ASHRAE, 2007). The review paper by Wang and Ma (2008)

provides a summary of different optimization algorithms used in building control applications. Optimization algorithms are numerous, and highly dependent on the intended application. They include basic least square methods, simplex search, dynamic programming, and Lagrange methods.

In the last quarter of a century, the application of optimal control to buildings has received considerable attention. A landmark work is the study carried out by Braun (1990), essentially focused on cooling. By performing numerical simulations, Braun compared conventional night setback and three optimal dynamic control strategies. The three control strategies consisted of: (a) minimizing energy consumption without time-of-use (TOU) rates, (b) minimizing energy consumption with TOU rates, and (c) minimizing peak demand. Braun (1990) concluded that the use of free-cooling with optimal control reduces electricity peak loads even when peak load reduction is not the objective function, and that in general, optimal control outperforms conventional control. The optimization method used in this study was the direct search complex method.

Rabl and Norford (1991) studied peak load reduction strategy by pre-cooling a building at night. In this study, a simplified model with relatively few inputs is used.

Morris *et al.* (1994) published an experimental study applying Braun's optimization method to a test facility. Optimal temperature set-points were designed using energy consumption and peak demand as objective functions. Figure 2.2 shows some of the results. It is interesting to observe that the temperature set-point profile of the optimal control strategy differs considerably from a night setback. However, the performance of the optimal control strategy is remarkably good.

Drees and Braun (1996) continued work in the field of ice storage systems by developing rule-based approaches based on optimal control strategies.

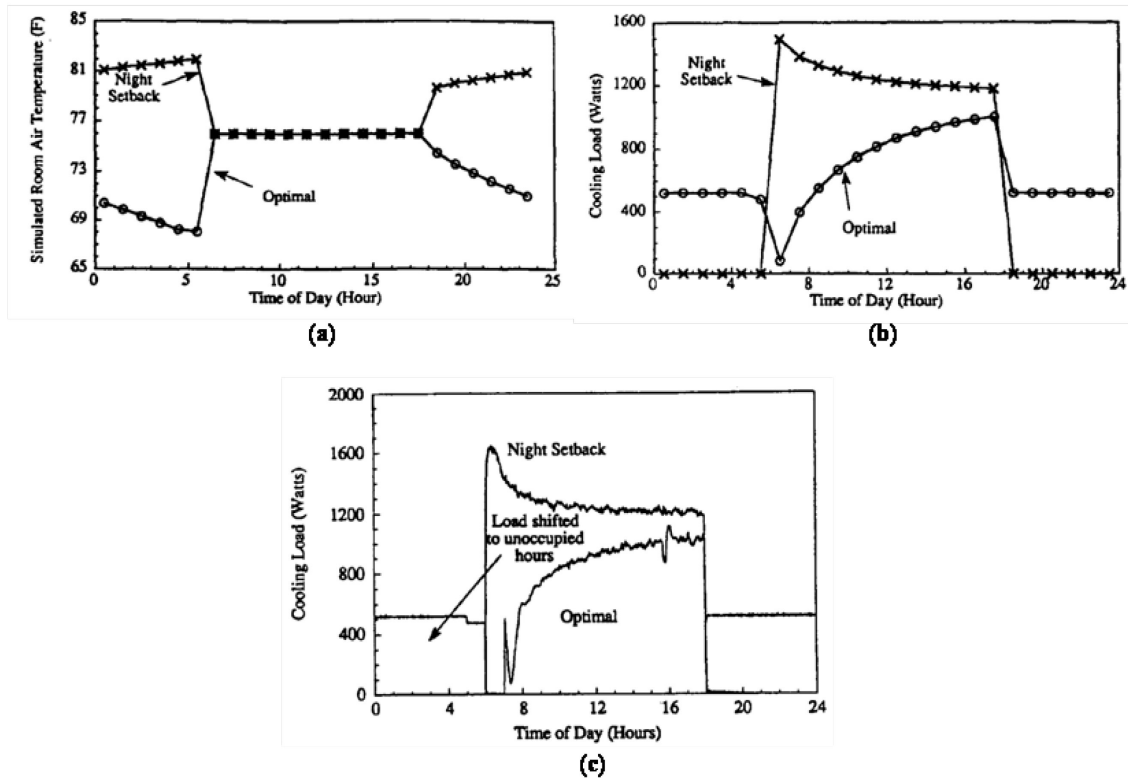


Figure 2.2. Set-points, simulation results and experimental results for night setback and optimal energy control, from Morris *et al.* (1994). (a) Set-points for night set-back and optimal energy consumption. (b) Simulation results of cooling load for the same conditions. (c) Experimental results for the cooling load with night setback and optimal control.

Kinter-Meyer and Emery (1995) presented one of the first studies considering optimal control of both active and passive storage. A simple model of a building and a mechanical system with a cooling tower and two chillers (one for direct supply of cooling and another for an ice-storage system) were examined. The plant model included a representation of the compressor as a simple function of the load and the temperatures of the cooling tower and the chilled water. Simple analogy relationships were used for the power consumed by the circulating pumps. The objective function to be minimized was

defined as the sum of the electric power consumed by each device and a penalty for demand charges. Two variables were determined: the cooling power provided directly to the space, and the charge rate of the TES system (which can be positive or negative). Kintner-Meyer and Emery pointed out that matching a pre-determined cooling load is not a requirement for an HVAC system: what is important is to maintain satisfactory thermal comfort conditions when the building is occupied. Kintner-Meyer and Emery employed a commercial non-linear optimization program (NPSOL) in their investigation.

The study by House *et al.* (1991) of optimal control of a thermal system addressed the problem by dividing one day into 24 discrete one-hour time steps. A sequential quadratic programming optimization algorithm was used. In France, Bénard and collaborators also studied the application of optimal control techniques for building control (Bénard *et al.*, 1992a, b) by using system identification to create low-order RC models for a group of buildings of a university campus. The cases studied included buildings with both low and high thermal inertia. A state-space representation was then used for designing optimal control strategies with good results.

Henze and collaborators have carried out extensive work on the application of optimal control techniques for predictive control of thermal energy storage (TES) in large buildings (Figure 2.3), in particular ice-storage systems. One of the key motivations for using TES is to take advantage of reduced utility rates during off-peak hours; however, lack of proper control strategies was cited as the cause of the poor performance of these systems (Henze *et al.*, 1997). Early research efforts of Henze's group focused on one controlled variable: the rate of charge of the ice thermal storage. This rate can also take negative values (i.e., discharge) when the stored cooling capacity is used to supply the

building needs (Henze, 1995; Henze *et al.*, 1997a; Henze *et al.*, 1997b; Henze & Krarti, 1999; Krarti *et al.*, 1999).

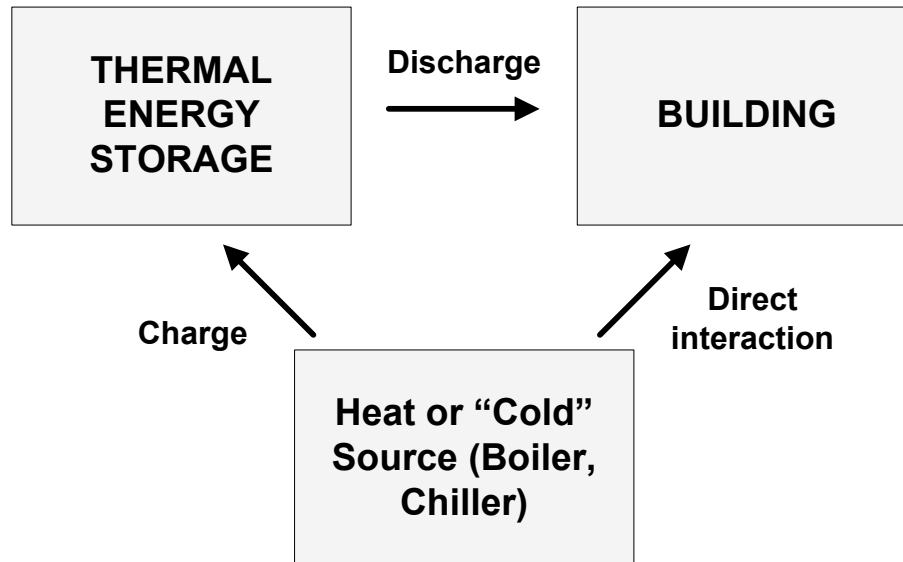


Figure 2.3. Schematic of a TES system, adapted from ASHRAE (2007). The chiller can provide cooling (i.e., remove heat from) the ice storage system or the building itself.

In the configuration shown in Figure 2.3, lower efficiencies are expected when the chiller is used to charge the ice TES than when it is used to supply the cooling load (ASHRAE, 2007). For this reason, a conventional control strategy is “chiller priority”; as its name indicates, the chiller is used in the first place to satisfy the cooling load and the use of the ice storage is minimized. “Chiller priority” is used when there are nearly flat rates for energy cost and there is no demand charge: the main benefit is then the reduction of the chiller rating.

Another strategy is “storage priority”, in which the chiller is used to make as much ice as possible during off-peak hours, and the ice TES is used as much as possible to satisfy the cooling load. The chiller only provides cooling directly to the space when the capacity of the TES is exceeded.

Henze *et al.* (1997) compared the performance of several conventional control strategies with the optimal control algorithm developed in this study. The control strategies included “chiller priority”, “storage priority” and “constant proportion” (the chiller and the ice storage share the load in a constant proportion). The optimal control strategy outperformed the three conventional strategies in terms of savings, especially for complex rate structures.

In recent years, Henze and collaborators (Henze *et al.*, 2004a; Henze *et al.*, 2005; Liu, 2005; Zhou *et al.*, 2005) have published studies on numerical simulations and experimental applications of optimal control in the coordination of active and passive thermal storage for large commercial buildings (see Fig. 2.3). In these studies, two variables (temperature set-points and discharge rate of the TES) are used as controlled variables in a dynamic programming strategy. Other studies carried out by this group have addressed:

- The effect of using different levels of building modeling accuracy on the optimal control strategy (Henze *et al.*, 2005; Liu, 2005). Construction materials, internal heat gains and characteristics of the HVAC plant were found to be among the most important factors for the design of optimal control strategies.
- The effect of forecasting uncertainty (Henze & Krarti, 1999). It was found that even imperfect forecasts enable the optimal predictive controller to perform better than conventional strategies do.
- The impact of the accuracy of weather forecasting models on a predictive optimal controller (Henze *et al.*, 2004b). A “perfect prediction” was used as

the reference. It was found that even simple weather forecasting models provide satisfactory results.

- The impact of the length of the planning horizon (Karti *et al.*, 1999). It was concluded that a planning horizon of 24 hours is often enough, unless two conditions occur simultaneously in the long term: (a) that all the energy stored in the TES is used and (b) the system needs more than one day to fully charge the TES.
- Parametric analysis of optimal control of active and passive cooling storage (Zhou *et al.*, 2005). In general, the conclusions of this study confirmed previous intuitive expectations: (a) optimal control provided more benefits in buildings with larger thermal mass; (b) more potential for savings was found for stronger incentives in the TOU utility rate structure; (c) more savings were obtained for a hotter, drier location in summer; (d) optimal control had a tendency to keep the set-point in the upper limit if other thermal comfort considerations were not included with a penalty function; (e) the capacity of the system affected the proportion of active and passive TES used; (f) an economizer was more useful wherever nights were cooler.

2.2.3 Model-Based Predictive Control of Solar Buildings

Studies on the dynamic control of *solar* buildings have tended to focus on specific aspects (e.g., the control of one piece of equipment) rather than on a global, comprehensive approach. The main goal of these investigations has often been the control of passive solar buildings. Dorato and Knudsen (1979) studied the use of steady

periodic models of solar radiation and exterior temperature, which were represented by Fourier series, to determine the optimal control strategy for auxiliary heating in a simplified model of an enclosure with a solar heating system. The objective function was analyzed by simple calculus (finding the values at which the derivative of the objective function is equal to zero). Albeit practical, this kind of strategy can only be used when simple curves are used to model the inputs (i.e., solar radiation and temperature).

Winn and Winn (1985) presented an implementation of optimal control to a solar house without active generation or TES systems. The residence used in this investigation had a Trombe wall and an electrically heated floor. Winn and Winn point out the importance of weather forecast for optimal control. It is also mentioned that a larger thermal mass mitigates the effect of imperfect predictions. This study is also noteworthy for its detailed presentation of the theoretical derivation of the control algorithms.

A predictive control algorithm for heating of massive buildings with high solar gains was presented by Athienitis (1988). Predictions of temperature and clearness index for the following day were used to determine the amplitude of a half-sinusoidal curve for solar radiation and the amplitude of a sinusoidal curve for temperature. These curves were applied to a linear thermal network of the building, and frequency domain techniques were used to determine the variation of the indoor temperature. The algorithm allowed the user to modify the “level” of the set-point curves, as well as the maximum heating power of the system. Five set-point profiles were designed: constant set-point, night set-back and three different ramp profiles. The algorithm classified the day as (a) cloudy (needing heating all day); (b) intermediate (heating is needed part of the day); and (c) sunny (there is risk of overheating). The heating power needed to follow each of the

five set-point profiles was determined. If at some point the heating power takes a negative value or exceeds the prescribed maximum, adjustments are made. Finally, the set-point profile that provided the smallest energy consumption was chosen, provided that the heating load did not exceed the preset capacity of the heater, and the air temperature was lower than the allowable maximum at all times.

Athienitis *et al.* (1990) stated that the proper design and operation of a building requires an *integrated analysis* of the building's response to load changes and the performance of its HVAC system.

“The time lags introduced by the building, its HVAC system and the sensor-control system are one of the major causes of complexity in controlling indoor environments.” (Athienitis *et al.*, 1990)

The paper mentions two approaches traditionally followed to attain this integrated analysis: (a) detailed numerical simulation with specialized software and (b) simplified analytical models dealing with specific interactions. Athienitis *et al.* (1990) developed an alternative methodology based on thermal networks with distributed parameter elements and lumped elements. Distributed parameter elements, which are used to represent exterior walls as two-port networks, provide a mathematically exact solution for heat fluxes and temperatures through them. Lumped elements (typically a single thermal capacitance) are used to represent constituents such as the room air and provide only an approximate solution. The resulting network model with two kinds of elements can then be solved in the frequency domain by applying methods borrowed from the analysis of electrical networks. In simple cases, the transfer functions between inputs and outputs can be determined analytically; in more complex cases, inputs and outputs are found at

discrete frequencies, and numerical methods can then be used to obtain an approximate analytical expression. The building transfer functions can be used for control studies (Athienitis & Shou, 1991) and for energy and load calculations..

Athienitis, Chen and collaborators have investigated the application of thermal network-based methods on the control of radiant floor heating systems with large thermal mass (Athienitis & Chen, 1993, 1997) and in particular on the effect of solar radiation on these systems (Athienitis & Chen, 1997a, 2000; Chikh, 2005). Chen has worked on the expansion of the concept of thermal networks for buildings (Chen, 2003), devised a weather prediction algorithm based on qualitative forecasts and historical records (Chen & Athienitis, 1996), designed a real time identification system (Chen, 1997), and has worked on the use of model predictive control in radiant floor heating systems (Chen, 2001, 2002; Chen & Athienitis, 2003). Chen has also used dynamic programming for the selection of set-points (Chen, 1997; Chen, 2001).

Numerical and experimental investigations in the Netherlands (Paassen, 1988; Lute & Paassen, 1989; Paassen, 1989; Lute & Paassen, 1990) and France (Vinot, 1988, 1989) addressed the application of predictive control in a room with adjustable window devices. These research projects are among the first to integrate the regulation of solar heat gains as part of the overall temperature control strategy. A linear discrete model of the room was used to calculate the room temperature as a function of solar heat gains, outdoor temperature and heating/cooling power. A room controller dashboard enabled communication with the occupants.

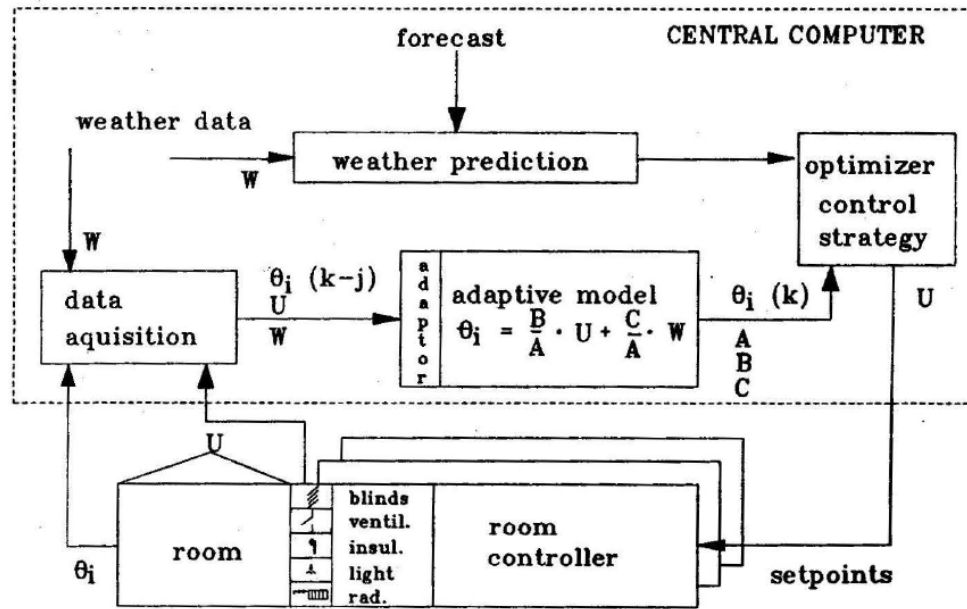


Figure 2.4. Office building control system (Lute & Paassen, 1989; Paassen, 1989).

Dounis *et al.* (1995a) compared the performance of traditional control, optimal control and knowledge based control (including fuzzy logic). While this paper strongly advocates the use of fuzzy logic techniques, it suggests that a combination of optimal and adaptive control techniques with fuzzy logic at lower levels might produce better results.

Simulation studies using optimal stochastic control, a technique that considers prediction uncertainty in dynamic programming, were carried out by Nygård-Ferguson for the control of the heating system of a passive solar room (Nygård-Ferguson & Scartezzini, 1988, 1989a; Nygård-Ferguson, 1990). The performance of the optimal stochastic control is compared with conventional strategies and is only outperformed by a hypothetical perfect prediction. The predicted mean vote (PMV) is used as a performance criterion. The objective function was formed by a weighted combination of energy consumption for each discrete step and PMV. In 1989, Nygård-Ferguson and Scartezzini stated that the main difficulty of implementing this advanced control strategy was the

computational requirement (2.8 MB of memory at the time!). Experimental studies were also made in a test building during which the occupants were given questionnaires to determine the PMV (Nygård-Ferguson & Scartezzini, 1989b, 1992). Although the optimal stochastic control performed better than conventional control strategies, overheating was reported.

2.2.4 Recent Developments in Model-Based Predictive Control

In recent years, model-based predictive control has received significant attention and is gradually becoming more “mainstream” (Cooperman *et al.*, 2010). Florita and Henze (2009) compared different models for weather forecasting (as opposed to using online weather forecasts) for predictive control. The authors point out that forecasts produced by meteorological institutions and companies may not provide the information required (hourly or sub-hourly forecasts of solar radiation), are subject to service interruption (e.g., communication failure), and may not be available for the specific location. Local forecasting has the advantage of enabling the creation of data-driven models, based on on-site measurements of weather variables and determination of trends. Florita and Henze conclude that although more complex models (typically, neural-network based) have been applied, the performance of simpler time series methods (e.g., simple prior moving average) is often satisfactory.

May-Ostendorp *et al.* (2011) have recently looked at the utilization of model predictive control of window operation in commercial buildings, with the purpose of extracting rules which may be easily computed and implemented in commercial buildings.

The *OptiControl* project, carried out in Switzerland by several academic institutions, government agencies and industrial partners, has produced interesting developments in the area of model predictive control (Gyalistras & OptiControlTeam, 2010). This team has looked at the utilization of thermally activated building systems (TABS) for energy storage (Gwerder *et al.*, 2008; Gwerder *et al.*, 2009; Tödli *et al.*, 2009), the development of advanced control algorithms for peak load reduction and climate control (Oldewurtel *et al.*, 2010a; Oldewurtel *et al.*, 2010b), and the improvement of weather forecasts for the purpose of building control (Stauch *et al.*, 2010).

The relevance of model complexity has become a common theme model predictive control research, both for building simulation and weather forecasting. Selecting the right level of modeling resolution is no easy task. For example, in page 7 of the final report of the *OptiControl* project, it is stated:

“In the selection of the computer modelling approach we had to balance the conflicting requirements arising from the needs for sufficient process detail, good modelling accuracy, and a high temporal resolution (≤ 1 hour) on the one hand, and for minimizing the input data needs, and maximizing the simplicity, robustness, and computational efficiency of the model on the other hand.. The chosen solution was a 12th order[†] bilinear thermal Resistance-Capacitance (RC) network modelling approach that lumps the radiative and convective heat transfer processes.” (see Figure 2.5).

[†] The order of the model is equal to the number of capacitances.

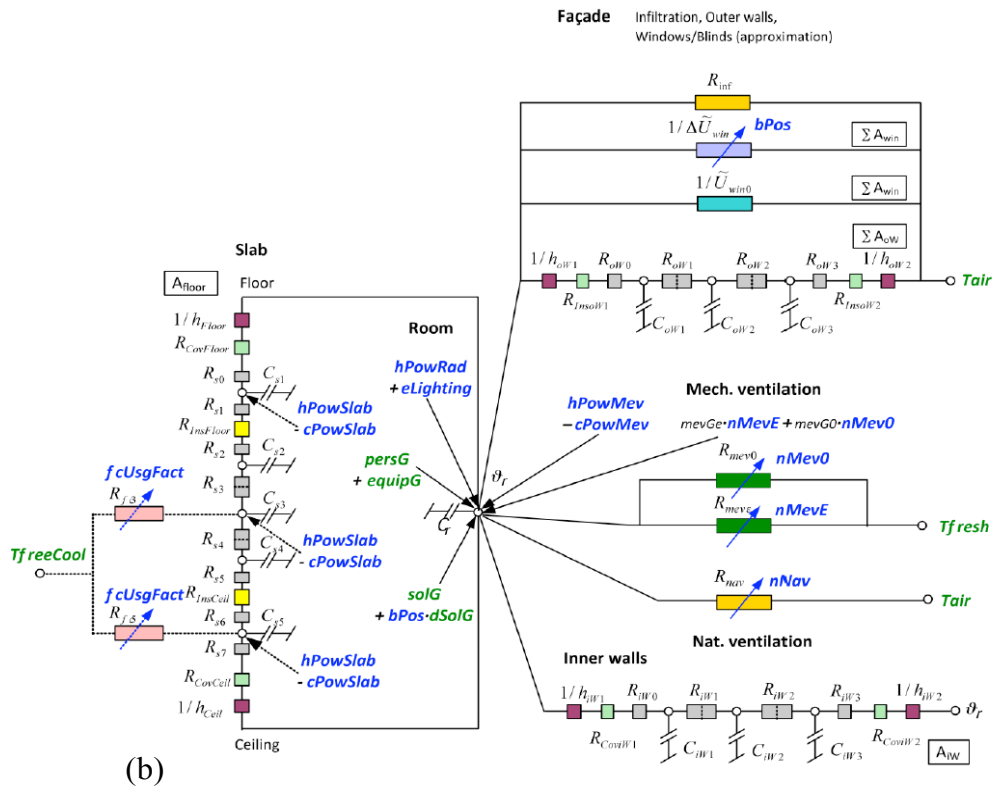
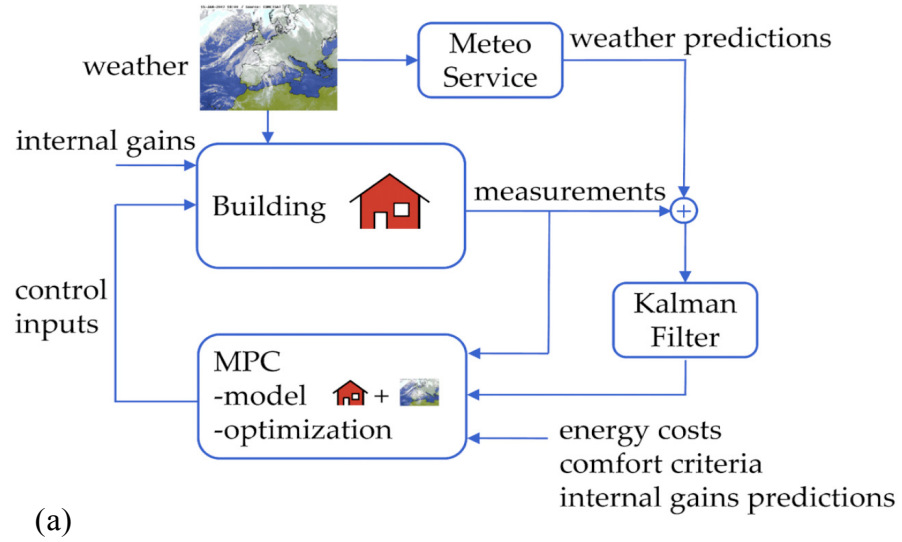


Figure 2.5. Approach of the *OptiControl* project (a). Simplified model (b). Adapted from (Gyalistras & OptiControlTeam, 2010).

It is worth mentioning that the procedure used to select this level of resolution is not described in the report. Apart from the work carried out by the *OptiControl* group and

other researchers of the ETH Zürich [e.g. (Bianchi, 2006)], several research groups around the world are currently working on Model Predictive Control. They include:

- The University of Colorado at Boulder and collaborators (Henze *et al.*, 2005; Zhou *et al.*, 2005; Henze *et al.*, 2007; Liu & Henze, 2007; Florita & Henze, 2009; Henze *et al.*, 2010; Morgan & Krarti, 2010; May-Ostendorp *et al.*, 2011). This group has focused on optimal control strategies for the control of passive and active thermal energy storage (in particular, for cooling) in commercial buildings.
- Purdue University (Braun, 2003; Lee & Braun, 2004, 2006; Braun, 2007b; Lee *et al.*, 2007; Lee & Braun, 2008b, a) in collaboration with LBNL, the Lawrence Berkeley National Laboratories (Xu *et al.*, 2004; Xu *et al.*, 2006). This group, which includes some of the pioneers in the field, has been looking into the application of optimal control for reducing peak demand in commercial buildings.
- Borrelli and collaborators at the University of California at Berkeley (with some links to the LBNL), while working on control theory and applications in other fields (vehicle dynamic controls), have also examined MPC in buildings (Borrelli *et al.*, 2006; Ma *et al.*, 2009; Coffey *et al.*, 2010; Ma *et al.*, 2010).
- Several French institutions (Dumur *et al.*, 1997a, b; Déqué *et al.*, 2000; Fraisse *et al.*, 2002; Morosan *et al.*, 2010a, b) have worked on predictive control, including distributed predictive control of multizone buildings.

- Kummert and collaborators in Belgium and Canada (Kummert *et al.*, 2001; Kummert & André, 2005; Kummert *et al.*, 2006) have worked on the specific case of solar buildings.
- The Catholic University of Paraná and other Brazilian researchers (Freire *et al.*, 2005; Bauchspiess *et al.*, 2006; Donaisky *et al.*, 2007; Freire *et al.*, 2008b; Freire *et al.*, 2008a; Vieira *et al.*, 2008; Reginato *et al.*, 2009) have studied predictive control based on system identification strategies.
- A group in the Czech Republic has recently been active on system identification based on statistical tools and model predictive control (Ferkl & Siroký, 2010; Ferkl *et al.*, 2010; Siroký *et al.*, 2010; Prívvara *et al.*, 2011; Siroký *et al.*, 2011).
- In Austria, Mahdavi and collaborators have studied the utilization of a room model to adjust the position of blinds and the state of luminaires based on occupancy and outdoor daylight level (Mahdavi, 2008; Mahdavi *et al.*, 2009). Although this is “model-based” control, it is not exactly “predictive”, as it deals with lighting phenomena, which do not have lag effects. Mahdavi has also worked on the more general problem of natural ventilation and in general in the incorporation of simulation into building control (Mahdavi, 2003; Mahdavi & Pröglhöf, 2005; Mahdavi *et al.*, 2009).
- Wang, at the University of Hong Kong, has published a review on supervisory and optimal control of buildings (Wang & Ma, 2008). Chen, from the same institution, has continued work initiated at Concordia University on predictive control of radiant floor heating systems (Chen, 2001, 2002).

- Other groups have also studied predictive control in Denmark (Wittchen *et al.*, 2005), Japan (Nagai, 1999), Sweden (Elizalde, 2008), Spain (Castilla *et al.*, 2010) and the UK (Hudson & Underwood, 1999; Yu & Dexter, 2009).

Despite the emerging interest in the application of MPC for building control applications, MPC research projects specifically devoted to solar homes are still rather limited. Moreover, investigations tend to focus more on the optimization algorithms for the controllers than the implementation in the building. Many papers have been presented or published in specialized conferences or journals for control engineering, with limited exposure to the HVAC and solar engineering research communities.

2.3 Artificial Intelligence Techniques for Building Control

Artificial intelligence (AI) techniques, such as artificial neural networks (ANN), fuzzy logic and genetic algorithms, have been applied to HVAC control since the 1990s (Dounis *et al.*, 1992; Curtiss *et al.*, 1993; Dounis *et al.*, 1995b; Curtiss *et al.*, 1996; Argiriou *et al.*, 2000; Morel *et al.*, 2001; Argiriou *et al.*, 2004; LeBreux *et al.*, 2006; Dounis & Caraiscos, 2009; Moon *et al.*, 2009). ANN have also been used in optimal control (Morel *et al.*, 2001; Massie, 2002).

Dounis and Caraiscos (2009) support the use of AI techniques. Dounis and Caraiscos, who are pioneers in the application of AI techniques (Dounis *et al.*, 1992), mention some disadvantages of model-based control: the obvious need for a model; the sensitivity of parameters to noise during online identification; and nonlinearities when dealing with comfort (PMV as an index rather than temperature). A key point mentioned about optimum and predictive control strategies is that “no industrial development has followed

these scientific studies”. However, as advocates of AI methods, their view on model-based control seems overly pessimistic. As illustrated in the previous section, model-based control remains an active research area.

Although AI techniques are not dependent on a previously found model, the need for a training period represents a serious limitation (Wang & Ma, 2008). As pointed out by Coffey *et al.* (2010), the lack of building physics in ANN means that they are not as useful for diagnostics, and they do not handle changes in conditions well.

Liu and Henze (2007) have also studied the use of “reinforcement learning”, i.e. algorithms that extract information from the operation of the system with an ANN for designing an optimal control strategy online. Instead of using a model, the cost of each control action is learned through the operation of the system. Genetic algorithms have also been used to incorporate occupants’ wishes in an optimal supervisory control strategy (Guillemin, 2003).

Research on multi-agent control systems (MACS), also known as distributed artificial intelligence, has received significant attention during the last decade (Mo & Mahdavi, 2003; Abras *et al.*, 2006; Dounis & Caraiscos, 2009; Wang *et al.*, 2010). Since agents are autonomous control units that sense their environment and react to it while mutually interacting with each other (Vlassis, 2007), they offer several advantages: robustness, flexibility, computational efficiency, scalability and ease of assembly in a hierarchical structure. These features of MACS offer possibilities for the development of community energy systems, while offering a structure that facilitates the integration of classical and modern control techniques. MACS can also be used as a method to include human behaviour (Callaghan *et al.*, 2000).

2.4 Relevant Technologies and Tools for Solar Homes

The field of solar energy engineering is quickly moving in many directions. Since the possibilities of storage and control are highly dependent on available technologies, it is important to keep track of the most recent innovations, where breakthroughs can dramatically change design scenarios. A complete review of the numerous recent technological advances relevant for solar homes is not intended here. Rather, the goal is to provide an overview of the most salient trends in research and development, and to illustrate the possibilities of technologies that are ready to be implemented in Canadian scenarios. Building energy modeling tools are also briefly discussed.

2.4.1 Passive Solar Design

Passive solar design (Anderson, 1990b; Balcomb, 1992; Athienitis & Santamouris, 2002; Haggard *et al.*, 2010) consists of a set of design techniques intended to take advantage of solar heat gains in order to supply a substantial portion of the heating needs of a building. The basic principles have been known since antiquity: Anderson (1990a) cites examples from ancient Egypt, Greece and Rome, including evidence of double-glazed windows in bathing rooms at Herculaneum (near Pompeii). Indian cultures in the American Southwest provided solar exposure to their dwellings (Anderson, 1990a). In spite of the intuitiveness of the concept, passive solar design requires a careful quantitative approach for its successful implementation. The term *passive* indicates that, in general, these methods do not require the intervention of mechanical systems or moving parts.

Passive solar design relies on features such as high levels of thermal insulation in the building envelope, air-tight construction, high-performance windows with an equatorial orientation (towards the South in Northern Hemisphere, and towards the North in Southern Hemisphere). Passive solar design also includes increased levels of thermal mass that can store heat while mitigating temperature fluctuations, properly sized overhangs to prevent solar gains in summer and measures to encourage natural ventilation and passive cooling. Passive solar design not only allows energy consumption and cost reduction; it also significantly improves thermal comfort.

The maximum contribution of passive solar gains to supply heating loads is difficult to quantify, as it is not clear which conditions should be used as a reference. When comparing solar gains to heat loss through the building envelope figures between 30 and 50% have been reported for different Canadian cities (CMHC, 2006c). As pointed out in (CMHC, 2006c), passive solar design is particularly suited for Canada's cold and sunny winters.

Overheating is a common problem found in poor passive solar design (CMHC, 2006c). In Canada, where wood-frame construction is traditional, thermal mass can play a significant role in preventing this problem. Other measures, such as set-point adjustment and air circulation to distribute the heat in the space, are also advisable.

2.4.2 BIPV and BIPV/T Systems

Photovoltaic generation provides the most practical way to generate electricity at a building scale when compared, for instance, with wind generators or CHP systems. When PV panels are integrated seamlessly into the building envelope, they are called "building

integrated photovoltaic” (BIPV) systems. This approach can reduce total cost since the PV panels are a working element of the building envelope, which replaces cladding or shingles, therefore even contributing to improving the aesthetics of the building. Most residential photovoltaic systems are “grid-connected” (Ayoub *et al.*, 2001). This approach provides a backup for the user of a BIPV system, obviating the need for a battery system or any other storage device. Photovoltaic generation can be used to offset the consumption of appliances and lighting. In 2001, a typical detached Canadian house consumed about 8720 kWh of electricity per year for lighting and appliances. Interestingly, even in the early 1990s, it was possible to reduce this figure to about 4,300 kWh by using energy-efficient appliances and lighting systems (Ayoub *et al.*, 2001). A quick calculation shows that this corresponds to the energy generated by a 3.5-4.0 kW_e PV system in Montréal.

When a BIPV installation has the additional goal of recovering heat, it is called a “building integrated photovoltaic/thermal” (BIPV/T) system. Research projects at Concordia University have studied the properties of BIPV/T systems by using air as the heat recovery fluid (Charron & Athienitis, 2006; Liao *et al.*, 2007; Candanedo (L.) *et al.*, 2010a). BIPV/T systems remain an important research area at the Concordia Solar Laboratory. Given their importance for the case study investigated in this thesis, details of the modeling of BIPV/T systems are presented in Chapter 4.

Two types of PV cells are commonly manufactured today: crystalline silicon (either single-crystal or polycrystalline) and thin-film panels. Crystalline panels are currently the dominant technology, but it is expected the thin-film technology will have a more important share of the market in the future (Hoffmann, 2006). Although the main

obstacle for BIPV systems remains their elevated cost, there is a continuous trend towards lower prices. Hoffmann (2006) indicates that a price of 1 € per W_p will be reached in the 2020s. As of May 2011, the price of PV is reported to be \$3.12 per W_p in the US and about €2.73/ W_p in Europe. Although for several years the price of PV remained steady, there is a clear downward trend (Figure 2.6).

Hoffmann also distinguishes between the advantages offered by bulk power generation and peak power. He projects that PV generation will be competitive with peak power utility rates by 2020 in Central Europe and before that date in Southern Europe. Competitiveness with bulk power prices should be attained by 2030.

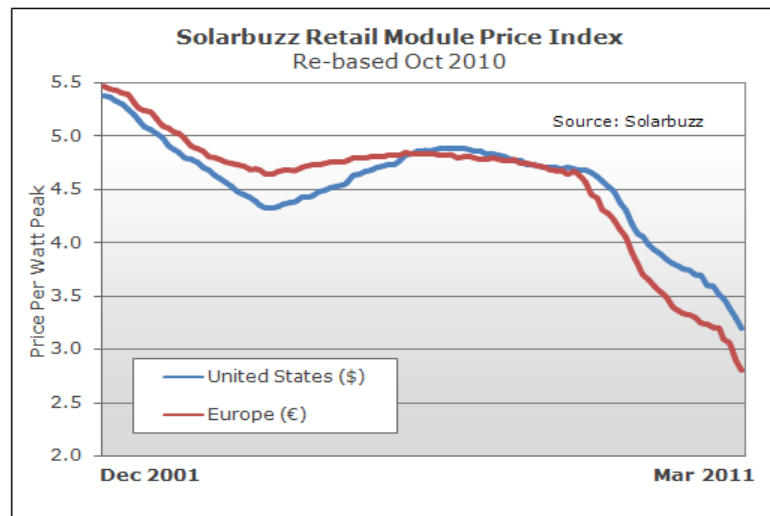


Figure 2.6. Progression of PV price over the last decade (Solarbuzz, 2011).

Rowlands (University of Waterloo) has been working on the potential impact of TOU rates and other incentive measures to encourage the installation of PV systems in Canadian buildings (Rowlands *et al.*, 2004; Rowlands, 2005b, a). Rowlands has observed that the period of maximum availability of solar energy coincides with the time of peak

load in the electrical distribution grid for several Canadian locations, and therefore, widespread installation of PV modules could reduce peak electricity loads.

2.4.3 Solar Thermal Collectors

Perhaps the most commonly used collectors for the solar heating of DHW are the glazed flat-plate solar collector and the vacuum tube solar collector. For the theory of operation of flat plate solar thermal collectors, the text by Duffie and Beckman (2006) is an excellent reference. These collectors consist simply of a plate designed to absorb solar radiation (the “absorber plate”), typically covered by glazing, on top of a piping system in which a circulating fluid (water or water-glycol mixture) removes the heat from the absorber plate. A circulating pump, together with a storage tank, completes the system. The circulating pump may be eliminated by placing the storage tank above the collector and relying on the thermosyphon effect.

In a vacuum tube solar collector, a specially designed heat pipe is encapsulated within a glass tube in which a vacuum has been made to reduce heat losses to the exterior. The heat pipe collects the heat and delivers it to a fluid circulating around a metal tip (the condenser of the heat pipe) inserted within a header or manifold.

Figure 2.7, obtained from a manufacturer’s website, displays typical curves for solar collectors. Efficiency, the fraction of energy recovered from solar radiation, is usually plotted versus the ratio of the temperature difference between the fluid’s temperature and the ambient temperature divided by solar irradiance. The curves are approximately linear. Although the y-axis intercept may vary, flat plate collectors tend to perform better at high solar radiation and smaller temperature differences (i.e., towards the left of the graph);

however, their performance drops rapidly when these conditions change. Because of their low heat losses, vacuum tube solar collectors have excellent performance in cold winter conditions; they can also operate at higher water temperatures than flat-plate collectors (50-95 °C versus 30-70 °C) (NRCan, 2006). Evacuated tube collectors are, however, typically more expensive than flat-plate collectors (NRCan, 2006).

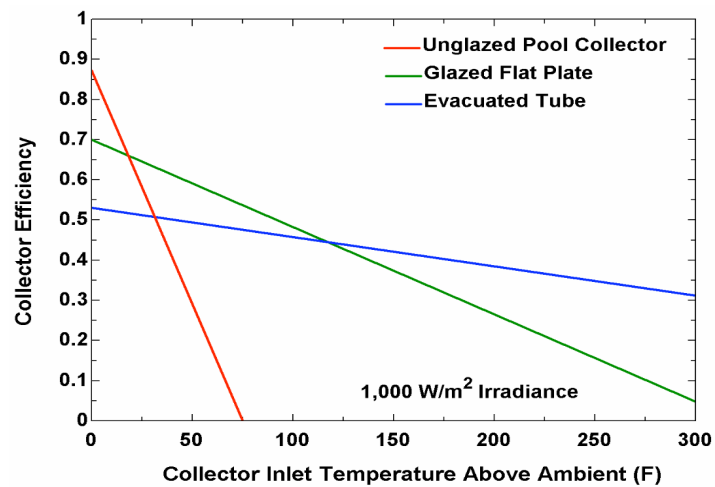


Figure 2.7. Comparison of the performance of different kinds of solar collectors (SunEarth Inc., 2005).

Work remains to be done to encourage the use of solar thermal collectors in Canada. As seen in Table 2.1, in 2000 Canada had comparatively few solar collectors (this situation remains largely unchanged). With only 2.5 times the population of Canada, Germany had in the year 2000, nearly 33 times the area of glazed flat-plate collectors, and nearly 800 times the area of evacuated tube collectors. However, the most densely populated areas in Canada receive more solar radiation than Germany. There is a significant potential for the growth of the solar thermal collector market in Canada.

Table 2.1. Installed area (m²) of several types of solar collectors in some IEA member countries in 2000 (Weiss & Faninger, 2002).

Country	Unglazed flat-plate	Glazed flat-plate	Evacuated tube
Canada	493,000	72,000	509
Germany	615,000	2,399,000	392,000
Japan	N/A	11,445,008	307,481

2.4.4 Heat Pumps

The principles of heat pump operation is described in any basic thermodynamics text (Karlekar, 1983). Air-source and ground-source heat pumps are the most common for heating applications. NRCan presents a brief overview of heat pump technologies for the Canadian climate (NRCan, 2005a).

The coefficient of performance (COP, the ratio of heat delivered to electricity consumed) of air-source heat pumps for heating applications ranges can be as high as 3.3. Air-source heat pumps are typically restricted to a minimum exterior temperature of (-15 °C); below which their COP drops below 1.0 (NRCan, 2005a).

An article by Spitler (2005) reviews the state of research on ground source heat pumps; in Canada, Bernier and collaborators have carried out investigations in this area (Bernier, 2001; Kummert & Bernier, 2008). Because the temperature of their source remains relatively stable, ground source heat pumps are quickly gaining popularity as a technology to supply the heating needs of Canadian homes.

A promising new development is the introduction of heat pumps with CO₂ as the refrigerant (Stene, 2005). Not only CO₂ has a smaller global warming potential than conventional refrigerants; it also works with sources at temperatures as low as -20 °C.

The integration of heat pumps with solar installations is receiving increasing attention (Citherlet *et al.*, 2008). For example, heat pumps are also being introduced to recover heat from hot air coming from BIPV/T installations (see Chapter 4) (Candanedo & Athienitis, 2008b), and in general to recover heat from roofs (Puren, 2007). The high temperature of the source allows very high COPs (> 5) to be obtained.

2.4.5 Thermal Energy Storage

Energy storage systems are essential for solar-optimized buildings, not only because of the obvious extension of energy availability, but also because they can be used to take advantage of changing electric utility rates.

Reviews of currently available thermal energy storage (TES) technologies have been presented by Dincer (2002), Nielsen (2003) and Bales *et al.* (2005). The latter presented the findings of Task 32 of the International Energy Agency (IEA), dedicated to advanced storage systems in single-family houses, with the purpose of obtaining a high solar fraction (i.e., fraction of thermal energy provided by the sun), focusing on latitudes of 45° (coincidentally, the latitude of Montréal). IEA's research has been focused on three types of active thermal storage systems: water-based, phase change materials (PCM) and thermochemical systems. This classification roughly coincides with the one presented by Dincer (2002) who mentions three storage methods: sensible heat storage (by changing the temperature of a medium like water or rock), latent heat storage (PCM materials, icewater storage), and chemical systems.

2.4.5.1 Sensible heat storage

Water is a popular storage medium for solar applications because of its availability and high specific heat. Although the energy storage density of water systems is not as high as PCMs or thermochemical systems, the obvious advantages of these systems are their simplicity, low cost and experience with their use (Bales *et al.*, 2005). Thermal stratification helps to improve the performance of a water storage tank, as hot water from the top can be used to supply heat to the space, or as the source of domestic hot water (DHW); colder water from the bottom can be used to obtain heat from any primary heat source. Technologies exist to enhance thermal stratification and delay the onset of thermal equilibrium in the tank. For example, baffles are installed in the tank as obstacles to natural convection (Kulacki *et al.*, 2007) and perforated pipes or special manifolds are used to reduce the speed of the water entering or leaving the tank, thus avoiding mixing the water in the tank (Duffie & Beckman, 2006). Multiple-tank configurations, with tanks at different temperatures, can also be employed (Cruickshank & Harrison, 2006).

A limitation of water is the fact that it can only store heat below 100 °C at atmospheric pressure. Above this temperature, pressure vessels are needed, a fact which considerably increases the price of the system (Dincer, 2002), and represents a safety issue. Heat resistant oils can store heat in a wide range of temperatures from -20 °C to +320 °C, but their specific heat is only about half that of water. Molten salts and molten metals are also used to store heat at high temperatures (Dincer, 2002).

Rocks have also been used for thermal storage (Dincer, 2002). They occupy more space per unit energy than water, but they are easy to implement. Dincer (2002) points

out that combining water with air/rock thermal storage has become practically a standard TES system for solar applications.

2.4.5.2 Latent heat storage

Ice storage systems are a mature technology to store cooling power (Dincer, 2002). They require a chiller for ice making and a piping distribution system. The chiller can be the same that provides direct cooling to the space, or a different one. In general, ice storage systems represent savings because of the use of electricity in off-peak hours and the reduction of initial cost due to a smaller system, but as discussed by Henze *et al.* (1995), these advantages depend on the operation strategy. Dincer (2002) discusses two basic schemes: (a) full storage TES, providing all the cooling needs during on-peak hours; and (b) partial storage TES, aiming to reduce only the peak load (this is the preferred system when the peak load are much higher than the average load).

PCMs are specifically designed to undergo a phase change (generally liquid-solid, but also solid-solid) at a given temperature, the “Phase Change Temperature” (PCT) (Bales *et al.*, 2005). Typical PCM materials are paraffins, fatty acids, or inorganic salt hydrates. By keeping them in a vessel, PCMs can be used as a backup for the thermal storage system. PCMs can also be incorporated into the building envelope, contributing to the passive storage of the building’s structure. According to Bales *et al.* (2005), typical PCTs are: 5-18 °C for cold storage, 22 °C for building envelope integration, and 60 °C for hot storage.

2.4.5.3 Thermochemical storage

Sorption can be defined as “the process in which one substance takes up or holds another (by either absorption or adsorption)” (WordNet, 2008). In a thermochemical

storage system, heat from a solar collector or other source is supplied to separate a sorbate –the sorbed substance– from a sorbent –the material that contains it (Bales *et al.*, 2005; Jähnig *et al.*, 2006). This process, called the desorption stage, requires energy and is therefore endothermic. The sorbate and sorbent can then be stored in separate vessels for as long as required. When the heat is needed, the substances can be combined, triggering the exothermic sorption stage, which releases energy. Most of the work of Task 32 has focused on systems using water as the sorbate, or operating substance.

Thermochemical systems have the advantage of providing a high density of energy storage. Nielsen (2003) gives the figure of 1 MWh/m³. In comparison, 1 m³ of water can store roughly 58 kWh of heat within a 50 K temperature range.

Figure 2.8, borrowed from a recent presentation by Hauer (2010), compares the energy storage capacity of thermochemical (TCM) systems, PCMs and water. Evidently, there is significant potential in thermochemical storage. However, engineering solutions including TCM are still needed, due to the complexities of the technology required.

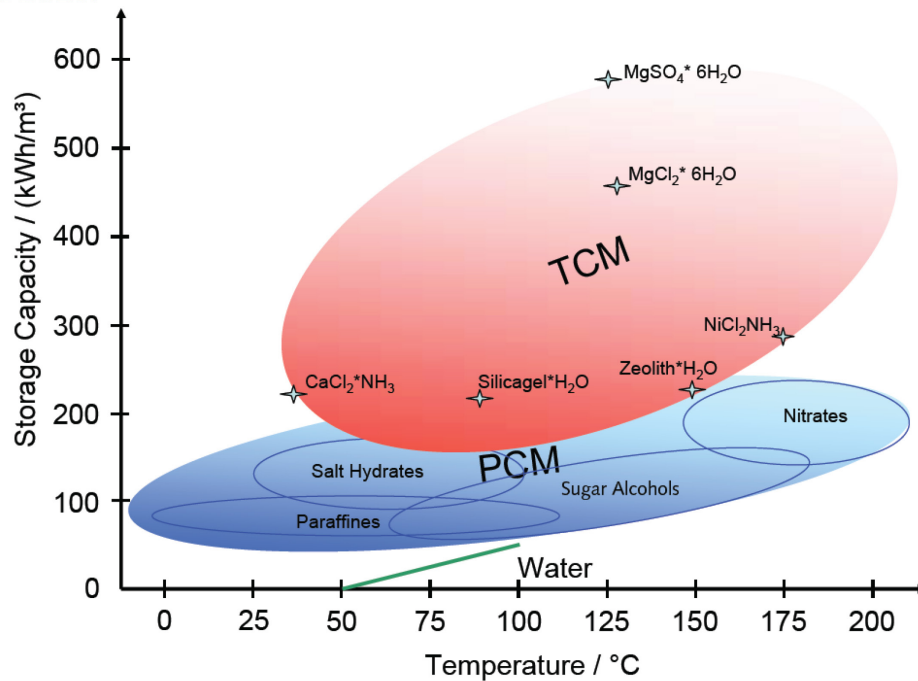


Figure 2.8. Comparison of different TES systems (Hauer, 2010).

2.4.6 Advanced Fenestration

2.4.6.1 High insulation windows

Technological developments have allowed the increase of the insulation value (R-value) of windows, which is often much lower than the insulation value of walls. Windows have been described as the “weak spot” of the building envelope (Hutcheon & Handegord, 1983). According to Arasteh *et al.* (2006), windows account for 30% of the heating and cooling energy in buildings in the US, and despite recent significant advances “[windows] are still significant energy liabilities”. The window-to-wall ratio (WWR) has always been an important parameter in the design of a building. Choosing an appropriate

WWR value usually implies a trade-off between increasing solar heat gains and daylighting and avoiding heat losses from the heated space.

In cold climates, two panes of glass have been traditionally used in windows to increase their total insulating value. The air gap between the window panes acts as an additional layer of insulation. Beyond a gap thickness of about 13 mm the R-value (i.e., thermal insulation) of the window does not change, since the most important heat transfer phenomenon is radiation between the two glazings (Athienitis & Santamouris, 2002). Frames made of conductive material such as aluminum can act as “thermal bridges”, with thermal resistance values even lower than the window glazing. Advances have been made in the framing system to include insulating materials to “break” the thermal bridge (Hutcheon & Handegord, 1983). Thermal bridges can also favour the appearance of condensation, which can have serious detrimental effects on the building enclosure (Hutcheon & Handegord, 1983). The addition of a third pane of glass, to create “triple-glazed windows” has further increased the R-value of windows.

Low emissivity coatings improve the R-value dramatically by reducing long wave radiation heat transfer between window panes. They have become quite popular since the 1980s, since replacing conventional windows with low-e windows is one of the easiest and cheapest ways to improve the energy performance of a building. In 2005, these windows represented about 50% of the US window market share, and their savings since their implementation have been estimated as \$US 37 billion (Arasteh *et al.*, 2006).

It is considered that U (conductance) values of $0.1 \text{ BTU}/(\text{ft}^2 \cdot \text{hr} \cdot ^\circ\text{F})$, which corresponds to R-10, are within reach (Arasteh *et al.*, 2006). Arasteh *et al.* indicate three promising areas of research: (a) **aerogels** which are silica-based porous coating materials,

currently in the research stage, that trap air and increase the insulating value while letting light through (Apte *et al.*, 2003); (b) **vacuum glazings**, already available in Japan, which try to completely eliminate convection and conduction heat losses, currently reach U values of 0.2 BTU/(ft²·hr·°F); and (c) **gas-filled low-e windows**, which use three or more glazings, low emissivity coatings and cavities filled with argon.

Low-e coatings also affect the SHGC (solar heat gain coefficient), the fraction of solar heat that ultimately reaches the living space. Whereas a low SHGC can be beneficial in cooling-dominated regions, it can have a detrimental effect in cold climates, where heat gains are desirable in winter. Although low-e windows with high SHGC are being developed (Apte *et al.*, 2003), the trade-off is not easy to determine, as in summer it is still convenient to reduce solar heat gains.

2.4.6.2 Switchable glazing and “smart windows”

Several new technologies, at different stages of research and development, offer the possibility of adjusting the impact of fenestration on heating loads, cooling loads and daylighting in a building. For example, it might be convenient to increase the opacity of a window during the summer months in order to reduce the cooling load, and increase their transmittance during winter to increase solar heat gains. Some of these new technologies are briefly presented below:

- **Electrochromic (EC) windows.** This technology takes advantage of chemical reactions, triggered by the sudden application of a voltage, to change the opacity of a material. Electrochromic windows, usually formed by several

layers, can vary their transmittance over a wide range, between a few and 70 percent (Apte *et al.*, 2003).

- **Thermochromic windows.** These windows change their optical properties as a function of temperature. Thermochromism is a well-known phenomenon that is used in a wide range of applications (Fraunhofer IAP, 2008). The main disadvantage of thermochromic windows is that they are not as easily controllable as electrochromic windows.
- **Photochromic windows.** Photochromic windows change colour when exposed to bright lights (CEC, 2006). Their main application could be glare prevention. They may not be the best technology for cold climates, as they can limit solar heat gains, especially in winter.
- **Gasochromic windows.** A gasochromic window has a layer of an active film (WO_3) which reacts when extremely dilute hydrogen fills the cavity, changing the colour and transparency of the window (Georg *et al.*, 1998; Wilson *et al.*, 2002). This change can be reverted by filling the cavity with dilute oxygen. Their switching speed can be faster than that of electrochromic windows (Carmody, 2003).
- **Other technologies.** Windows using polymer dispersed liquid crystals (PDLC), the technology used in LCD screens, have been considered for modifying properties of window glazings (Bonsor, 2001; Richardson *et al.*, 2001). This technology offers privacy by scattering light, but there is no control of solar heat gains. Suspended particle devices (SPDs) were created as a commercial product by Research Frontiers, Inc. (Bonsor, 2001; Research

Frontiers, 2010), although other companies are developing the idea (SPD Control Systems, 2006) based on principles discovered nearly a hundred years ago: millions of particles in a liquid suspension block the light when in random distribution (Bonsor, 2001). When a voltage is applied, they become aligned, consequently allowing the light to pass through.

2.4.6.3 Controllable motorized blinds and control algorithms

Although blinds, curtains and shades have been used for centuries to adjust the passage of light through windows, it is only in the last decades that they have been used as automated “control actuators” of solar heat gains and daylighting. Taking into account the architectural trend towards buildings with large glazing areas (Bessoudo, 2008), these devices will play an increasing role in building energy management.

The inherent complexity of the physical heat transfer phenomena and their effects on thermal comfort makes controlling the position of blinds, curtains or shades a difficult task. However, automatic control of these devices is a necessity.

The published literature in the field of blind controls is vast. Some of the relevant recent investigations have been carried out at the Concordia Solar Laboratory (Park & Athienitis, 2003; Tzempelikos & Athienitis, 2003; Tzempelikos, 2005; Tzempelikos & Athienitis, 2005). The potential of controllable blinds for reducing electricity load and energy consumption in buildings has been underscored (see Figure 2.9).

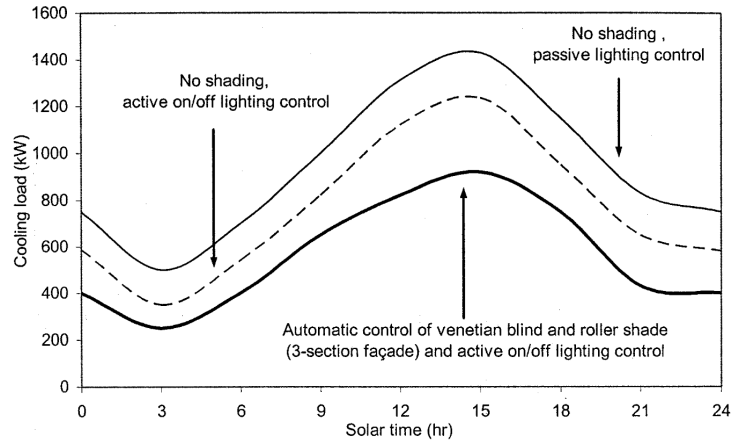


Figure 2.9. Cooling load curves for a hot summer day under different control conditions of lighting, as well as venetian and roller blind control (Tzempelikos, 2005).

Controlling solar heat gains and internal temperature in a house by adjusting the position of roller blinds according to an algorithm working with weather forecasts has been explored at the Concordia Solar Laboratory (Candanedo *et al.*, 2007a). A detailed discussion about these investigations is presented in Chapter 5. Studies on the control of venetian blinds have been carried out by Park and Athienitis (2003), Kuhn (2006), O'Neill & Athienitis (2007) and O'Neill (2008).

2.4.7 Technology Trends in Building Controls

Wireless technologies, such as ZigBee™ (Egan, 2005; Duan & Li, 2008) are becoming more widely available. Although wireless sensors are still relatively costly, the savings in terms of wiring and installation costs are turning them into an interesting alternative for retrofit projects. Some wireless devices are able to harvest different kinds of energy (electromagnetic waves, solar, thermal and vibration). Moreover, the implementation of wireless devices converges with the trend towards distributed control architecture, in which smaller, low-cost processing devices are closer to sensors. Control

system installations are shifting from centralized to de-centralized (Braun, 2007a; Guo & Zhou, 2009). This development contributes to their robustness and flexibility.

In recent years, efforts have been made towards the creation of open-source network protocols expected to ease the design of integrated HVAC solutions, such as BACNet™ (Bushby, 1997; Holmberg & Bushby, 2009) and LonWorks (Echelon, 2009) in North America, and KNX/EIB in Europe (KNX, 2011). These protocols have opened the doors for the participation of more control companies in the HVAC market (Braun, 2007a).

The emergence of embedded intelligence in devices promises to supply valuable information for building operators, maintenance crews and even building occupants (Braun, 2007a). It will be possible to obtain information not only from the central control system, but also from individual components (air-handling units, fans, heat exchangers, etc.). This information will most likely include documentation of the device, and it may also include performance maps that could provide accurate estimates of power consumption, flow rates, temperatures and other variables, working as “virtual sensors” (Braun, 2007a).

Web and mobile (e.g., iPhone™) interfaces (Negron & Hayes, 2009) and energy dashboards (Fehrenbacher, 2009) are bringing home automation closer to reality. By facilitating the exchange of information with the occupants, these devices are expected to have a significant impact on user behaviour (Agarwal *et al.*, 2009; Bartram *et al.*, 2010), by allowing the occupants to change their consumption habits based on relevant information.

2.4.8 Building Simulation Methodologies and Tools

Software tools, based on some of the concepts discussed above, are often used to calculate the energy performance of buildings. These calculation engines can be focused on components, systems, zones, or the entire building. The website of the US Department of Energy presents an exhaustive list of building simulation tools (DOE, 2007), along with comments on their strengths and weaknesses, number of users, cost, audience and so on. An inter-institutional report by Crawley *et al.* (2005) also presents a description of the features of several popular software packages.

Building simulation software packages are numerous. The selection of a program depends on several factors: the objective (building design, research, design of control systems, consultancy, verification of code-compliance), level of detail required, and of course, cost. It is important to bear in mind that notwithstanding the level of sophistication of the tool, code development takes time, and it will always lag somewhat behind the most recent technological advances. A few of the most relevant programs used in Canada are listed below:

ESP-r is a tool originally created at the University of Strathclyde in Scotland about 30 years ago (ESP-r, 2010). It is one of the most popular and powerful tools for researchers in building engineering. A vast community of users makes continuous contributions to ESP-r. It has detailed models for building heat transfer, HVAC systems, climate analysis, air movement, shading-insolation analysis and view factor calculations. ESP-r heat transfer analysis is based on a control volume finite difference scheme. Developed to run in UNIX operating systems, ESP-r is distributed free of charge with a GPL (general public license). A common complaint is ESP-r's lack of user-friendliness: as stated in

(DOE, 2007): “*It is a general purpose tool and the extent of the options and level of detail slows the learning process. Specialist features require knowledge of the particular subject. Although robust and used for consulting by some groups, ESP-r still shows its research roots.*” Even on the ESP-r website (ESP-r_Overview, 2008), it is stated that “*ESP-r is much better learned via interactions with a mentor than by self-instruction*”. Although it might not be the most practical program for a back-of-the-envelope calculation, ESP-r remains one of the leading computational tools in the field.

TRNSYS (Beckman *et al.*, 1994) was developed at the University of Wisconsin-Madison, for the dynamic simulation of solar energy systems. TRNSYS (“transient systems”) employs the response factor method to calculate conduction through building walls. TRNSYS components can be connected in a visual and intuitive way within an environment called the Building Simulation Studio, exchanging inputs and outputs. TRNSYS modules or “Types” include common HVAC and building components, as well as many solar engineering modules such as photovoltaic panels, thermal collectors and heat pumps (Crawley *et al.*, 2005). Another advantage of TRNSYS is that it easily interacts with other calculation software running in the Windows environment (e.g., MATLAB, Excel). On the downside, TRNSYS is not intended specifically for building modeling, and it is a relatively costly software package.

EnergyPlus was created by the US Department of Energy (DOE) in the late ‘90s (Crawley *et al.*, 2001; EnergyPlus, 2010). EnergyPlus, which incorporates features of older programs (such as BLAST and DOE-2, both developed by the DOE), employs by default the response factor method. A more recent version enables the alternative use of the finite difference method for calculating heat conduction through walls. EnergyPlus is

a well-documented tool. It is easy to find which mathematical model is used for a calculation. EnergyPlus input files (IDFs) can be easily modified with the IDF Editor. The data analysis of EnergyPlus output files is relatively straightforward. OpenStudio (NREL, 2009), a plug-in developed by NREL, enables the use of a drawing tool (Google SketchUp) to create the geometry of a building. With this approach, a basic estimate of the heating and cooling needs of a house can be made in minutes. However, the lack of a graphical user interface (GUI), especially for the configuration of an HVAC system, is still one of the shortcomings of EnergyPlus, although several other third party tools (e.g., CYPE-Building Services, DesignBuilder, EFEN and EPlusInterface among others) use EnergyPlus as their working engine (EERE, 2010).

A recent development in building energy modeling is the utilization of Modelica, an object-oriented equation-based language (Wetter, 2009). Wetter points out the shortcomings of traditional building simulation programs (such as ESP-r or EnergyPlus), which are written with imperative languages, such as C++ or FORTRAN. In imperative languages, variables are assigned values calculated with a mathematical expression. The variables needed are calculated sequentially, through a procedure designed beforehand by the programmer. This approach has severe limitations. As stated by Wetter “*the lack of separation between models, data and solvers makes it hard to integrate models from different disciplines for co-simulation...*” This rigidity is a hurdle for testing advanced control strategies. In contrast, Wetter argues that by using Modelica, a declarative language in which equations can be stated without necessarily assigning values, it is easier to mimic the structure of a typical HVAC installation, which should enable rapid prototyping, model reutilization and integration, and test alternative control

strategies. Based on this approach, a promising development is the creation of the “Building Controls Virtual Test Bed” (BCVTB) (Wetter & Haves, 2008), a software tool that brings together the capabilities of EnergyPlus, Modelica, MATLAB/Simulink and Radiance. BCVTB is expected to facilitate the implementation in BACNet of the control strategies developed.

In a similar line of research, Åkesson has developed “Optimica”, a module in Modelica for solving optimization problems (Åkesson, 2007; Åkesson *et al.*, 2009).

2.4.8.1 Tools used in Canada for specific purposes

In Canada, some tools have been developed for specific objectives, such as feasibility studies, early stage design of renewable systems, and daylight modeling, among others.

They include:

- **EE4-CBIP:** This tool was developed by NRCan (EE4, 2008) to verify the compliance of buildings with the Commercial Building Incentive Program (CBIP) by comparing the simulation results with the Model National Energy Code of Canada for Buildings (NRC, 1997). EE4 uses the former flagship software package of the US Department of Energy, DOE-2, as its calculation engine.
- **HOT2000:** Created by NRCan as a design tool for the house building industry, HOT2000 (HOT2000, 2003) employs the bin method[‡] for calculating energy consumption. HOT2000 allows the user to select between four levels of thermal mass: “light, wood frame”, “medium, wood frame”, “heavy, masonry” and “very

[‡] The bin method uses historical data of the occurrence of a set of given weather conditions (usually temperature). The instantaneous heating or cooling load is estimated for each temperature, and the result is multiplied by the time of occurrence.

heavy, concrete”, and correction factors are then used in the simulations. HOT2000 was the required tool in the recent EQUilibrium Housing Initiative (CMHC, 2008). An improved version of this tool, HOT3000 (HOT3000, 2008), is expected to be released during 2011. HOT3000 will incorporate more renewable energy technologies and will perform dynamic simulations using ESP-r as its engine.

- **RETScreen:** Perhaps the best known Canadian software tool used for planning renewable energy projects, RETScreen (RETScreen, 2008) is a useful tool for the sizing and feasibility studies of solar systems, including photovoltaic installations, solar thermal collectors and transpired solar collectors, among similar systems. User friendly (based on Microsoft Excel macros), it is available at no charge in 26 languages, contains an extensive database of weather data and equipment and performs financial analysis. A new version (RETScreen 4) has recently been released.
- **Daysim:** This tool has been designed through a collaboration between the Institute for Research in Construction (IRC), which is a subdivision of the Canadian National Research Council (NRC), and the Fraunhofer Institute for Solar Energy Systems in Germany (Reinhart, 2006). This program, also available free of charge, is used for daylighting design by using Radiance as its calculation engine.

2.4.9 Advanced Solar Homes in Canada: a Brief Overview

In Canada, the construction of the project called *La Macaza Solar House* began in 1975, led by a team from the McGill School of Architecture. Concordia University,

through its Centre for Building Studies, performed monitoring of this house in the late 1970s (Yager, 1980). More recently, Gerbasi (2000) investigated the energy performance of the NOVTEC Advanced House. During the year of monitoring reported in this study, this 220 m² house consumed slightly more than 13,200 kWh, which is about 40% less than the energy consumed by a house complying with the R-2000 standard.

Since 2002, the U.S. Department of Energy (DOE) has organized the “Solar Decathlon” (DOE, 2011), a student competition intended to showcase the application of advanced solar technologies to residential building construction. In this competition — organized in 2002, 2005, 2007, 2009 and 2011— twenty teams from different American and international universities present their house projects at the Washington Mall during several days, in which they present their projects to the general public while maintaining prescribed thermal comfort conditions and generating enough power to supply predetermined loads. The name “decathlon” refers to the ten categories used to evaluate the buildings (architecture, market appeal, engineering, communications, affordability, comfort, hot water, appliances, home entertainment and energy balance). The first Canadian entry, *Northern Light*, was built for the 2005 event by a team from Concordia University (Pasini, 2006). This house featured a 7-kW BIPV/T system, advanced lighting controls, a battery system intended for energy autonomy, power for an electric vehicle, and several passive solar design features (other details shown in Section 5.2). This house, which came 14th in the overall scoring (out of 20 teams), won a special award for the integration of the PV panels in its roof (Pasini, 2006).

The last two Solar Decathlon events have also featured Canadian projects. In 2007 a project was presented by *Team Montréal* (Université de Montréal, McGill University,

École de Technologie Supérieure), in which Concordia University played a consulting role. This house (final standing, 8th place) is now permanently in display at Jean Drapeau park in Montréal near the Biosphere Museum. In 2009, there were two Canadian entries: *Team Ontario* (University of Waterloo, Ryerson University and Simon Fraser University), which came in 4th place, closely followed by *Team Alberta* (University of Calgary), in 6th place.

In 2006, Canada Mortgage and Housing Corporation organized the *Equilibrium Housing Initiative*, intended to showcase readily available state-of-the-art technologies for housing. As described on the CMHC website, this contest was conceived with five “keywords” in mind: Health, Energy, Resources, Environment, and Affordability (CMHC, 2008). Concordia University played a leading role in the design of two of the twelve original winning entries: the ÉcoTerra House, and the Alstonvale Net Zero House. The latter was used as a case study in this investigation, and a detailed account is presented in Chapter 4.



Figure 2.10. The ÉcoTerra House (photo: YuXiang Chen).

Figure 2.10 shows the ÉcoTerra House (Chen *et al.*, 2007; Noguchi *et al.*, 2008; Chen *et al.*, 2010b; Doiron *et al.*, 2011), whose construction was completed in November 2007. This house, located near Eastman (Québec), about 100 km east of Montréal, is a near net-zero house which relies heavily on passive solar design. For example, it includes R-36 insulation on its wall, 0.8 ACH at 50 Pa, triple-glazed windows (window-to-wall ratio of 40% on its south façade) and concrete floors to add thermal mass. It has 2.8 kW BIPV/T roof. Apart from its electric energy output, the BIPV/T roof is used to preheat outdoor air; the heated air is then used to deliver thermal energy to a hollow-core concrete slab installed in the basement. The BIPV/T air may also be used to preheat the domestic hot water and to supply air to the dryer. The main heating system of the house is a 3-ton ground-source heat pump linked to a forced air system. Energy efficient appliances and advanced lighting complete the energy design of the house, which consumes about 10,000 kWh/year (Doiron, 2011).

Other noteworthy projects developed for the *EQuilibrium Initiative* include: (a) the *Avalon Discovery 3* in Red Deer, Alberta (Avalon, 2008) which relies heavily on a “combi” system with solar thermal collectors providing heat to radiant floor heating system; (b) the *Abondance Le Soleil* near downtown Montréal (Écocité, 2010), which employs ground-source heat pumps and a 14-kW PV panel system on its roof; (c) and the *Riverdale Net Zero Project* in Edmonton, Alberta (Riverdale, 2008).

The Riverdale project, designed with passive solar design features, includes a 5.3 kW PV system, and a solar thermal system with a 17,000-L tank for thermal energy storage. Since the construction of the house, the project managers have gradually abandoned the utilization of the solar thermal system due to problems during the operation. Considering

that heating loads are of the order of a couple of kW, a rather unorthodox approach for space heating has been used: baseboard heaters fed with PV electricity (!). While this measure arguably makes economic sense, using electric baseboards has several important shortcomings: it does not contribute to the reduction of peak loads, it is thermodynamically wasteful, and it is far from being the best approach in terms of thermal comfort. In Alberta, where electricity is generated with natural gas, this could potentially increase GHG emissions.

In spite of all these inadequacies, electricity-based space heating may be the subject of further investigation. Instead of baseboard heaters, there is a significant product development opportunity: small heat pumps, with heating capacities as small as ½ ton, could be used to deliver heat to a RFH system, thus complementing the advantages of passive solar design.

3. Theoretical Considerations

3.1 Research Needs in Control of Solar-Optimized Homes

The literature review presented in Chapter 2 dealt with control strategies used in buildings, techniques for simulation and load calculation, and available technologies for solar optimized buildings. However, much work remains to be done in control strategies for solar-optimized buildings. In particular:

- Research in control of solar buildings has focused on **passive** solar buildings. Work is needed in solar-optimized buildings, including active systems. As discussed in Section 1.1, solar-optimized buildings –which use devices like photovoltaic panels, solar collector or active thermal energy storage–, require a special approach.
- There have been relatively few investigations, especially in recent years, on the application of optimal control to the specific case of solar homes (Winn & Winn, 1985; Paassen, 1988; Nygård-Ferguson & Scartezzini, 1989b, a; Lute & Paassen, 1990; Chen, 2001). In these cases, the control has focused on a single variable, typically the rate of heat delivery to the space.
- Although work has been done in handling active and passive storage in large commercial buildings (Kintner-Meyer & Emery, 1995; Henze *et al.*, 2004a; Zhou *et al.*, 2005), similar efforts are still needed for solar-optimized homes. Active storage in particular has rarely been considered in the control strategies of solar-optimized buildings. Moreover, it is important to bear in mind that

unlike most commercial buildings, which need cooling most of the time and therefore have ice storage systems, solar-optimized homes (especially in the Canadian climate) are usually heating-dominated and therefore appropriate heat storage devices must be integrated in the control system. Moreover, TES systems are rarely used at the residential level partially due to the flat rates for electricity applied by utilities.

- Modeling of renewable energy devices (such as BIPV/T or solar collectors) must be integrated into solar-optimized buildings.
- Most efforts in the control of blinds have dealt with local control, which is very important for daylighting as well as thermal and visual comfort. In spite of the enormous potential of active fenestration and motorized blinds for controlling solar heat gains, they are often not included in the supervisory control strategy.
- Complex calculations used for optimal control were restricted as recently as 10 or 15 years ago because of the computational capacity available at the time. The accessibility of online weather forecasts with abundant information also opens up new possibilities.
- The examined planning horizon has usually been 24 hours, but when energy autonomy is an issue, longer planning horizons (two days or longer) must be considered.

3.2 Thermal Networks for Building Energy Modeling

Thermal networks, in which thermal phenomena are modeled based on electric network analogies, are commonly used for building energy modeling. Conduction heat transfer through opaque building envelope components is commonly modeled with two different approaches: (a) conduction transfer functions (CTF) and (b) control volume finite difference methods (CVFD).

3.2.1 Analytical Methods and Conduction Transfer Functions

The exact analytical solution for heat conduction through a one-dimensional solid is found by modeling it as a two-port network element (Pipes, 1957; Davies, 2004). One of the faces of the solid is treated as an “input” side, with a corresponding temperature and heat flux (analogous respectively to voltage and temperature) while the other face is treated as an “output” side, with its corresponding temperature and heat flux. In a two-port network, knowledge of two variables allows finding the other two. “Input” and “output” are easily interchangeable.

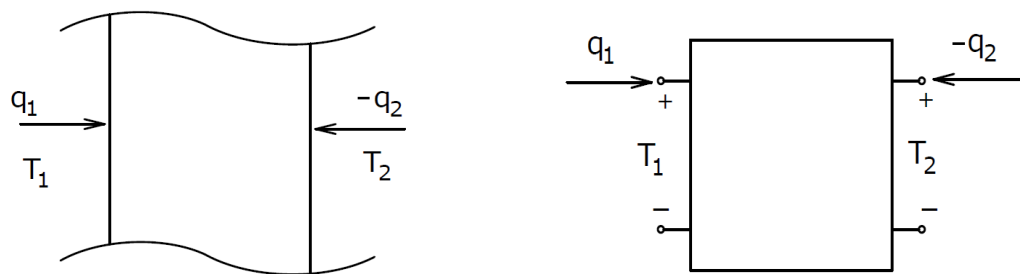


Figure 3.1. Two-port network model for a wall, adapted from (Athienitis, 1985).

The relationship between the parameters in the two-port network model is given by two equations (Athienitis & Santamouris, 2002).

$$\begin{aligned} T_1 &= AT_2 + B(-q_2) \\ q_1 &= CT_2 + D(-q_2) \end{aligned} \quad (3.1)$$

In a matrix representation:

$$\begin{bmatrix} T_1 \\ q_1 \end{bmatrix} = \begin{bmatrix} A & B \\ C & D \end{bmatrix} \begin{bmatrix} T_2 \\ -q_2 \end{bmatrix} \quad (3.2)$$

The negative sign has been introduced so that the heat fluxes on both sides (q_1 and q_2) follow the same direction (by convention, in two-port networks the “current” on both sides is represented entering the network). By writing the heat conduction differential equations, it is possible to find the steady-periodic solution for a sinusoidal fluctuation with a frequency of ω rad/s, which is given by:

$$\begin{bmatrix} T_1 \\ q_1 \end{bmatrix} = \begin{bmatrix} \cosh(\gamma L) & \sinh(\gamma L)/k\gamma \\ k\gamma \sinh(\gamma L) & \cosh(\gamma L) \end{bmatrix} \begin{bmatrix} T_2 \\ -q_2 \end{bmatrix} \quad (3.3)$$

in this equation, k is the thermal conductivity of the material and L its thickness. The variable γ is given by:

$$\gamma = \sqrt{\frac{s}{\alpha}} \quad (3.4)$$

in which s is the Laplace transform operator ($s = j\omega$) and α is the thermal diffusivity of the material. For the case of a multilayered wall, the two-port network for all the layers can readily be found by applying a “cascade” multiplication of the matrices representing each two-port model (Davies, 1973). As presented in (Athienitis & Santamouris, 2002):

$$\begin{bmatrix} T_1 \\ q_1 \end{bmatrix} = \begin{bmatrix} A_1 & B_1 \\ C_1 & D_1 \end{bmatrix} \begin{bmatrix} A_2 & B_2 \\ C_2 & D_2 \end{bmatrix} \dots \begin{bmatrix} A_N & B_N \\ C_N & D_N \end{bmatrix} \begin{bmatrix} T_N \\ -q_N \end{bmatrix} \quad (3.5)$$

The exact heat conduction solution for any periodic signal can be found by using this method. The treatment of a wall as a two-port network facilitates its integration as an element in a thermal network, and allows Thévenin or Norton equivalent circuits to be found. The components of these equivalent circuits depend on the frequency. For instance, in Figure 3.2, the quantity U_o stands for the equivalent conductance of the exterior film coefficient (h_o) of a wall of area A_o in series with a layer of insulating material with insulation value R_{ins} :

$$U_o = \frac{A_o h_o}{1 + h_o R_{ins}} \quad (3.6)$$

It can be shown that the Norton “current” (i.e., heat source) is given by the negative of the product of the “transfer admittance” (Y_T), a parameter derived from the two-port model, and the sol-air temperature, an equivalent temperature which includes the effect of solar radiation. The Norton conductance is equal to the “self admittance” of the wall.

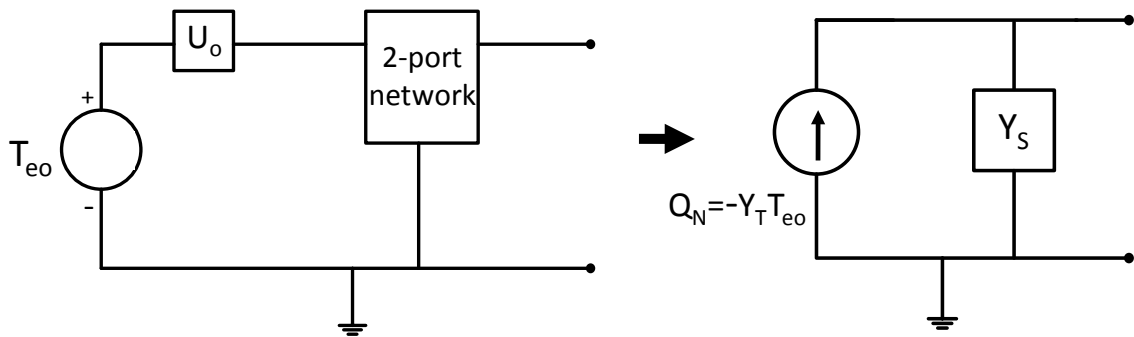


Figure 3.2. Norton equivalent for a wall with an exterior insulating layer of negligible thermal mass. Adapted from Athienitis & Santamouris (2002).

The sol-air temperature is given by:

$$T_{eo} = T_o + \frac{\alpha_w G}{h_o} \quad (3.7)$$

where T_o is the outdoor temperature, G is the incident solar irradiance in W/m^2 and α_w is the absorptance of the wall. In this case, the self admittance of the wall is given by:

$$\mathbf{Y}_s(\omega) = \frac{U_o + A_o k \gamma \tanh(\gamma L)}{\frac{U_o}{A_o k \gamma} \tanh(\gamma L) + 1} \quad (3.8)$$

The transfer admittance is given by:

$$\mathbf{Y}_T(\omega) = -\frac{A_o}{\frac{A_o}{U_o} \cosh(\gamma L) + \frac{\sinh(\gamma L)}{k \gamma}} \quad (3.9)$$

Both the self admittance and the transfer admittance are a function of γ , which means that the circuit parameters shown at the right side of Figure 3.2 are a function of frequency (ω). Note that for steady state (i.e. $\omega = 0$), $\mathbf{Y}_s(0) = U_o$ and $\mathbf{Y}_T(0) = -U_o$. Distributed parameter elements such as Norton equivalent circuits for walls can be combined with lumped parameters (i.e., containing a single thermal capacitance) for energy modeling and control (Athienitis *et al.*, 1990).

Analytical solutions for heat conduction through walls have been used in the derivation of conduction transfer function (CTF) factors (Mitalas & Stephenson, 1967; Stephenson & Mitalas, 1971). CTFs basically consist of z-transforms[§], which are used to calculate the heat flux at the inner surface of opaque components based on previous and current temperatures (at the exterior and interior surface), as well as previous heat fluxes

[§] A more detailed explanation of z-transforms is given in Section 3.2.4.

(Davies, 2004). CTFs are a key component in the ASHRAE's Heat Balance Method, HBM, (Rees *et al.*, 2000; McQuiston *et al.*, 2005). As its name indicates, the HBM consists of writing heat balance equations for the nodes of interest (i.e., exterior surfaces, interior surfaces, air node), and solving the equations simultaneously. Periodic response factors (PRFs) are a simpler version of CTFs; they are used in ASHRAE's Radiant Time Series (RTSM) method (Spitler *et al.*, 1997; McQuiston *et al.*, 2005), a simplified version of the HBM method used for cooling load calculations. After calculating the coefficients of the CTFs and RTFs, the rest of the calculations are rather straightforward, computationally efficient and easily programmable into a software tool, or even a spreadsheet in the case of the RTSM. Conduction transfer function factors are used in popular software tools, such as EnergyPlus or TRNSYS.

CTFs and PRFs, used respectively in the HBM and the RTSM, depend on the assumption that the wall, floor or roof behaves as a linear system. This represents a limitation for modeling components with a non-linear behaviour such as PCMs.

3.2.2 Control Volume Finite Difference (CVFD) Method

This approach is based on a space discretization of the solid into control volumes (Athienitis, 1994; Underwood & Yik, 2004), each one of which describes a layer, as shown in Figure 3.3. A node is located at the centroid of the control volume. The heat flux between adjacent nodes is described by using resistance analogies: the flux is calculated as proportional to the difference between the temperatures of the two nodes. Between control volumes shaped like a rectangular prism, as is often the case in walls or floors, the conductance is calculated simply as kA/L , where k is the thermal conductivity

of the material, A the area of the surface of contact, and L the distance between adjacent nodes.

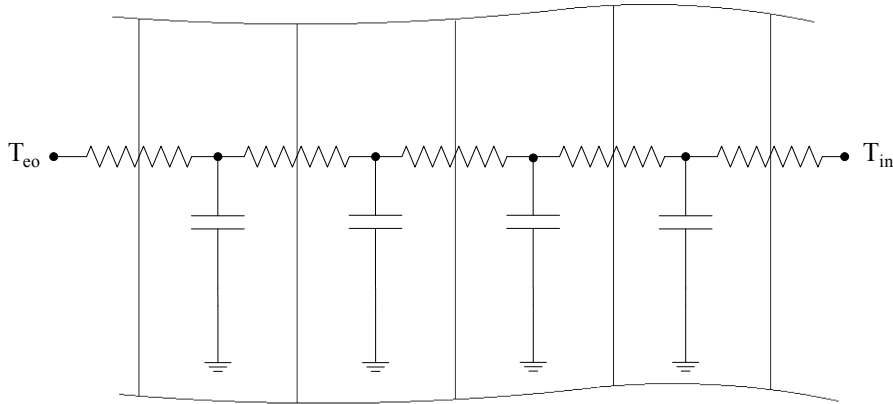


Figure 3.3. Control volume discretization.

If the node has considerable thermal mass, a node may also be assigned a capacitance, which represents the heat storage capacity of the control volume. By performing a heat balance analysis on the control volume, the differential equation of a node can then be written as (Athienitis *et al.*, 1990; Athienitis and Santamouris, 2002):

$$C_i \frac{dT_i}{dt} = Q_i + \sum_{j=i}^n U_{i,j} (T_j - T_i) \quad (3.10)$$

where Q_i represents the heat generated at a node or received directly by it from source(s), $U_{i,j}$ represents the thermal conductance (inverse of the resistance), T is the temperature, and C is the thermal capacitance of each node.

A commonly followed strategy to find the transient solution is the application of a time discretization (Athienitis & Santamouris, 2002), for which several approaches exist to carry out this task. The **fully explicit** approach assumes that the current temperature of a given node depends only on its temperature and the temperature of the surrounding

nodes at the previous time step (Patankar, 1980; Athienitis, 1994). The term having the time derivative can then be discretized as follows (Athienitis, 1994):

$$C_i \frac{dT_i}{dt} \approx C_i \frac{\Delta T_i}{\Delta t} = C_i \left(\frac{T_i^{p+1} - T_i^p}{\Delta t} \right) \quad (3.11)$$

By solving for the temperature at the next time step (Athienitis, 1994):

$$T_i^{p+1} = \frac{\Delta t}{C_i} \left(Q_i^p + \sum_{j=1}^n U_{i,j} (T_j^p - T_i^p) \right) + T_i^p \quad (3.12)$$

Heat conduction calculations based on the CVFD method are applied in building simulation tools such as ESP-r and the most recent versions of EnergyPlus. While being more computationally intensive, CVFD has the advantage of flexibility for handling nonlinearities in the system.

3.2.3 Thermal Network Analysis and Transfer Functions

Regardless of the method employed for the calculation of conduction through massive building envelope components, these sub-circuits become a part of a larger “thermal network” representing the zone being analyzed (often linked to other zones).

Figure 3.4 shows a schematic of a simple one-zone thermal network. For clarity's sake, radiative exchange between the internal surfaces is not shown. The air node (T_{air}) is linked to the internal surfaces by interior film coefficients. It is also linked to the outdoor temperature directly by a resistance representing infiltration and conduction through elements of negligible thermal mass (windows and doors). The air node also receives a heat contribution from the heating system (Q_{HS}). The internal surfaces of the walls,

ceiling and floor receive solar heat gains. The external surfaces are connected to their corresponding "sol-air temperatures".

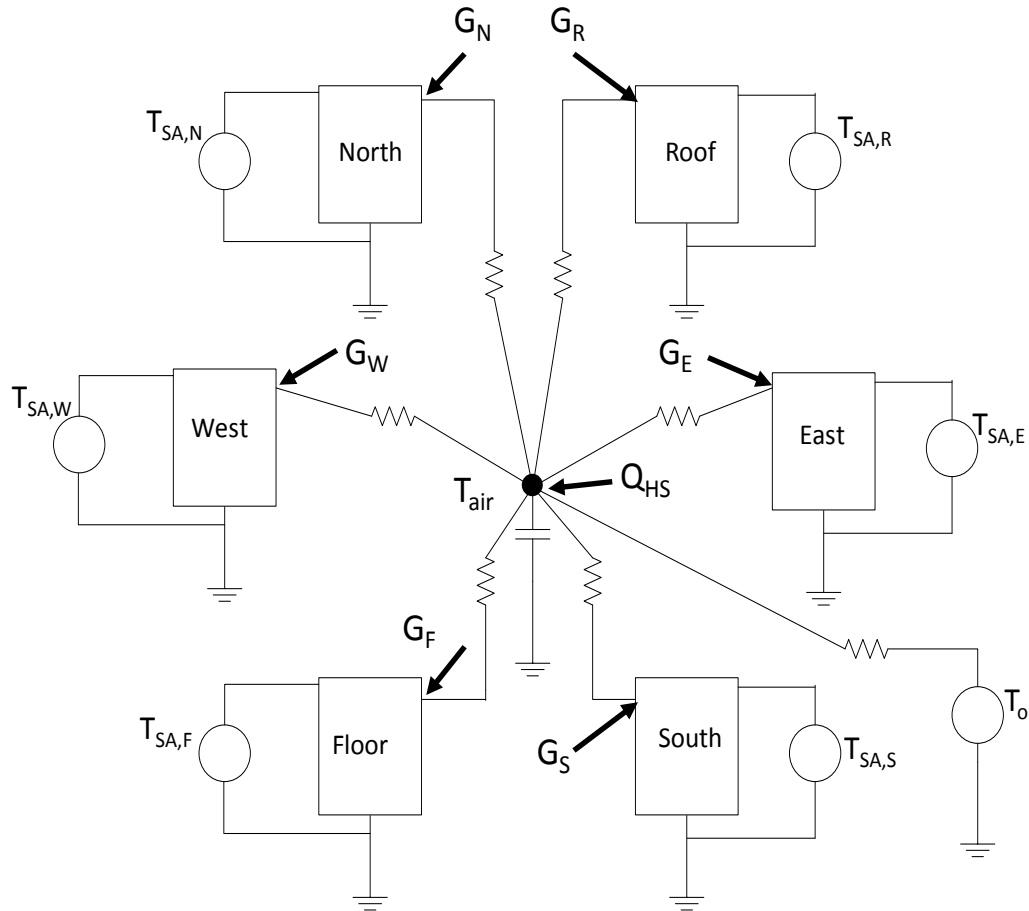


Figure 3.4. Thermal network representation of a single-zone room (radiative exchange between the internal surfaces is not shown). Each part of the building envelope is exposed to sol-air temperatures (T_{SA}) and to solar radiation hitting its internal surface.

By representing radiation and convection with linear approximations, tools from circuit analysis can then be used to study the building. For example, by introducing the admittances associated with the capacitances of the nodes (sC), the following equation can be written in matrix form.

$$\begin{pmatrix} sC_1 + \sum_{j=1}^n U_{1,j} & -U_{1,2} & -U_{1,3} & \cdots & -U_{1,n} \\ -U_{1,2} & sC_2 + \sum_{j=1}^n U_{2,j} & -U_{1,3} & \cdots & -U_{2,n} \\ \cdots & \cdots & \cdots & \cdots & \cdots \\ -U_{n,1} & -U_{n,2} & -U_{n,3} & \cdots & sC_n + \sum_{j=1}^n U_{n,j} \end{pmatrix} \begin{pmatrix} T_1 \\ T_2 \\ \cdots \\ T_n \end{pmatrix} = \begin{pmatrix} Q_1 \\ Q_2 \\ \cdots \\ Q_n \end{pmatrix} \quad (3.13)$$

In Equation (3.13), the term U_{ij} is the conductance between nodes i and j , T_i is the temperature of node i , and Q_i is the heat source at node i . In a simpler notation:

$$\mathbf{YT} = \mathbf{Q} \quad (3.13)$$

By solving for the temperatures, the thermal admittance matrix (\mathbf{Y}) is then inverted to become the thermal impedance matrix ($\mathbf{Z} = \mathbf{1/Y}$). Equation (3.13) becomes:

$$\mathbf{T} = \mathbf{ZQ} \quad (3.14)$$

As mentioned by Athienitis *et al.* (1990), the temperature of a node can be found by adding the contributions of each heat source:

$$T_i(s) = \sum_{j=1}^n \mathbf{Z}_{i,j}(s) Q_j \quad (3.15)$$

where Z , with units of impedance, is a transfer function between the source and the output written in terms of s . This transfer function can be expressed analytically in terms of s when there are relatively few nodes (Athienitis *et al.*, 1990). However, the problem quickly becomes more complex as the number of nodes increases.

In the previously mentioned paper by Athienitis *et al.* (1990), thermal networks are also proposed as a tool that can link building design and control. The effect of each disturbance (i.e., heat source) on the room air temperature or any other suitable thermal

comfort variable can be represented by a transfer function (see Figure 3.5). The total effect is then calculated by applying the superposition principle.

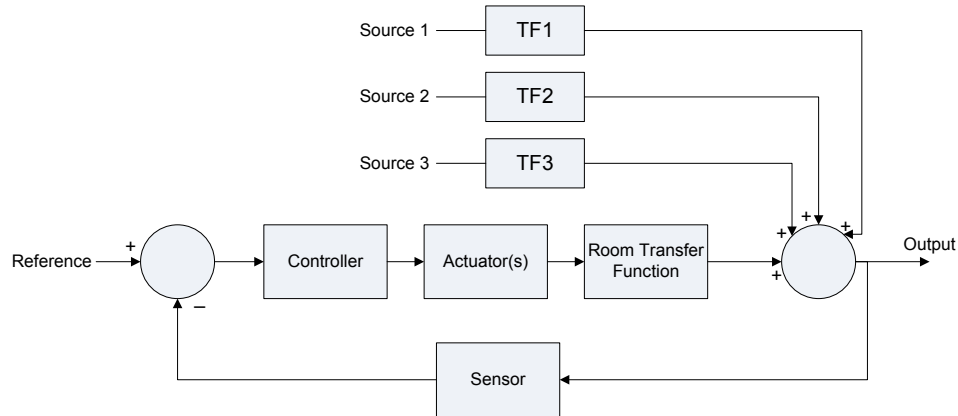


Figure 3.5. Building control diagram based on transfer functions. Adapted from Athienitis *et al.* (1990).

Transfer functions can be found in several ways. If the network is relatively simple, the admittance matrix is written in terms of s , and is then inverted to find the impedance matrix, which in turn can be used to find analytical expressions for the transfer functions. For more complex networks, an exact mathematical transfer function based on the different building parameters is harder to find. However, an exact solution for the transfer function may not be necessary for design and control applications. Moreover, these parameters (insulation, surface areas, etc.) are also subject to uncertainty and the search for an exact solution is an excessive and futile effort.

Athienitis *et al.* (1990) proposed the numerical inversion of the admittance matrix at discrete frequencies for complex networks. The resulting discrete values (magnitude and angle) of the transfer functions can then be plotted in a Bode diagram of the response. A transfer function, written as the ratio of two polynomials in terms of s , is found by applying interpolation techniques (Levy, 1959).

Figure 3.6, borrowed from the article by Athienitis *et al.* (1990) shows the response found at discrete frequencies for a sample transfer function, between node 1 (the air node) and node 7 (basement temperature). Equation (3.16) shows a third-order approximation for the transfer function.

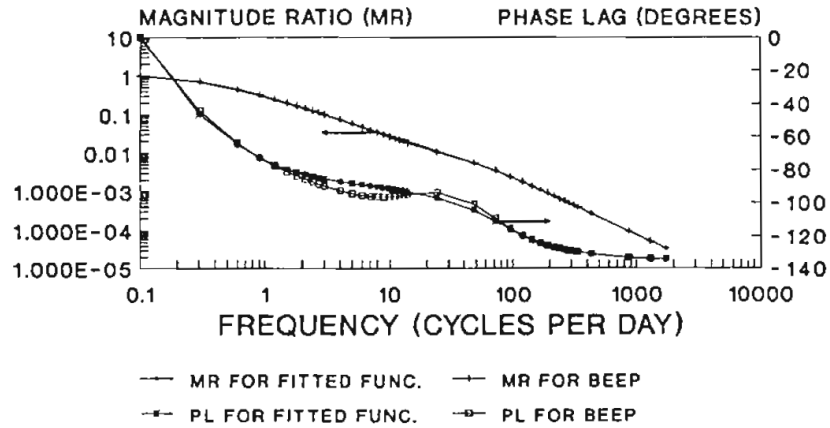


Figure 3.6. Numerical determination of a transfer function for a sample building (Athienitis *et al.*, 1990). This figure shows the Bode diagram of exact discrete responses found with a computer program (BEEP, see Athienitis *et al.* (1990) for details) and a curve-fitted third-order transfer function.

$$Z_{1,7}(s) = \frac{0.00804 + 10.5s + 55.2s^2 - 10.5s^3}{1 + 4.01 \times 10^{-4}s + 6.64 \times 10^7 s^2 + 2.63 \times 10^9 s^3} \quad (3.16)$$

3.2.4 Discrete-Time Transfer Functions Using z -Transforms

The z -transform is the discrete counterpart of the Laplace transform. A presentation of the z -transform can be found, for example, in the books by Stephanopoulos (1984) and Seborg *et al.* (1989). An introduction of the use of z -transforms in building control is presented by Underwood (1999) and Davies (2004). A more in-depth discussion of the theory of z -transforms can be found in the texts by Ogata (1987), Houpis (1992) and Moudgalya (2007) among others. Moudgalya (2007) defines the z -transform as follows:

“The z-transform of a sequence $\{u(n)\}$ is denoted by $U(z)$ and it is calculated using the formula

$$U(z) = \sum_{n=-\infty}^{\infty} u(n)z^{-n} \quad (3.17)$$

where z is chosen such that $\sum_{n=-\infty}^{\infty} |u(n)z^{-n}| < \infty$.”

The definition above is called the “bilateral” z-transform, as it takes into account values before and after $n = 0$ (Mathworld, 2008). When only values such that $n \geq 0$ are considered, the term “unilateral” or “one-sided” z-transform is used.

The importance of the z-transform lies in the fact that it can be shown (Stephanopoulos, 1984) that it represents a special case of a Laplace transform of a train of known impulses occurring with a period T . By definition, the Laplace transform of a function $y(t)$ is given by:

$$Y(s) = \int_0^{\infty} y(t)e^{-st} dt \quad (3.18)$$

Let $y(t) = y_0$ at time $t = 0$, y_1 at time $t = T$, y_2 at time $t = 2T$, and so forth. Equation (3.18) can then be written as:

$$Y(s) = \sum_{n=0}^{\infty} y(nT)e^{-snT} \quad (3.19)$$

By assuming that the auxiliary variable z is given by the following expression:

$$z = e^{sT} \quad (3.20)$$

Equation (3.19) becomes:

$$Z(y(t)) = Y(z) = \sum_{n=0}^{\infty} y(nT)z^{-n} \quad (3.21)$$

In process control, a variable is sampled at discrete time intervals. In this case, the z -transform of a sequence occurring at times $0, T$ and $2T$ is given simply by a polynomial in terms of z^{-1} , with a degree **equal to the number of terms minus one, and coefficients equal to the elements of the series**. For instance, if the sequence is $u(0) = 1, u(1) = 0.8$ and $u(2) = -0.5$, its z -transform is $U(z) = 1 + 0.8z^{-1} - 0.5z^{-2}$.

In continuous-time, a transfer function between an output $y(t)$ and input $u(t)$ is defined as the ratio of their Laplace transforms when the initial conditions are zero, i.e. $Y(s)/U(s)$. Likewise, in the discrete-time transfer function is the ratio of the z -transforms of the input and output:

$$G(z) = \frac{Y(z)}{U(z)} \quad (3.22)$$

The advantage of a z -transfer function is that it can easily be associated with a difference equation. For example, the transfer function given by:

$$\frac{Y(z)}{U(z)} = \frac{2 + 3z^{-1} + 4z^{-2}}{1 + 2z^{-1} + 3z^{-2} - 4z^{-3}} \quad (3.23)$$

can be written as:

$$Y(z)(1 + 2z^{-1} + 3z^{-2} - 4z^{-3}) = U(z)(2 + 3z^{-1} + 4z^{-2}) \quad (3.24)$$

The translation theorem states that:

$$Z(y(t - nT)) = z^{-n}Z(y(t)) \quad (3.25)$$

Equation (3.24) can be written as:

$$Y(z) + 2Y(z)z^{-1} + 3Y(z)z^{-2} - 4Y(z)z^{-3} = 2U(z) + 3U(z)z^{-1} + 4U(z)z^{-2} \quad (3.26)$$

By applying the translation theorem, and then inverting the z -transform, the following difference equation can be written:

$$y(t) + 2y(t-T) + 3y(t-2T) - 4y(t-3T) = 2u(t) + 3u(t-T) + 4u(t-2T) \quad (3.27)$$

By rearranging the equation above, one can express the current value of the output as a function of previous values of both the input and the output, and the current value of the input:

$$y(t) = -2y(t-T) - 3y(t-2T) + 4y(t-3T) + 2u(t) + 3u(t-T) + 4u(t-2T) \quad (3.28)$$

Such an approach is easily programmable and can be used for real time control as well as for simulation studies. It is the method used in Simulink (MathWorks, 2010).

A continuous-time transfer function, such as the one presented in Equation (3.16), can be transformed in an equivalent discrete-time transfer function in several ways. One method could be to find the signal in the time-domain by applying an inverse Laplace transform (e.g., with a partial fraction expansion), and then finding the corresponding z -transform for a sampling time T . Another alternative is to use the so-called Tustin or bilinear method (Seborg *et al.*, 1989). In this method, a Padé approximant is used to define an approximate value for the value of z as defined in Equation (3.20):

$$z = e^{sT} \approx \frac{2 + sT}{2 - sT} \quad (3.29)$$

By solving for s in the equation above:

$$s \approx \frac{2}{T} \left(\frac{z-1}{z+1} \right) = \frac{2}{T} \left(\frac{1-z^{-1}}{1+z^{-1}} \right) \quad (3.30)$$

Equations (3.29) and (3.30) can be used to convert numerically between continuous-time and discrete-time transfer functions.

As mentioned above, the Heat Balance Method (HBM) recommended by ASHRAE for load calculations is based on the determination of Conduction Transfer Functions (CTF). These CTFs are essentially z -transforms transfer functions for conduction through solid building envelope components (Davies, 2004). Readily programmable and computationally efficient, they are used in EnergyPlus as the default conduction heat transfer method. Research continues on methods to improve their performance and applicability (Cellura *et al.*, 2003; Beccali *et al.*, 2005b, a).

3.3 Predictive Control Methodology for Solar-Homes

3.3.1 System Identification of Simplified Models

A simplified linear model, such as a set of transfer functions or a state-space model, facilitates the implementation of advanced control strategies. These control strategies would be difficult to handle with a full-scale model, either created with a building energy modeling tool, or built from first principles by the user.

Several building simulation software tools, such as ESP-r and EnergyPlus (Crawley *et al.*, 2001; ESP-r, 2010), achieve accurate representations of buildings through a careful integration of detailed models of physical phenomena into a single, comprehensive tool. Such a model provides a reliable representation of the building's response to external impulses and its HVAC system, which is particularly useful for research purposes.

However, this approach is often unnecessarily detailed for many applications. In other words, simplicity is compromised in search of accuracy.

With a full-scale building simulation tool, testing and design of advanced control strategies can be quite cumbersome. For example, anticipatory control strategies, such as optimal control strategies used to select set-point trajectories (Kummert *et al.*, 2001; Henze *et al.*, 2004a; Henze *et al.*, 2005) require estimating the effect of an action such as turning on a piece of equipment or changing the position of a valve based on expected loads. Model Predictive Control (MPC) has been applied to manage the large time scales associated with large thermal masses based on a known building model and weather forecasts (Chen, 2001; Oldewurtel *et al.*, 2010a). Predictive control calculations imply performing full building energy simulations at regular intervals with a moving time-horizon (Coffey *et al.*, 2006). This approach can be difficult to implement with a full-scale building model, especially if optimal control algorithms are used. It is clear that simpler models, requiring fewer inputs, are needed in control applications for solar homes (Kummert *et al.*, 1996).

The need for simpler models has been recognized in other computationally demanding tasks. For instance, simplified models have been proposed as a tool for community level studies (Kämpf & Robinson, 2007). These simplified building models have commonly been based on thermal network representations with a limited number of thermal resistances and capacitances (Fraisse *et al.*, 2002; Kämpf & Robinson, 2007).

It is known –and experimentally confirmed (Barakat, 1987; Lefebvre *et al.*, 1987; Freire *et al.*, 2005; Mustafaraj *et al.*, 2009)– that simplified linear models (e.g., transfer function models) can offer a suitable representation of a small building. This in itself is a

powerful yet often overlooked fact. However, it is hard to decide *a priori* the level of complexity that is appropriate for a given application. This difficulty of this task lies in deciding which details can be neglected without jeopardizing the validity of the conclusions. Therefore, validation is necessary when creating a simplified model. Physical models whose parameters are obtained from system identification of measurements or building simulation results comply with this requirement.

Two fundamental assumptions are applied for the selection of linear models:

1. Solar homes have higher levels of insulation and air-tightness, while having large fenestration areas. This implies that their response is heavily dependent on the incoming solar gains, the outdoor temperature and internal loads, and less dependent on other inputs that typically affect a conventional house, such as ground temperature, sky temperature, humidity, wind speed and others.

2. The models identified do not need to perform well under every circumstance: the models only need to perform adequately for the range of time-scales or frequencies typically found in building modeling. These models can also be season-dependant. For example, the response to solar gains in winter will be different from the response in summer, due to the change in solar angles.

The problem consists then in determining the transfer functions corresponding to each of the relevant forcing functions, following an approach similar to the one presented in the previous section. The use of a building simulation model enables the possibility of “virtual experiments” not feasible in a real building. For example, by applying a stimulus or forcing function (temperature or radiation) at discrete frequencies, while “turning off”

the rest of the stimuli, the impact of each input variable can be studied independently. The output will typically be the indoor room air temperature, the operative temperature or other indicator of thermal comfort. In a linear system, the superposition principle is applicable: the output can be calculated by adding the effect of each input (Figure 3.7).

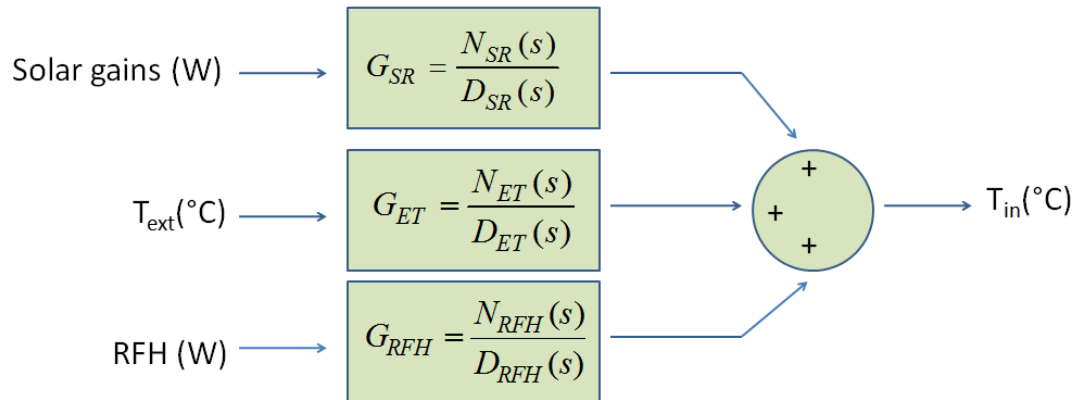


Figure 3.7. Superposition principle applied to a simplified model, with three inputs used: solar gains, outdoor temperature and heat delivered by a RFH system.

A wide range of system identification (SI) techniques can be used to find approximate transfer functions or state-space models for a solar house. A full description of SI techniques is beyond the scope of this thesis. For more information, the reader is referred to the books by Ljung (1999) and Box *et al.* (1994). MATLAB’s System Identification Toolbox (Ljung, 2010) was instrumental in the determination of simplified models. A brief overview of SI methods is also presented in the manual of this Toolbox.

In essence, two kinds of models, as presented in MATLAB’s Toolbox (Ljung, 2010), are used in this investigation:

- **Simple process models.** This scheme assumes that a continuous-time, low-order model, can accurately describe the performance of the system. Simple

process models in the SI toolbox are up to second order for the numerator (two zeros) including a time-delay, and up to third order for the denominator (three poles):

$$G(s) = \frac{Ke^{-T_d s}(1 + T_z s)}{(1 + T_{p1}s)(1 + T_{p2}s)(1 + T_{p3}s)} \quad (3.31)$$

In this type of model, the SI Toolbox directly determines the optimal value of the parameters, according to the order selected by the user. The user can adjust the order of the models, until he/she is satisfied with the selection. During the course of this investigation (in particular for the response to the heat of a radiant floor heating system) it was found that a first-order RC model was often sufficient:

$$G(s) = \frac{K}{1 + T_p s} \quad (3.32)$$

- **Linear parametric models.** In this case, higher order discrete-time (z -transforms) transfer functions are found. In this investigation, the two most commonly used models parametric linear models are the autoregressive model with exogenous input (ARX), and the autoregressive moving average model with exogenous input (ARMAX)**. The word “autoregressive” refers to the fact that the current value of the $y(t)$ output depends on its own previous values, while the “exogenous input” refers to the influence of the input

** Many other schemes exist: Output-error (OE), Box-Jenkins, ARIMAX, ARARX, etc. Ljung, L. (1999). *System Identification: Theory for the User*. Second Edition. Prentice Hall, Upper Saddle River, New Jersey.

variable $u(t)$. Both of them are *time series* models (Box *et al.*, 1994). Their general form is given by (Ljung, 2010):

$$A(q)y(t) = \sum_{i=1}^{nu} B_i(q)u_i(t - nk_i) + e(t) \quad [\text{ARX}] \quad (3.33)$$

$$A(q)y(t) = \sum_{i=1}^{nu} B_i(q)u_i(t - nk_i) + C(q)e(t) \quad [\text{ARMAX}] \quad (3.34)$$

in which $A(q)$, $B(q)$ and $C(q)$ represent polynomials in terms of q^{-1} , the “backward-shift operator”, equivalent to the z^{-1} , $y(t)$ is the sequence of output values, $u_i(t)$ is the sequence corresponding to the input i , nu is the number of inputs, and $e(t)$ is the sequence of noise values. In the case of a single input, Equations (3.33) and (3.34) become:

$$A(q)y(t) = B(q)u(t - nk) + e(t) \quad (3.35)$$

$$A(q)y(t) = B(q)u(t - nk) + C(q)e(t) \quad (3.36)$$

The polynomials $A(q)$, $B(q)$ and $C(q)$ provide an abbreviated notation for the difference equations (Ljung, 2010):

$$\begin{aligned} A(q) &= 1 + a_1q^{-1} + a_2q^{-2} \dots \\ B(q) &= b_1q^{-1} + b_2q^{-2} \dots \\ C(q) &= 1 + c_1q^{-1} + c_2q^{-2} \dots \end{aligned} \quad (3.37)$$

For example, Equation (3.36) stands for:

$$\begin{aligned} y(t) + a_1y(t-1) + \dots + a_{n_a}y(t-n_a) = \\ b_1u(t-n_k) + \dots + b_{n_b}u(t-n_k-n_b+1) + \\ c_1e(t-1) + \dots + c_{n_c}e(t-n_c) + e(t) \end{aligned} \quad (3.38)$$

The difference between an ARX and ARMAX is the presence of the polynomial $C(q)$, which is used to model the impact of white noise separately.

After finding the transfer function models, it is necessary to estimate the “goodness of the fit” between the original input and output data and each of the transfer functions models. MATLAB’s SI toolbox defines the fit variable as follows:

$$FIT = \left(1 - \frac{\left(\sum_{n=1}^N (y(n) - \hat{y}(n))^2 \right)^{1/2}}{\left(\sum_{n=1}^N (y(n) - \bar{y})^2 \right)^{1/2}} \right) 100\% \quad (3.39)$$

in which y is the measured output, \bar{y} is the arithmetic mean of the output, \hat{y} is the output calculated by the model and N is the number of measurements. In a “perfect fit”, $FIT = 100\%$ (i.e., the estimated outputs are equal to the measured outputs). The variable FIT is a good indicator of how well a model performs, but it is not the only criterion for assessing a model. Other criteria to consider are:

- **Stability of the model.** Adding more parameters (i.e., coefficients) to the model implies accounting for higher frequencies. It is equivalent to the addition of more capacitors in a thermal network. However, this implies that smaller time-steps are then required in a simulation in order to maintain stability. As pointed out in the paper by Beccali *et al.* (2005a), “*the best model is not always the largest in terms of number of poles*”.
- **Phase matching.** Peaks and troughs should coincide in both the model and the fed-in data. For example, for an adequate description of the thermal

response of a house, predicting when a minimum or maximum temperature value will be achieved is an important consideration.

When a satisfactory discrete-time transfer-function model has been found, it is often useful to find an approximation for a continuous-time transfer function. Such an approximation can provide information on the frequency response of the building. By applying Equation (3.29), and after some algebraic manipulation, continuous-time transfer functions can be found.

A transfer function representation can provide valuable information about the building's dynamics. For instance, information can be determined about the input delays (i.e., the time it takes for an input to cause an observable effect), time constants and relevant frequencies (e.g., cut-off frequencies). Moreover, transfer functions can be used to estimate the relative weight of each of the inputs on the total response, and could become a useful addition to research on sensitivity analysis.

Another advantage of a transfer function representation is that the information describing the building response may be communicated with a few numerical parameters, namely the coefficients of the transfer functions. In this way, building engineering professionals could easily exchange valuable information about the dynamic behaviour of the building.

3.3.2 Model Predictive Control (MPC) of Radiant Floor Heating

Predictive control has different applications. On the subject of the control of a heating system in a house with significant thermal storage, two clearly distinct although closely related objectives can be identified:

- a. Selection of optimal set-point trajectories for the house and for TES systems.
- b. Finding a method to track the set-points as closely as possible.

By optimally selecting the set-point trajectory, the building's thermal mass may be used to store energy. However, tracking the set-point is non-trivial in a house with significant thermal mass due to the long time constants involved.

In this investigation, MPC strategies have been used to address the problem of tracking the set-point trajectories. MPC is the collective name of a group of techniques aimed at achieving optimal tracking of the reference values by using forecast values of the disturbances. MPC is popular in the chemical and petroleum industries, where system responses are slow (Moudgalya, 2007). Solar homes, with high thermal mass and insulation are also characterized with long time constants. Generalized predictive control (GPC) algorithms, a subset of MPC algorithms, have been used by Chen (1997; 2001, 2002) for the control of radiant floor heating systems, in research efforts which began at Concordia University.

Having a z -domain model (either a model derived from first principles or resulting from the identification process), and a forecast of the forcing functions or disturbances, control measures can be taken beforehand in order to minimize the deviation (or error) from the set-point. This is accomplished by carrying out an optimization of an objective function at each time step.

Bemporad *et al.* (2010) introduce a simple presentation of MPC based on the minimization of the sum of square deviations S_k between the output and the set-point for

all the values from a current time step (k) to a future time step P (prediction horizon). For a single output,

$$S_k = \sum_{i=1}^P \{w[r_{k+i} - y_{k+i}]\}^2 \quad (3.40)$$

in which, r_{k+i} and y_{k+i} are respectively the reference and output at the time step $k+i$, and w is a weighting factor. The linear model obtained from system identification can be supplied to the MPC controller, along with a forecast of expected “disturbances” (e.g., weather variables) affecting the system. This information is then used to calculate the value(s) of the manipulated variable(s) that will minimize S_k .

As this minimization is carried out at regular intervals with a moving target, MPC is also often called “receding horizon” control, as shown in Figure 3.8, borrowed from the user guide of MATLAB’s MPC Toolbox (Bemporad *et al.*, 2010).

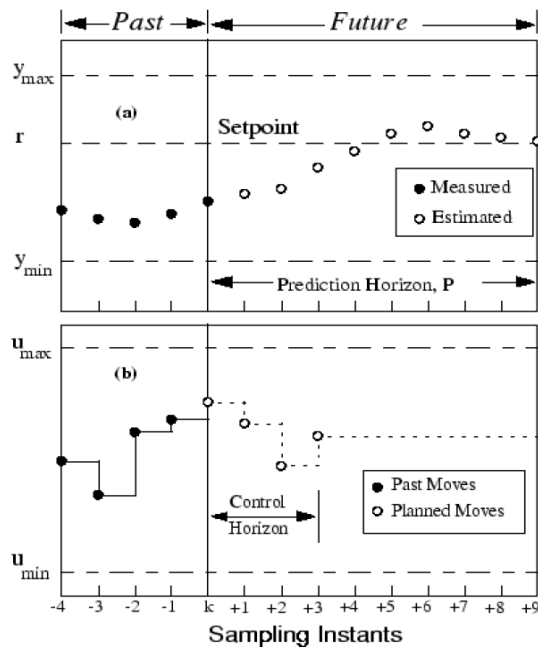


Figure 3.8. Receding horizon control, as presented by Bemporad *et al.* (2010).

At a given time step, a model-based predictive controller reads the load forecast over a certain number of time steps called the “prediction horizon”. The optimization problem is then solved for a period called the “control horizon” (typically, only a few time steps long). The calculation is then repeated at the next time step.

A complete presentation of the techniques used for solving the optimization problem presented in Equation (3.40) is beyond the scope of this thesis. For more information, the interested reader is referred to the texts by Bemporad *et al.* (2010), Rossiter (2003), Wang (2009) and Camacho & Bordons (2004).

3.3.3 Optimal Set-point Sequence for Solar-Heated TES Tank

When a TES device is used, advanced control strategies are recommended. When charging a TES system requires significant energy expenditure, keeping the system “fully charged” is a naive approach. A “fully-charged” TES guarantees, of course, the supply of thermal energy. However, following this strategy means that in many cases the TES would be charged unnecessarily. For example, if a TES system is used for residential space heating, it will not be necessary to keep the tank “fully-charged” before a sequence of clear sunny days, when solar heat gains would take care of space heating needs.

The state of charge of the tank should depend on the expected loads and energy availability. This problem has been addressed in the case of ice storage systems, in which the operation of the chiller must be carefully planned (Henze, 1995; Henze *et al.*, 1997).

For this investigation, dynamic programming was applied for defining a set-point trajectory for a TES water tank. Dynamic programming can be readily implemented in a computer program, it can include nonlinearities and complex models, and it handles

constraints with relative ease. This method has been used before for dynamic control of buildings (Henze, 1995; Henze *et al.*, 1997; Henze & Krarti, 1999; Nagai, 1999; Chen, 2001; Liu, 2005). The term “programming” is not related to computer programming, but it is rather used as a synonym of “planning” (Dreyfus, 2002).

3.3.3.1 Principle of Optimality

The following discussion is based on the presentation of the principle of optimality as introduced in the texts by McCausland (1969), Dreyfus & Law (1977) and Kirk (2004). In general, in a system changing between discrete states, the overall cost (often energy expenditure) is represented as the summation of a series of costs of control actions, which depend on the state of the system and the action taken at a time t_k . The total cost J_0 of going from the stage 0 to stage N can be represented as:

$$J_0 = \sum_{k=0}^N C(\mathbf{x}_k, \mathbf{u}_k, \mathbf{w}_k) \quad (3.41)$$

in which C is a cost function which depends on the vector of states (\mathbf{x}_k), the vector of controlled inputs (\mathbf{u}_k), and the vector of disturbances (\mathbf{w}_k). The problem consists of finding the sequence of control operations (\mathbf{u}_k^*) that provides an optimum value J_0^* for the period under consideration:

$$J_0^* = \min(J_0) = \min\left(\sum_{k=0}^N C(\mathbf{x}_k, \mathbf{u}_k, \mathbf{w}_k)\right) \quad (3.42)$$

Finding J_0^* implies finding the optimal sequence of intermediate states \mathbf{x}_k^* . To solve this problem, dynamic programming makes use the principle of optimality (Bellman, 1957),

also known as the Bellman equation. It has been stated by Dreyfus & Law (1977) as follows:

“The best path from A to B has the property that, whatever the initial decision in A, the remaining path to B, starting from the next point after A, must be the best path from that point to B.”

This principle is useful for reducing the number of operations to determine optimal paths. Figure 3.9 illustrates this principle.

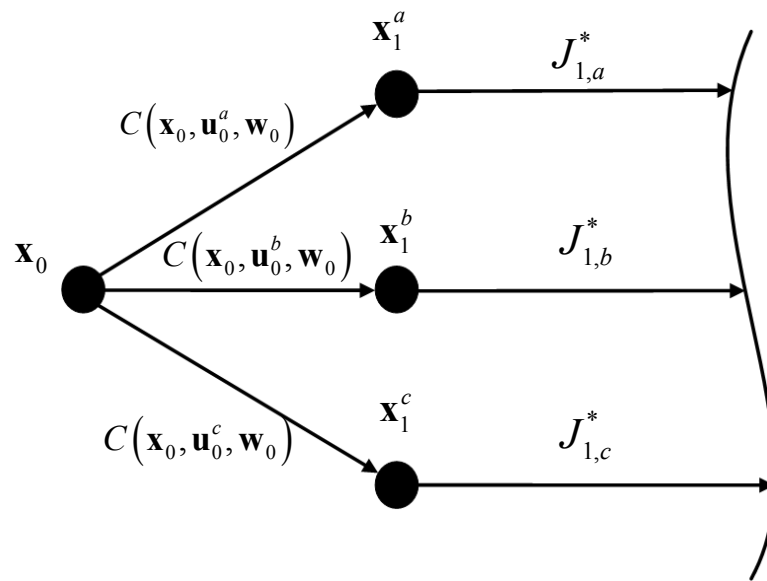


Figure 3.9. Principle of optimality: if the optimal path includes \mathbf{x}_1^a , then it has to contain the optimal path from \mathbf{x}_1^a until the end.

Let the initial state be \mathbf{x}_0 . Let us assume that there are only three possible states to be reached after the first control action: \mathbf{x}_1^a , \mathbf{x}_1^b and \mathbf{x}_1^c . Therefore, there are three possible

costs, namely $C_0(\mathbf{x}_0, \mathbf{u}_0^a, \mathbf{w}_0)$, $C_0(\mathbf{x}_0, \mathbf{u}_0^b, \mathbf{w}_0)$, $C_0(\mathbf{x}_0, \mathbf{u}_0^c, \mathbf{w}_0)$. If the optimal routes from each of these points are somehow known, then the optimum value can be found as:

$$J_0^* = \min \begin{pmatrix} C_0(\mathbf{x}_0, \mathbf{u}_0^a, \mathbf{w}_0) + J_{1,a}^* \\ C_0(\mathbf{x}_0, \mathbf{u}_0^b, \mathbf{w}_0) + J_{1,b}^* \\ C_0(\mathbf{x}_0, \mathbf{u}_0^c, \mathbf{w}_0) + J_{1,c}^* \end{pmatrix} \quad (3.43)$$

Generalizing,

$$J_0^* = \min(C_0(\mathbf{x}_0, \mathbf{u}_0, \mathbf{w}_0) + J_1) \quad (3.44)$$

The advantage of Equation (3.44) is that it defines a recurrence relationship that considerably reduces the number of calculations. The application of this principle is significantly more efficient than an exhaustive search. An example of the application of the dynamic programming algorithm is presented in Chapter 5.

4. Design and Control of a Solar House

4.1 The Alstonvale Net Zero House

The Alstonvale Net Zero House (ANZH) was developed within the framework of the aforementioned *EQuilibrium Initiative*. In keeping with the spirit of the competition, the ANZH was conceived to display advanced solar technologies, energy efficiency and environmentally friendly design, providing a comfortable and healthy environment for the occupants at a reasonable price. The Alstonvale project was selected among the twelve winners of *EQuilibrium* out of 72 submissions. Descriptions of the design of the Alstonvale House have been presented in (Candanedo *et al.*, 2007b; Candanedo & Athienitis, 2008b; Pogharian *et al.*, 2008).

The ANZH was a two-storey detached house (see Figure 4.1), located in the town of Hudson, a suburb of Montréal located 50 km west of the city centre. Considering the need for an integrated approach, the design of the ANZH was carried out through very close collaboration among different professionals: architects, engineers in different fields, and solar engineering experts, among others. Members of Concordia University, including the author of this thesis (who played a key role in the energy modeling), were members of this team.

This house has a number of features that make it especially appropriate as a case study for control strategies for a solar home:

- Passive solar design features
- Motorized curtains

- A building-integrated photovoltaic/thermal roof
- Active thermal energy storage
- Highly efficient appliances
- Use of a plug-in electric vehicle
- Advanced control systems



Figure 4.1. Alstonvale Net Zero House (January 2010).

4.2 Design Procedure and Building Simulation

The design of the house started with a “charrette” (October 2006), a guided brainstorming session in which several professionals including architects and engineers from different fields contribute ideas to the design of the building. The need for a high-quality building envelope and passive solar design was emphasized during this meeting. The basic architectural features of the house were then decided by the architect-builder.

Although there was agreement on the most desirable features of the house (large south facing windows, high levels of insulation and air-tightness, high levels of thermal mass), a detailed quantitative analysis was needed to decide on the optimal values of the main design and control parameters.

4.2.1 Preliminary Simulations

The software tool used for the preliminary analysis of the building's performance was HOT2000. This tool was also a requirement for the *EQuilibrium* competition.

As mentioned in Chapter 2, HOT2000 uses the bin method to calculate heating and cooling loads. HOT2000 treatment of thermal mass is relatively coarse: adjustment of heating loads is carried out by correction factors according to four different thermal mass levels, from “light construction, wood frame” to “very heavy, concrete” (this level was used in the simulations). HOT2000 cannot be used for dynamic simulations, and therefore it is not suitable for the evaluation of control strategies. Its capabilities for assessing the performance of renewable energy systems are also rather limited. For instance, numerous systems are not available (TES tank models, BIPV/T models, etc.), and the contributions of renewable are only accounted globally (for the entire year), rather than dynamically. Despite these limitations, HOT2000 gives a quick assessment of the quality of the building envelope, and it is adequate for parametric analysis of windows and walls.

The output of HOT2000 is used to calculate the EnerGuide Rating System for houses (ERS, previously known as EGH) according to the following equation:

$$ERS = 100 - 20 \left(\frac{\text{Annual Energy Consumption}}{\text{Reference}} \right) \quad (4.1)$$

in which the “Annual Energy Consumption” includes the energy used for heating, cooling, appliances, and lighting (either electric or fuel). Since the ERS was designed for all Canadian regions and all types of residential units, the “Reference” value in the denominator depends on the size of the house, the number of heating degree days (to account for climatic differences) and the primary heating method (either electricity or fuel). Details about the calculation of the reference value are presented in the appendix.

The EnerGuide rating was created for the R-2000 program (NRCan, 2005b). To qualify for the R-2000 label, the house has to reach an ERS value of 80. By introducing local energy generation, the *net* Annual Energy Consumption can then become zero and the corresponding ERS value of a net-zero energy home would then be 100.

4.2.1.1 HOT2000 climate data

The *Equilibrium* rules also required that the basic weather data available in HOT2000 would be used for the simulations. Some of the key variables available from the HOT2000 weather file are listed in Table 4.1 and 4.2.

Table 4.1. Degree-days and design temperatures corresponding to Montréal used by HOT2000 (HOT2000, 2003).

Annual heating degree days (18 °C)	4,471
Design heating temperature (°C)	-23
Avg. deep ground temperature (°C)	6.4
Design cooling dry bulb temp. (°C)	30
Design cooling wet bulb temp. (°C)	23

Table 4.2. Weather parameters corresponding to Montréal used by HOT2000 (monthly values) (HOT2000, 2003).

	Dry bulb (°C)	Wet bulb (°C)	Amplitude (°C)	St. Dev. (°C)	Wind speed (km/h)	Global hor. rad. (MJ/m ² /day)	South vert. rad. (MJ/m ² /day)
Jan	-10	-10.6	8.9	2.6	18.3	5.27	2.86
Feb	-8.8	-9.5	9.1	2.5	17.9	8.61	4.34
Mar	-2.4	-3.8	8.3	2	17.9	12.42	5.81
Apr	5.6	3	9.8	1.4	16.9	16.38	6.7
May	13.1	9.3	11.1	1.9	15.3	19.11	8.09
Jun	18.4	14.6	10.7	1.1	14.5	20.8	9.12
Jul	20.9	17	10.5	1.1	13.1	20.79	9.36
Aug	19.6	16.2	10.5	1.2	12.2	17.8	7.86
Sep	14.8	12.1	10.3	1.4	13.1	13.19	5.9
Oct	8.7	6.5	9.2	1.6	14.8	8.41	3.96
Nov	2.1	0.7	6.9	1.7	16.6	4.36	2.54
Dec	-6.8	-7.5	7.8	2.8	16.8	3.87	2.29
Ann	6.27	4	9.42	1.77	15.62	12.6	5.74

4.2.1.2 ERS rating for the building envelope

During the design of the Alstonvale House, HOT2000 was used primarily to select the level of insulation in the building envelope, the size of the windows and the awnings. In order to qualify for the *EQuilibrium* competition, it was necessary to show that the house could reach an ERS rating of 82 with a conventional heating system (i.e., without renewable energies). This requirement was introduced to guarantee high standards of quality for the building envelope.

To establish a baseline for the basic ERS rating, the simulation had to be run with a number of pre-set values established in the rules of the competition.

Table 4.3 presents the values of these parameters:

Table 4.3. Parameters used by HOT2000 as standard operating conditions (CMHC, 2006a).

Main floor heating set point (°C)	21
Basement heated	Yes
Basement cooled	No
Basement set point (°C)	19
Basement separate thermostat	No
Allowable daily temperature rise Medium	2.8
Interior loads, lighting (kWh/day)	3
Interior loads, appliances (kWh/day)	14
Interior loads, other (kWh/day)	3
Average exterior use [including dryer] (kWh/day)	4
Hot water load (L/day)	225
Hot water temperature (°C)	55
Fraction of internal gains in basement	0.15
Adult occupants	2, at home 50% of time
Child occupants	2, at home 50% of time
Terrain, building site	Suburban, Forest
Local shielding, walls	Very Heavy
Local shielding, flue	Light local shielding
Ventilation ac/h (natural plus mechanical)	0.3
Ventilation sizing including HRV	As per CSA Standard F326

Simulations indicated that diminishing returns appear when adding more insulation in the walls of the house. Infiltration and heat loss through the fenestration became more important. This has important economical repercussions: financial resources that would otherwise be used for the insulation can then be invested, for example, in renewable energy systems. The ERS rating for different levels of insulation is given in Table 4.4.

Table 4.4. Space heating and DHW loads, and corresponding ERS Rating. Basic HOT2000 default values applied without renewable energy systems.

Average Wall Insulation (R-value) [h·°F·ft²/BTU]	Space Heating + DHW [MJ]	ERS Rating
32	42,686.73	85
40	39,950.97	85
50	37,477.30	86
51	37,267.19	86

The requirements of the competition indicated the need to show whether mechanical cooling was needed. In order to have a quantitative criterion, it was requested that the HOT2000 simulations show that the annual cooling load was below 1500 MJ (416.7 kWh), for a cooling set-point of 25.6 °C. The size of the awnings was adjusted until this prerequisite was met.

Table 4.5 presents the final main parameters chosen for the building envelope and other key facts of the house layout.

Table 4.5. Relevant parameters of the house layout and building envelope.

Component/Detail	Parameter value	Comments
Habitable area, main floor	84 m ²	
Habitable area, upper floor	112 m ²	
Garage	50 m ²	
Basement/mech. room	28 m ²	
Average wall insulation	R32	Québec code requires R20
Average insulation under floor slab	R26	
Average ceiling insulation	R68	
Window R-value	R7	Triple-glazed, two low emissivity coatings, argon-filled.
Solar heat gain coefficient	0.57	
Visible transmittance	65.2%	
Total solar transmittance	45.5%	
South-facing windows	50 m ²	
Window-to-wall ratio (south façade)	42%	
East windows	10 m ²	
West windows	2.5 m ²	
North windows	0 m ²	No windows on north side
Concrete floor thickness (main floor)	6 in (15 cm)	
Concrete floor thickness (upper floor)	2.5 in (6.35 cm)	

In summary, the Alstonvale Net Zero House design includes a high-performance, air-tight building envelope, triple-glazed south-facing windows (about 40% of the south façade) and heavy thermal mass (6-inch concrete floors, a masonry wall) designed for the storage of solar heat gains. Overhangs of appropriate size were intended to protect the house from excessive solar radiation during the summer, thus preventing overheating.

Another relevant detail of the house is a motorized solar chimney, facing east, which can be opened during the summer to enhance natural convection in order to remove warm air from the house.

4.2.1.3 Reduction of electric energy and hot water use

The ERS rating presented in Equation 4.1 can be modified to account for the *Net Annual Energy Consumption* on the numerator. This value can be reduced in two ways: (a) by reducing energy consumption or (b) by introducing renewable energy generation.

Energy accounted for 40 points in the competition (out of 100). Although the net-zero energy target was not mandatory, the scoring system strongly favoured approaching or achieving it (Figure 4.2). For example, an ERS Rating of 94 meant that the house would receive a score of 38 in the energy category. Achieving net-zero (ERS = 100) meant that it would receive full marks (100% = 40 points) in this category. The use of renewable energy systems was necessary to reach the net-zero goal. As the capabilities of HOT2000 for simulating renewable energy systems are rather limited, it was strongly recommended to present supporting simulations with other software tools. RETScreen was the tool suggested for estimating the output of PV and solar thermal systems.

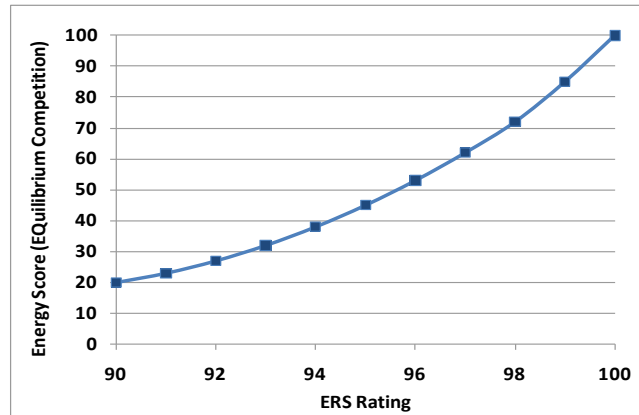


Figure 4.2. Scoring system in the energy category as a function of ERS rating. Adapted from (CMHC, 2006a).

Lowering the energy used by hot water, lighting, appliances and plug-loads was a necessary step. However, in order to avoid unrealistic assumptions, regulations were put in place by the organizers to guarantee comfortable conditions for the building occupants without dramatic changes in their lifestyle. As stated in one of the documents issued by CMHC: “...*This constitutes designing people rather than houses, and is not allowed*” (CMHC, 2006b). Although the author of this thesis does not concur with some of these rules (e.g., no clotheslines were allowed), this approach was necessary to guarantee reasonable solutions.

Each of the assumptions of reduced energy consumption had to be justified by the design team. A minimum value was also prescribed by the organizers for lighting energy consumption (1 kWh/day).

The energy consumed by major appliances was estimated at 3.93 kWh/day (or 1435 kWh/year), a significant reduction from the 14 kWh/day used by default in Table 4.3. This reduction was achieved by selecting highly-efficient equipment, with EnergyStar®

labels. Table 4.6 shows the rated annual energy consumption values of these appliances (the dryer was included in a different category).

Table 4.6. Energy use of major appliances. Adapted from Pogharian (2007).

Appliances	Annual Energy Consumption (kWh)
Dishwasher	194
Oven	208
Cooktop	117
Refrigerator	430
Washing machine	125
Freezer	361
TOTAL	1,435

A value of 3 kWh/day was used for other internal loads. This assumption is justified based on the values presented in Table 4.7.

Table 4.7. Energy use of minor appliances. Adapted from Pogharian (2007).

Appliance	Power (W)	Units	minutes/day	kWh/day
Hair dryer	1,850	1	3	0.09
Microwave	1,460	1	10	0.24
Toaster	1,600	1	10	0.27
Coffemaker	980	1	30	0.49
Other kitchen appliances	1,000	1	2	0.03
Computer	350	2	90	1.05
Computer monitor	60	2	90	0.18
TV	110	1	120	0.22
DVD player	30	1	60	0.03
Stereo	40	1	180	0.12
TOTAL				2.73

It was considered that the value of 1 kWh/day for internal lighting could easily be achieved by using 15 fluorescent light bulbs (13 W each) during 5 hours per day. Finally, by using a highly efficient dryer (385 kWh/year) and fluorescent lighting for exterior luminaires, a value of 1.3 kWh/day can be achieved. The dryer is considered an “exterior” load as most of its heat is released to the outdoor environment and therefore does not contribute to the internal heat gains.

In summary, the values employed for electrical energy use were: 3.93 kWh/day for major internal appliances, 1 kWh/day for lighting, 3 kWh/day for other appliances and 1.3 kWh/day for exterior appliances.

Hot water usage can also be significantly reduced by using showers with low-flow nozzles, faucets with aerators, and appliances with low water consumption. The energy consumed by the hot water system can be further reduced by employing a drain heat recovery system (Powerpipe™). It was estimated that the hot water needs of the house could be reduced from 225 L/day to 125 L/day at 55 °C.

4.2.1.4 HOT2000 simulations: preliminary energy estimates

The simulations were carried out by assuming that the main heating system was an air-source heat pump with an average COP of 4.0 and a very low cut-off temperature (-20 °C), and the backup system was an electric furnace. The reason for assuming such a high COP value is explained in the next section. Two evacuated-tube solar collector systems (with a combined annual output of 24,800 MJ) satisfied the large majority of the DHW needs.

The space heating needs of the house were estimated to be about 23,000 MJ (21.8 x 10⁶ BTU), with a peak heating load 12 kW at -23°C.

Table 4.8 presents a summary of the electric energy usage in the house. From these values it was then estimated that a photovoltaic system generating about 7 MWh per year would offset the house energy use.

Table 4.8. Estimated annual electric energy consumption (kWh).

Appliances and lighting	3,370
Ventilation Fans	790
Electricity used for heating	2,920
Domestic water heating	140
TOTAL	7,220

4.2.1.5 First RETScreen Calculations

Calculations were carried out with RETScreen (RETScreen, 2008) to estimate the production of 32 polycrystalline PV panels (arranged in two rows, see Figure 4.3), each with a nominal power output of 175 W (total 5.6 kW) under Montréal weather conditions. For a perfectly due-South azimuth angle and an inclination of 45°, the energy output is about 6.9 MWh (Figure 4.4), which practically satisfies the estimated electric energy use (only 300 kWh short).

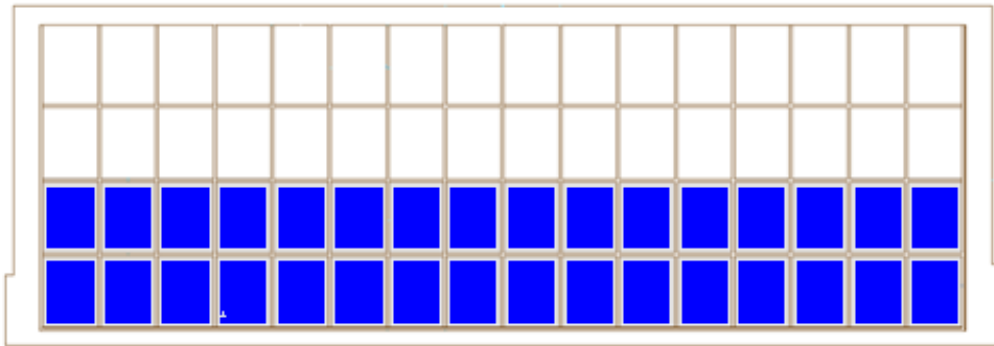


Figure 4.3. First roof configuration (PV panels in blue, glass panels in white).

RETScreen® Energy Model - Photovoltaic Project		Training & Support	
Site Conditions		Estimate	Notes/Range
Project name		Alstonvale Project	See Online Manual
Project location		Hudson, QC	
Nearest location for weather data	-	Montreal, QC	→ Complete SR&SL sheet
Latitude of project location	°N	45.5	-90.0 to 90.0
Annual solar radiation (tilted surface)	MWh/m²	1.44	
Annual average temperature	°C	6.1	-20.0 to 30.0
System Characteristics		Estimate	Notes/Range
Application type	-	On-grid	
Grid type	-	Central-grid	
PV energy absorption rate	%	100.0%	
PV Array			
PV module type	-	poly-Si	
PV module manufacturer / model #		Day4	See Product Database
Nominal PV module efficiency	%	13.2%	4.0% to 15.0%
NOCT	°C	45	40 to 55
PV temperature coefficient	% / °C	0.40%	0.10% to 0.50%
Miscellaneous PV array losses	%	5.0%	0.0% to 20.0%
Nominal PV array power	kWp	5.60	
PV array area	m²	42.4	
Power Conditioning			
Average inverter efficiency	%	90%	80% to 95%
Suggested inverter (DC to AC) capacity	kW (AC)	5.0	
Inverter capacity	kW (AC)	6.0	
Miscellaneous power conditioning losses	%	0%	0% to 10%
Annual Energy Production (12.00 months analysed)		Estimate	Notes/Range
Specific yield	kWh/m²	161.9	
Overall PV system efficiency	%	11.2%	
PV system capacity factor	%	14.0%	
Renewable energy collected	MWh	7.631	
Renewable energy delivered	MWh	6.868	
	kWh	6,868	
Excess RE available	MWh	0.000	Complete Cost Analysis sheet
Version 3.2		© Minister of Natural Resources Canada 1997 - 2005.	NRCan/CETC - Varennes

Figure 4.4. Energy output for Montréal of a 5.6 kW PV system.

A section of glass panels over an absorber plate, located above the PV modules, was intended for thermal energy recovery (details explained in Section 4.3).

4.2.2 Dynamic Simulation of Thermal Phenomena

Considering the limitations of HOT2000 (e.g., bin method, lack of a proper thermal mass model, numbers reported monthly, etc.), dynamic simulations were necessary in order to evaluate the performance of the renewable energy systems and the effect of control strategies.

The dynamic simulations of the Alstonvale House were developed first in Mathcad (Mathsoft, 2001), a mathematical programming tool, then in MATLAB M-files, and finally in MATLAB/Simulink. All of these implementations are based on the use of thermal network analogies and a fully explicit finite difference method scheme.

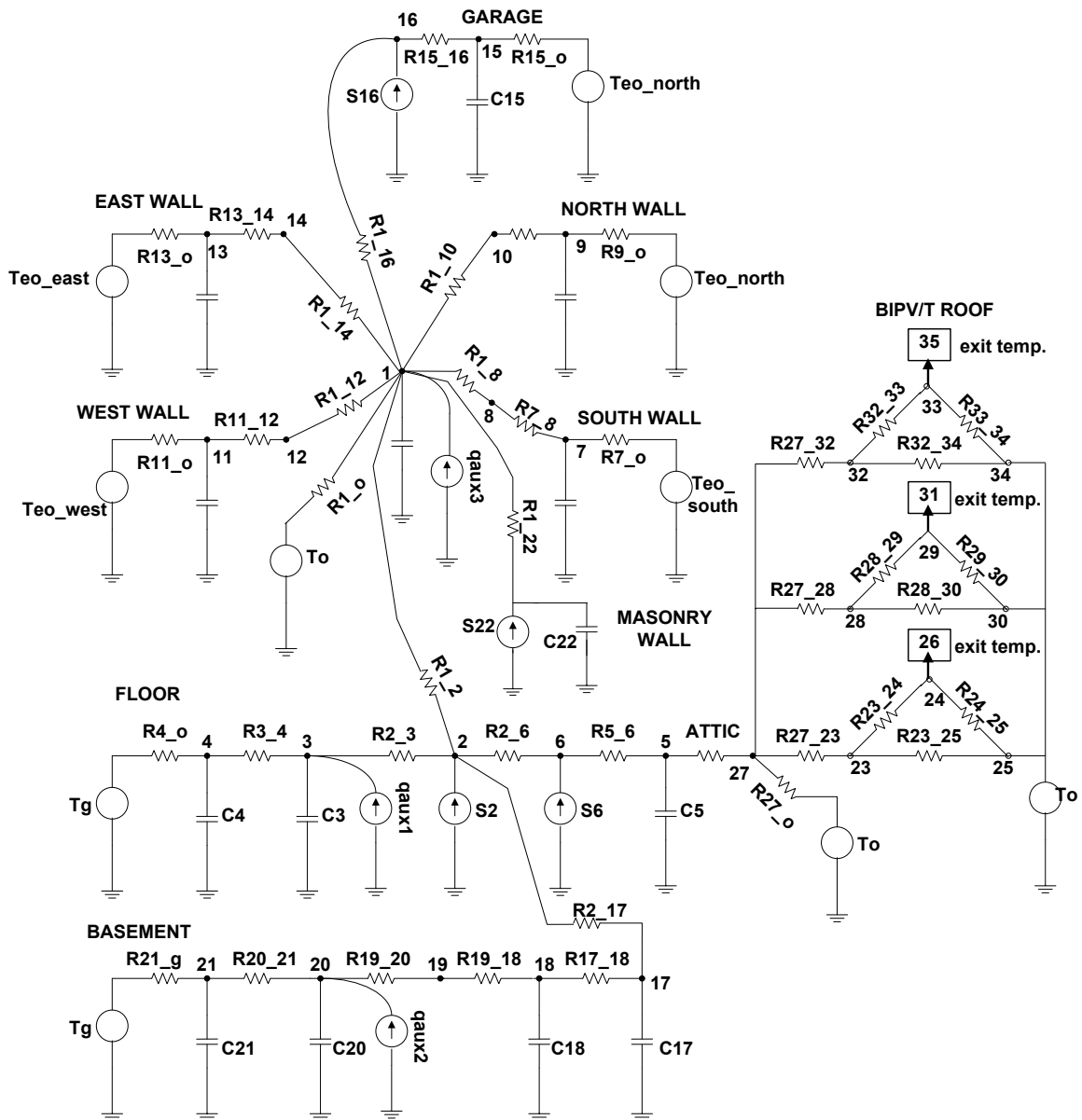


Figure 4.5. Thermal network used in the preliminary dynamic simulations of the Alstonvale Net Zero House. Resistances corresponding to radiation exchange between the surfaces are not shown.

The first dynamic simulations –the ones supplied in the report submitted to CMHC–, were carried out in Mathcad. Hourly data for a year (8760 hours), obtained from a TMY2 (meteorological file) for Montréal were used. Beam radiation and diffuse horizontal radiation were used –along with astronomical calculations for the solar angles– to calculate solar irradiance on the surfaces of interest (namely, the façades of the house and its two roofs) by applying an implementation of the Perez model (Perez *et al.*, 1990) developed by the author of this thesis. The time step used for the simulations was 150 s.

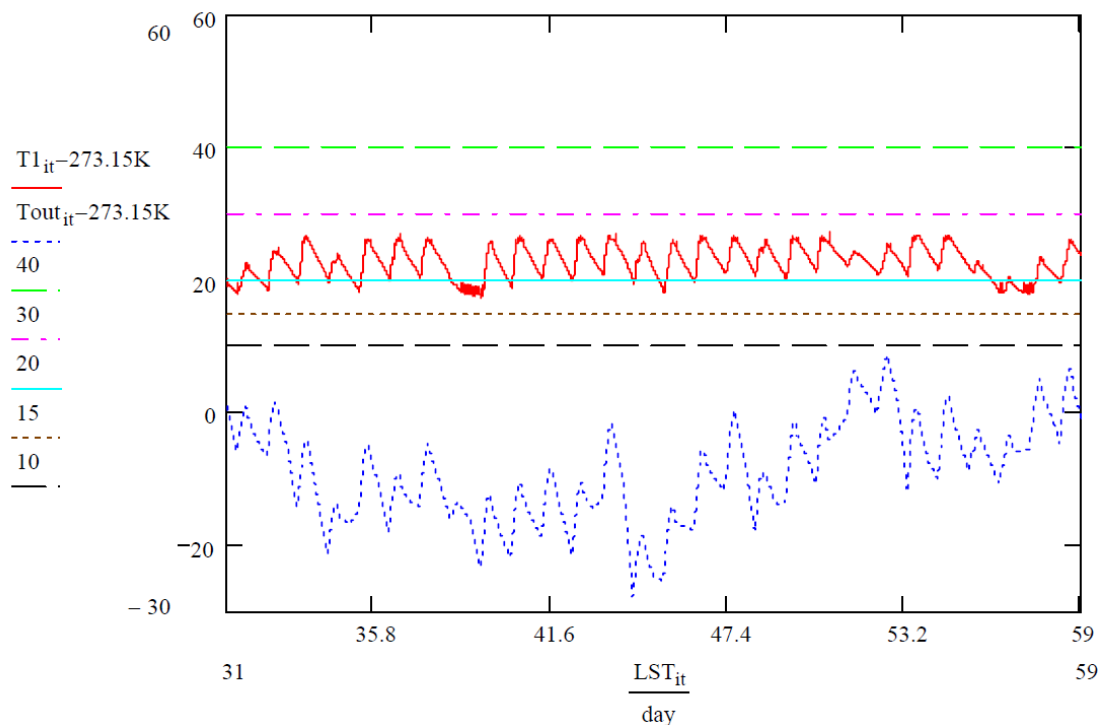


Figure 4.6. Typical results obtained with the Mathcad model.

At a later stage, a decision was made to use MATLAB as a dynamic simulation tool, first through M-files, and then with Simulink (MATLAB’s graphical interface for dynamic simulation and control). A typical implementation of an equation in an M-file is shown below (see the appendix for the complete code):

```

%%%%%%%%%%%%%%%%%%%%%%%%%%%%%%%%%%%%%%%%%%%%%%%%%%%%%%%%%%%%%%%%%%%%%%%%
T(1,i+1)= T(1,i) + (dt/CAP(1))*((T(2,i)-T(1,i))/R(1,2) +...
+ (T(6,i)-T(1,i))/R(1,6) + (T(8,i)-T(1,i))/R(1,8) +...
(T(10,i)-T(1,i))/R(1,10) + (T(12,i)-T(1,i))/R(1,12) +...
(T(14,i)-T(1,i))/R(1,14) + (T(16,i) -T(1,i))/R(1,16) +...
+ (Temp(j(i))-T(1,i))/R1_OUT +...
+ (T(22,i)-T(1,i))/R(1,22) + qaux3(i)); %Node1 AIR

```

Figure 4.7. shows a typical representation of MATLAB/Simulink of a node equation.

Other details about the Simulink model are presented in the appendix.

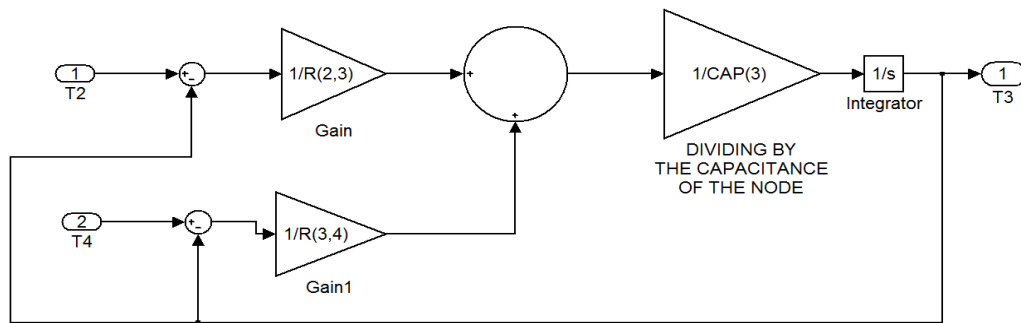


Figure 4.7. Typical node equation in a Simulink representation.

The numbers obtained with the Simulink model compared relatively well with the results obtained in HOT2000 (Table 4.9), which confirmed that this model could be used for control studies. The largest difference (December), may be attributable to differences in the weather data used. December is particularly cloudy in Montréal, a fact that has an significant impact on the heating load, and which may be handled better in a dynamic simulation. The peak heating load estimated with Simulink was about 9-10 kW, compared with about 12 kW as estimated with the steady-state calculation of HOT2000.

Table 4.9. Comparison between the Simulink and HOT200 models, heating energy from December through March (Candanedo & Athienitis, 2010a).

	Simulink Model, MJ (kBTU)	HOT2000, MJ (kBTU)
December	9254 (8771)	6633 (6287)
January	5769 (5468)	6276 (5949)
February	5096 (4830)	4056 (3844)
March	2952 (2798)	2178 (2064)

MATLAB/Simulink has been increasingly used in recent years in building simulation because of the flexibility that it provides in prototyping control strategies (Hudson & Underwood, 1999; Kummert *et al.*, 2001; Riederer, 2005; van Schijndel & Hensen, 2005; Yu & Dexter, 2009). MATLAB/Simulink was also the tool chosen for the core of the research presented in this thesis. Selecting the right tool was an essential decision. Some of the advantages of MATLAB/Simulink that were taken into consideration were its general programming capabilities, the relative ease of implementation of new renewable energy technologies, and its focus on controls (not necessarily building controls) with “toolboxes” for system identification, model predictive control, signal processing, etc.

4.2.3 Addition of Electric Vehicle and Roof Design Modifications

Taking into consideration the significant fraction of worldwide energy use attributable to transportation of people and goods, as well as to food production, Sevag Pogharian, the leader of the Alstonvale project, decided to go beyond the original goals of the project by including both factors into the original design (Pogharian *et al.*, 2008). Consequently, additional generation capacity was added for an electric vehicle. The car selected for this project was the ZENN: this car, designated as a neighbourhood vehicle, has a maximum speed of 40 km/h, and a range of about 50-80 km per charge (ZENN, 2008). If the car is charged three times per week, and assuming 10 kWh per charge, the total energy needed would be 1,500 kWh. For this reason, eight additional photovoltaic modules were added to the roof (Figure 4.8.) in order to increase the nominal capacity of the system by 1.4 kW to a total of 7.0 kW. It was estimated that this change could raise the annual energy output of the roof by 1,600-1,700 kWh.

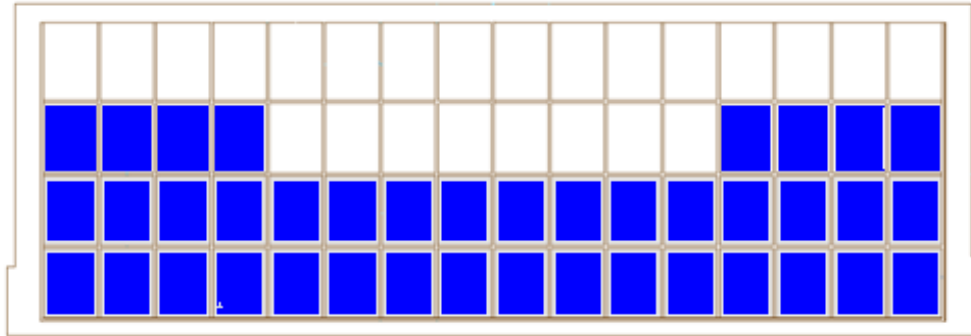


Figure 4.8. Second roof configuration (8 additional PV modules, for a total of 40).

Finally, partly due to aesthetic considerations, and partly to account for the influence of unknowns such as snow accumulation and equipment breakdowns, eight more panels were added to the roof (Figure 4.9), for a total of 48 PV panels with a nominal output of 8.4 kW. The estimated annual output in this case is 10,400 kWh.

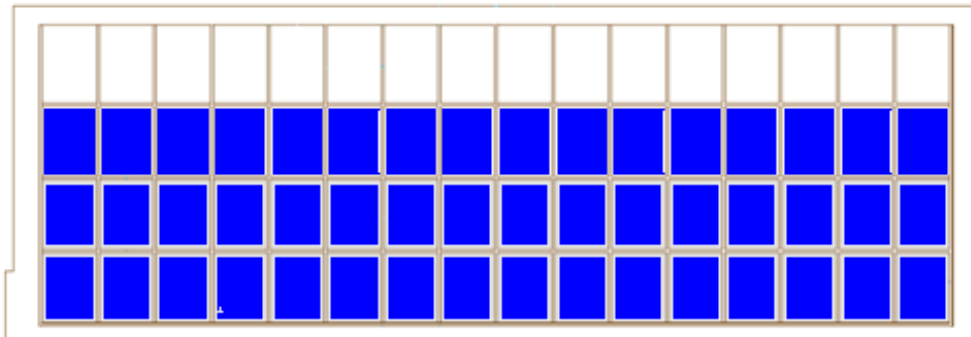


Figure 4.9. Final roof configuration with 48 PV modules.

4.3 Heating System

4.3.1 BIPV/T Roof

4.3.1.1 Description and Basic Principle of Operation

Apart from the heat provided by passive solar heat gains, the main heat source of the Alstonvale House was its BIPV/T roof (Figure 4.10). Table 4.10 summarizes some key parameters of the BIPV/T roof, in its final configuration.



Figure 4.10. BIPV/T roof of the ANZH.

Table 4.10. Parameters of BIPV/T roof in the ANZH.

Width of the roof	18.5 m
Length (streamwise)	5.7 m
Approximate area	105 m ²
Slope	45°
Azimuth	0° (due South)
Number of PV modules	48
Voltage (MPP)	23.5 V
Current	7.5 A
Nominal power	175 W
Nominal electric power (total)	8.4 kW
Number of glass modules	16
Estimated thermal output	20-25 kW

A large south-facing roof was designed for collection of thermal and electric energy. Figure 4.11 illustrates the principle of operation of the BIPV/T system. Outdoor air is taken near the edge of the roof, and is drawn under the PV panels with a variable speed fan. As it moves upwards, the air stream removes heat from the PV panels, and its temperature increases. The glazing section significantly increases the air temperature, since most of the solar radiation passes through the glass and impinges on the absorber plate underneath.

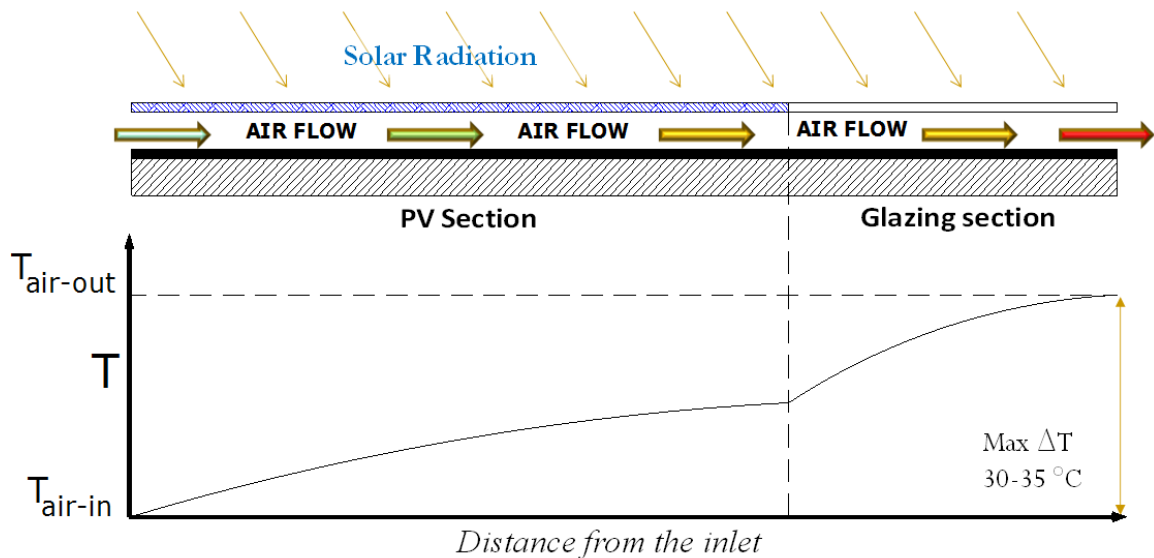


Figure 4.11. Principle of operation of the BIPV/T Roof.

As mentioned above, in the first configuration, half the roof was covered with PV panels, and the other half with glass panels. Adding more PV panels to increase the electric energy output for an electric car implied a reduction in the thermal energy output, since the glazing section was reduced by half. To compensate for this effect, it was decided to include a low-emissivity surface for the absorber plate underneath the glazing section (Figure 4.12). The product used for the absorber plate was TiNOX[®], with a rated infrared emissivity of 4% (TiNOX, 2010). While this implied a relatively minor

additional cost, it was largely beneficial for the thermal performance of the system and nearly offset the detrimental effect of reducing the glazing area.



Figure 4.12. Low-emissivity absorber plate (TiNOX).

4.3.1.2 BIPV/T System Modeling

Figure 4.13 shows a conceptual representation of the code used in the calculation of the BIPV/T outlet temperature, which depends on several input variables. As a simplifying assumption, thermal capacitance effects in the roof were neglected (i.e., the outlet temperature at a given time t depends only on the conditions at that time).

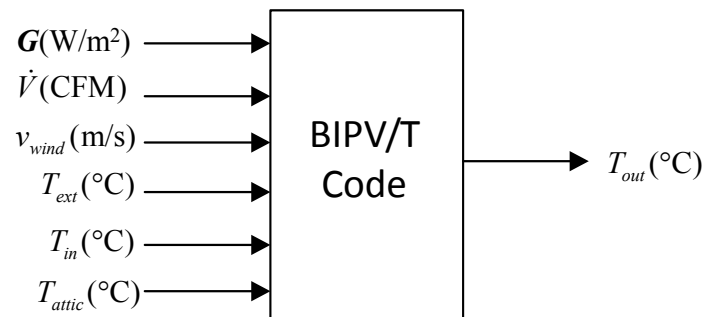


Figure 4.13. Conceptual representation of the code used for the BIPV/T system.

In order to model the system, the roof was divided into several one-dimensional control volumes in the streamwise direction (Figure 4.14). An energy balance was then performed for each control volume. This approach (i.e., to divide the roof into several sections, usually not more than five or six) is the customary procedure when modeling the output of a BIPV/T roof (Bazilian *et al.*, 2001; Candanedo (L.) *et al.*, 2010a; Candanedo (L.) *et al.*, 2010b). The exit temperature of each control volume is the inlet temperature used in the following control volume. Each control volume spans the entire width of the roof (w_{PV}). The length of each control volume in the streamwise direction is L_{CV} . An energy balance equation is written for three nodes in each control volume: the PV panel, the air in the channel and the bottom of the channel. The three equations are:

$$(T_{PV} - T_{ext})h_o + (T_{PV} - T_{bot})h_r + (T_{PV} - T_{ma})h_{ct} + P_{elec} = \alpha G \quad (4.2)$$

$$(T_{ma} - T_{PV})h_{ct} + (T_{ma} - T_{bot})h_{cb} + q_{rem} = 0 \quad (4.3)$$

$$\frac{(T_{bot} - T_{attic})}{R_{ins}} + (T_{bot} - T_{ma})h_{cb} + (T_{bot} - T_{PV})h_r = 0 \quad (4.4)$$

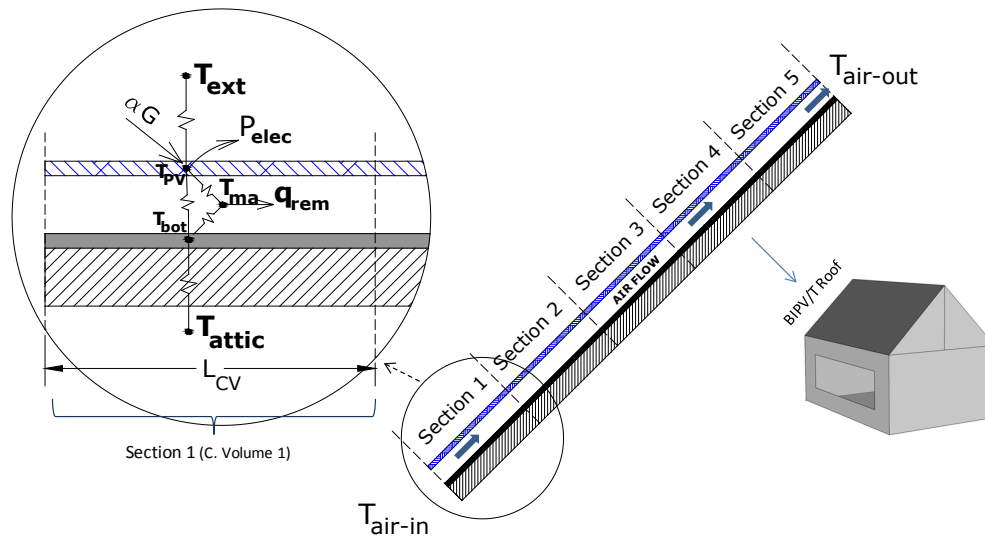


Figure 4.14. Modeling of the BIPV/T roof.

For the glazing section, one term is added in Equation 4.4 to account for the solar radiation passing through the glass:

$$\frac{(T_{bot} - T_{attic})}{R_{ins}} + (T_{bot} - T_{ma})h_{cb} + (T_{bot} - T_{PV})h_r + \alpha_{AB}\tau_g G = 0 \quad (4.5)$$

The equations above are solved iteratively until a convergence criterion is satisfied (less than 0.1% of difference between the values obtained in consecutive iteration).

Within each iteration, the following additional variables are calculated:

- The heat removed by the air flow (q_{rem})

$$q_{rem} = \dot{V}_{air} \rho_{air} c_{p-air} (T_{af} - T_{ai}) = \dot{m}_{air} c_{p-air} (T_{af} - T_{ai}) \quad (4.6)$$

- The average air temperature within the control volume (T_{ma})

$$T_{ma} = \frac{1}{L_{CV}} \int_0^{L_{CV}} \frac{h_{ct} T_{PV} + h_{cb} T_{bot}}{h_{ct} + h_{cb}} + \left(T_{ai} - \frac{h_{ct} T_{PV} + h_{cb} T_{bot}}{h_{ct} + h_{cb}} \right) e^{-\frac{w_{PV}(h_{ct} + h_{cb})t}{\dot{m}_{air} c_{p-air}}} dt \quad (4.7)$$

- The electrical efficiency (η_e) as a function of the PV temperature

$$\eta_e = 0.126 - 0.00055(T_{PV} - T_{STC}) \quad (4.8)$$

- The electric power output (P_{elec})

$$P_{elec} = \eta_e \alpha G \quad (4.9)$$

- A linearized radiative heat transfer coefficient (h_r).

$$h_r = \frac{4\sigma}{\frac{1}{\varepsilon_b} + \frac{1}{\varepsilon_t} - 1} \left(\frac{T_{PV} + T_{bot}}{2} \right)^3 \quad (4.10)$$

In Equation 4.2, the McAdams formula (McAdams, 1954) was used for calculating the exterior heat transfer coefficient (h_o):

$$h_o = 5.7 + 3.8v_{wind} \quad (4.11)$$

in which the wind speed is given in m/s and the heat transfer coefficient in $\text{Wm}^{-2}\text{K}^{-1}$. The determination of the convective heat transfer coefficients h_{cb} and h_{ct} used in Equations 4.2 through 4.5 is a complex issue. These factors depend on details such as the framing of the BIPV/T roof, the air flow rate, entrance effects, among many others. Considerable research effort on the determination of these coefficients in BIPV/T systems has been carried out at Concordia University. For this investigation, convection heat transfer values, similar to the ones measured in other demonstration projects, such as the ÉcoTerra house (Chen *et al.*, 2010a; Doiron, 2011) and experimental facilities, were used, typically between 7 to $12 \text{ Wm}^{-2}\text{K}^{-1}$. Figure 4.15 shows the simulated temperature rise in the BIPV/T roof for three different wind speeds (3, 5 and 7 m/s). It is clear from this picture that the wind speed has an important effect on the performance of the BIPV/T system. For the conditions considered in this example, the temperature rise is between 23.6 and 30.5 °C between the inlet and outlet.

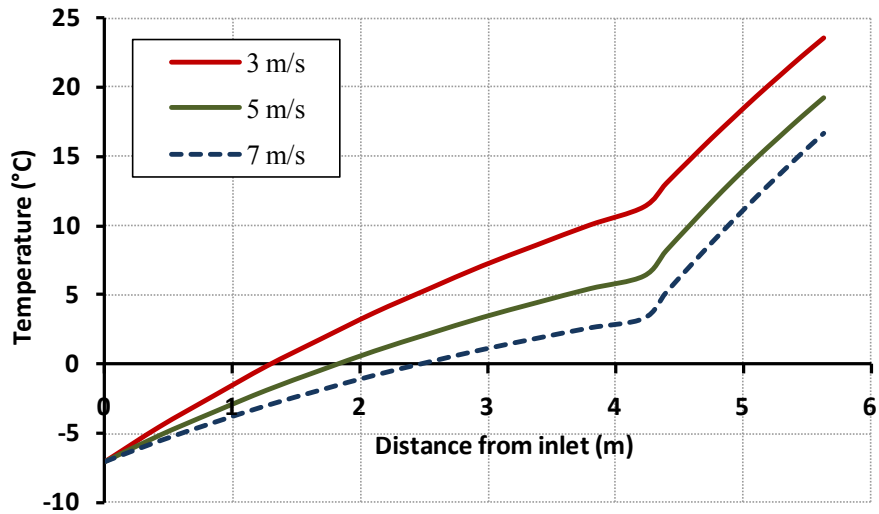


Figure 4.15. Temperature change as a function of distance from inlet in the Alstonvale BIPV/T roof for different wind speeds. Irradiance = 900 W/m², Outdoor temperature = -10°C, air flow rate = 1300 CFM, attic temp. = 10 °C.

A variable speed fan can be used to change the air flow rate in the channel. Figure 4.16 shows the BIPV/T exit temperature for three different flow rates. As expected, lower air flow rates permit reaching higher exit temperatures (up to 30 °C higher than the inlet).

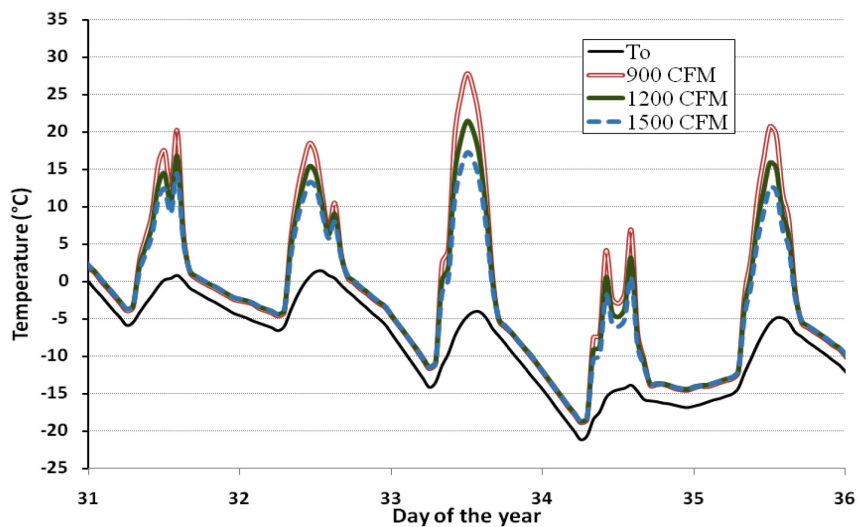


Figure 4.16. Outdoor dry-bulb temperature and BIPV/T exit temperatures for different flow rates. Montréal TMY2 weather file.

Despite lower exit temperatures, higher flow rates have a higher heat carrying capacity and thus remove thermal energy from the BIPV/T roof more efficiently (Table 4.11). The selection of an air flow rate depends on factors, such as the intended application and the operating range of the equipment (e.g., heat pumps).

Table 4.11. Heat capacity rates, temperature rises and heat removed for different flow rate conditions at noon, Feb. 5th (35th day of the year).

Flow rate (CFM)	C_{air} (W/K)	ΔT (K)	Heat removed (kW)
900	509.7	32.6	16.6
1200	679.6	26.2	17.8
1500	849.5	22.0	18.7

4.3.2 Solar-Assisted Heat Pump System and TES Tank

In spite of the significant temperature rise achievable with the BIPV/T system, the temperature of the exit air is often not high enough for its direct use for space heating in the house. A heat pump is used to raise the quality of the collected heat.

On the other hand, when high solar radiation levels allow the use of the BIPV/T system for energy recovery, solar gains can completely satisfy the space heating needs of the house. In other words, the energy collected by the BIPV/T is not intended to be used immediately. It is therefore necessary to store the thermal energy recovered from the roof, so it can be used later. A concrete tank, able to store 4500 L of water, was built to be used as a thermal energy storage (TES) device (Figure 4.17).



Figure 4.17. TES Tank (before insulation was applied).

This tank size was selected in order to store one day's worth of heating: if the average heating load of the house is assumed to be about 6-7 kW, then the required amount of energy for a 24-hr period would be about 144-168 kWh. If the temperature of the tank is allowed to fluctuate over a 30 °C range, the required volume is between 4.1 and 4.8 m³. Tank sizing is a non-trivial issue. In this case, the period of storage (i.e., one day's worth of heating) was chosen considering that this was approximately the amount of heat that could be collected during one sunny day. Moreover, this tank size could be reasonably fit into the basement of a typical house.^{††}

An air-to-water heat exchanger was installed in the ceiling of the garage to transfer thermal energy from the BIPV/T air to the mechanical system. This heat exchanger has the capacity to remove up to 20 kW of thermal energy (see the appendix for more details on the heat exchanger). Two parallel ducts coming from the roof of the house bring the stream of hot air from the roof to the heat exchanger, as shown in Figure 4.18.

^{††} Research on TES tank sizing could investigate, for example, the likelihood of having a sequence of a given number of sunny days, followed by another sequence of cloudy days.

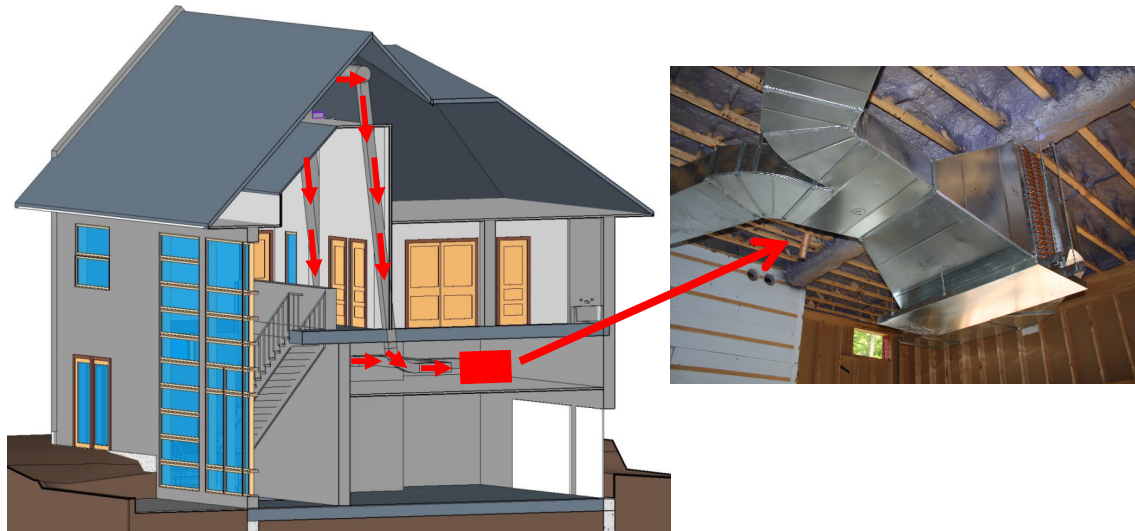


Figure 4.18. Left: ducting system used to bring hot air to the heat exchanger (drawing courtesy of Kwang-Wook Park). Right: air-to-water heat exchanger.

The TES tank could be charged in four ways, mainly depending on the temperature of the BIPV/T air.

1. **Mode A: Direct charge with heat exchanger.** When the BIPV/T air temperature is significantly hotter (e.g., 5 °C) than the temperature of the bottom of the TES tank, the heat can be sent directly to it by using a heat exchanger.
2. **Mode B: BIPV/T air with two heat pumps (or two stages).** For lower temperatures, then the BIPV/T air is used as the source of two heat pumps.
3. **Mode C: BIPV/T air with a single heat pump (or single stage).** For even lower temperatures, the BIPV/T air is used as the source of only **one** heat pump.
4. **Mode D: One heat pump with a ground source.** A ground source heat pump loop will be used as the backup system when the temperature of the BIPV/T air is not high enough for the heat pumps. The ground source loop replaces a previously considered backup system consisting of a wood pellet boiler.

Figure 4.19 summarizes conceptually the four modes of operation.

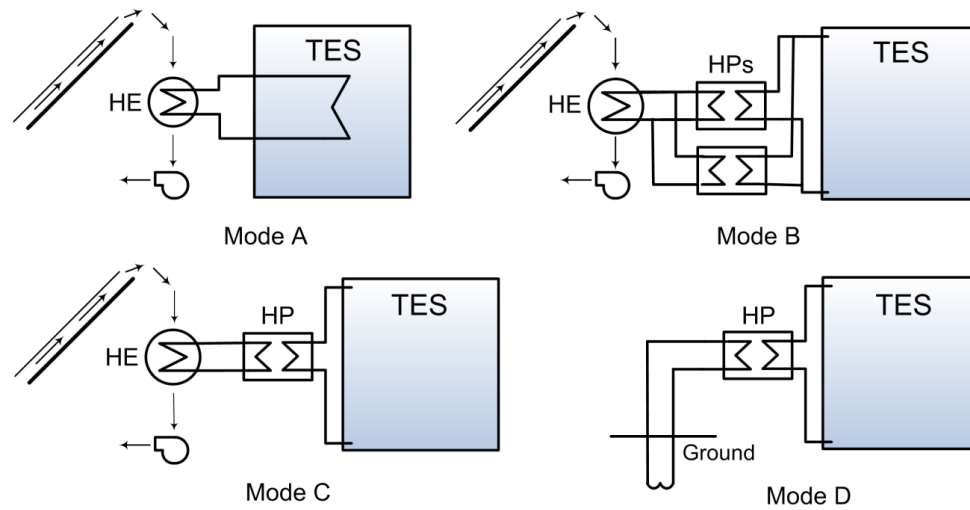


Figure 4.19. The four charging modes for the TES tank.

The heat stored in the TES reservoir is delivered to the house through a hydronic radiant floor heating (RFH) system. This system is expected to improve the thermal comfort of the occupants of the house, and to extend the use of the concrete floor as a heat storage device. Twelve heating zones were planned for the RFH system (see Figure A.3 and Figure A.4 in the appendix). The RFH system was designed with an electronic manifold, intended to regulate the supply water temperature (and thus the delivered heat) according to the commands from the supervisory system, by mixing the return water from the RFH with the water coming from the tank.

The decision to use an air-to-water heat exchanger linked to two heat pumps, instead of a commercial air-source heat pump system, was based on two factors: (a) the possibility of operating in Mode A (i.e., bypassing the heat pumps); (b) the need to work with variable and relatively low air flow rates.

The selection procedure of the heat pump system is described in detail by Candanedo & Athienitis (2008b). A brief outline is presented below.

As previously discussed, the exit temperature of the BIPV/T can be found for a set of values of solar radiation, outdoor temperature, wind speed and air flow rate. With this information, and manufacturers' data on the heat exchanger and the heat pump, it is possible to determine the operating point of the equipment. Figure 4.20 shows a conceptual representation of the group formed by the heat exchanger, heat pump and TES tank. Heat pump manufacturers usually provide the specifications sheets based on temperatures and flow rates on the source side (evaporator side), as well as temperatures and flow rates for the sink or load side (condenser side).

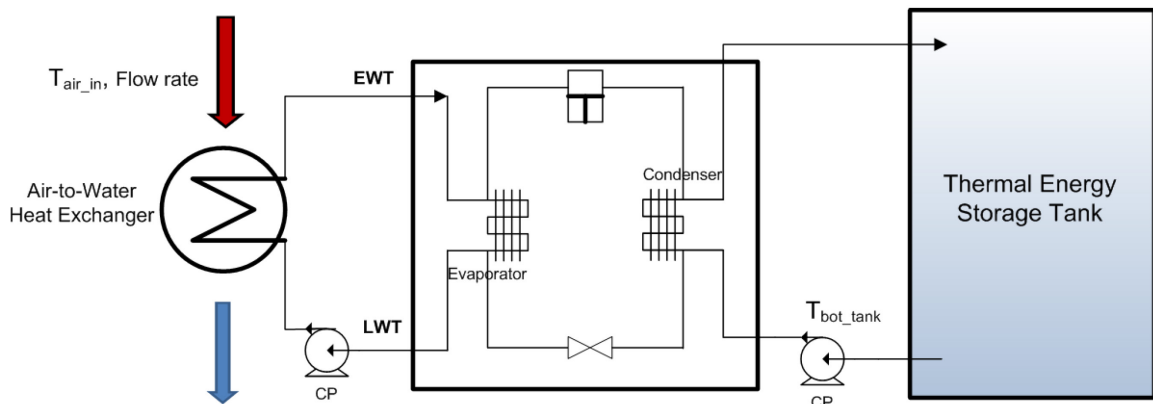


Figure 4.20. Heat exchanger-heat pump-TES tank group.

4.3.2.1 Determination of heat pump/heat exchanger operating point

Assuming that flow rates on both sides are kept constant, the heat extracted (Q_{rem}) by the heat pump at the evaporator side is given as a function of the entering water-glycol temperature (EWT) on the evaporator side and the “load” temperature (T_{bot_tank}) at the condenser side:

$$Q_{rem} = f(EWT, T_{bot_tank}) \quad (4.12)$$

This function was programmed as a look-up table by using data from the manufacturer's spec sheet and then applying a double interpolation. This heat removed (Q_{rem}) is approximately equal to the thermal energy removed from the BIPV/T air stream. If it is assumed that 5% of the energy is released to the surroundings, then we can write

$$Q_{rem} = 0.95C_{air}\varepsilon_{HX}(T_{air} - LWT) \quad (4.13)$$

where C_{air} is the heat carrying capacity of the BIPV/T air stream (W/K), ε_{HX} is the effectiveness of the heat exchanger, T_{air_in} is the temperature of the BIPV/T air entering the heat exchanger, and LWT is the temperature of the water-glycol mix leaving the heat pump. Finally, the temperature change in the water-glycol mixture is given by:

$$EWT - LWT = \frac{Q_{rem}}{C_{wg}} \quad (4.14)$$

in which C_{wg} is the heat carrying capacity of the liquid. The effectiveness of the heat exchanger (ε_{HX}) was estimated using the following equation, corresponding to a single-pass cross-flow heat exchanger with both fluids unmixed (Incropera & DeWitt, 2002) :

$$\varepsilon_{HX} = 1 - e^{\left(\frac{NTU^{0.22}}{C_r} \left(e^{-C_r NTU^{0.78}} - 1\right)\right)} \quad (4.15)$$

An estimate of $(uA)_{HX}$, the conductance of the heat exchanger walls, is used:

$$NTU = \frac{(uA)_{HX}}{C_{min}} \quad (4.16)$$

$$C_{min} = \min(C_{air}, C_{wg}) \quad (4.17)$$

Equations 4.12 through 4.15 are solved simultaneously by applying numerical methods (in the case of two heat pumps, a factor of 2 is used in Equation 4.12).

A function was created in MATLAB to find the operation point following the procedure described above. Five inputs were used (Figure 4.21): the temperature of the BIPV/T air (T_{air}), the temperature of the bottom of the TES tank, the BIPV/T air flow rate, the liquid flowrate at the source side (evaporator) of the heat pump, and the liquid flow rate at the sink side (condenser).

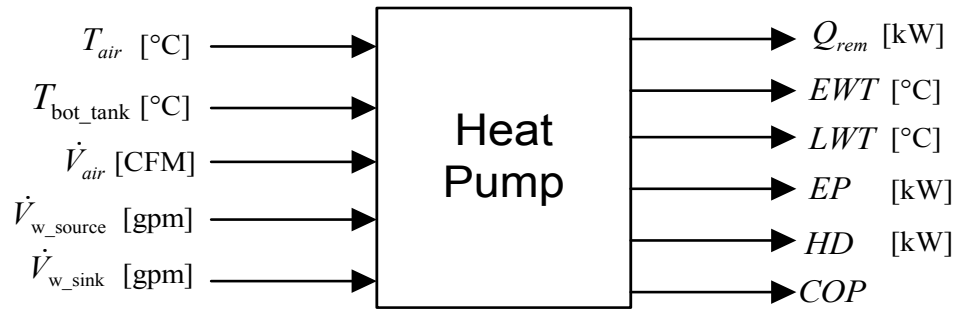


Figure 4.21. Schematic of the function used to model the heat pump operation.

The heat extracted by the heat pump (Q_{rem}), the electric power consumed by the heat pump(s) (EP), the entering water temperature at the source side (EWT) and the temperature of the water leaving the source side (LWT) are calculated from the technical specifications sheets. The heat delivered (HD) to the tank and the COP are calculated as:

$$HD = 0.95Q_{rem} + EP \quad (4.18)$$

$$COP = \frac{HD}{EP} \quad (4.19)$$

Simulations were carried out to study the performance of one and two heat pumps under different conditions, and some preliminary results were presented in (Candanedo &

Athienitis, 2008b). Figure 4.22 shows the HD to the tank, while Figure 4.23 shows the COP for different conditions of BIPV/T flow rate and temperature. In near-optimal conditions (high flow rates and high BIPV/T temperatures), over 20 kW could be delivered to the tank with a COP higher than 5.

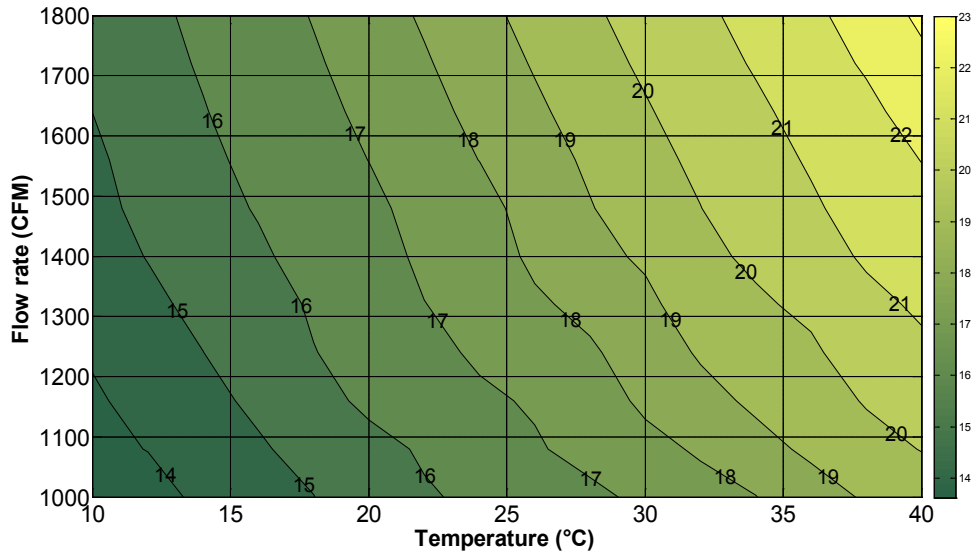


Figure 4.22. Heat delivered to the TES tank in mode B (two heat pumps operating in parallel). $T_{bot_tank} = 33$ °C. pumps used: Genesis GSW036.

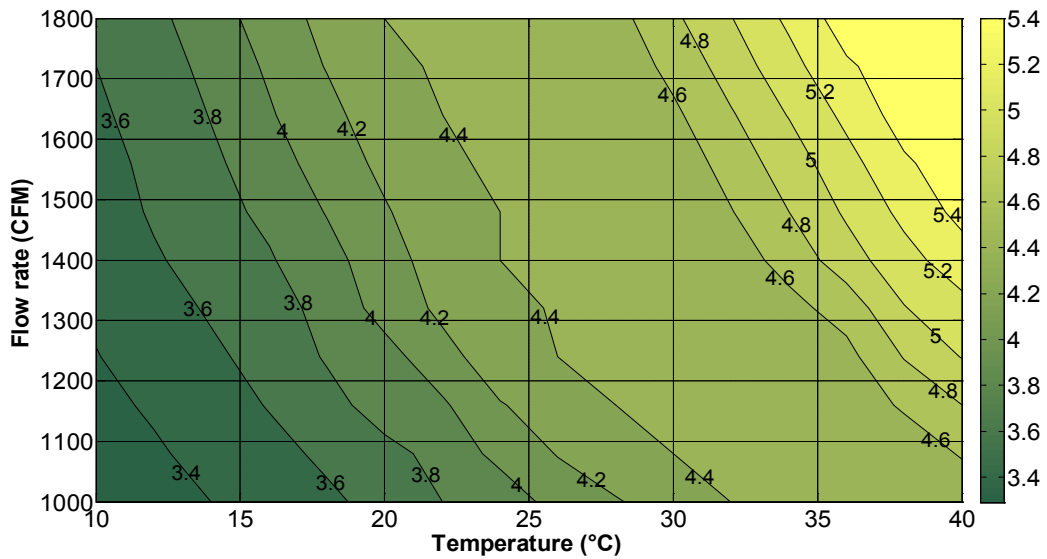


Figure 4.23. COP in mode B (two heat pumps in parallel). $T_{bot_tank} = 33$ °C. Heat pumps GSW036.

The use of two heat pumps instead of one meant that the operation of the equipment at partial loads would be better. Most importantly, this strategy also implied that the operation range of the heat pump would be wider. Heat delivery rates with the heat pump system could range from about 7 kW to more than 23 kW of thermal energy, for BIPV/T temperatures going from -2 °C to more than 40 °C. For an average heat delivery output rate of about 14-15 kW, eight hours of operation (typically, between 8:00 and 16:00) could deliver about 112-120 kWh of thermal energy to the TES tank, which represents about one day of heating autonomy.

The heat pumps initially selected for this project, Genesis[®] GSW036 (manufactured by ClimateMaster), employed R22 as refrigerant. This refrigerant was phased-out in the United States and Canada in 2010, because of its effect as greenhouse gas. For this reason, these two heat pumps were replaced by two EW020 (manufactured by Waterfurnace), which use R410a. Although their name might suggest a nominal capacity of 20 kBTU/hr, the performance of these heat pumps is similar to that of the previously selected model. The specifications sheets of both heat pumps are included in the appendix.

4.3.2.3 Simulation of tank stratification

The stratification in the thermal energy storage tank has been modeled with the multi-node model described by Duffie and Beckman (2006a). In this case, the tank has been divided into 4 horizontal nodes (Figure 4.24). The flow coming from the heat pumps or from the flow rates will mix with the water from one of the four nodes, depending on their temperature. The flow rates between nodes are calculated using mass flow balances.

An accurate calculation of thermal stratification in the TES tank would require more complex methods (e.g., CFD simulations). However, it has been found that three to five nodes are usually enough for practical purposes (Duffie & Beckman, 2006).

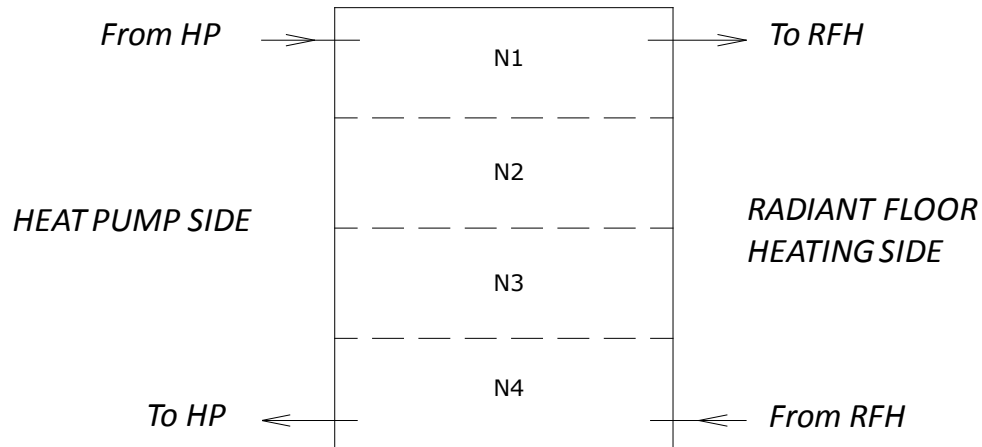


Figure 4.24. Stratification in TES tank modeled with 4 nodes, as per Duffie and Beckman (2006a).

Although the heat pump(s) can deliver a large amount of energy (over 20 kW) to the water tank, a high flow rate is required and therefore the temperature rise created by the heat pump(s) between the supply and return water is between only 5 and 10 °C (9 and 18 °F). Under these conditions, it is nearly impossible to stratify the tank more than this temperature difference. Regardless, simulations indicate that the system operation remains satisfactory even in the worst-case scenario (a fully mixed tank).

4.3.2.4 Fan and motor selection

Ducting and piping systems conceived to reduce pressure drop, as well as efficient circulating pumps and fans, are important elements in designing a net-zero energy house.

In the case of the Alstonvale House, the pressure drop for a flow rate of 1800 CFM was estimated to be 275-375 Pa (Figure 4.25).

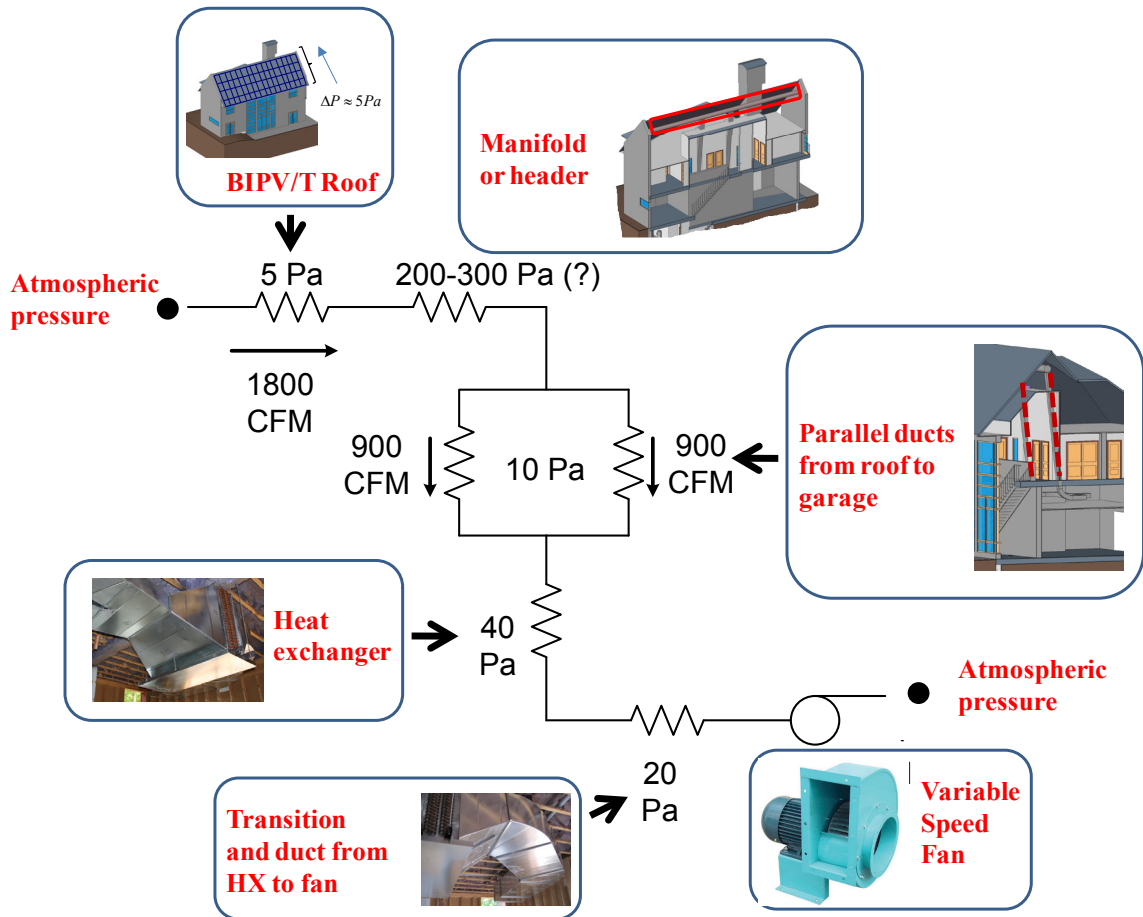


Figure 4.25. Pressure drop in BIPV/T ducting system.

The two parallel runs of duct from the roof to the garage helped to significantly reduce the pressure drop for the system. The largest pressure drop was estimated to be in the manifold of the duct, where sixteen 4" diameter ducts brought the BIPV/T air to a larger 18" duct. Based on the upper pressure drop estimate (375 Pa) and a flow rate of 1800 CFM and cost considerations, a fan with the curve shown below was selected (Figure 4.26). This piece of equipment selected is a backward inclined, centrifugal fan.

The main considerations were high mechanical efficiency (over 73%), low noise levels, and cost.

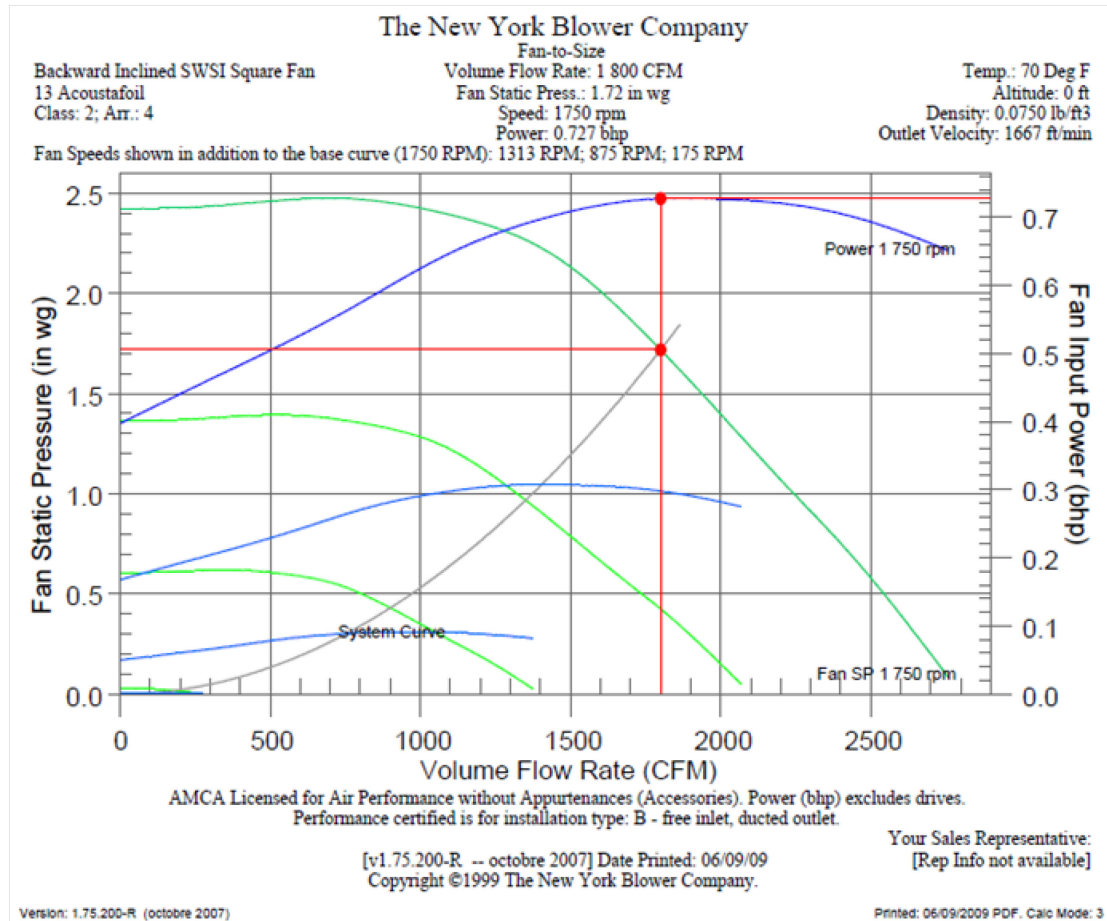


Figure 4.26. Static pressure/flow rate curve for the fan used in the Alstonvale House (NYB, 2007).

A curve for a slightly different fan (with marginally better performance, but significantly more expensive), is shown in the appendix.

Manufacturer’s data indicates that the fan input power (bhp) corresponding to the selected fan is 0.727 HP (550 W). A high-efficiency, 3-phase motor, rated at 1 HP (756 W) was selected for this fan.

A fan speed controller was installed in order to adjust the flow rate as required. In May 2010, a team from the Concordia Solar Laboratory, used a balometer to take flow measurements for different fan speeds (Figure 4.27).

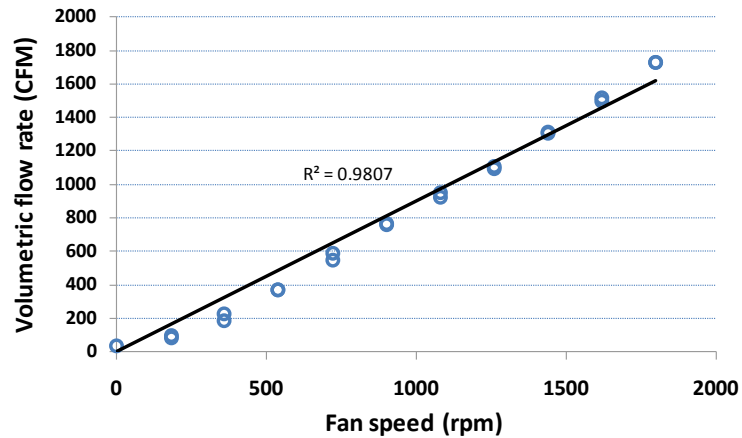


Figure 4.27. Measured flow rate vs. fan speed (Allard *et al.*, 2010)

As expected, there was a linear relationship between flow rate and fan speed. The flow rate measured for maximum fan speed was 1729 CFM, which confirmed the calculations used for the fan selection.

4.4 Final Schematic and Control Sequences

The Alstonvale House unfortunately suffered severe damage in a fire in May 2010, which prevented the collection of data from the operation of the mechanical system and the passive response of the building. Newspaper reports attributed the fire to faulty application of spray foam insulation (Defendorf, 2010).

At that moment, the development of the control sequences was at an advanced stage by a group from Concordia University led by the author of this thesis (Candanedo *et al.*, 2010). The “control sequences” are the technical document used by the installer of the

control system for the actual implementation of the algorithms. A full description of the details of the mechanical schematic is beyond the scope of this thesis. However, an overview of the final schematic is presented in Figure 4.28.

CG 8 : MISCELLANEOUS

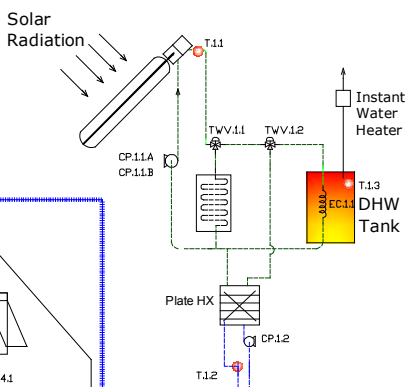
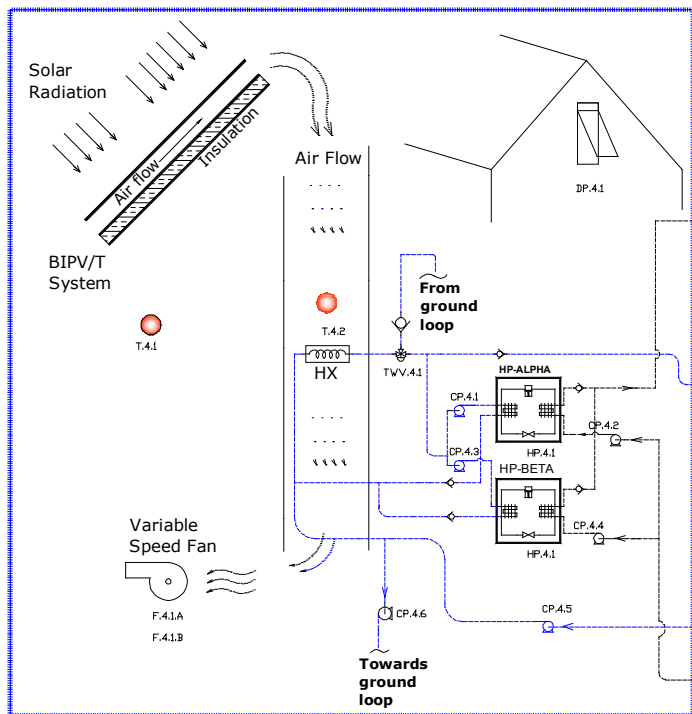
Curtains
CUR.8.1

CG 1: SOLAR THERMAL
COLLECTOR AND DHW LOOP

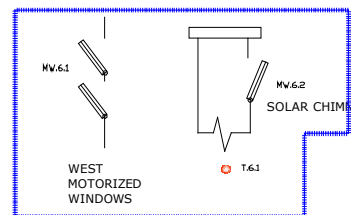
HRV.7.1.A
HRV.7.1.B
VDR.7.1 VDR.7.4
VDR.7.2 VDR.7.5
VDR.7.3 VDR.7.6

CONTROL GROUP 7 :
HRV AND VENTILATION

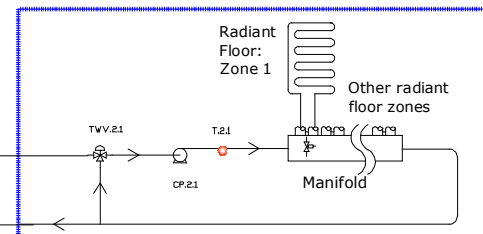
CONTROL GROUP 4:
BIPV/T, HEAT PUMPS, GROUND LOOP



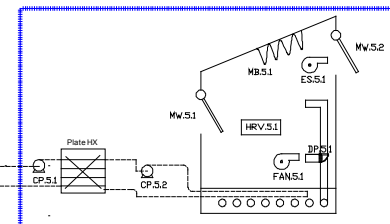
CONTROL GROUP 6 : NATURAL COOLING



CONTROL GROUP 2 : RFH SYSTEM



CG 5: GREENHOUSE



CG 3: TES AND HDS TANKS

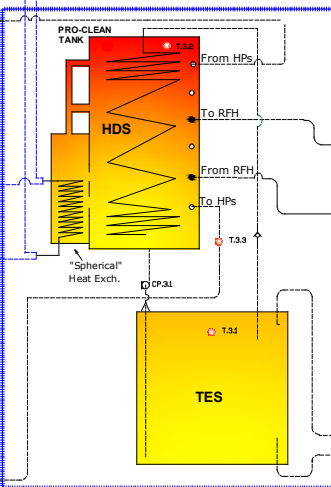


Figure 4.28. Near-final control schematic of the Alstonvale House. Adapted from Candanedo *et al.*, (2010).

4.5 Design Suggestions for Other Cases: the ÉcoTerra House

The design and control approaches proposed for the Alstonvale House can be suitably applied in other advanced solar homes. For example, the idea of a BIPV/T-assisted heat pump system could be a realistic heating alternative for Canadian homes. As an illustration of the potential of such a system, simulations were carried out for the BIPV/T system of the ÉcoTerra House, which was presented in section 2.4.9.

The BIPV/T roof of this house (Figure 4.29) has a tilt angle of 30° , and is approximately 10.4 m wide by 5.1 m long in the streamwise direction. The PV system, consisting of flexible amorphous silicon panels, has a nominal PV electric output of 2.8 kW under standard test conditions. As in the Alstonvale House, outdoor air is driven under the BIPV/T roof of the ÉcoTerra House. In the current system, the heated air can be used to: (a) heat a hollow-core concrete slab in the basement; (b) to preheat domestic hot water or (c) to supply hot air to a dryer. A schematic of the mechanical system is shown in Figure 4.30. The main heating system of the ÉcoTerra House is 2.2 ton ground-source heat pump (Chen, 2009).

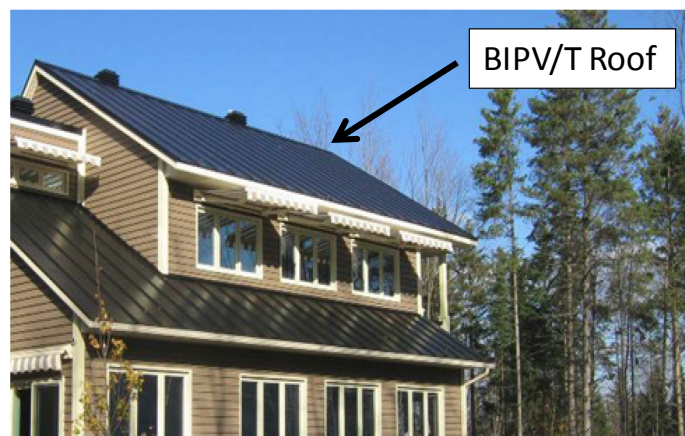


Figure 4.29. BIPV/T roof of the ÉcoTerra House.

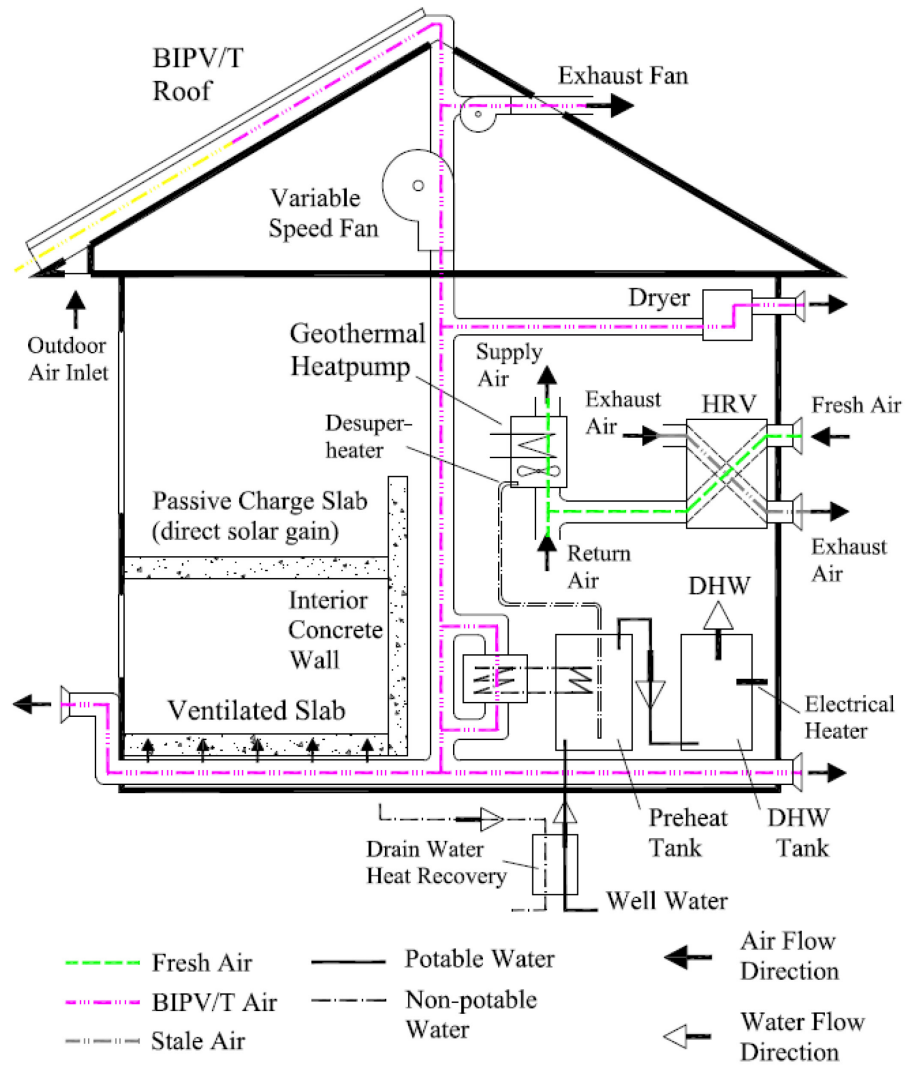


Figure 4.30. Mechanical system of the ÉcoTerra House (Chen, 2009).

To illustrate the potential of a heat pump assisted by the BIPV/T roof of the ÉcoTerra House, an air-source heat pump designed for cold climates was selected. The heat pump chosen for the simulation was the NIBE F2025-A (as shown in the next chapter, this heat pump was also used for the development of optimal control strategies). The heat delivered by this heat pump ranges from 3 to 8 kW (0.9 to 2.3 tons, approximately). For these proof-of-concept simulations, it was assumed that the heat pump delivered thermal energy to a TES tank with a constant temperature of 30 °C. It was also assumed that heat

pump could not operate if the air temperature was lower than -10 °C. Other details on this heat pump are presented in the next chapter.

The BIPV/T model presented in section 4.3.1.2 was modified for the geometry and materials used in the ÉcoTerra House. To model the BIPV/T roof with amorphous panels, it was assumed that their efficiency varied as a linear function of temperature:

$$\eta_e = 0.06 - 0.00022(T_{PV} - T_{STC}) \quad (4.20)$$

For the simulations, the design flow rate of 800 CFM under the PV panels was assumed. In the existing configuration, the air flow rate is about 450 CFM, because of some issues with the installation of the ducting system.

Figure 4.31 shows the results for the COP of the NIBE heat pump corresponding to a 10-day period between January 15 and 25 under Montréal weather conditions.

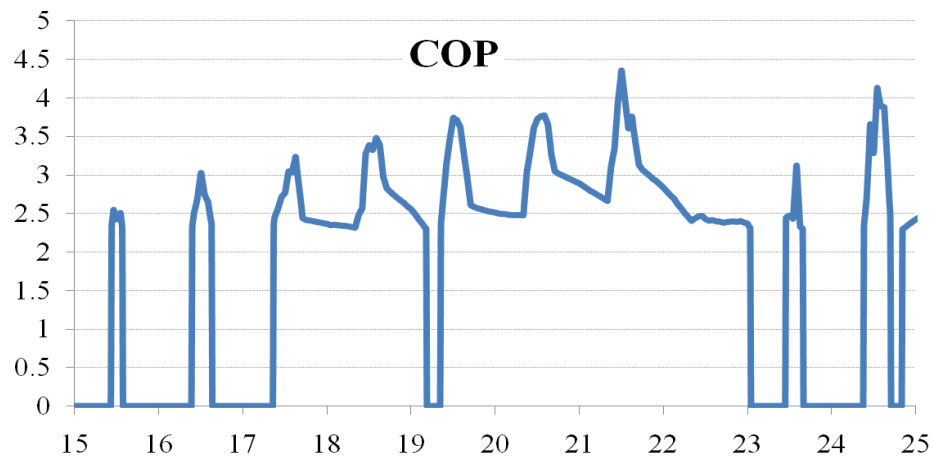


Figure 4.31. COP of the BIPV/T assisted heat pump. ÉcoTerra BIPV/T roof with an air flow rate of 800 CFM.

Table 4.12 shows the energy delivered and consumed by the heat pump from December through March. For this period, the total energy delivered by the heat pump is 7,693 kWh. It is interesting to compare these numbers with the measurements of the

actual system at the ÉcoTerra House. Doiron (2011) reports that the heating energy supplied by the ground-source heat pump system is 7,459.8 kWh for the entire heating season. Therefore, the numbers obtained with this preliminary study for a BIPV/T-assisted heat pump suggest that such a system could supply the heating energy for the house, *provided that a suitable heat pump is used*. Most of the air-source heat pumps used in North America are not designed to operate with very low temperature. Special heat pump products using BIPV/T air as a heat source could be developed (with features such as variable speed compressor to manage partial loads and low cut-off temperatures). A TES tank would help in managing solar radiation availability.

Table 4.12. Heating energy and power consumption. Simulations for a BIPV/T-assisted heat pump at the ÉcoTerra house.

	December	January	February	March
Heating Energy (kWh)	2563	2401	1816	913
Power Consumption (kWh)	837.4	819.2	554.7	248
Effective COP	3.06	2.93	3.27	3.68

The COP of the heat pump, calculated above for a sink at a constant 30 °C, could be significantly improved if advanced control strategies are used to select the temperature of the TES (the following chapter presents optimal control strategies for a similar system). Moreover, in contrast with the roof of the Alstonvale, in the BIPV/T system of the ÉcoTerra there is no glazing section to boost the air temperature and improve the COP.

The utilization of a BIPV/T-source heat pump would be a cheaper option than a ground-source heat pump, since no expensive drilling (which could cost more than \$10,000) is required. There would be a single system (solar) rather than two (solar + geothermal), an elegant and economical option. Considering that having a photovoltaic system is practically necessary in a net-zero energy house, a BIPV/T-based heating

system could be a suitable choice. Finally, another advantage of this system is that the period of heat collection (i.e., when the heat pump operates) coincides with the maximum generation of the PV system, which means that the impact on the grid is considerably reduced.

There is considerable opportunity for developing heat pump products designed specifically for BIPV/T-assisted configurations. It was estimated that the ground loop would be the source of heating of the Alstonvale House about 1/3 of the time. This is because the heat pump/heat exchanger system selected could only work with air temperatures of 2-3 °C or higher. In contrast, some European heat pumps currently not available in North America, such as the abovementioned NIBE and the Vitocal 300-A (Viessmann, 2010), report that they can work with temperatures as low as -15 °C or even -20 °C. The COP of the Vitocal 300-A for an air-source at 2 °C and 35 °C for the sink is reported to be 3.7.

5. Predictive Control Strategies

5.1 Introduction

Predictive control strategies developed for advanced solar houses are presented in this chapter. It begins by describing preliminary work performed at the Concordia Solar House. Then, rule-based control strategies developed for the Alstonvale Net Zero House are then presented. The procedure used for system identification of a simplified model is described. The application of MPC strategies for a radiant floor heating system in a room with large solar gains is discussed. Finally, the dynamic programming algorithm used for determining the optimal set-point trajectory for a TES tank is presented.

5.2 Experimental Work at the Concordia Solar House

While it was not possible to collect information on the passive response of the Alstonvale Net Zero House, experimental evidence of the validity of a simplified model for a solar house was collected at the Concordia Solar House (Loyola Campus, Concordia University) (Candanedo *et al.*, 2007a). This house, built for the 2005 Solar Decathlon (Pasini, 2006), has insulation levels (R-32) and a high window-to-wall ratio (over 40%). The thermal mass of the house was relatively small (wooden structure, bamboo floors).



Figure 5.1. *Northern Light* (a.k.a. Concordia Solar House) at the Loyola campus.

The team working at the house noticed that the temperature fluctuation of the Concordia Solar House followed a rather regular, repetitive pattern on sunny days. The shape of the response also looked similar to that of a simple RC circuit. Figure 5.2 shows the free-floating response (i.e., without temperature control) of the house during a few days in February 2007.

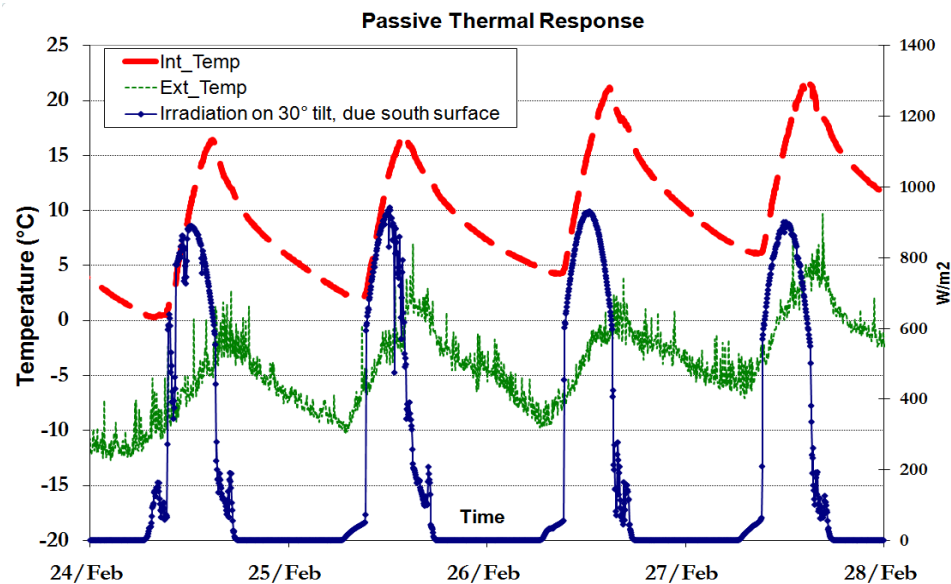


Figure 5.2. Passive thermal response of the Concordia Solar House for February 2007. Pyranometer used for irradiance measurements, temperatures measured with type T thermocouples. Measurements every 200 s. Adapted from Candanedo *et al.* (2007a).

As expected, solar radiation has a significant impact on indoor temperature fluctuations. Consequently, indoor temperature swings are often larger than the exterior temperature fluctuation. Moreover, the house behaves as a low-pass filter: while noise accounts for part of the measured outdoor temperature variations, the indoor thermocouple does not register this type of high-frequency fluctuation. Finally, while the solar radiation measured is not a perfect curve, it follows a clear pattern: there is some

morning shading due to a neighbouring building east of the house, and some afternoon shading, due to a tree located at the west side.

Based on these observations, it was assumed that the house's thermal response could be modeled through the following circuit (Figure 5.3):

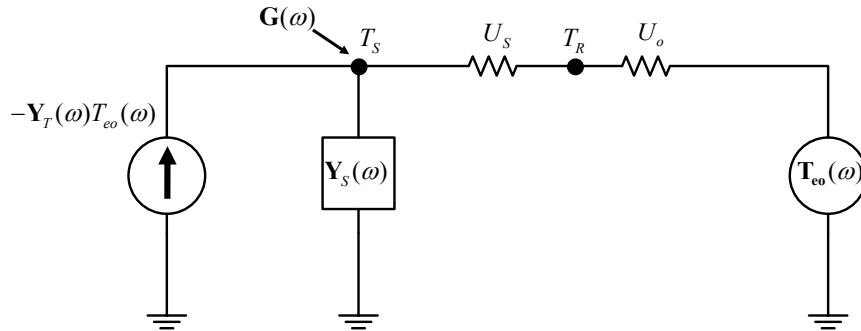


Figure 5.3. Simplified thermal circuit used to model the Concordia Solar House (Candanedo *et al.*, 2007a).

In this model, two nodes are considered as a model of the Concordia Solar House: a surface node (T_S), which accounts for all the surfaces in the room, and a room air node (T_R). Both nodes are connected by a conductance U_S . The entire building envelope is represented by a Norton equivalent similar to the one shown in Figure 3.2, in which the transfer admittance (Y_T) is used to account for the effect of outdoor temperature, and the self admittance (Y_S) describes the response of the mass in the building envelope to heat transmitted through the envelope and by solar gains impinging on the internal surface. The effect of ventilation, infiltration and conduction through windows and doors is represented by U_o .

By applying the superposition principle, the response of the room temperature is obtained by adding the contributions of solar radiation and outdoor temperature. The contribution of solar radiation is given by:

$$T_1(\omega) = \left(\frac{G(\omega)}{\mathbf{Y}(\omega) + \frac{U_S U_o}{U_S + U_o}} \right) \left(\frac{1}{1 + \frac{U_o}{U_S}} \right) \quad (4.21)$$

and that of the exterior temperature:

$$T_2(\omega) = \left(\frac{\frac{1}{\mathbf{Y}_S(\omega)} + \frac{1}{U_S}}{\frac{1}{\mathbf{Y}_S(\omega)} + \frac{1}{U_S} + \frac{1}{U_o}} \right) T_o(\omega) \quad (4.22)$$

The total temperature response is then given by:

$$T_R(\omega) = T_1(\omega) + T_2(\omega) \quad (4.23)$$

Given that the building is highly insulated and that the infiltration is negligible, one can assume that $U_o \ll U_S$. In this case, the denominator in Equation (4.22) becomes very large, and T_2 becomes very small. The room temperature will only depend on T_1 and will be given by:

$$T_R(\omega) \approx \frac{G(\omega)}{\mathbf{Y}_S(\omega) + U_S} \quad (4.24)$$

If the denominator of Equation (4.24) is represented by a single admittance, then:

$$T_R(\omega) \approx \frac{G(\omega)}{\mathbf{Y}_{Eq}(\omega)}, \quad \text{or} \quad (4.25)$$

$$\mathbf{Y}_{Eq}(\omega) \approx \frac{G(\omega)}{T_R(\omega)} \quad (4.26)$$

The transfer function between the indoor room air and solar gains, i.e., the inverse of Equation (4.26), has units of thermal impedance. The admittance Y_{Eq} can be found at discrete frequencies: one cycle per day, two cycles per day, and so forth.

A Fourier analysis was applied to the irradiance $[S(t)]$ and indoor temperature response (T_R) presented in Figure 5.2 to find their equivalent in the frequency domain. By definition, the Fourier series is:

$$\hat{S}(n) = \frac{1}{P} \int_a^{a+P} S(t) e^{-j\omega_n t} dt \quad (4.27)$$

A numerical approximation can be found in this way (Athienitis, 1994):

$$\hat{S}(n) = \frac{1}{P} \sum_{k=0}^N S(t_k) \cdot e^{-j\omega_n t_k} \Delta t \quad (4.28)$$

in which P is the period (24 hours), t_k is the time in seconds of sample k , and Δt is the sampling period (200 s). The signal can be reconstructed to the time domain as follows:

$$S(t) = \sum_{n=-\infty}^{\infty} \hat{S}(n) \cdot e^{j\omega_n t} \quad (4.29)$$

Numerically, having N_H frequencies, $S(t)$ is given by:

$$S(t) = S(0) + 2 \sum_{n=1}^{N_H} \text{Re} \left(\hat{S}(n) \cdot e^{j\omega_n t} \right) \quad (4.30)$$

The factor of 2 accounts for the integration of frequencies from $-\infty$ to 0. Note that the solar gains into the space are given as the product of the irradiance, the area of the windows (A_w), and an equivalent transmittance (τ_w):

$$G(t) = S(t) \cdot A_w \cdot \tau_w \quad (4.31)$$

The Fourier analysis can also be applied to the indoor temperature (T_R):

$$\hat{T}_R(n) = \frac{1}{P} \sum_{k=0}^N T(t_k) \cdot e^{-j\omega_n t_k} \Delta t \quad (4.32)$$

The admittance as a function of frequency is then given as the ratio:

$$\mathbf{Y}_{Eq}(n) = \frac{\hat{S}(n) \cdot A_w \cdot \tau_w}{\hat{T}_R(n)} \quad (4.33)$$

The advantage of Equation (4.33) is that the $\mathbf{Y}_{Eq}(n)$ is a property of the building. The values of $\mathbf{Y}_{Eq}(n)$ of the Concordia Solar House *were experimentally found by measuring the solar irradiance on a vertical surface and the indoor temperature fluctuation*. This equivalent admittance can be used to predict the response to any given solar radiation profile. For this reason, additional physical details of the house are not needed for control, as Equation (4.33) represents a model derived from system identification.

Different solar irradiance profiles on a **due-South vertical surface**, intended to represent solar radiation curves of archetypical days, were designed.

$$S(t) = \begin{cases} S_{\max} \cos(\omega t - \pi), & 9:00 < t < 18:00 \text{ hr} \\ 0.1S_{\max} \cos(\omega t - \pi), & 6:00 < t < 9:00 \text{ hr} \\ 0, & \text{otherwise} \end{cases} \quad (4.34)$$

S_{\max} values of 250, 500, 750 and 1030 W/m² were used. Figure 5.4 shows the four curves, which represent overcast, partially cloudy, partially sunny and clear sunny days.

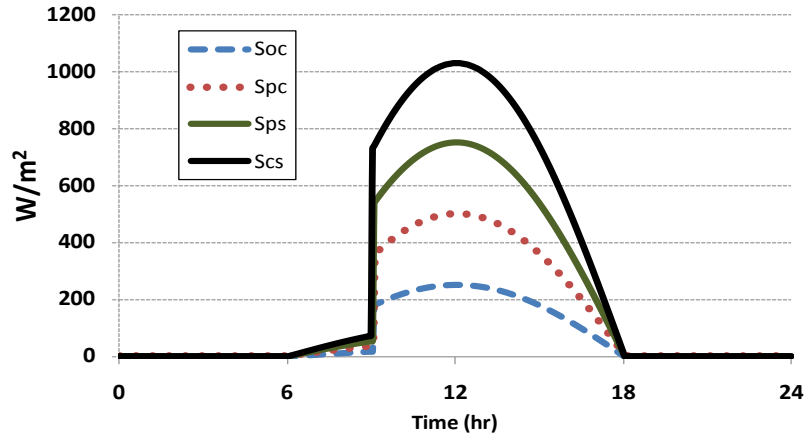


Figure 5.4. The four curves used to represent solar radiation conditions: Soc (overcast day), Spc (partially cloudy), Sps (partially sunny), Scs (clear sunny).

Since the solar gains also depend on the transmittance of the fenestration, by adjusting the position of the roller blinds (shown in Figure 5.1) it is possible to mitigate the impact of solar radiation. It was assumed that the transmittance of the window without the roller blind is 65%. When the roller blind is fully closed, the transmittance of the group window-plus-blind is 40%. Therefore, by adjusting the position of the blind, the transmittance can be adjusted between $\tau_{open} = 65\%$ and $\tau_{closed} = 40\%$. A linear variation between these values was assumed:

$$\tau_{eq} = r\tau_{open} + (1-r)\tau_{closed} \quad (4.35)$$

For a control strategy, it is reasonable to expect that the roller blind will take only a limited number of discrete values. In this case, it was assumed that the roller blind could take only five values: 0, 25, 50, 75 and 100%, where 100% means “fully open”. By combining the five roller blind positions with the four solar radiation curves, a look-up table can be built to predict the temperature swing for a given day (Table 5.1).

Table 5.1. Temperature swing in °C as a function of blind position and radiation. Adapted from (Candanedo *et al.*, 2007a).

Condition	Blind Position				
	0%	25%	50%	75%	100%
Overcast	2.4	2.7	3.1	3.5	3.8
Partially cloudy	4.7	5.4	6.2	6.9	7.6
Partially sunny	7.1	8.2	9.3	10.4	11.5
Sunny	9.4	10.9	12.3	13.8	15.3

An algorithm was designed to limit the temperature swing by selecting the blind position at 6:00 a.m. depending on the expected solar radiation for that day. Details of the algorithm are presented in Candanedo *et al.* (2007a). An experiment was carried out at the Concordia House during the last days of March 2007 by introducing the weather forecast manually for the following day. The agreement for the predicted temperature fluctuation was good in general (Table 5.2). On April 1st, solar radiation was lower than expected, and therefore the temperature swing was smaller than predicted.

Table 5.2. Measured and expected temperature swings. Adapted from Candanedo *et al.* (2007a).

	March 29 th	March 30 th	March 31 st	April 1 st
Predicted condition	Clear sunny	Partly sunny	Clear sunny	Partly sunny
Blind position	25%	75%	25%	75%
Expect. temp. swing	10.9	10.4	10.9	10.4
Measured temp. swing	11	9.8	10	8.3

The measured temperature fluctuation also followed the predicted temperature fluctuation (Figure 5.5). The “average” level is relatively hard to predict: in this case, the initial temperature is provided at midnight.

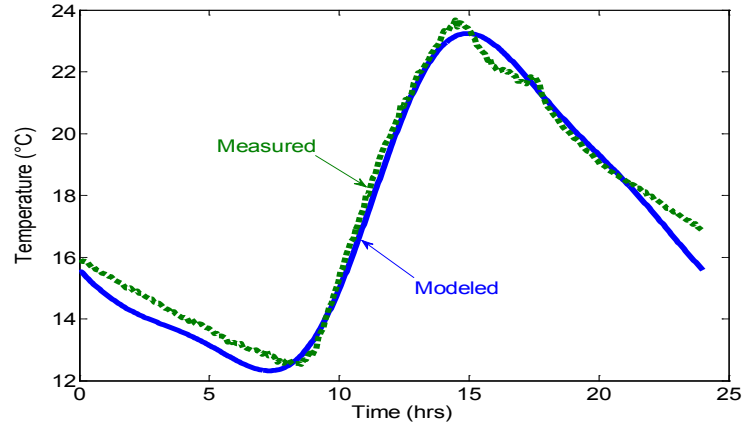


Figure 5.5. Temperature fluctuation modeled and predicted, March 29th, 2007 (note: initial measured temperature at 0:00 was “fed-in” into the program).

The investigations carried out at the Concordia Solar House provided the basis for further research on this subject using the house as a case study (Malys, 2007). Malys developed a recursive algorithm in which the current interior temperature (T_{int}) depends on its value at the previous time-step and on the solar gains received:

$$T_{int,i+1} = T_{int,i} + \Delta t (AG_{vr} - BT_{int,i}) \quad (4.35)$$

in which A and B are found by a least-square method based on experimental measurements. In essence, the approach followed by Malys is equivalent to a first-order transfer function in the z -domain.

5.3 Rule-Based Predictive Control

Simple predictive control strategies, based on the application of heuristic rules, were applied to the model of the Alstonvale Net Zero House described in the previous chapter. These strategies, which are described below, dealt with the controlled use of the TES capacity of the water tank and the building itself. Results of these investigations were

presented in Candanedo & Athienitis (2008a, 2009; 2010a). While these simple strategies were not based on formal mathematical optimization, the core of the predictive control principles, namely decision-making based on expected loads, is present in these works, and were the basis of future developments.

5.3.1 Simple Weather Scenarios for Building Control Prototyping

Building simulation tends to be used for assessing the performance of buildings over relatively long periods, typically months or years. This approach has the advantage of providing an all-encompassing standardized evaluation, which includes the building's response to diverse weather conditions. Since energy bills are supplied monthly, most building labelling programs are based on monthly or annual building simulations or measurements. Annual energy balances are commonly used for categorizing a building as “net-zero energy”. However, simulations at shorter time-scales provide significant information, in particular for the testing of control strategies.

Figure 5.6 shows three solar radiation scenarios used for testing predictive control in a solar house (Candanedo & Athienitis, 2008a; Candanedo & Athienitis, 2010a). These scenarios were designed based on three “typical” solar conditions: sunny (S), intermediate (M), and cloudy (C). In these sequences, a sunny day was assigned a daily clearness index (K_T) of 0.7, an intermediate day was assigned a K_T of 0.5, and a cloudy day was assigned a K_T of 0.3. For example, the sequences shown in Figure 5.6 correspond to SCCCC, SCSCC and SSMCC.

The model of Liu and Jordan, as described in (Duffie & Beckman, 2006), was used to find a typical distribution of hourly clearness indexes (k_T) as a function of daily clearness

indices and solar angles for Montréal. The Erbs model (Erbs *et al.*, 1982), was used to calculate the ratio diffuse/global horizontal radiation. Finally, the Perez model (Perez *et al.*, 1990) was used to calculate radiation on different surfaces.

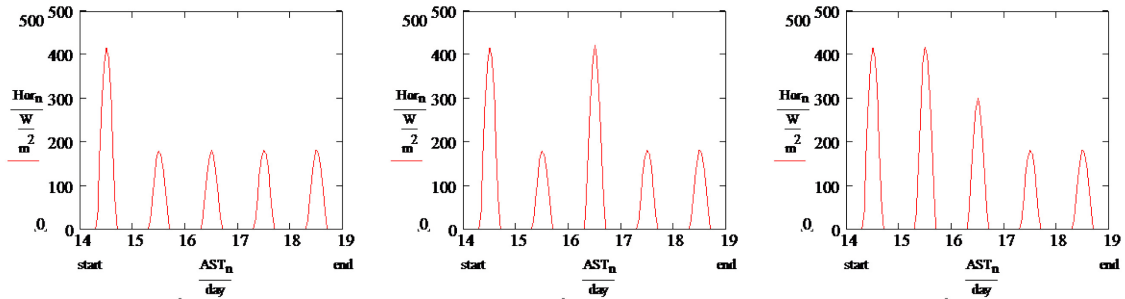


Figure 5.6. Global horizontal radiation according to scenarios designed for testing control strategies. (Candanedo & Athienitis, 2008a).

Temperatures were modeled with steady-periodic curve using an average value and average fluctuation range for the corresponding month, and the design day data (quasi-sinusoidal) proposed by ASHRAE (ASHRAE, 2005). Wind speed data (used for the calculation of convective heat transfer coefficients) was taken from a TMY2 file.

5.3.2 Comparison of Heuristic Control Strategies

The work presented in Candanedo & Athienitis (2009) compares the performance of heuristic predictive control strategies applied to TES tank of the Alstonvale House.

Strategy 1 – No predictive control. The tank set-point is fixed at 48 °C and the room air set-point is fixed at 23 °C. The BIPV/T fan flow rate is kept constant at 1600 CFM. The modes of operation are selected as follows:

- If the exit air temperature is at least 3 °C higher than that of the top of the TES tank, then direct exchange between the heat exchanger and the tank (mode A) takes place.

- If the exit air temperature is below 48.9 °C (the operation limit of the heat pump) but above 10 °C, then two heat pumps are used (mode B).
- If the air temperature is between 3.5 °C and 10 °C then only one heat pump is used (mode C).
- Finally, if the air temperature is below 3.5 °C and the tank top temperature is below 35 °C, then mode D (ground source operation) is activated. In this latter mode, the ground source is operated until the tank temperature is 2 °C above the 35 °C limit (in other words, 37 °C).

Strategy 2 – Predictive control with fixed BIPV/T fan speeds. Same as above, but the control system decides on the tank set-point according to the solar radiation expected for the next two days (see section 5.3.3 for details). For instance, if the current day is expected to be sunny and the next day to be overcast, then the tank set-point is increased to 48 °C. For two consecutive sunny days, the tank set-point is 40 °C.

Strategy 3 – Predictive control with variable fan speeds. Similar to Strategy 2, but in this case the flow rate varies between 1040 and 1600 CFM depending on mainly on the expected solar radiation.

$$\text{Fan Speed Control Signal} = \begin{cases} 0\%, & \text{if } T_{\text{Tank_top}} \geq T_{\text{Tank_set-point}} \\ \text{else} \\ 100\%, & \text{if } S_{\text{roof}} > 950 \text{ W/m}^2 \\ 91.25\%, & \text{if } 800 \text{ W/m}^2 < S_{\text{roof}} \leq 950 \text{ W/m}^2 \\ 82.5\%, & \text{if } 500 \text{ W/m}^2 < S_{\text{roof}} \leq 800 \text{ W/m}^2 \\ 73.75\%, & \text{if } 300 \text{ W/m}^2 < S_{\text{roof}} \leq 500 \text{ W/m}^2 \\ 65\%, & \text{if } S_{\text{roof}} \leq 300 \text{ W/m}^2 \text{ and } T_{\text{ext}} > 5 \text{ }^\circ\text{C} \\ 0\%, & \text{if } S_{\text{roof}} \leq 300 \text{ W/m}^2 \text{ and } T_{\text{ext}} \leq 5 \text{ }^\circ\text{C} \end{cases} \quad (4.36)$$

Strategy 4 – Similar to strategy 3, but in this case:

- Mode B (with two heat pumps) is activated when the air temperature is between 20 °C and 48.9 °C.
- Mode C (one heat pump) is activated between 3.5 °C and 20 °C,
- Mode D (ground source) is activated when the air is below 3.5 °C.

Strategy 5 – Similar to strategy 3, but the ground source loop is used only if the tank temperature drops to under 30 °C (instead of 35°C).

Strategy 6 – Similar to strategy 3, but the ground source is used only if the TES temperature drops to below 28 °C.

A summary of the control strategies tested is presented in Table 5.3.

Table 5.3. Summary of control strategies (relevant features of each strategy are highlighted). T_{exit} is the exit temperature of the BIPV/T air, and T_{bot_tank} is the temperature of the bottom of the TES tank. The green shading indicates the change with respect to the previous strategy.

	Strategy 1	Strategy 2	Strategy 3
Mode A	$T_{exit} > T_{bot_tank} + 3^{\circ}\text{C}$	$T_{exit} > T_{bot_tank} + 3^{\circ}\text{C}$	$T_{exit} > T_{bot_tank} + 3^{\circ}\text{C}$
Mode B	$10^{\circ}\text{C} \leq T_{exit} \leq 48.9^{\circ}\text{C}$	$10^{\circ}\text{C} \leq T_{exit} \leq 48.9^{\circ}\text{C}$	$10^{\circ}\text{C} \leq T_{exit} \leq 48.9^{\circ}\text{C}$
Mode C	$3.5^{\circ}\text{C} \leq T_{exit} < 10.0^{\circ}\text{C}$	$3.5^{\circ}\text{C} \leq T_{exit} < 10.0^{\circ}\text{C}$	$3.5^{\circ}\text{C} \leq T_{exit} < 10.0^{\circ}\text{C}$
Mode D	$T_{bot_tank} < 35^{\circ}\text{C}$	$T_{bot_tank} < 35^{\circ}\text{C}$	$T_{bot_tank} < 35^{\circ}\text{C}$
Fan Speed	Fixed	Fixed	Variable
Comment	Reference case (without predictive control)	Predictive control variable set-points	Predictive control, variable fan speed
	Strategy 4	Strategy 5	Strategy 6
Mode A	$T_{exit} > T_{bot_tank} + 3^{\circ}\text{C}$	$T_{exit} > T_{bot_tank} + 3^{\circ}\text{C}$	$T_{exit} > T_{bot_tank} + 3^{\circ}\text{C}$
Mode B	$20^{\circ}\text{C} \leq T_{exit} \leq 48.9^{\circ}\text{C}$	$10^{\circ}\text{C} \leq T_{exit} \leq 48.9^{\circ}\text{C}$	$10^{\circ}\text{C} \leq T_{exit} \leq 48.9^{\circ}\text{C}$
Mode C	$3.5^{\circ}\text{C} \leq T_{exit} < 20.0^{\circ}\text{C}$	$3.5^{\circ}\text{C} \leq T_{exit} < 10.0^{\circ}\text{C}$	$3.5^{\circ}\text{C} \leq T_{exit} < 10.0^{\circ}\text{C}$
Mode D	$T_{bot_tank} < 35^{\circ}\text{C}$	$T_{bot_tank} < 30^{\circ}\text{C}$	$T_{bot_tank} < 28^{\circ}\text{C}$
Fan Speed	Fixed	Variable	Variable
Comment	Reference case (without predictive control)	Predictive control variable set-points	Predictive control, variable fan speed

As expected, it was found that the control strategy selection had an important effect on the energy consumed by the heat pump (variable fan speeds accounted for significant reductions in fan energy). Table 5.4 shows the results found by using Montréal’s weather

file for the month of February. Similar room temperatures were obtained (typically between 21 °C and 23 °C) for the six control strategies, as the control of the TES tank was the focus of the control strategies presented in this section.

Table 5.4. Heat delivery and heat pump power consumption for the six control strategies (kWh), corresponding to the month of February (TMY2 file).

	Strategy 1	Strategy 2	Strategy 3	Strategy 4	Strategy 5	Strategy 6
Mode A	0	0	0	0	3	8
Mode B	1,670	1,089	1,394	987	1,757	1,806
Mode C	345	296	80	473	84	87
Mode D	1,055	1,400	1,313	1,327	917	836
TOTAL	3,070	2,785	2,787	2,787	2,761	2,737
HP elect. energy use	821	700	700	683	645	628

The heat pump energy consumption of Strategy 2, when predictive control is introduced, is about 15% lower than that of Strategy 1. However, the heat output is only 9% smaller. The use of Strategy 6 accounts for an additional 10% reduction of energy consumed, although the heat output remains practically equal.

Strategy 6 is the one with the smallest energy consumed by the heat pump; this strategy also maximizes the contribution of the “Mode B” (the two heat pumps operating in parallel). The significance of the temperature limit used for the operation of the ground loop is noteworthy: a change in 5 °C from Strategy 4 to Strategy 5 accounted for a 5.6% reduction in energy consumption. When this “limit temperature” is lowered again from 30 to 28 °C, a further reduction of 2.7% is achieved. In all the strategies, the contribution of Mode A (direct heat exchange) is negligible. The BIPV/T air temperature will rarely exceed the TES tank temperature by more than 3 °C.

The heat delivered by all the strategies is approximately the same, although the contribution of each operating mode varies significantly. The introduction of a variable fan speed (change from Strategy 2 to Strategy 3) practically does not affect the heat pump

energy consumption; however, it increases significantly the energy delivered by Mode B. In all cases, there is always a need for a considerable amount of energy from the ground loop, between 30% (Strategy 6) and 50% (Strategy 2).

5.3.3 Set-point modification based on forecast

In a later investigation (Candanedo & Athienitis, 2010a), the solar radiation expected for the current day and the next day was used to select three variables: (a) the TES tank set-point; (b) the house temperature set-point; and (c) the blind position.

5.3.3.1 Description of the approach

The three aforementioned variables were selected by reading the weather file for global horizontal and beam radiation, then by calculating the roof irradiance with the Perez model (Perez *et al.*, 1990), and finally by integrating over the periods of interest.

$$RAD_{TODAY} = \int_0^{24h} G_{roof} dt \quad (4.37)$$

$$RAD_{TOM} = \int_{24h}^{48h} G_{roof} dt \quad (4.38)$$

A simple rule-based algorithm (Figure 5.7) has been designed to use the BIPV/T-heat pump(s)-TES group when conditions are favourable, and to manage the storage in the house thermal mass. For example, if it is sunny today, and cloudy conditions are expected tomorrow, it may be advisable to raise both the house and the TES set-points to increase the amount of stored thermal energy.

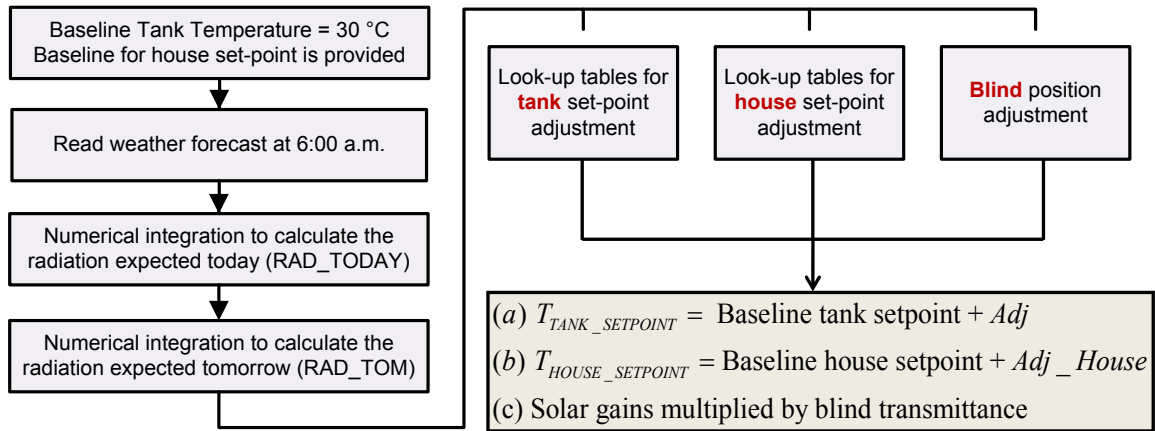


Figure 5.7. Summary of rule-based algorithm for adjusting set-points based on expected solar radiation (RAD_TODAY and RAD_TOM are given in MJ/m²).

The look-up tables used for calculating the “adjustment values” for the tank and house set-points are shown in Table 5.5. They are based on reasonable expectations for energy collection and storage for both days. For example, if it is sunny today and cloudy conditions are expected tomorrow, it may be advisable to raise both the house and TES set-points to increase the amount of stored thermal energy.

Table 5.5. Adjustment values for the tank set-point and the house set-point according to the solar radiation expected on the roof over the next two days.

TANK SET-POINT ADJUSTMENT (°C)					
		RAD TOMORROW (MJ/m2)			
		> 10	6.5 - 10	4.1 - 6.5	< 4.1
RAD TODAY (MJ/m ²)	> 10	10.0	12.7	15.3	18.0
	6.5 - 10	8.7	9.3	12.0	14.7
	4.1 - 6.5	5.3	6.0	8.7	11.3
	< 4.1	0.0	2.7	5.3	8.0
HOUSE SET-POINT ADJUSTMENT (°C)					
		RAD TOMORROW (MJ/m2)			
		> 10	6.5 - 10	4.1 - 6.5	< 4.1
RAD TODAY (MJ/m ²)	> 10	1.5	2.0	3.0	4.0
	6.5 - 10	1.0	1.3	2.0	3.0
	4.1 - 6.5	0.5	0.8	1.0	2.0
	< 4.1	0.0	0.3	0.5	1.0

In order to prevent room overheating while collecting solar gains, the position of the blinds behind the windows is adjusted based on the solar radiation expected for the current day only (RAD_{TODAY}), by using weather data available at 6:00 am. The effective transmittance τ_{eff} of the blinds is calculated as a function of the position of the blinds.

$$\tau_{eff} = \begin{cases} 64\%, & \text{if } RAD_{TODAY} > 10 \text{ MJ/m}^2, \text{ fully closed} \\ 76\%, & \text{if } 6.5 \text{ MJ/m}^2 < RAD_{TODAY} \leq 10 \text{ MJ/m}^2 \\ 88\%, & \text{if } 4.1 \text{ MJ/m}^2 < RAD_{TODAY} \leq 6.5 \text{ MJ/m}^2 \\ 100\%, & \text{if } RAD_{TODAY} \leq 4.1 \text{ MJ/m}^2, \text{ fully open blinds} \end{cases} \quad (4.39)$$

In section 4.3.2, the four modes of operation for charging the tank were presented. Figure 5.8 shows the procedure followed in (Candanedo & Athienitis, 2010a) to select the mode of operation depending on: (a) the temperature of at the top of the tank, (b) the BIPV/T air temperature, (c) the required tank set-point. This algorithm is similar to “Strategy 6” presented in the previous section.

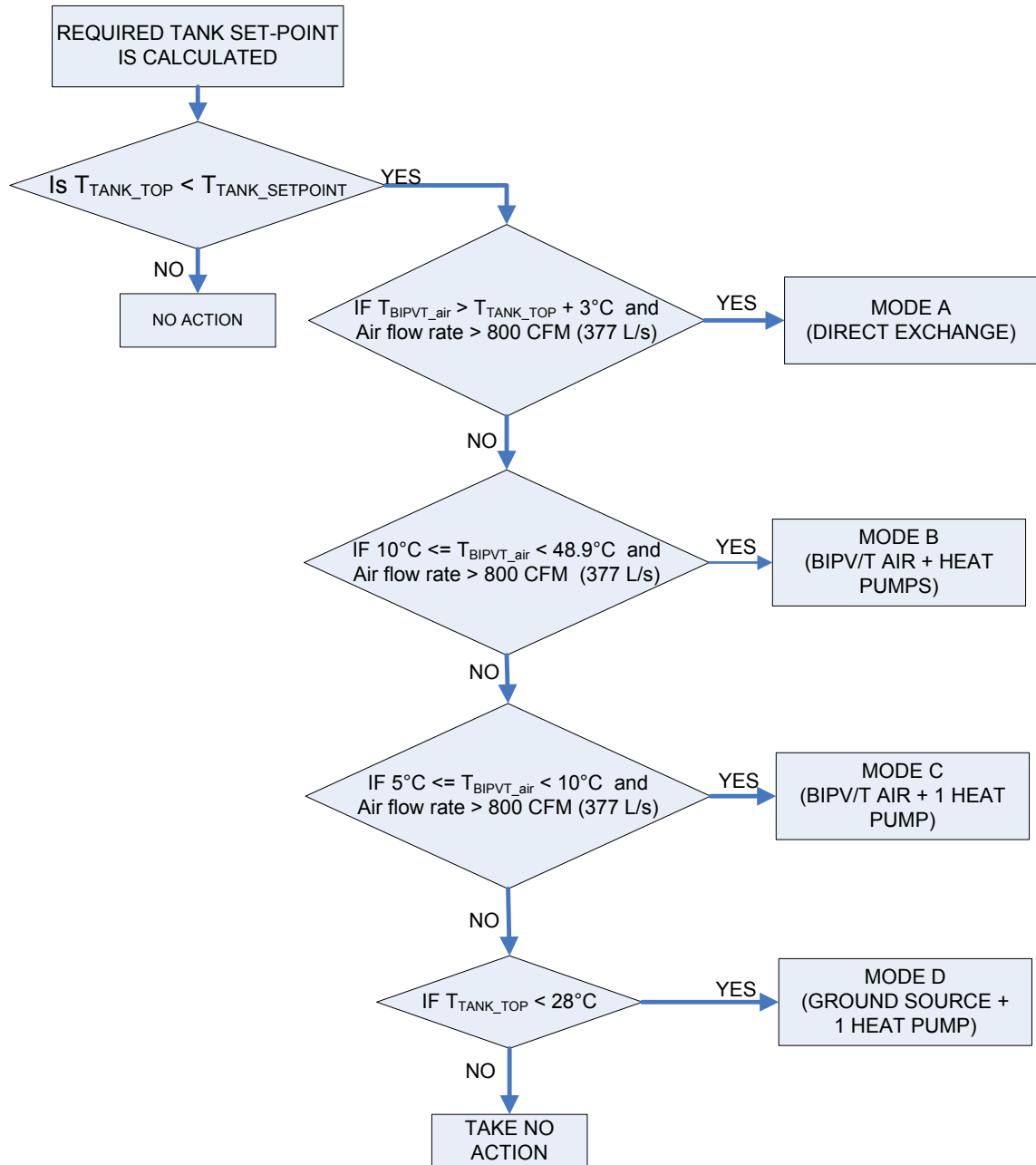


Figure 5.8. Algorithm for selecting the mode of operation for the BIPV/T-heat pump group.

In all cases, the fan speed was adjusted depending on the current solar radiation and outdoor temperature according to the following equation:

$$\text{Fan Speed Control Signal} = \begin{cases} 0\%, & \text{if } T_{\text{TANK_TOP}} \geq T_{\text{TANK_SETPOINT}} \\ \text{else} \\ 100\%, & \text{if } G_{\text{roof}} > 950 \text{ W/m}^2 \\ 91.25\%, & \text{if } 800 \text{ W/m}^2 < G_{\text{roof}} \leq 950 \text{ W/m}^2 \\ 82.5\%, & \text{if } 500 \text{ W/m}^2 < G_{\text{roof}} \leq 800 \text{ W/m}^2 \\ 73.75\%, & \text{if } 300 \text{ W/m}^2 < G_{\text{roof}} \leq 500 \text{ W/m}^2 \\ 65\%, & \text{if } G_{\text{roof}} \leq 300 \text{ W/m}^2 \text{ and } T_{\text{ext}} > 5 \text{ }^\circ\text{C} \\ 0\%, & \text{if } G_{\text{roof}} \leq 300 \text{ W/m}^2 \text{ and } T_{\text{ext}} \leq 5 \text{ }^\circ\text{C} \end{cases} \quad (4.40)$$

As shown in Equation (4.40), the fan is turned off if the set-point value is reached, or if the low solar radiation values (below 300 W/m² on the roof) coincide with low temperatures: in this case, the BIPV/T air will not work as an efficient source of heating.

5.3.3.2 Results

Some typical results found by applying these control strategies to the Alstonvale House model are presented from Figure 5.9 through Figure 5.13.

Energy storage in the building thermal mass and thermal comfort may be in conflict. This is illustrated in Figures 5.9 and 5.10. Figure 5.9 shows the indoor air room temperature and TES tank temperatures (top and bottom nodes) when the blinds (or curtains) are kept fully open for a sequence of three sunny days followed by two cloudy days in January. As expected, the TES tank set-point is raised on the 16th of January to take advantage of the current sunny conditions and prepare for the cloudy days. In general, the TES tank temperature follows the set-point, which means that the BIPV/T and heat pumps supply enough heat to the tank, and solar gains supply the heating load. In fact, the maximum daily temperature keeps increasing from the 14th to the 16th of January, in which overheating clearly occurs (temperatures near 30 °C).

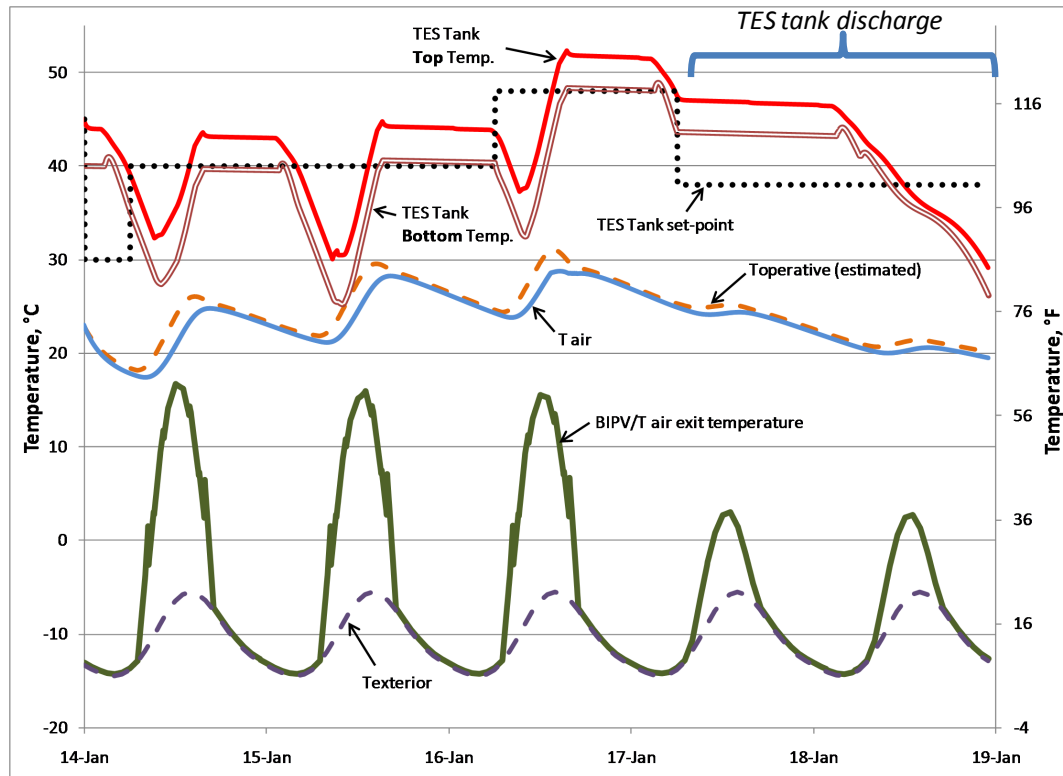


Figure 5.9. Set-point adjustments with blinds fully open.

The TES tank provides enough heating to satisfy the heating load on the 18th and 19th of January, when cloudy conditions prevail. The corresponding electric energy used by the heat pumps 67.8 kWh for that 5-day period.

If the blind position is adjusted to prevent overheating (as per the algorithm shown in Figure 5.7), the results are significantly different. Not enough heat is stored in the building's thermal mass, and therefore heat must be taken from the tank to satisfy the heating requirements. The TES tank set-point is therefore not reached and the heat pumps consume more energy: 89.5 kWh.

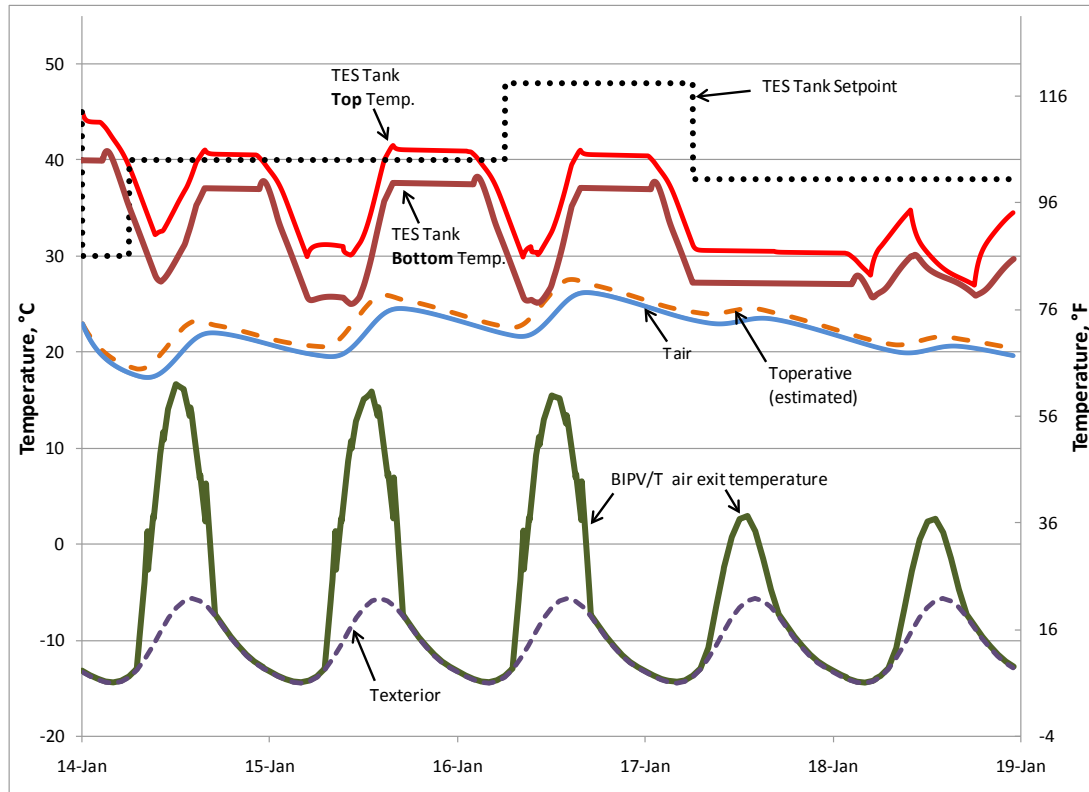


Figure 5.10. Position of blinds adjusted based on the expected radiation.

Figure 5.11 shows the power consumed by the heat pump system, as well as the power generated by the PV system (nominal power 7 kW_p) under the two scenarios described above. Most of the time, the power generated exceeds the power consumed; however, in the case of the “blind position adjustment”, the heat pump operates under cloudy conditions. This example illustrates that the BIPV/T seems an option that could be used to shift peak loads, since the period of maximum heat collection coincides with the maximum electric power generation. The energy stored in the TES tank can then be used at night or during later days.

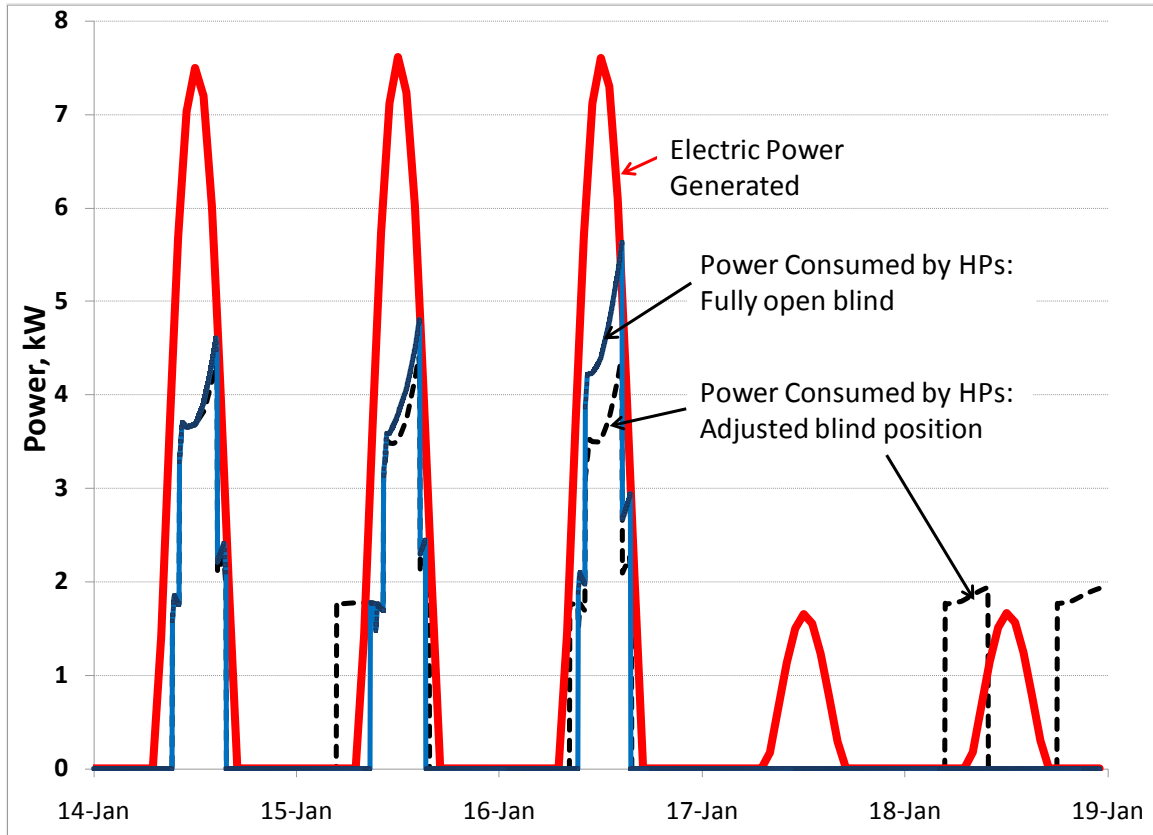


Figure 5.11. Power generated by PV and used by heat pumps.

Finally, Figures 5.12 and 5.13 show the performance of the system with a typical meteorological year (TMY) file instead of a paradigmatic sequence of days. The tank shows a cycle of charge/discharge which depends on both solar radiation and outdoor temperature. On March 5th, when cloudy conditions are expected to follow a sunny day, the set-point of the TES tank is raised.

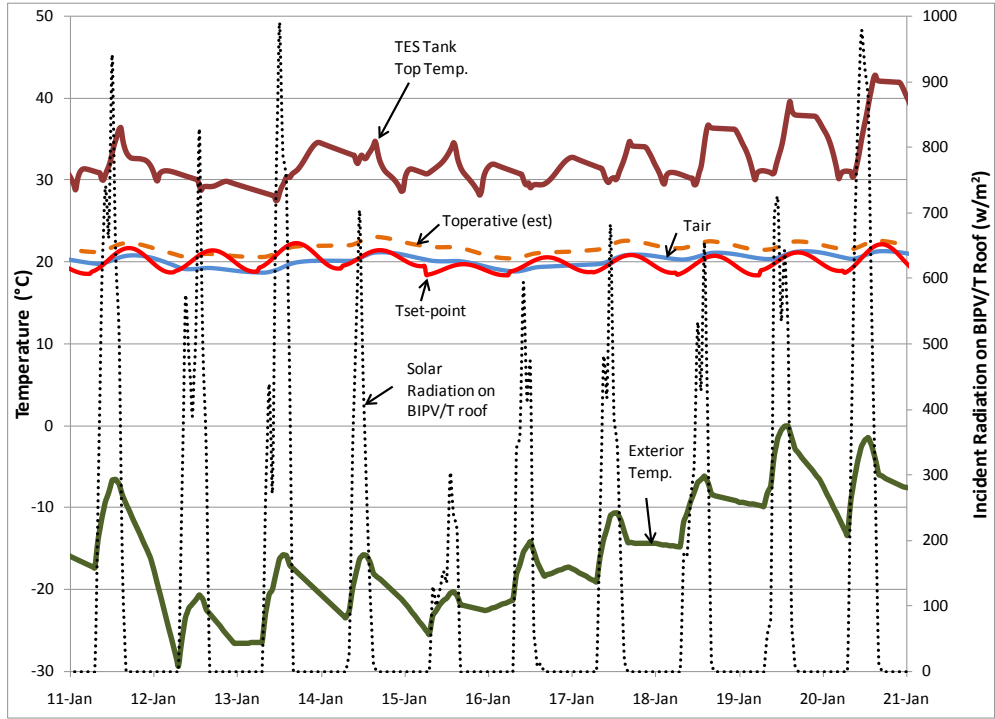


Figure 5.12. System's performance over 10 days in January (TMY2 file).

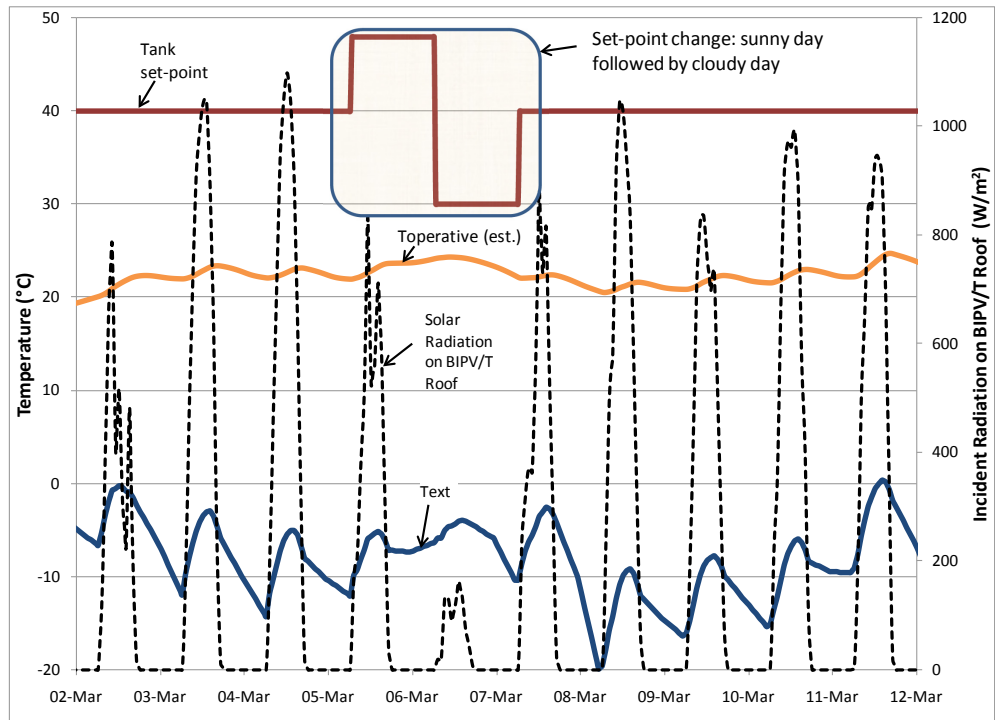


Figure 5.13. System's performance over 10 days in January (TMY2 file). Note the set-point change when a cloudy day follows a sunny day.

5.4 System Identification of Simplified Model

The control strategies presented in Section 5.1 consist of heuristic rules based on information from weather forecasts. While control strategies were developed for the case of the Alstonvale Net Zero House, a generalized methodology is advisable. A key problem encountered during the development of predictive control strategies was the complexity of the model used in the simulation. As mentioned before, simple models can often be reliable enough for the implementation of control strategies. However, it is difficult to select which is appropriate complexity level. The methodology used in this investigation, which is of general applicability, can be summarized in the following steps:

1. Create a detailed model of the building. This model can be created in any given simulation tool (ESP-r, EnergyPlus). A customized model may also be created using a programming tool (Mathcad, MATLAB, Python). Both approaches have been used during the course of this investigation.
2. Investigate the response of the building to “forcing functions”, typically solar gains, outdoor temperature and input from the house’s heating system. In a building simulation tool, each response can be studied independently by “turning off” the inputs that are not being considered. The output selected can be the indoor air temperature, operative temperature, the temperature of a surface, etc.
3. Apply a system identification algorithm to find transfer functions corresponding to each of the inputs being considered.
4. Create a simple model of the house consisting of the transfer functions found.
5. Compare the response of a simple model with a more detailed simulation.

6. Applied the simplified model to develop MPC algorithms for local-loop control, and for the development of optimal control strategies for supervisory control.

Figure 5.14 summarizes these steps:

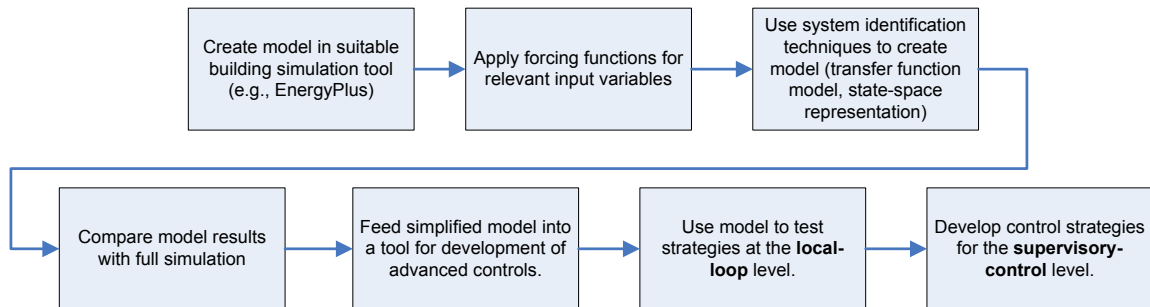


Figure 5.14. Methodology for system identification and model-based predictive control implementation.

As an exercise in the application of this methodology, a model was developed based on the basic geometry of the kitchen/dining room of the Alstonvale House (Figure 5.15). This building was the basis of the studies presented in two conference papers and two journal articles (Candanedo & Athienitis, 2010b; Candanedo *et al.*, 2011b, a; Candanedo & Athienitis, 2011).

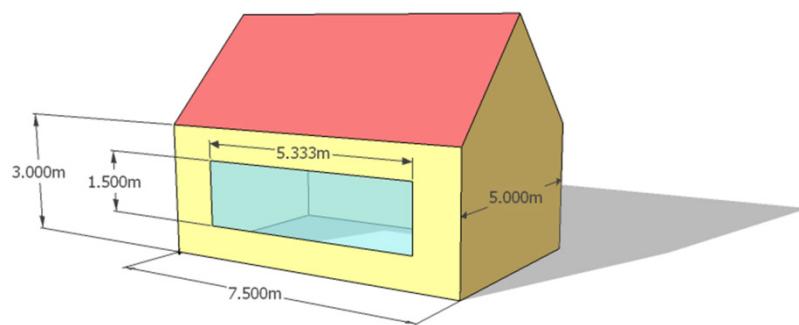


Figure 5.15. Geometry of the shed used for system identification and modeling of MPC strategies.

As in the case of the Alstonvale House, this “shed” had high levels of insulation on its walls and roof, a roof tilted at 45° facing due South, and a thick concrete slab. In this building, the only window is a large south-facing, argon-filled, triple-glazed window with two low emissivity coatings. The infiltration is kept constant at a fixed rate. No internal gains are considered.

A radiant floor heating system has been installed near the bottom of the floor slab. Contractors tend to prefer radiant floor heating installations made near the surface of the floor, because this kind of system has shorter time constants, which make them easier to control.

It is assumed that the main variables affecting the indoor temperature of the shed are the solar gains passing through the windows, the outdoor temperature and the heat delivered by the radiant floor heating system. In order to study the response to each of these inputs, three different forcing functions were created and applied to the model (Figure 5.16).

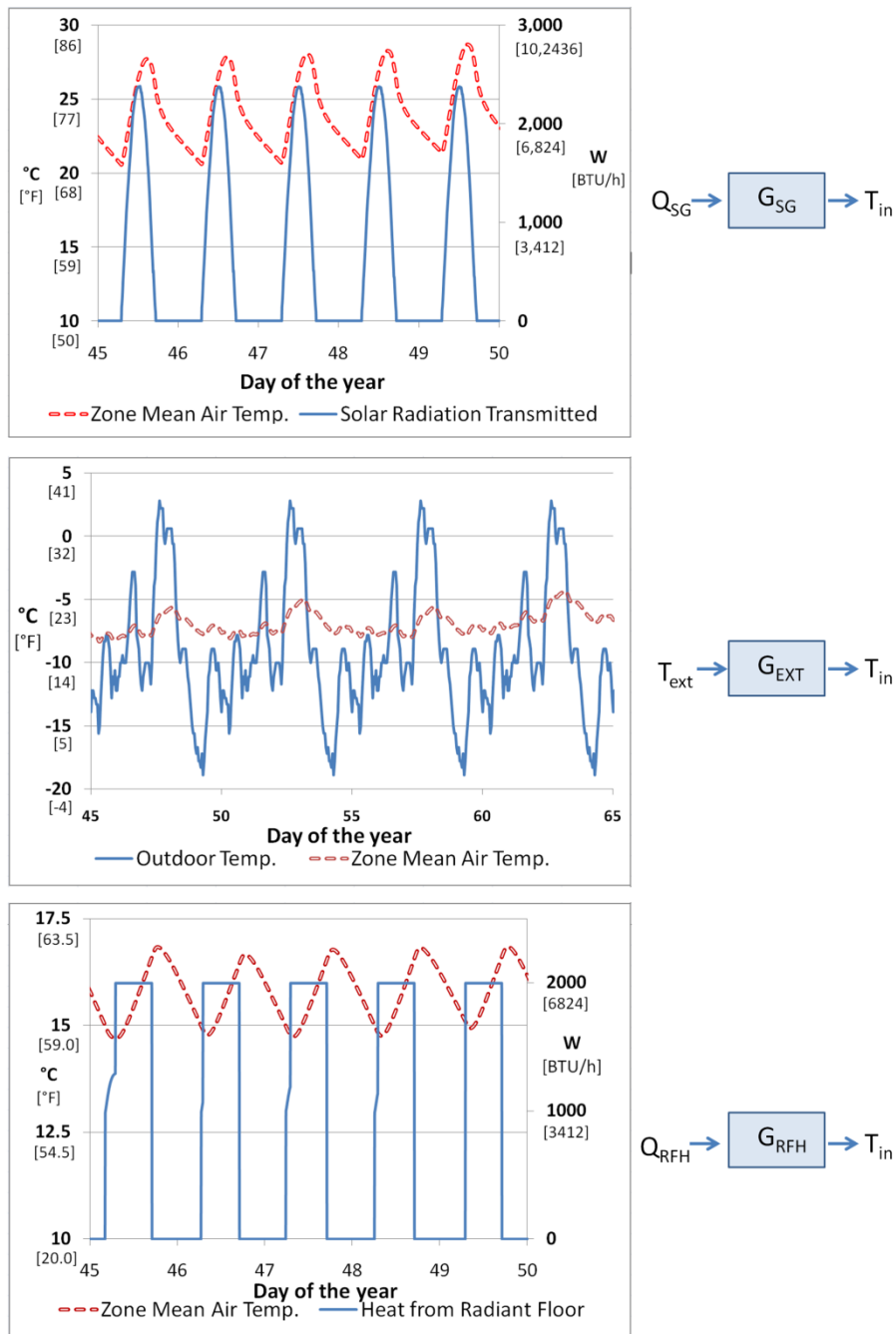


Figure 5.16. Input signals (forcing functions) used to study the response of a simple building to weather variables and heat from a radiant floor heating system. (Candanedo & Athienitis, 2011).

The forcing functions were selected to observe the response of the building for fluctuations with a daily period, as well as its response to lower-frequency phenomena

(with time constants of the order of days). As shown in Figure 5.16, the response of the building tends to follow a predictable pattern, especially in the cases of the response to solar gains and heat injected by the RFH.

Although the pattern of the response to outdoor temperature is less predictable (intermediate graph), its influence is smaller. Note that the amplitude of the indoor temperature fluctuations is about 5 °C while the outdoor temperature changes more than 20 °C.

As described in Candanedo & Athienitis (2011), MATLAB's system identification (SI) toolbox (Ljung, 2010) was used to find approximations for the three transfer functions:

$$\tilde{G}_{SG}(s) = \frac{2.27 \times 10^{-6} s^2 + 4.21 \times 10^{-10} s + 3.12 \times 10^{-14}}{s^3 + 4.17 \times 10^{-3} s^2 + 2.48 \times 10^{-7} s + 7.06 \times 10^{-13}} \text{ [K/W]} \quad (4.41)$$

$$\tilde{G}_{EXT}(s) = \frac{2.63 \times 10^{-5} s^2 + 7.53 \times 10^{-9} s + 3.00 \times 10^{-13}}{s^3 + 1.62 \times 10^{-4} s^2 + 1.03 \times 10^{-7} s + 3.78 \times 10^{-13}} \text{ [K/K]} \quad (4.42)$$

$$\tilde{G}_{RFH}(s) = \frac{0.01836}{1 + 4.254 \times 10^5 s} \text{ [K/W]} \quad (4.43)$$

The “free floating” response (i.e., without the intervention of the heating system), was tested with the transfer function model and with EnergyPlus (Figure 5.17).

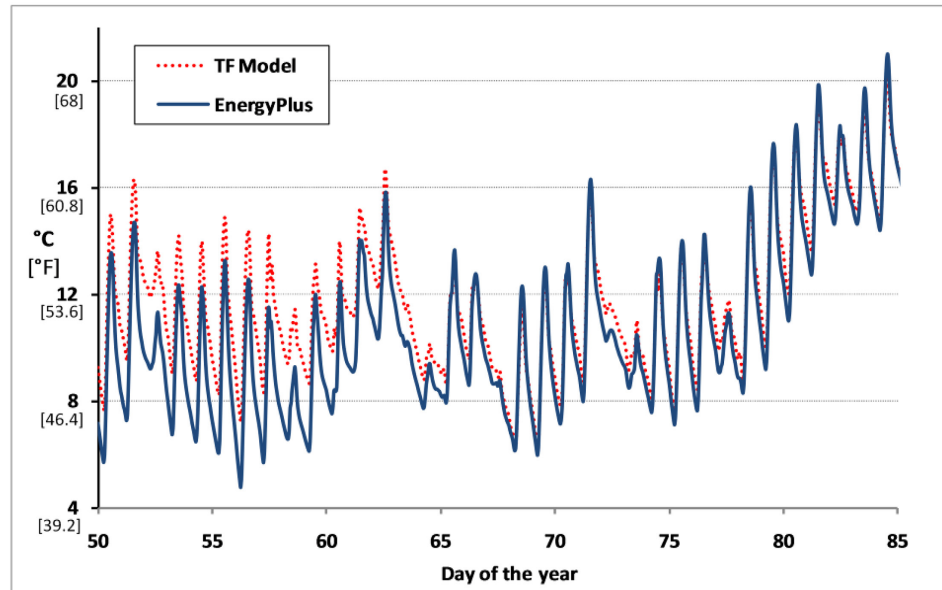


Figure 5.17. Comparison between EnergyPlus and TF model (Candanedo & Athienitis, 2011).

For the period shown in Figure 5.17, the results were considered satisfactory. The difference between the simplified model and the EnergyPlus model is less than 2 °C (3.6 °F) 76% of the time and a root mean square error between both signals of 0.88 °C. The FIT parameter was equal to 65%. It is interesting to note that the time constant of the RFH is 425,000 s, or nearly five days. Considering that 99% of the effect of a step input is perceived at 3τ (15 days), the difficulty of effectively controlling the heat released by the RFH without predictive control can be appreciated.

5.5 MPC for Radiant Floor Heating (RFH)

Linear models (transfer functions, state space, etc.) can be readily introduced in MATLAB's MPC toolbox for dealing with the second objective (effective set-point tracking). Figure 5.18 shows an implementation in Simulink of an MPC algorithm designed for the control of the RFH of the example shown in the previous section.

The input signals have been built from EnergyPlus weather files. The outdoor temperature has been incorporated directly with the MATLAB function *signalbuild*. Solar gains have been found by running a simulation with the EnergyPlus model and setting the radiation transmitted through the windows as an output of the EnergyPlus simulation.

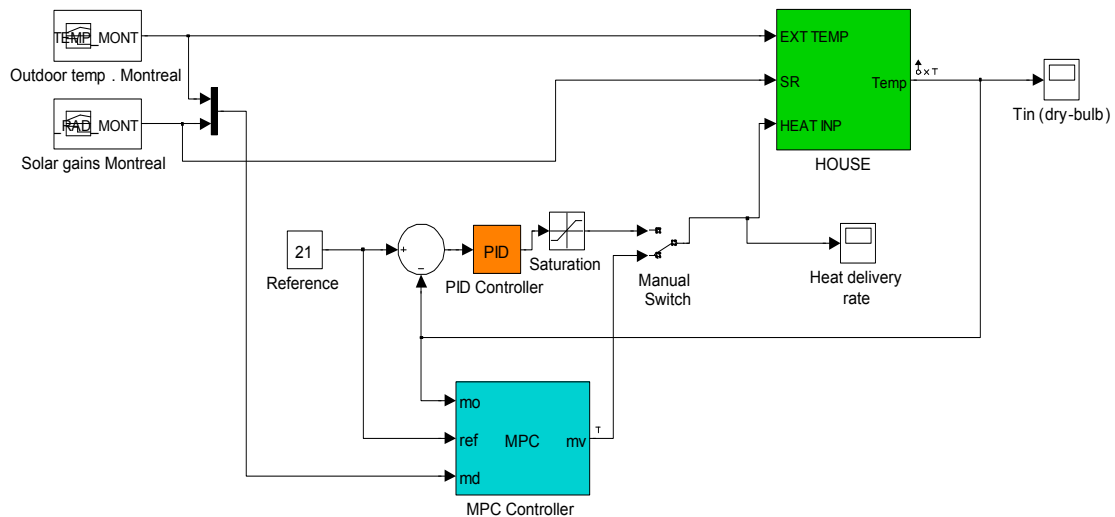


Figure 5.18. MPC in MATLAB/Simulink (Candanedo et al., 2011a).

Both input signals are sent to the input port “md” (measured disturbances) in the MPC block. The MPC block contains a complete description of the room model. The model has been created by using several commands for the treatment of linear systems available in MATLAB:

```

GEXT = tf(NUMEXT,DENEXT);    %Transfer functions
GSRE = tf(NUMGHR,DENGHR);
GRFH = tf(NUMRFH,DENRFH);

GEXT.InputName = 'Temp';    %Input names
GSRE.InputName = 'Rad';
GRFH.InputName = 'Heat';

GEXT.OutputName = 'y1';    %Output names
GSRE.OutputName = 'y2';
GRFH.OutputName = 'y3';

```

```
Suma = sumblk('Tin','y1','y2','y3');    %Sum block  
SISTEMA = connect(GEXT,GSRE,GRFH,Suma,{'Temp' 'Rad' 'Heat'},'Tin');
```

The linear system “SISTEMA” is then used to create an MPC block. In this case, the time step used is 900 s (15 min), with a prediction horizon of 192 time steps (48 hours) and a control horizon of 16 time steps (4 hours). The output of the RFH system is kept within 0 W (i.e., no cooling) and 1500 W. A fixed set-point temperature of 21 °C was applied.

Figure 5.19 shows results obtained for a period of 15 days between January and February (data from a TMY2 file was used) with an MPC algorithm applied to the system presented in the previous section. Although significant fluctuations are observed in the room temperature, mainly because there is no cooling power, the room temperature is maintained within comfortable limits (between 18 and 25 °C), while taking advantage of solar gains.

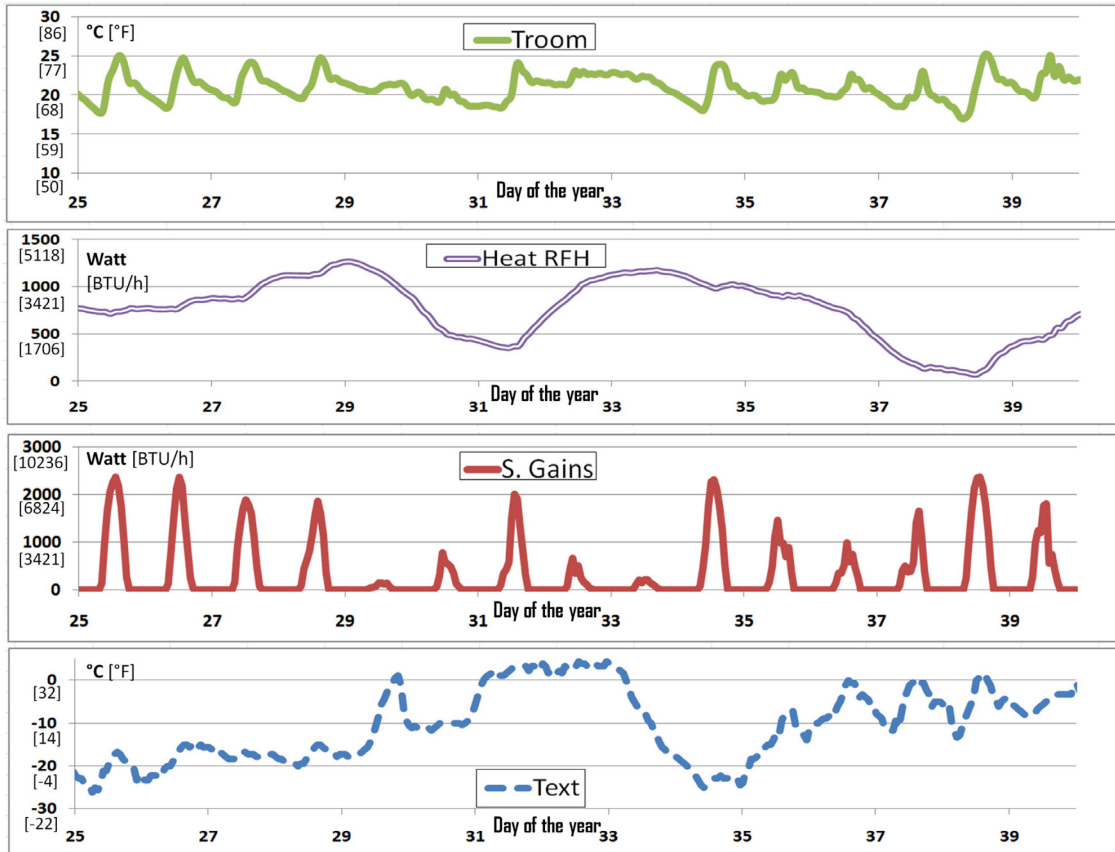


Figure 5.19. Results obtained with the MPC controller for Montréal weather.

When a series of cloudy days is expected (just before day 29) the heat delivery rate is higher. Conversely, when it is expected that high solar gains will coincide with relatively high temperatures, the heat delivery rate is reduced (as before day 31). The heat output rate increases again to compensate for the cloudy conditions of days 32 and 33.

5.6 MPC for RFH and Blind Position

One way to improve the performance of the MPC is to include some way to regulate the impact of solar gains. This problem was investigated in (Candanedo *et al.*, 2011b, a). In this case, the model used was created in MATLAB based on a thermal network representation. Details of the model are provided in (Candanedo *et al.*, 2011a). Although

a customized model was used, the same methodology can be applied to a model created in EnergyPlus, ESP-r or any similar program.

The strategy consists of assuming that a motorized roller blind, electrochromic windows or similar devices have the net effect of multiplying the solar gains by an adjusting factor τ_{adj} (Figure 5.20). This factor is assumed to vary between 100% (e.g., when the roller blinds are fully open) and a minimum value. In this example, the minimum value was taken to be 65%, which implies assuming that when the blind is fully closed, about 35% of the solar gains are rejected. This coincides with the assumption used in the experiment at the Concordia Solar House. In this case, the system has four inputs instead of three (the additional input is the value of the adjusting factor).

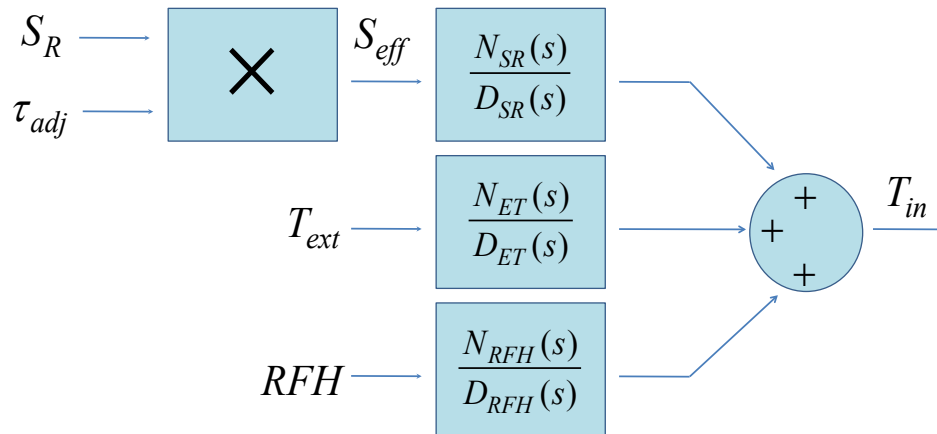


Figure 5.20. Multiplication of solar gains by and adjustment factor (“equivalent transmittance”) to account for the presence of a roller blind or similar device.

The multiplication of two signals is not a linear operation. Given that the MPC algorithm applied in this case requires a linear system, the system shown in Figure 5.20 is replaced with a linearized equivalent. The linearization is accomplished by breaking down the solar gains and the adjusting factor into two parts: a mean value at an operating point and a deviation from that value:

$$S_R = \bar{S}_R + \Delta S_R \quad (4.44)$$

$$\tau_{adj} = \bar{\tau}_{adj} + \Delta \tau_{adj} \quad (4.45)$$

The product of both variables can be expressed as:

$$\begin{aligned} S_{eff} &= \tau_{adj} S_R = (\bar{\tau}_{adj} + \Delta \tau_{adj})(\bar{S}_R + \Delta S_R) \\ &= \bar{\tau}_{adj} \bar{S}_R + \bar{\tau}_{adj} \Delta S_R + \Delta \tau_{adj} \bar{S}_R + \underbrace{\Delta \tau_{adj} \Delta S_R}_{\text{neglected}} \end{aligned} \quad (4.46)$$

If the product of the two deviations is neglected, then the variable S_{eff} is a linear function of ΔS_R and $\Delta \tau_{adj}$.

$$\tilde{S}_{eff} = \bar{\tau}_{adj} \bar{S}_R + \bar{\tau}_{adj} \Delta S_R + \Delta \tau_{adj} \bar{S}_R \quad (4.47)$$

Since $\Delta S_R = S_R - \bar{S}_R$ and $\Delta \tau_{adj} = \tau_{adj} - \bar{\tau}_{adj}$, after some algebraic manipulation:

$$\tilde{S}_{eff} = S_R \bar{\tau}_{adj} + \bar{S}_R \tau_{adj} - \bar{S}_R \bar{\tau}_{adj} \quad (4.48)$$

The resulting system is shown in Figure 5.21.

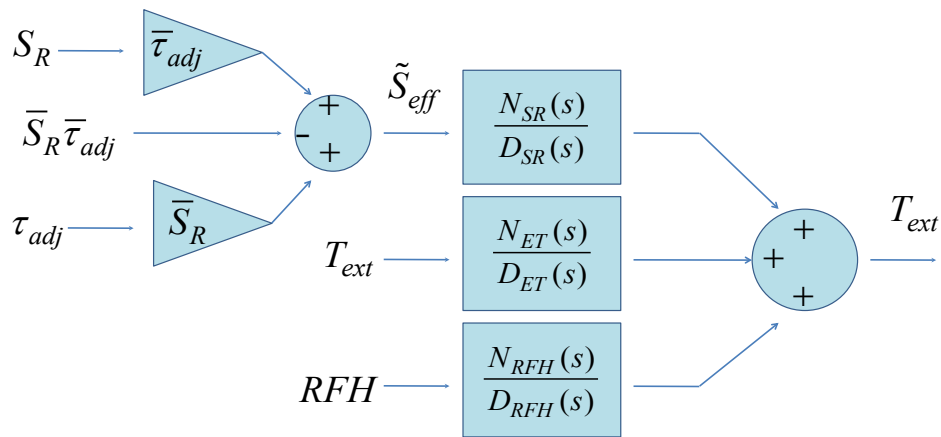


Figure 5.21. Linearized equivalent of system shown in Figure 5.20.

Although the system now has *five* inputs, one of them, the product of both mean values, is a constant. The operating point was selected taking into account that the control

of solar gains is more important when solar gains are relatively high; the mean value selected for solar gains was 1500 W. The mean value for the adjusting factor corresponds to a “50% open” position, $\bar{\tau}_{adj} = 0.825$, the midpoint between 65% and 100%.

Based on this discussion, an MPC block with two control variables was incorporated in a Simulink model (Figure 5.22).

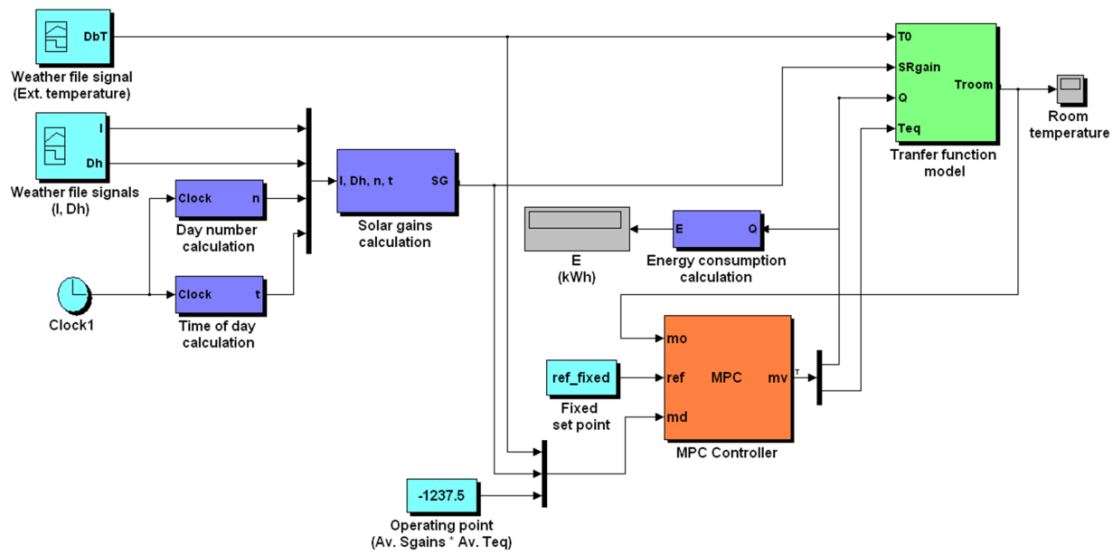


Figure 5.22. Simulink model with an MPC block generating two controlled variables (RFH heat output and blind position).

The system’s performance with and without blind control is shown respectively in Figures 5.23 and 5.24.

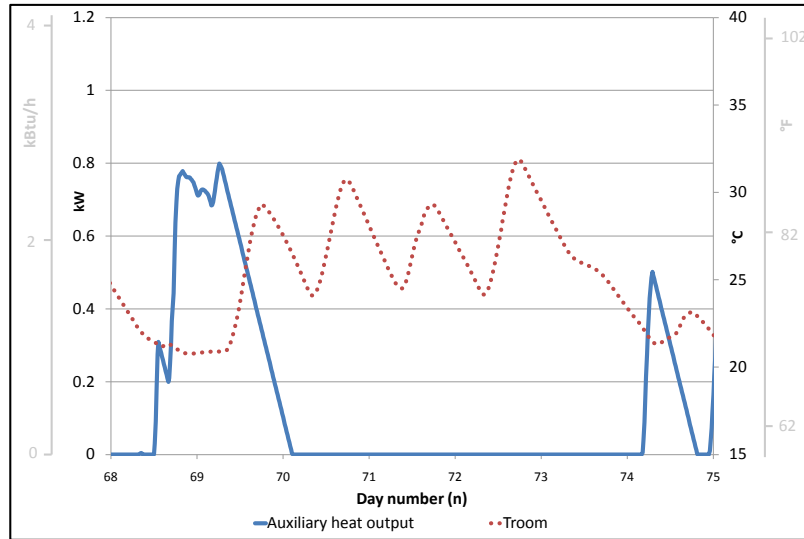


Figure 5.23. RFH heat delivery rate and room temperature without blind control.

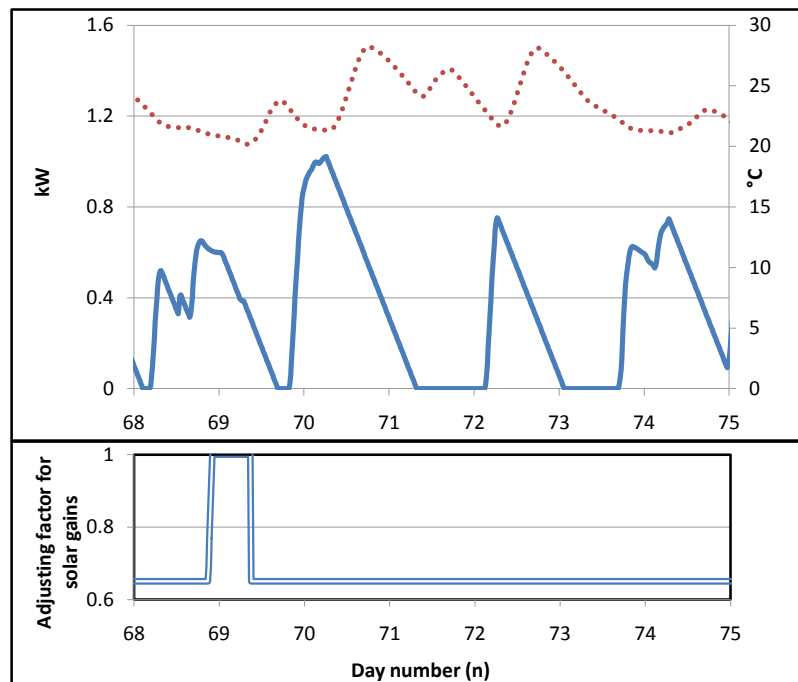


Figure 5.24. RFH heat delivery rate, adjusting factor and room temperature with blind control.

As seen in Figure 5.24, adjusting the position of a roller blind mitigates the problem of overheating, although it does not prevent it completely (the potential for heat rejection of an internal blind is limited). It is also interesting to observe that, in contrast with

Figure 5.23, the RFH system delivers heat between days 70 and 74. The blind position is either fully open (as in the first part of day 69) or fully closed (the rest of the time), practically without intermediate positions. Presumably, if the dynamic fenestration system had a higher capacity for heat rejection, intermediate positions would be more likely to occur.

5.7 Optimal Control of TES Tank Set-point

As shown in section 5.3, the first approach used in this investigation consisted of rule-based strategies. Recently, an optimal control algorithm has been used to select a set-point trajectory for the TES tank (Candanedo & Athienitis, 2010b, 2011).

5.7.1 System Description

Consider the system shown in Figure 5.25 (similar to the heating system of the Alstonvale House). A BIPV/T roof is used to heat outdoor air. The heated air is then used as the source of a heat pump. The condenser of the heat pump is linked to TES water tank, which itself is linked to the radiant floor heating system of the house.

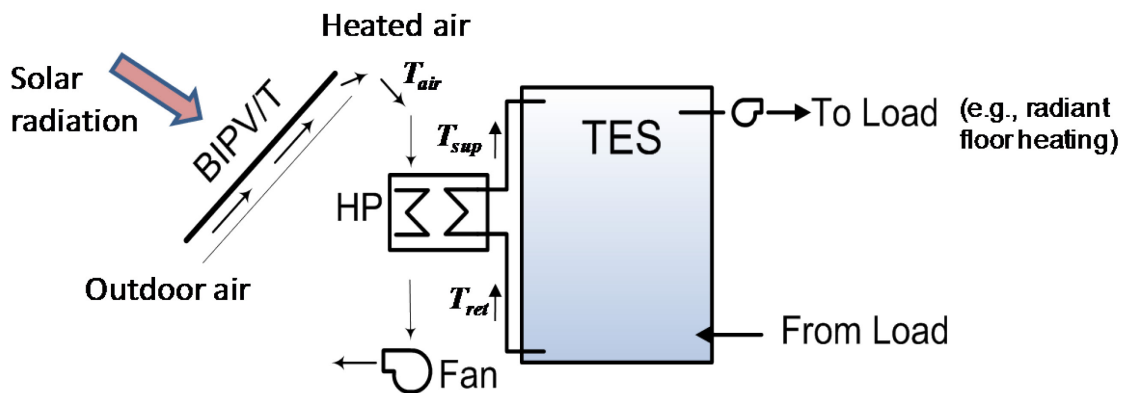


Figure 5.25. BIPV/T assisted heat pump used to heat a TES water tank.

In the example used in this investigation, the building shown in Figure 5.15 was used for the heating load calculations. The south-facing roof of the building was assumed to consist of a BIPV/T system. A 1000-L TES tank was used.

Technical data from a commercial air-source heat pump designed for cold climates, NIBE F2025-6, was used in the simulations (NIBE, 2010).

Table 5.6. Heating capacity (HC) and electric power consumption of the heat pump used in this example as a function of the air-source temperature and the temperature of the water supplied to the reservoir [Manufacturer’s data (NIBE, 2010)].

Air temp.		Temperature of Water Delivered to Sink (Output Temperature, T_{sup})								
		35 °C (95 °F)			45 °C (113 °F)			55 °C (131 °F)		
°C	°F	HC (kW)	HC (kBTU/h)	P_{HP} (kW)	HC (kW)	HC (kBTU/h)	P_{HP} (kW)	HC (kW)	HC (kBTU/h)	P_{HP} (kW)
-15	5.0	3.14	10.71	1.42	3.12	10.64	1.67	3.07	10.47	2.00
-7	19.4	4.34	14.80	1.56	4.25	14.49	1.77	3.94	13.44	2.16
2	35.6	5.90	20.12	1.55	5.56	18.96	1.81	5.23	17.83	2.26
7	44.6	6.78	23.12	1.53	6.44	21.96	1.84	6.07	20.70	2.26
15	59.0	8.11	27.66	1.56	7.78	26.53	1.87	7.35	25.06	2.30

In this investigation, the nominal air-flow rate required by the heat pump (1320 m³/hr or 780 CFM) was used in the simulations. Rather than using a look-up table, the following correlations were used to calculate the heat delivered by the heat pump and the electric energy consumed:

$$HC = 5.27 + 0.1514T_{air} \quad [\text{kW}] \quad (4.49)$$

$$P_{HP} = \left(\frac{T_{air} + 273.15}{258.15K} \right) \left(4 \times 10^{-4} T_{sup}^2 + 7 \times 10^{-3} T_{sup} + 1.18 \right) \quad [\text{kW}] \quad (4.50)$$

Note the HC is only a function of the air temperature, while P_{HP} is a function of both the T_{air} and T_{sup} .

The information which is usually available is the temperature of the BIPV/T air (T_{air}) and the temperature of the return water coming from the tank (T_{ret}), as shown in Figure 5.25. In order to calculate the point of operation for any given condition, the water output temperature (T_{sup}) is calculated by using the nominal water flow rate of the heat pump (0.16 L/s, 2.54 gal/min) with the following equation:

$$T_{sup} = T_{ret} + \frac{HC}{\dot{m}_w c_{pw}} \quad (4.51)$$

5.7.2 Dynamic Programming Algorithm

Charging the TES tank has a cost associated mainly with the electric power consumption of the heat pump, although the circulating pumps and the BIPV/T fan also represent a sizeable portion. The key idea is that any change from state to state will take a certain amount of energy, which will vary depending on the conditions. The problem lies in determining the optimal set-point trajectory for the TES tank.

This problem was addressed with a dynamic programming (DP) algorithm in Candanedo & Athienitis (2010b, 2011) with a single state variable (average tank temperature). Although there will certainly be stratification in the tank, a single node was used for two reasons: (a) it represents a “worst-case scenario” (no stratification), (b) it can be used as a proof of concept of the algorithm.

To start, taking into account the availability of reliable weather forecasts released by Environment Canada, a 48 hr prediction horizon (F_H) was chosen. For this example, the control horizon is assumed to be equal to the prediction horizon and therefore set-point values are also calculated over a two-day period.

Another important decision was the time discretization: how often should the set-point be changed? Once more, considering that weather forecasts from the Canadian Meteorological Service are tabulated at 3 hour intervals (Poulin *et al.*, 2006), it seemed reasonable to update the tank set-point every three hours. Moreover, changing the set-point more frequently would be unnecessary and would impose a heavy duty cycle (i.e., excessive switching between ON/OFF) for the heat pump. Consequently, the determination of the optimal set-point trajectory means finding 16 values at 3 hour intervals.

From the manufacturer's data, it was determined that the heat pump could work with temperatures at the "sink side" (i.e., condenser side) ranging from 30 to 55 °C. This domain was discretized in 11 values, spaced at intervals of 2.5 °C. The eleven possible set-point values (PSV) are:

$$PSV = \{30.0, 32.5, 35.0, 37.5, 40.0, 42.5, 45.0, 47.5, 50.0, 52.5, 55.0\} \text{ °C} \quad (4.52)$$

If there are 16 time slots after the initial time, and 11 possible temperature values in each one of them, the total number of possible paths is $11^{16} = 4.6 \times 10^{16}$ values. This figure is not manageable with an exhaustive search: assuming that the calculation of the cost of each trajectory takes 0.01 s, an evaluation would take more than 14 million years.

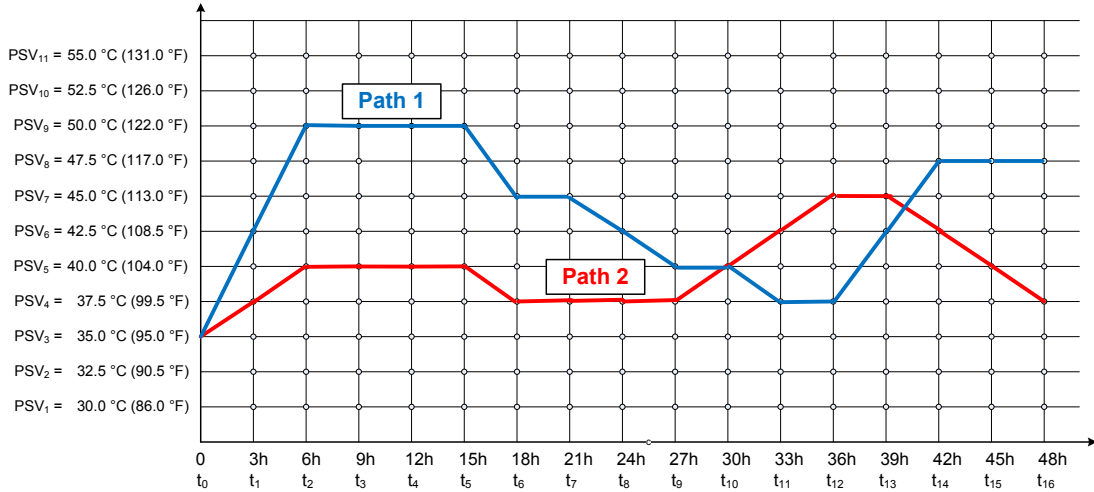


Figure 5.26. Two possible set-point trajectories for the TES tank set-point (state variable).

A DP algorithm is used to find the optimal set-point trajectory, as it significantly reduces the number of required calculations. The DP algorithm is implemented through the following steps.

1. For a given time step t_0 , the control horizon (48 hr) is divided into 16 future times:

$$\text{future time steps} = \{t_1, t_2, \dots, t_{16}\} \quad (4.53)$$

2. At any of these times, the temperature can take any of the values presented in Equation (4.52). A nomenclature based on two indices is adopted. The state $S_{i,j}$ means that at time i , the temperature set-point is j . For example, the state $S_{4,8}$ means that at the 4th time step (twelve hours from the beginning), the 8th set-point value is used (47.5 °C).

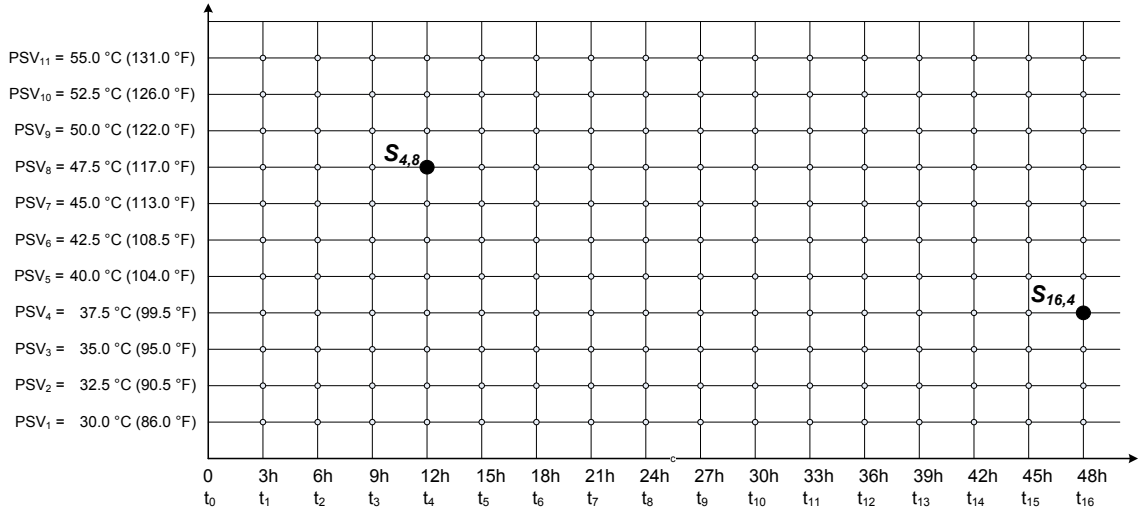


Figure 5.27. Nomenclature used and two sample points.

3. A guess value is assigned to the last temperature. In other words, the last state is $S_{16,guess_value}$. For example, let us assume that this value is $S_{16,6}$.
4. Now, we need to evaluate the minimum cost of moving from any second-to-last state until the final state. Since there are no intermediate states, this minimum cost of moving from t_{15} until the end is simply the result of evaluating the cost function:

$$J_{15,j} = C(S_{15,j}, S_{16,4}) \quad (4.54)$$

There are 11 possible ways of carrying out this operation. The **global minimum cost** will be the minimum of these 11 values:

$$JG_{15} = \min(J_{15,1}, J_{15,2}, \dots, J_{15,11}) \quad (4.55)$$

An important detail is that the optimum sequence of points must also be recorded:

$$OS_{15} = \{x_{15}, x_{16}\} \quad (4.56)$$

These variables hold the temperatures of the 15th and 16th time steps.

5. Now, we move backwards in time. The minimum cost of going from **any given point** at time t_{14} ($S_{14,j}$) until the final state will be given by:

$$J_{14,j} = \min \left\{ \begin{array}{l} C(S_{14,j}, S_{15,1}) + J_{15,1} \\ C(S_{14,j}, S_{15,2}) + J_{15,2} \\ C(S_{14,j}, S_{15,3}) + J_{15,3} \\ C(S_{14,j}, S_{15,4}) + J_{15,4} \\ C(S_{14,j}, S_{15,5}) + J_{15,5} \\ C(S_{14,j}, S_{15,5}) + J_{15,6} \\ C(S_{14,j}, S_{15,5}) + J_{15,7} \\ C(S_{14,j}, S_{15,5}) + J_{15,8} \\ C(S_{14,j}, S_{15,5}) + J_{15,9} \\ C(S_{14,j}, S_{15,5}) + J_{15,10} \\ C(S_{14,j}, S_{15,5}) + J_{15,11} \end{array} \right. \quad (4.57)$$

The global minimum cost for advancing from time t_{14} to the final state is then:

$$JG_{14} = \min(J_{14,1}, J_{14,2}, \dots, J_{14,11}) \quad (4.58)$$

The sequence of states corresponding to the JG_{14} is then recorded:

$$OS_{14} = \{x_{14}, x_{15}, x_{16}\} \quad (4.59)$$

It is important to remember that **the optimal sequences are re-calculated**. For example, the value of x_{15} may be different in OS_{14} and OS_{15} .

6. We move backwards in time again. The minimum cost of going from **any given point** in the time slot t_{13} (i.e., state $S_{13,j}$) will be:

$$J_{13,j} = \min \left\{ \begin{array}{l} C(S_{13,j}, S_{14,1}) + J_{14,1} \\ C(S_{13,j}, S_{14,2}) + J_{14,2} \\ C(S_{13,j}, S_{14,3}) + J_{14,3} \\ C(S_{13,j}, S_{14,4}) + J_{14,4} \\ C(S_{13,j}, S_{14,5}) + J_{14,5} \\ C(S_{13,j}, S_{14,6}) + J_{14,6} \\ C(S_{13,j}, S_{14,7}) + J_{14,7} \\ C(S_{13,j}, S_{14,8}) + J_{14,8} \\ C(S_{13,j}, S_{14,9}) + J_{14,9} \\ C(S_{13,j}, S_{14,10}) + J_{14,10} \\ C(S_{13,j}, S_{14,11}) + J_{14,11} \end{array} \right. \quad (4.60)$$

Then, the global minimum cost for advancing from time t_{13} to the final state is:

$$JG_{13} = \min(J_{13,1}, J_{13,2}, \dots, J_{13,11}) \quad (4.61)$$

The advantage of the method becomes more evident: the costs $J_{14,1}$, $J_{14,2}$, etc. are already known. The corresponding sequence of states is then recorded:

$$OS_{13} = \{x_{13}, x_{14}, x_{15}, x_{16}\} \quad (4.62)$$

7. The same operations are repeated until the global minimum cost (JG_0) for the initial state is reached, and the optimal sequence OS_0 is obtained. The initial state is often known (i.e., the user usually knows the current temperature set-point), allowing this step to be omitted.

The advantage of the DP algorithm described above is that for each “backward jump”, only $11 \times 11 = 121$ additional cost calculations must be performed. In total, the number of cost calculations is $11 \times 11 \times 16 = 21,296$.

If necessary, the sequence can then be repeated with different guess values for the final state. For the 11 possible set-point values, this would imply a total of $11 \times 21,296 = 234,256$ cost calculations: a large number, but still significantly smaller than that of an exhaustive search.

5.7.3 Cost of Switching from State to State

In the previous calculations, reference has often been made to the cost of switching between states. In this case, the cost function is the electric energy used by the heat pump to change the tank's temperature. The following factors must be considered:

- Thermal energy is being drawn from the tank to supply the heating load, which depends on the set-point values, solar gains and outdoor temperature.
- Thermal energy is given to the tank by the heat pump.

With these factors in mind, the following steps are taken to calculate the cost function:

1. Assuming a uniform temperature in the tank, the change of internal energy given by the set-point change will be:

$$\Delta U_{AB} = V_{\text{tank}} \rho_w c p_w (T_{spB} - T_{spA}) \quad (4.63)$$

For example, a set-point change from 35 °C to 40 °C in a 1,000-L tank represents a change in internal energy of 5.8 kWh.

2. During the period between the set-point change, energy will be drawn from the tank by the loads. This thermal energy is calculated by integrating the

value of the heating load by applying the trapezoidal rule (i.e., the mean of the heating load multiplied by the time period):

$$E_{del,AB} = \left(\frac{Q_{H,A} + Q_{H,B}}{2} \right) \Delta t \quad (4.64)$$

For example, if the load at 3:00 p.m. is 2 kW, and the load at 6:00 p.m. is 1 kW, the energy delivered over this three-hour period will be 4.5 kWh.

3. Changing the set-point will require heating the tank while at the same time compensating for the heat delivered to the loads. Therefore, the total energy required from the heat pump is given by:

$$E_{req,AB} = \Delta U_{AB} + E_{del,AB} \quad (4.65)$$

Continuing with the example, raising the set-point from 35 to 40 °C, while delivering heat to the house, will require 5.8 kWh + 4.5 kWh = 10.3 kWh.

4. If $E_{req,AB} \leq 0$, this means that the set-point can be changed without receiving additional energy from the heat pump. Therefore, the heat pump does not need to operate and the cost of the set-point change from A to B is zero:

$$C_{AB} = 0 \quad (4.66)$$

5. If $E_{req,AB} > 0$, then the **heat pump needs to deliver heat to the tank**. The cost will be the electric energy consumed by the heat pump over that period. The electric energy used by the heat pump depends on the radiation received by the roof, outdoor temperature, air-flow rate, the temperature of the tank and other factors.

- a. The first step is to calculate the time-average BIPV/T air temperature over the interval of interest. This is accomplished by using the model presented in section 4.3.1.2.

$$T_{air_avg,AB} = \frac{1}{\Delta t} \int_{t_A}^{t_B} T_{air} (G, T_{ext}, T_{attic}, w_{speed}, \dot{m}_{air}) dt \quad (4.67)$$

- b. The available thermal energy is calculated by introducing the average air temperature into the heat pump correlation (4.49), and then multiplying by the time step (Δt).

$$H_{HP,AB} = \Delta t \cdot HC(T_{air_avg,AB}) \quad (4.68)$$

- c. The average of both set-points is used to calculate the return water temperature ($T_{ret,AB}$) in order to calculate the average supply temperature ($T_{sup,AB}$), and finally the electric power consumption (EE_{AB}).

$$T_{ret,AB} = \frac{TSP_{AB} + TSP_{AB}}{2} \quad (4.69)$$

$$T_{sup,AB} = T_{ret,AB} + \frac{HC(T_{air_avg,AB})}{\dot{m}_w c_{pw}} \quad (4.70)$$

$$EE_{AB} = \Delta t \cdot P_{HP}(T_{sup,AB}, T_{air_avg,AB}) \quad (4.71)$$

It is possible that the average air temperature during that period is too cold for the operation of the heat pump. To account for this, when the average BIPV/T temperature falls below -15°C , P_{HP} is assigned a very large value (1 MW), guaranteeing that any path involving such an operation would be left out.

6. The potential thermal energy recovered from the roof $H_{HP,AB}$, which was calculated in Equation (4.68), can be larger or smaller than the heat required to change set-points calculated in Equation (4.65), $E_{req,AB}$. If $H_{HP,AB} > E_{req,AB}$, then the heat pump will not need to run during the entire time step. The electric energy use is adjusted proportionally as follows:

$$C_{AB} = EE_{AB} \cdot \left(\frac{E_{req,AB}}{H_{HP,AB}} \right) \quad (4.72)$$

7. If the heat required is equal to the heat available ($H_{HP,AB} = E_{req,AB}$), then the cost is equal to the electricity usage calculated in Equation (4.71):

$$C_{AB} = EE_{AB} \cdot \underbrace{\left(\frac{E_{req,AB}}{H_{HP,AB}} \right)}_1 = EE_{AB} \quad (4.73)$$

8. Finally, if the available heat is smaller than the required heat for the set-point change ($H_{HP,AB} < E_{req,AB}$) then this set-point transition is impossible and the path is discarded. This is accomplished in the algorithm by making the cost tend to infinity:

$$C_{AB} = \infty \quad (4.74)$$

A summary of this algorithm is presented in Figure 5.28. The MATLAB code used in the implementation of the cost function and the dynamic programming algorithm is included in the appendix.

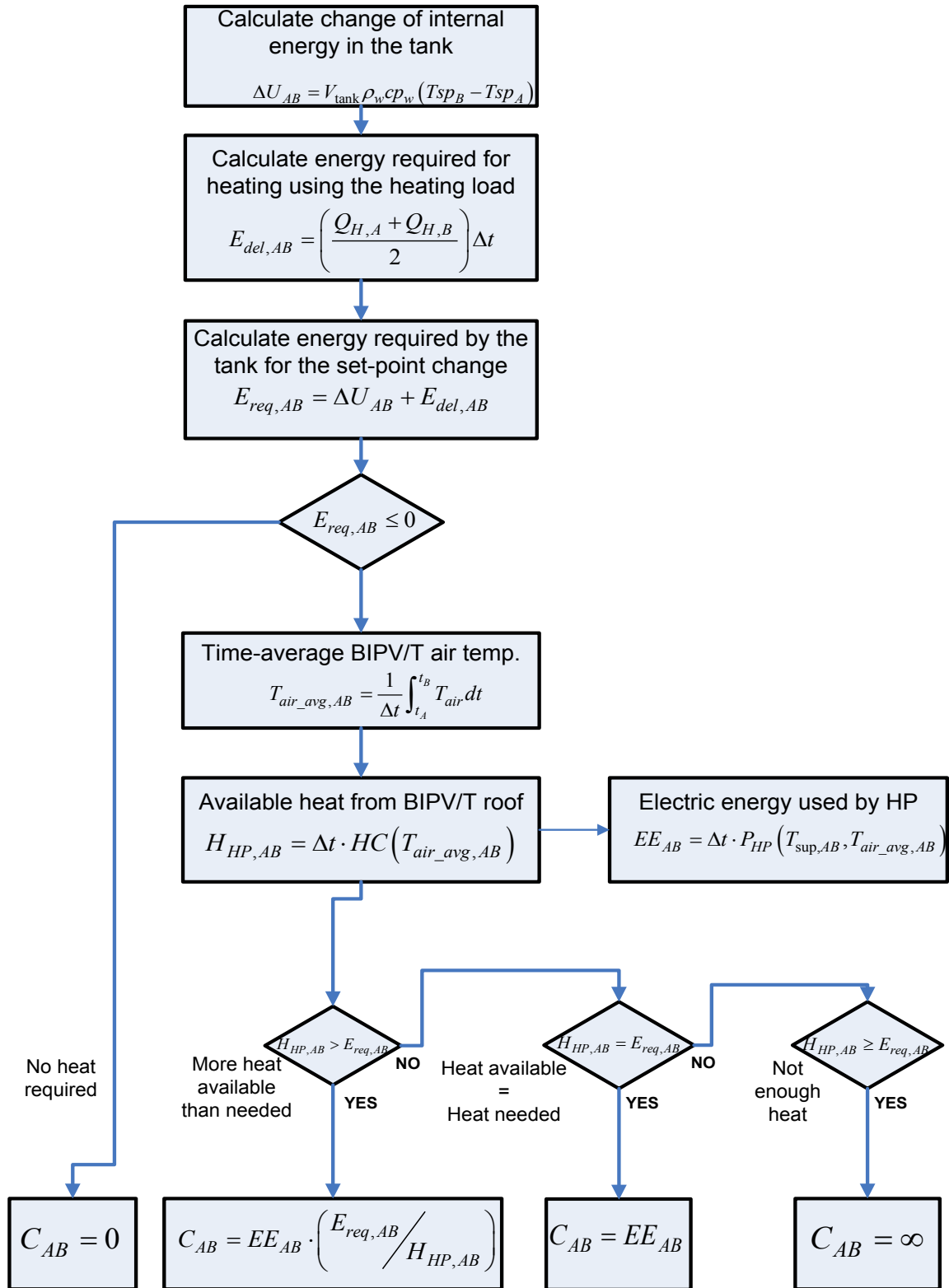


Figure 5.28. Algorithm used to calculate the cost of moving from set-point A to set-point B.

5.7.4 Results of Dynamic Programming Algorithm

Montréal weather data and results from load calculations with an MPC algorithm^{‡‡} were used to calculate optimal set-point trajectories using the procedure described above. The data correspond to the period starting at 0:00 on January 24 and ending at 0:00 of January 26. The initial and final states were assumed to be 37.5 °C and 30.0 °C, respectively. Two paths are shown in Figure 5.29: a “plausible” path in which the TES set-point increases during the daytime (a decision likely to be made by a human operator), and an optimal set-point trajectory. Although both strategies provided heating to the building, the energy consumed by the optimal set-point trajectory is 11.3 kWh while the “plausible” path 15.6 kWh; the optimal path represents energy savings of 38%.

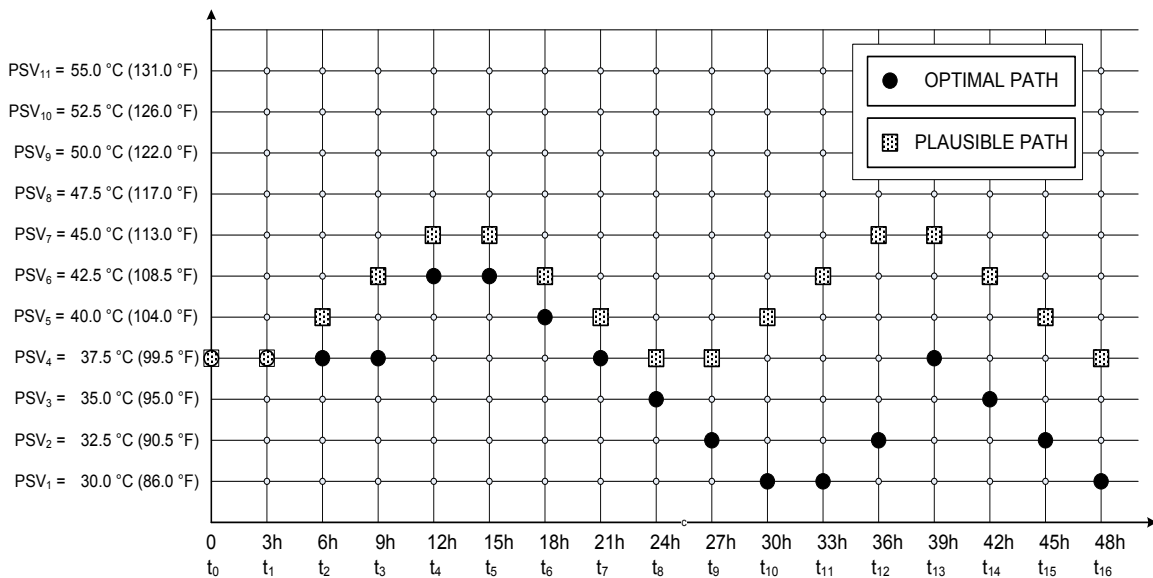


Figure 5.29. Comparison of an optimal set-point trajectory and a plausible trajectory for the TES tank.

^{‡‡} Details of the MPC algorithm were presented in sections 5.5 and 5.6.

The application of the DP algorithm to other times of the year provides insight on its capabilities. Figure 5.30 shows the weather conditions and the load calculated with an MPC algorithm for a period between January 10 and 12; Figure 5.31 shows the set-point trajectory corresponding to the same period. The second day is somewhat less sunny than the first day; however, the temperature drops significantly (about 20 °C) in this period.

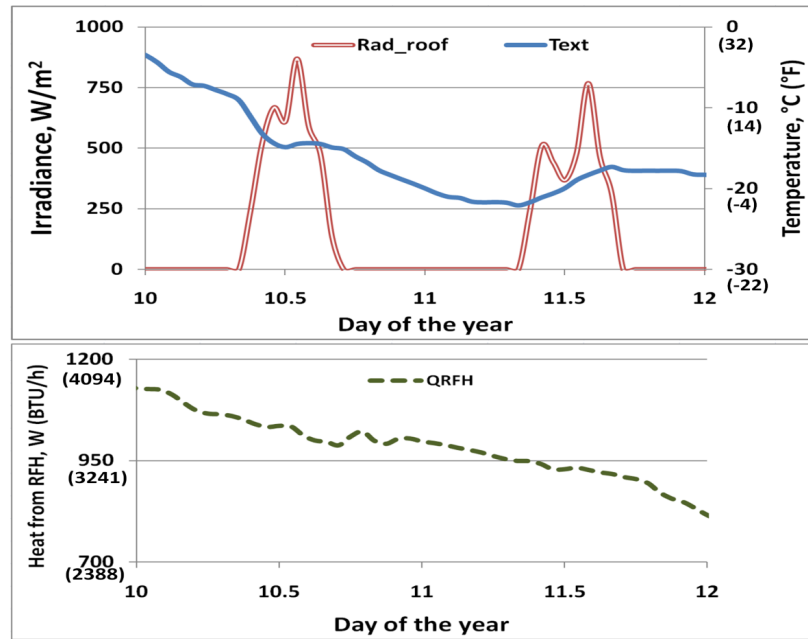


Figure 5.30. Weather conditions and RFH heat output calculated by MPC algorithm (Jan. 10th - 12th).

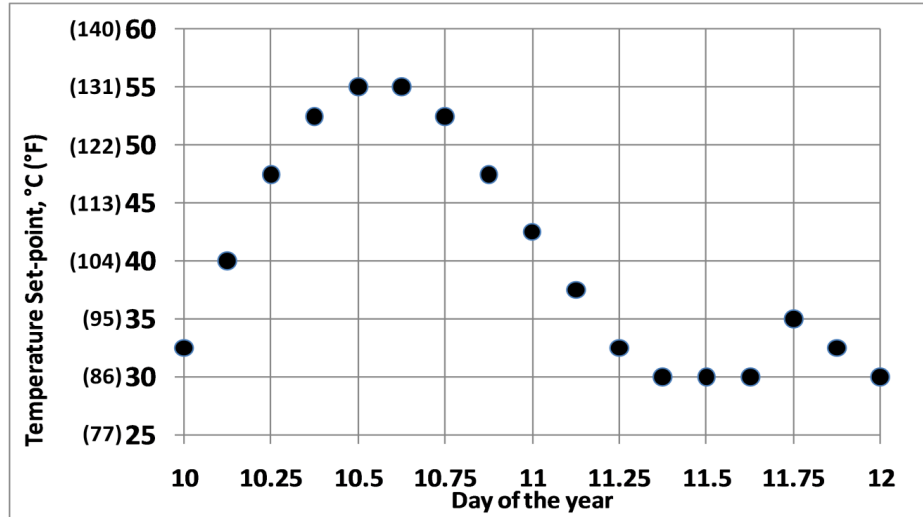


Figure 5.31. Optimal TES set-point trajectory (Jan. 10th to 12th).

On the first day (Figure 5.31), the combination of relatively warm outdoor temperatures and sunny conditions is optimal for the operation of the BIPV/T-assisted heat pump. Therefore, the DP algorithm raises the tank set-point to 55 °C on the first day to collect as much heat as possible. The first day is used for heat collection (both in the building’s thermal mass and in the TES tank).

Figure 5.32 shows the weather conditions and calculated RFH load for two days in December (Dec 9th at 0:00 until Dec 11th at 0:00).

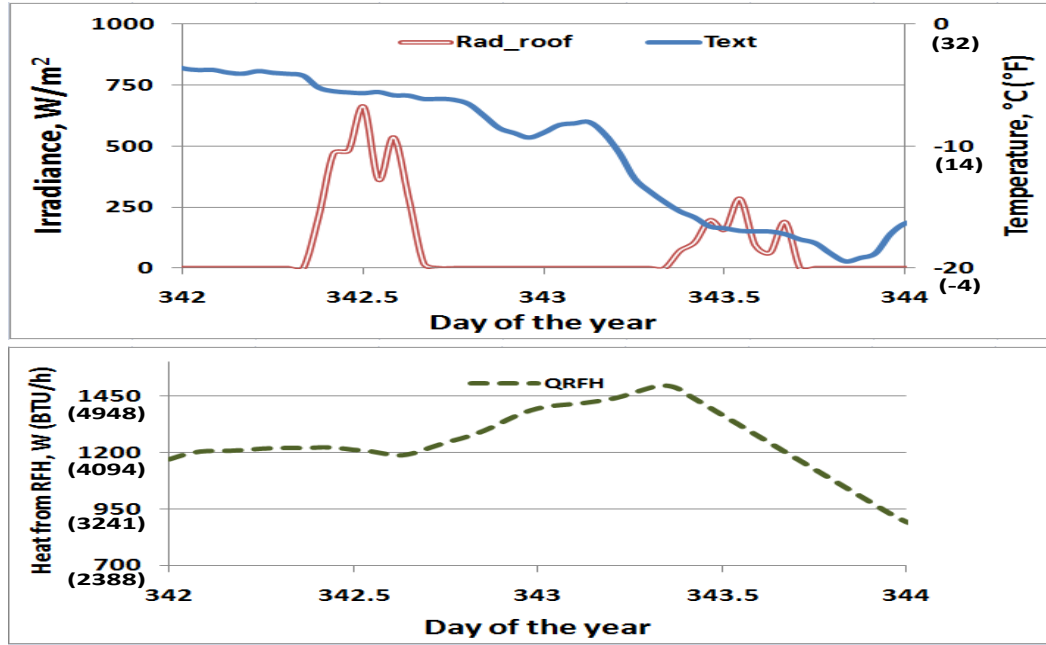


Figure 5.32. Weather conditions and RFH heat output calculated by MPC algorithm (Dec. 9th – Dec. 11th).

In this case, the output of the DP algorithm shows relatively low set-points for both days (Figure 5.33). The set-point values during the first day are slightly higher, since solar radiation is also slightly higher.

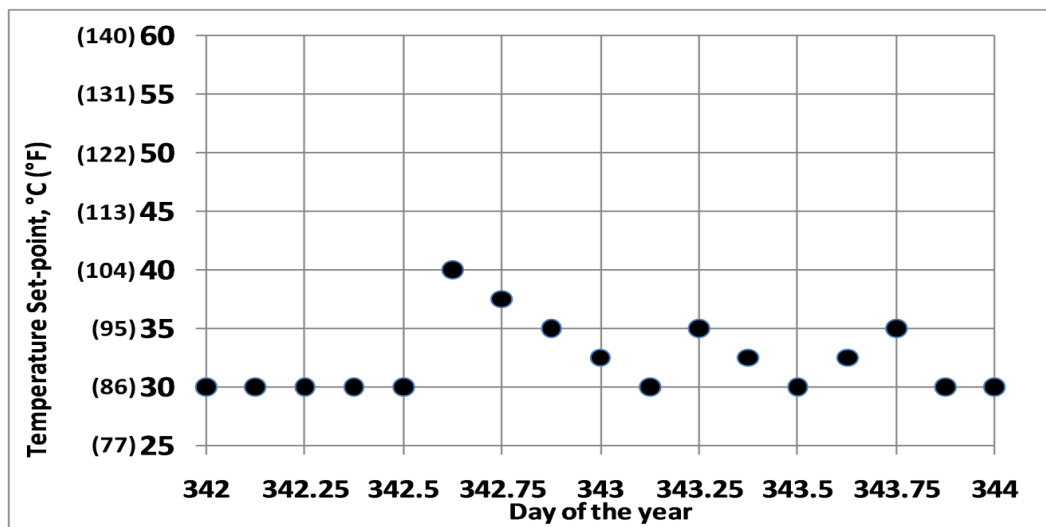


Figure 5.33. Optimal TES set-point trajectory (Dec 9th to Dec 11th).

While the algorithm presented here used only the electric energy use of the heat pump as the cost function, the energy consumed by the fan, pumps and other auxiliary equipment should be taken into account in further research.

6. Conclusions

6.1 Summary

This thesis investigated predictive control strategies for optimally designed solar homes. The design approach of these homes relies on the use of solar energy by incorporating passive solar design as well as active solar technologies, along with energy efficiency and conservation measures. As expected, it has been found that predictive control can be beneficial in dealing with the variability of solar radiation and weather conditions, by planning the charge and discharge of active and passive TES as a function of the expected availability of solar energy and heating loads of the house.

A literature review was presented, including optimal and predictive control techniques for buildings, technologies for advanced homes, modeling tools and Canadian examples of advanced houses. This review underlined the need for further research on advanced control strategies for solar-optimized homes. Increased computational power and the availability of online weather forecast data should be leveraged in the development of these strategies. Moreover, most research in the field of predictive control has dealt with large, cooling-dominated, commercial buildings. This can be partly attributed to the existence of incentives like time-of-use rates and demand response charges for commercial buildings, as well as the fact that electricity is less often used for heating purposes, especially in warmer climates. The application of innovative rate structures at the residential level and the gradual adoption of smart meters and smart grid technologies could promote the use of TES devices and advanced control strategies in optimally designed solar homes.

A review of the theoretical tools used in the thesis was presented in Chapter 3. An introduction to the applied modeling approaches, system identification techniques and predictive control algorithms was presented. The simplified transfer-function model used in the predictive control studies was introduced and the basic assumptions employed to justify a simplified linear system were explained.

The development of the Alstonvale Net Zero House, a case study whose systems provided the basis for investigations on control strategies, was presented. It is estimated that this house would consume about 7,000 kWh of electricity per year, all of which could be provided by its BIPV/T system. The PV installation was designed to have an energy surplus for an electric vehicle. The BIPV/T system was also designed to provide thermal energy for the space heating needs of the house. The modeling approach used to find the operating point of the BIPV/T-heat pump system was presented. Passive solar design can provide a significant portion of the heating loads (40-50%, depending on the reference used, set-point and other factors). For the designed configuration, simulations indicate that the BIPV/T-assisted heat pump system could provide about two-thirds of the remaining heating needs, while the ground loop could provide one-third.

Chapter 5 discusses in detail the predictive control strategies investigated. Early work carried out at the Concordia Solar House (a.k.a. *Northern Light*) was presented. These investigations confirmed that a linear model, obtained at discrete harmonics of a daily frequency, could provide a good approximation for the response of a well-insulated and airtight advanced solar house. It was also shown that such a model could be used for predictive control strategies for the control of a roller blind in order to mitigate indoor temperature fluctuations.

Rule-based control strategies developed for the BIPV/T-assisted heat pump of the Alstonvale House were presented. Sequences of sunny, intermediate and cloudy days were designed to test these control strategies. Predictive control had a significant effect on reducing the energy used by the heat pump (15%). It was found that the selection of the minimum allowable tank temperature (used to decide when to switch from BIPV/T-source operation to ground-source operation) also reduced the energy consumption by a further 10%.

Set-point adjustment strategies for both the room temperature and the TES tank were also studied. The impact of adjusting the position of a generic dynamic shading device according to the expected forecast was investigated. Partially blocking solar gains achieves the desired effect of preventing overheating. On the other hand, since less solar heat is received and stored the HVAC system must provide heat to the space. For a designed five-day sequence in January, the heat pump system consumes 89.5 kWh for the “adjusted blind position” case, in comparison with 67.8 kWh for the case of “blinds fully open”, which represents a 32% difference. There is a clear trade-off between overheating prevention and the use of the building thermal mass for energy storage. Other factors such as expected occupancy must therefore be included in the design of predictive control strategies. Results of this study were published in Candanedo & Athienitis (2010a).

Simplified models were also developed through system identification of more detailed models; these simpler models are more appropriate for the development of optimal and predictive control techniques. It is rather complicated to test predictive control strategies with detailed models, whether they are “custom” models or those created in an accepted simulation software tool such as EnergyPlus or ESP-r, which were

developed for other purposes, such as design or benchmarking. The simplified models created for this study were low-order transfer function models, using solar gains, outdoor temperature and the heat delivery rate of an RFH system as input variables. Simplified models not only facilitate the treatment of the control problem, but also provide useful information about the system's response, such as time constants, frequency response and relative weight of each input. Transfer function models were incorporated into a model predictive control (MPC) strategy for the radiant floor heating system of a sample room with large solar gains and a thick concrete slab. The control of the position of a shading device was added to the MPC strategy through the linearization of the product of solar gains and equivalent blind-window transmittance (Candanedo *et al.*, 2011b, a).

Finally, a dynamic programming (DP) algorithm was applied to the selection of the optimal set-point trajectory of a TES tank heated with a BIPV/T-assisted heat pump. This algorithm used as inputs the weather variables and the expected heating load (calculated with an MPC algorithm). It was found that a dynamic programming algorithm can successfully use weather forecasts and expected load data to control the level of charge of the TES tank. An example is shown in which the application of the DP algorithm for a two-day period results in savings of 38% in comparison with a plausible set-point path (Candanedo & Athienitis, 2011).

A discussion on the research contributions of this thesis, lessons learned, and recommendations for future lines of research is presented below.

6.2 Research Contributions

The main contributions of this investigation are summarized as follows:

1. Development of simplified linear models of solar homes using system identification techniques based on “virtual experiments”, which were carried out with both a customized model (created in MATLAB/Simulink) and a commercial building software tool (EnergyPlus). Work presented on this subject at the High Performance Building Conference in 2010 obtained the Second Best Paper Award (Candanedo & Athienitis, 2010b).
2. Design and predictive control simulations of a case study, the Alstonvale Net Zero House (Candanedo & Athienitis, 2010a). Techniques and approaches used in the design of the house can be generalized and extended to other solar houses, including:
 - Simulation of a BIPV/T-assisted heat pump, along with subroutines for modeling the BIPV/T roof, the heat exchanger, the heat pumps and the water tank.
 - Implementation of rule-based predictive control strategies, based on expected weather patterns for the radiant floor heating system and the TES tank.
3. Design of control strategies for simultaneous control of (a) a radiant floor heating system and (b) the effective transmittance of a dynamic fenestration system (section 5.6). A paper is currently in press for ASHRAE Transactions (Candanedo *et al.*, 2011b, a).

4. Optimal control of a TES tank charged with a BIPV/T-assisted heat pump. To the best knowledge of this author, this is the first time an optimal control strategy has been applied to the simulation of a BIPV/T-assisted heat pump. Results of this work are currently in press in the *ASHRAE Journal of HVAC & R Research* (Candanedo & Athienitis, 2011).

6.3 Lessons Learned

Lessons gathered throughout this investigation encompass technical and scientific findings, as well as some of a more practical nature. They include:

1. **Importance of design robustness.** Attempting to take advantage of every opportunity to recover energy from a building is a worthwhile goal. However, this should not be done at the expense of sacrificing design robustness. Complexity can be managed if it is incorporated in a modular, compartmentalized manner. Since the addition of interdependent components may reduce the reliability of the system, design integration should be made so that a fault in one component does not imply a complete malfunction of another. Strategies such as redundancy, fault detection and self-repairing control systems may help to increase the robustness of the system while enabling the introduction of advanced technologies.
2. **The role of building components.** It should not be forgotten that a building must fulfill its primary role of providing shelter to its occupants. This should be done while maintaining comfortable and healthy conditions inside the building and offering a pleasant exterior appearance. Consequently, the implementation of systems such as BIPV or BIPV/T must also take into account factors such as

aesthetics, prevention of leakage, accessibility for maintenance and durability of the building envelope.

3. **Design of ducting and auxiliary heating systems.** Conventional approaches to the design of ducting systems for ventilation and HVAC in houses have paid little attention to energy efficiency. Improperly sized ducts, unnecessary bends and 90-degree elbows contribute to pressure losses. This also applies to the selection of fans and circulating pumps for hydronic systems. Although these components represent a relatively small portion of the energy consumed in a conventional home, they become an important fraction of the energy used in an advanced solar house since other loads are significantly reduced. Auxiliary equipment should not be neglected. Measures taken at the Alstonvale Net Zero House to reduce energy loss associated with pumps and fans were presented in Chapter 4.
4. **The need for integration of the building industry.** Designing advanced houses requires a building industry with increased awareness and information on energy efficiency, comfort and health requirements, and environmental issues, and technical skills in different domains of engineering. With several notable exceptions, current practices of the building industry lag behind the needs for the development of products integrating renewable energy technologies appropriate for the Canadian climate and conditions. There should also be closer links with related sectors, such as HVAC equipment, controls and home automation.
5. **Importance of adequate design resolution and appropriate model complexity.** While accurate modeling tools are a valuable asset for building design—the next-best thing to actual measurements—their output should be treated with caution.

Although software tools such as EnergyPlus or ESP-r have been developed over the course of decades by teams of professionals using scientific research as a foundation, the creation of a model relies upon implicit or explicit assumptions, and there is inevitably significant uncertainty in key variables. For example, appliance loads and domestic hot water usage are notoriously difficult to predict. Input values of material properties are not accurately known. Infiltration, an essential factor for energy performance, depends significantly on the quality of the construction. On the other hand, the potential of simplified models for guiding the decision-making process and developing control strategies should not be underestimated. Even if precise numbers are not found, simplified models provide the basis for relative comparisons of design and control strategies.

6. **Importance of control strategies as part of the design.** Energy numbers are often reported, but it is less common to find detailed explanations on which control strategies were used, even on basic information such as set-points, dead-bands and allowable fluctuations. It is also rare to find that a building energy model used for design, has also been applied for the development of control strategies. Ideally, design and control strategies should be developed in parallel.
7. Although it is possible to identify guidelines of general applicability, **there is no universal solution for the design of net-zero homes.** One should keep in mind that successful and popular design approaches, such as the *Passivhaus* standard in Germany, have been developed for a particular climate and conditions. This or similar standards should be carefully analyzed and adapted before their use is recommended elsewhere.

6.4 Recommendations for Future Research Work

Further research in the following aspects is recommended:

1. Development of simple rule-based algorithms for optimal temperature set-point trajectories in advanced houses. These algorithms, derived from the application of optimal control algorithms, could use energy, peak loads and cost can be used as objective functions, while using thermal comfort as a constraint.^{§§}
2. The determination of optimal set-points for heating/cooling should be complemented with demand-response strategies for appliances.
3. Experimental research on the application of predictive control strategies to the control of a BIPV/T-assisted heat pump used to charge a TES tank. New experimental facilities at Concordia University (the Solar Simulator/Environmental Chamber Laboratory) should be used to study optimal system configurations.
4. A systematic approach should be developed for the system identification of simplified residential building models. In particular, simplified circuits (similar to the one presented in Section 5.2) should be identified from “numerical experiments” or from measurements in the actual building.
5. Research is needed on the frequency-domain analysis of advanced solar buildings. This could prove to be useful considering that many phenomena affecting buildings are periodic in nature and dominated by a few relevant

^{§§} Ongoing work by the author of this thesis will be presented at the ISES World Congress in 2011.

frequencies (e.g., one-cycle per day and its harmonics). A transfer function representation facilitates the analysis in the frequency domain.

6. Simple models can be used as a tool to quantify the relative importance of the input variables affecting the building indoor temperature.
7. More “top-down” work is needed for the modeling of buildings. The building should be analyzed as a system rather than as a detailed accounting of the contributions of smaller components. Data-driven approaches are needed. This will be facilitated by developments such as embedded intelligence in building components and the adoption of “smart meters”, which will collect data at an unprecedented scale.
8. Research on the application of system identification techniques for larger, multi-zone buildings deserves further attention. It may be possible to identify relationships between the coefficients of the models and the design parameters of the buildings, or groups of parameters (e.g., dimensionless groups). Correlations could expedite system identification.
9. Likewise, many predictive control strategies may be implemented and be even more successful at the community scale, or within a cluster of buildings, or a group of residential units. This is particularly true for the management of large-scale, long-term thermal energy storage and load management.
10. Incorporation of more statistical and probability analysis in building simulation, to account for the effect of uncertainties in the building parameters, weather patterns and occupant behaviour.

References

- Abras, S.; Ploix, S.; Pesty, S. & Jacomino, M. (2006). A Multi-Agent Home Automation System for Power Management. *Proceedings of the Third International Conference in Control, Automation and Robotics (ICINCO)*, Setúbal, Portugal.
- Agarwal, Y.; Weng, T. & Gupta, R.K. (2009). The energy dashboard: improving the visibility of energy consumption at a campus-wide scale. *Proceedings of the First ACM Workshop on Embedded Sensing Systems for Energy-Efficiency in Buildings*, 55-60, Berkeley.
- Åkesson, J. (2007). *Languages and Tools for Optimization of Large-Scale Systems*, Ph.D. Thesis. Lund University, Lund, Sweden.
- Åkesson, J.; Årzén, K.-E.; Gäfvert, M.; Bergdahl, T. & Tummescheit, H. (2009). Modeling and Optimization with Optimica and JModelica.org—Languages and Tools for Solving Large-Scale Dynamic Optimization Problems. *Computers and Chemical Engineering* **34**(11), 1737-1749.
- Allard, A.; Candanedo, J.A. & Saint-Germain, M. (2010). Preliminary report: flow measurements at the Alstonvale House. Report: *Concordia Solar Laboratory*. Montréal, Canada.
- Anderson, B. (1990a). Introduction. In *Solar Building Architecture*, ed. Anderson B. MIT Press, Cambridge, Massachusetts.
- Anderson, B., ed. (1990b). *Solar Building Architecture*. MIT Press, Cambridge, Massachusetts.
- Anonymous. (2011). Nouveau Record pour Hydro-Québec. *Journal Métro*. January 25th.
- Apte, J.; Arasteh, D. & Huang, Y.J. (2003). Future Advanced Windows for Zero-Energy Homes. *ASHRAE Transactions* **109**(2), 871-882.
- Arasteh, D.; Selkowitz, S.; Apte, J. & LaFrance, M. (2006). Zero Energy Windows. Report: *Lawrence Berkeley National Laboratory*. Berkeley, California, US.
- Argiriou, A.; Bellas-Velidis, I. & Balaras, C. (2000). Development of a neural network heating controller for solar buildings. *Neural Networks* **13**(7), 811-820.
- Argiriou, A.A.; Bellas-Velidis, I.; Kummert, M. & André, P. (2004). A neural network controller for hydronic heating systems of solar buildings. *Neural Networks* **17**(3), 427-440.
- ASHRAE. (2005). *Handbook-2005 Fundamentals*. American Society of Heating, Refrigerating and Air-Conditioning Engineers, Atlanta, USA.
- ASHRAE. (2007). *Handbook-2007 HVAC Applications*. American Society of Heating, Refrigerating and Air-Conditioning Engineers, Atlanta, USA.

- ASHRAE. (2009). *Handbook-2009 Fundamentals*. American Society of Heating, Refrigerating and Air-Conditioning Engineers, Atlanta, USA.
- Assimakopoulos, M.; Tsangrassoulis, A.; Guarracino, G. & Santamouris, M. (2004). Integrated energetic approach for a controllable electrochromic device. *Energy & Buildings* **36**(5), 415-422.
- Athienitis, A.K. (1985). *Application of Network Methods to Thermal Analysis of Passive Solar Buildings in the Frequency Domain* Thesis. University of Waterloo, Waterloo, Canada.
- Athienitis, A.K. (1988). A predictive control algorithm for massive buildings. *ASHRAE Transactions* **94**, 1050-1068.
- Athienitis, A.K. (1994). *Building Thermal Analysis*. Electronic Book Mathcad, MathSoft, Boston, USA.
- Athienitis, A.K. & Chen, T.Y. (1993). Experimental and theoretical investigation of floor heating with thermal storage. *ASHRAE Transactions* **99**(1), 1049-1057.
- Athienitis, A.K. & Chen, T.Y. (1997). Numerical study of thermostat setpoint profiles for floor radiant heating and the effect of thermal mass. *ASHRAE Transactions*.
- Athienitis, A.K. & Santamouris, M. (2002). *Thermal Analysis and Design of Passive Solar Buildings*. James & James, London, UK.
- Athienitis, A.K. & Shou, J.G. (1991). Control of Radiant Heating Based on the Operative Temperature. *ASHRAE Transactions* **97**(7), 787-794.
- Athienitis, A.K.; Stylianou, M. & Shou, J. (1990). A methodology for building thermal dynamics studies and control applications. *ASHRAE Transactions* **96**(2), 839-848.
- Avalon. (2008). Discovery 3 House. URL: http://www.avaloncentralalberta.com/html/build_green/discovery_3_technology.php.
- Ayoub, J.; Dignard-Bailey, L. & Filion, A. (2001). Photovoltaics for Buildings: Opportunities for Canada. *CANMET, Varennes*.
- Balcomb, J.D., ed. (1992). *Passive Solar Buildings*. MIT Press, Cambridge, Massachusetts.
- Bales, C.; Hadorn, J.-C.; Drück, H. & Streicher, W. (2005). Advanced storage concepts for solar houses and low energy buildings - IEA-SHC Task 32. *Proceedings of the ISES Solar World Congress 2005*.
- Barakat, S. (1987). Experimental determination of the z-transfer function coefficients for houses. *ASHRAE Transactions* **93**(1), 146-161.
- Bartram, L.; Rodgers, J. & Muise, K. (2010). Chasing the Negawatt: Visualization for Sustainable Living. *IEEE Computer Graphics and Applications*, 8-14.

- Bauchspiess, A.; Ishihara, J.Y.; Felgner, F. & Litz, L. (2006). First-Principles Structured Identification for Predictive HVAC Control. *Congresso Latino-Americano de Controle Automático (CLCA)*, Salvador de Bahia, Brazil.
- Bazilian, M.; Groenhout, N. & Prasad, D. (2001). Simplified numerical modelling and simulation of a photovoltaic heat recovery system. *17th European Photovoltaic Solar Energy Conference*, Munich.
- Beccali, G.; Cellura, M.; Lo Brano, V. & Orioli, A. (2005a). Is the transfer function method reliable in a European building context? A theoretical analysis and a case study in the south of Italy. *Applied Thermal Engineering* **25**, 341–357.
- Beccali, G.; Cellura, M.; Lo Brano, V. & Orioli, A. (2005b). Single thermal zone balance solved by Transfer Function Method. *Energy and Buildings* **37**(12), 1268-1277.
- Beckman, W.A.; Broman, L.; Fiksel, A.; Klein, S.; Lindberg, E.; Schuler, M. & Thornton, J. (1994). TRNSYS: The most complete solar energy system modeling and simulation software. *Renewable Energy* **5**(1).
- Bellman, R.E. (1957). *Dynamic Programming*. Princeton University Press, Princeton, NJ, US.
- Bemporad, A.; Morari, M. & Ricker, N.L. (2010). *Model Predictive Control Toolbox 3 User's Guide*. The Mathworks.
- Bénard, C.; Guerrier, B. & Rosset-Louërat, M.M. (1992a). Optimal building energy management. Part 1: Modeling. *Journal of Solar Energy Engineering* **114**(1), 2-12.
- Bénard, C.; Guerrier, B. & Rosset-Louërat, M.M. (1992b). Optimal building energy management. Part II: Control. *Journal of Solar Energy Engineering* **114**(1), 13-22.
- Bernier, M.A. (2001). Ground-coupled heat pump system simulation. *ASHRAE Transactions* **106**(1), 605-616.
- Bessoudo, M. (2008). *Thermal Comfort Conditions near Highly-Glazed Façades: an Experimental and Simulation Study*. Master's Thesis, Concordia University, Montréal, Québec, Canada.
- Bianchi, M.A. (2006). *Adaptive Modellbasierte Prädiktive Regelung einer Kleinwärmepumpenanlage*, Ph.D. Thesis. ETH Zürich, Zürich.
- Biaou, A.-L.; Bernier, M.A. & Ferron, Y. (2004). Simulation of Net Zero Energy Homes. *Proceedings of eSim2004 - Building Performance Simulation Conference*.
- Bonsor, K. (2001). How Smart Windows Work. *HowStuffWorks website*.
- Borrelli, F.; Bemporad, A.; Fodor, M. & Hrovat, D. (2006). An MPC/hybrid system approach to traction control. *IEEE Transactions of Control Systems and Technology* **14**(3), 541-552.

- Borresen, B. (1981). Thermal room models for control analysis. *ASHRAE Transactions* **87**(Part 2), 251-261.
- Box, G.E.P.; Jenkins, G.M. & Reinsel, G.C. (1994). *Time Series Analysis: Forecasting and Control*. Third Edition. Prentice Hall, New Jersey.
- Braun, J.E. (1990). Reducing energy costs and peak electrical demand through optimal control of building thermal storage. *ASHRAE Transactions* **96**(2), 876-888.
- Braun, J.E. (2003). Load Control Using Building Thermal Mass. *Journal of Solar Energy Engineering* **125**, 292.
- Braun, J.E. (2007a). Intelligent Building Systems - Past, Present and Future. In *Proceedings of the 2007 American Control Conference*, New York City, USA. July 11-13.
- Braun, J.E. (2007b). A near-optimal control strategy for cool storage systems with dynamic electric rates. *HVAC&R Research* **13**(4).
- Bushby, S. (1997). BACnet: a Standard Communication Infrastructure for Intelligent Buildings. *Automation in Construction* **6**, 529-540.
- Callaghan, V.; Clarke, G.; Pounds-Cornish, A. & Sharples, S. (2000). Buildings as Intelligent Autonomous Systems: A Model for Integrating Personal and Building Agents. *6th International Conference on Intelligent Autonomous Systems*, 25-32,
- Camacho, E. & Bordons, C. (2004). *Model Predictive Control*. Second Edition. Springer, London, UK.
- Candanedo (L.), L.M.; Athienitis, A.K.; Candanedo, J.; O'Brien, W. & Chen, Y. (2010a). Transient and steady state models for open-loop air based BIPV/T systems. *ASHRAE Transactions* **116**(1), 600-612.
- Candanedo (L.), L.M.; Athienitis, A.K. & Park, K.W. (2010b). Convective heat transfer coefficients in a building-integrated photovoltaic/thermal system. *Journal of Solar Energy Engineering (ASME)* **133**(2).
- Candanedo, J.; Allard, A. & Athienitis, A.K. (2011a). Predictive control of radiant floor heating and transmitted irradiance in a room with high solar gains. *ASHRAE Transactions* **117**(2).
- Candanedo, J.; Allard, A. & Athienitis, A.K. (2011b). Solar-assisted radiant floor heating in a net-zero energy residential building. *ASHRAE Symposium Paper*, Las Vegas, NV.
- Candanedo, J.A. & Athienitis, A.K. (2008a). Modelling of predictive control strategies in a net zero energy house with active and passive thermal storage. In *EuroSun 2008*, Lisbon, Portugal. October 7-10.

- Candanedo, J.A. & Athienitis, A.K. (2008b). Simulation of the performance of a BIPV/T system coupled to a heat pump in a residential heating application. In *9th International IEA Heat Pump Conference*, Zürich, Switzerland. May 20-22.
- Candanedo, J.A. & Athienitis, A.K. (2009). Application of predictive control strategies in a net zero energy solar house. In *Passive and Low Energy Architecture (PLEA) 2009*, Québec City, Canada. June 22-24.
- Candanedo, J.A. & Athienitis, A.K. (2010a). Investigation of anticipatory control strategies in a net-zero energy solar house. *ASHRAE Transactions* **116**(1), 246-259.
- Candanedo, J.A. & Athienitis, A.K. (2010b). Simplified linear models for predictive control of advanced solar homes with passive and active thermal storage. In *1st High Performance Building Conference*, Purdue University, Indiana. July 12-15.
- Candanedo, J.A. & Athienitis, A.K. (2011). Predictive control of radiant floor heating and solar-source heat pump operation in a solar house. *HVAC & R Research* **17**(3), 235-256.
- Candanedo, J.A.; Doiron, M.; Allard, A. & Bastien, D. (2010). Control Sequences - Alstonvale Net Zero House. Report: *Concordia University (Prepared for Régulvar)*. February 2010.
- Candanedo, J.A.; O'Neill, B.; Pantic, S. & Athienitis, A.K. (2007a). Studies of control strategies for the Concordia Solar House. *Proceedings of the Joint 2nd Solar Buildings Research Network - 32nd Solar Energy Society of Canada Inc(SESOCI), 2007 Conference*.
- Candanedo, J.A.; Pogharian, S.; Athienitis, A.K. & Fry, A. (2007b). Design and simulation of a net-zero energy house in Montréal. *Proceedings of the Joint 2nd Solar Buildings Research Network - 32nd Solar Energy Society of Canada Inc(SESOCI), 2007 Conference*.
- Carmody, J. (2003). *Window Systems for High-performance Buildings*. Norton.
- Castilla, M.; Álvarez, J.D.; Berenguel, M.; Pérez, M.; Rodríguez, F. & Guzmán, J.L. (2010). Técnicas de Control del Confort en Edificios. *Revista Iberoamericana de Automática e Informática Industrial* **7**(3), 5-24.
- CEC. (2006). Windows of the Future. *California Energy Commission, Consumer Energy Center website*.
- Cellura, M.; Giarrè, L.; Brano, V.L. & Orioli, A. (2003). Thermal dynamic models using z-transform coefficients: an algorithm to improve the reliability of simulations. In *Eighth International IBPSA Conference*, Eindhoven, Netherlands. August 11-14, 2003.
- Charron, R. & Athienitis, A.K. (2006). Optimization of the performance of double-façades with integrated photovoltaic panels and motorized blinds. *Solar Energy* **80**(5), 482-491.
- Chen, T. (1997). *A Methodology for Thermal Analysis and Predictive Control of Building Envelope Heating Systems*, Ph.D. Thesis. Concordia University, Montréal, Canada.

- Chen, T. (2001). Real-time predictive supervisory operation of building thermal systems with thermal mass. *Energy & Buildings* **33**(2), 141-150.
- Chen, T. (2002). Application of adaptive predictive control to a floor heating system with a large thermal lag. *Energy & Buildings* **34**(1), 45-51.
- Chen, T. (2003). A method for the direct generation of comprehensive numerical solar building transfer functions. *Solar Energy* **74**(2), 123-132.
- Chen, T. & Athienitis, A. (2003). Investigation of practical issues in building thermal parameter estimation. *Building and Environment* **38**(8), 1027-1038.
- Chen, T.Y. & Athienitis, A.K. (1996). Ambient temperature and solar radiation prediction for predictive control of HVAC systems and a methodology for optimal building heating dynamic operation. *ASHRAE Transactions* **102**(1), 26-35.
- Chen, Y. (2009). *Modeling and Design of a Solar House with Focus on a Ventilated Concrete Slab Coupled with a Building-Integrated Photovoltaic/Thermal System*, M.Sc. Thesis. Concordia University, Montréal.
- Chen, Y.; Athienitis, A.K. & Galal, K. (2010a). Modeling, design and thermal performance of a BIPV/T system thermally coupled with a ventilated concrete slab in a low energy solar house: Part 1, BIPV/T system and house energy concept. *Solar Energy* **84**(11), 1892-1907.
- Chen, Y.X.; Athienitis, A.K. & Galal, K. (2010b). Modeling, design and thermal performance of a BIPV/T system thermally coupled with a ventilated concrete slab in a low energy solar house: Part 1, BIPV/T system and house energy concept. *Solar Energy* **84**(11), 1892-1907.
- Chen, Y.X.; Athienitis, A.K.; Galal, K. & Poissant, Y. (2007). Design and simulation for a solar house with building-integrated photovoltaic/thermal system and thermal storage. In *ISES Solar World Congress I*, 327-332, Beijing, China. September 18-21.
- Citherlet, S.; Bony, J. & Nguyen, B. (2008). Analyse des Performances du Couplage d'une Pompe à Chaleur avec une Installation Solaire Thermique pour la Rénovation. Report: *Haut École d'Ingénierie et de Gestion du Canton de Vaud*. Yverdon-les-Bains, Switzerland.
- CMHC. (2006a). Net-Zero Energy Healthy Housing (NZEHH) Pilot Demonstration Initiative - Appendix C: NZEHH Energy Calculation Information and Example. Ottawa, Ontario.
- CMHC. (2006b). Net-Zero Energy Healthy Housing (NZEHH) Pilot Demonstration Initiative: Questions and Answers Set #8. Ottawa, Ontario. December 21.
- CMHC. (2006c). *Tap the Sun*. Canada Mortgage and Housing Corporation, Ottawa, Ontario.
- CMHC. (2008). The Five Principles of Equilibrium Housing. Retrieved on March 6th, 2008.
- Coffey, B.; Haghghat, F.; Morofsky, E. & Kutrowski, E. (2010). A Software Framework for Model Predictive Control with GenOpt. *Energy and Buildings* **42**, 1084-1092.

- Coffey, B.; Morofsky, E. & Haghghat, F. (2006). Model-based control of responsive building systems. In *Proceedings of the eSim 2006 - Building Performance Simulation Conference*, Toronto, Canada.
- Cooperman, A.; Dieckmann, J. & Brodrick, J. (2010). Using Weather Data for Predictive Control. *ASHRAE Journal*, 130-132.
- Crawley, D.B.; Hand, J.W.; Kummert, M. & Griffith, B.T. (2005). Contrasting the capabilities of building energy performance simulation programs. Report: *US Department of Energy, University of Strathclyde and University of Wisconsin-Madison Joint Report*. July.
- Crawley, D.B.; Lawrie, L.K.; Winkelmann, F.C.; Buhl, W.; Huang, Y.J.; Pedersen, C.O.; Strand, R.K.; Liesen, R.J.; Fisher, D.E.; Witte, M.J. & others. (2001). EnergyPlus: creating a new-generation building energy simulation program. *Energy and Buildings* **33**(4), 319-331.
- Cruickshank, C. & Harrison, S. (2006). Analysis of a modular thermal storage for solar heating systems. *Proceedings of the Joint 1st Solar Buildings Research Network - 31st Solar Energy Society of Canada Inc(SESOCI), 2006 Conference*.
- Curtiss, P.; Kreider, J. & Brandemuehl, M. (1993). Adaptive control of HVAC processes using predictive neural networks. *1993 Winter Meeting of ASHRAE Transactions Part 1*, 496-504.
- Curtiss, P.S.; Shavit, G. & Kreider, J.F. (1996). Neural networks applied to buildings- a tutorial and case studies in prediction and adaptive control. *ASHRAE Transactions* **102**(1), 1141-1146.
- Davies, M. (1973). The thermal admittance of layered walls. *Building Science* **8**(3).
- Davies, M.G. (2004). *Building Heat Transfer*. John Wiley & Sons, Liverpool, UK.
- Defendorf, R. (2010). An NZE project, a tragic fire and a will to rebuild. *GreenBuildingAdvisor.com*. August 6th.
- Déqué, F.; Ollivier, F. & Poblador, A. (2000). Grey boxes used to represent buildings with a minimum number of geometric and thermal parameters. *Energy & Buildings* **31**(1), 29-35.
- Dincer, I. (2002). On thermal energy storage systems and applications in buildings. *Energy & Buildings* **34**(4), 377-388.
- DOE. (2007). Building Energy Software Tools Directory. *US Department of Energy - Energy Efficiency and Renewable Energy Website*.
- DOE. (2011). Solar Decathlon History. U.S. Department of Energy. URL: <http://www.solardecathlon.gov/history.html>.
- Doiron, M.A. (2011). *Whole-Building Energy Analysis and Lessons Learned for a Near Net-Zero Energy Solar House*, Master's Thesis. Concordia University, Montréal, Québec.

- Doiron, M.A.; O'Brien, W. & Athienitis, A.K. (2011). Energy performance, comfort and lessons learned from a near net-zero energy solar house. *ASHRAE Transactions (In Press)*.
- Donaisky, E.; Oliveira, G.H.C.; Freire, R.Z. & Mendes, N. (2007). PMV-Based Predictive Algorithms for Controlling Thermal Comfort in Building Plants. In *16th IEEE International Conference on Control Applications*, Singapore, 1-3 October 2007.
- Dorato, P. & Knudsen, H. (1979). Periodic optimization with applications to solar energy control. *Automatica* **15**, 673-676.
- Dounis, A.; Santamouris, M. & Lefas, C. (1992). Implementation of artificial intelligence techniques in thermal comfort control for passive solar buildings. *Energy Conversion & Management* **33**(3), 175-182.
- Dounis, A.I. & Caraiscos, C. (2009). Advanced control systems engineering for energy and comfort management in a building environment - A review. *Renewable and Sustainable Energy Reviews* **13**, 1246-1261.
- Dounis, A.I.; Lefas, C.C. & Argiriou, A. (1995a). Knowledge-Based versus Classical Control for Solar-Building Design. *Applied Energy* **50**, 281-292.
- Dounis, A.I.; Santamouris, M.J.; Lefas, C.C. & Argiriou, A. (1995b). Design of a Fuzzy Set Environment Comfort System. *Energy and Buildings* **22**, 81-87.
- Drees, K. & Braun, J. (1996). Development and evaluation of a rule-based control strategy for ice storage systems. *HVAC & R Research* **2**(4).
- Dreyfus, S. (2002). Richard Bellman on the Birth of Dynamic Programming. *Operations Research* **50**(1), 48-51.
- Dreyfus, S.E. & Law, A.M. (1977). *The Art and Theory of Dynamic Programming*. Academic Press, New York, US.
- Duan, P. & Li, H. (2008). ZigBee Wireless Sensor Network Based Multi-Agent Architecture in Intelligent Inhabited Environments. *IET 4th International Conference on Intelligent Environments*, 1-6, Seattle.
- Duffie, J.A. & Beckman, W.A. (2006). *Solar Engineering of Thermal Processes*. John Wiley & Sons, Hoboken, New Jersey.
- Dumur, D.; Boucher, P.; Murphy, K.M. & Déqué, F. (1997a). Comfort Control in Residential Housing using Predictive Controllers. In *Proceedings of the 1997 IEEE International Conference on Control Applications*, Hartford, CT. October 5-7.
- Dumur, D.; Boucher, P.; Murphy, K.M. & Déqué, F. (1997b). On Predictive Controller Design for Comfort Control in Single Residential Housing. In *European Control Conference*, 109-114, Brussels. July.
- Echelon. (2009). Introduction to the LonWorks Platform. Report: *Echelon Corporation*.

- Écocité. (2010). Abondance Le Soleil Net-Zero Energy Triplex. URL: <http://www.ecocite.ca/abondance/LeSoleil.html>.
- EE4. (2008). CanmetEnergy Technology Centre (NRCan) website. Retrieved on April 2008 URL: http://www.sbc.nrcan.gc.ca/software_and_tools/ee4_soft_e.asp.
- EERE. (2010). EnergyPlus Version 5.0.0, Energy Simulation Software. U.S. DOE Energy Efficiency and Renewable Energy (EERE), Building Technologies Program. URL: <http://apps1.eere.energy.gov/buildings/energyplus/>.
- Egan, D. (2005). The emergence of ZigBee in building automation and industrial control *Computing and Control Engineering Journal* **16**(2), 14-19.
- Elizalde, E. (2008). *Weather Forecast Control: Prestudy of Installing a Predictive Heating Control System Based on Meteorological Forecast at Sandvik Site in Sandviken*, Master's Thesis. University of Gävle, Gävle, Sweden.
- EnergyPlus. (2010). EnergyPlus Version 5.0.0. U.S. Department of Energy, Energy Efficiency and Renewable Energy, Building Technologies Program.
- Erbs, D.G.; Klein, S.A. & Duffie, J.A. (1982). Estimation of the diffuse radiation fraction for hourly, daily and monthly-average global radiation. *Solar Energy* **28**(4), 293-302.
- ESP-r. (2010). Version 11.9. URL: <http://www.esru.strath.ac.uk/Programs/ESP-r.htm>.
- ESP-r_Overview. (2008). ESP-r website. Retrieved on March, 2008. URL: http://www.esru.strath.ac.uk/Programs/ESP-r_overview.htm.
- Fehrenbacher, K. (2009). Ten monitoring tools bringing smart energy home. <http://gigaom.com/cleantech/10-energy-dashboards-for-your-home/>.
- Ferkl, L. & Siroký, J. (2010). Ceiling radiant cooling: Comparison of ARMAX and subspace identification modelling methods. *Building and Environment* **45**, 205-212.
- Ferkl, L.; Siroký, J. & Prívára, S. (2010). Model Predictive Control of Buildings: the Efficient Way of Heating. In *2010 IEEE International Conference on Control Applications*, Yokohama, Japan. September 8-10.
- Florita, A.R. & Henze, G.P. (2009). Comparison of Short-Term Weather Forecasting Models for Model Predictive Control. *HVAC & R Research* **15**(5), 835-853.
- Fraisse, G.; Viardot, C.; Lafabrie, O. & Achard, G. (2002). Development of a simplified and accurate building model based on electrical analogy. *Energy and buildings* **34**(10), 1017-1031.
- Fraunhofer IAP. (2008). Thermochromic Polymers. *Fraunhofer Institute for Applied Polymer Research*.

- Freire, R.Z.; Oliveira, G.H.C. & Mendes, N. (2005). Development of single-zone predictive equations using linear regression for advanced controllers synthesis. In *Proceedings of the Ninth Building Simulation Conference*, Montréal, Canada.
- Freire, R.Z.; Oliveira, G.H.C. & Mendes, N. (2008a). Development of regression equations for predicting energy and hygrothermal performance of buildings. *Energy and Buildings* **40**, 810-820.
- Freire, R.Z.; Oliveira, G.H.C. & Mendes, N. (2008b). Predictive controllers for thermal comfort optimization and energy savings. *Energy and Buildings* **40**, 1353-1365.
- Gellings, C.W. (2009). *The Smart Grid: Enabling Energy Efficiency and Demand Response*. The Fairmont Press, Boca Raton, Florida.
- Gellings, C.W. & Talukdar, S. (1987). Load Management Concepts. *Load Management*, 3-27.
- Georg, A.; Graf, W.; Schweiger, D.; Wittwer, V.; Nitz, P. & Wilson, H. (1998). Switchable glazing with a large dynamic range in total solar energy transmittance (TSET). *Solar Energy* **62**(3), 215-228.
- Gerbasi, D. (2000). *The Energy Performance of the NOVTEC Advanced House*, Master's Thesis. Concordia University, Montréal, Québec.
- Guillemin, A. (2003). *Using Genetic Algorithms to take into account user wishes in an advanced building control system*, Ph.D. Thesis. École Polytechnique Fédérale de Lausanne, Lausanne, Switzerland.
- Guo, W. & Zhou, M. (2009). An emerging technology for building automation control. In *IEEE International Conference on Systems, Man and Cybernetics*, San Antonio, Texas. October.
- Gwerder, M.; Lehmann, B.; Tödtli, J.; Dorer, V. & Renggli, F. (2008). Control of Thermally-Activated Building Systems (TABS). *Applied Energy* **85**, 565-581.
- Gwerder, M.; Tödtli, J.; Lehmann, B.; Dorer, V.; Güntensperger, W. & Renggli, F. (2009). Control of thermally activated building systems (TABS) in intermittent operation with pulse width modulation. *Applied Energy*, 1606-1616.
- Gyalistras, D. & OptiControlTeam. (2010). Final Report: Use of Weather and Occupancy Forecasts for Optimal Building Climate Control (OptiControl). Report: *ETH Zürich*. Zürich, Switzerland.
- Haggard, K.; Bainbridge, D.A. & Aljilani, R. (2010). *Passive Solar Architecture Pocket Reference*. Earthscan, London, UK.
- Hauer, A. (2010). Compact Thermal Energy Storages: Potential and Limitations for Different Applications, ed. Bayern Z. Presentation at Eurosun 2010, Graz, Austria, Oct. 1st, 2010.

- Henze, G.P. (1995). *Evaluation of Optimal Control for Ice Storage Systems*, Ph.D. Thesis. University of Colorado, Boulder, Colorado, US.
- Henze, G.P.; Dodier, R.H. & Krarti, M. (1997). Development of a predictive optimal controller for thermal energy storage systems. *International Journal of HVAC&R Research* **3**(3), 233-264.
- Henze, G.P.; Felsmann, C. & Knabe, G. (2004a). Evaluation of optimal control for active and passive building thermal storage. *Int J Therm Sci* **43**(2), 173-183.
- Henze, G.P.; Florita, A.R.; Brandemuehl, M.J.; Felsmann, C. & Cheng, H. (2010). Advances in near-optimal control of passive building thermal storage. *Journal of Solar Energy Engineering* **132**.
- Henze, G.P.; Kalz, D.E.; Felsmann, C. & Knabe, G. (2004b). Impact of forecasting accuracy on predictive optimal control of active and passive building thermal storage inventory. *HVAC & R Research* **10**(2), 153-178.
- Henze, G.P.; Kalz, D.E.; Liu, S. & Felsmann, C. (2005). Experimental analysis of model-based predictive optimal control for active and passive building thermal storage inventory. *HVAC & R Research* **11**(2), 189-213.
- Henze, G.P. & Krarti, M. (1999). The impact of forecasting uncertainty on the performance of a predictive optimal controller for thermal energy storage systems. *ASHRAE Transactions* **105**(1).
- Henze, G.P.; Laguna, M. & Krarti, M. (1995). Heuristics for the optimal control of Thermal Energy Storage. *Proc of the Metaheuristics Int Conf Kluwer Academic Publishers, Norwell, MA*.
- Henze, G.P.; Pfafferott, J.; Herkel, S. & Felsmann, C. (2007). Impact of adaptive comfort criteria and heat waves on optimal building thermal mass control. *Energy and Buildings* **39**, 221-235.
- Hirsch, R.L. (2008). Mitigation of Maximum World Oil Production: Shortage Scenarios. *Energy Policy* **36**, 881-889.
- Hirsch, R.L.; Bezdek, R. & Wendling, R. (2005). Peaking of World Oil Production: Impacts, Mitigation and Risk Management. Report: *US Department of Energy*.
- Hoffmann, W. (2006). PV solar electricity industry: Market growth and perspective. *Solar Energy Materials and Solar Cells* **90**(18-19), 3285-3311.
- Holmberg, D.G. & Bushby, S.T. (2009). BACnet and the Smart Grid. *BACnet Today: A Supplement to ASHRAE Journal*, B8-B12.
- HOT2000. (2003). Canmet Energy Technology Centre (NRCan) website.
- HOT3000. (2008). Canmet Energy Technology Centre (NRCan) website.

- Houpis, C.H. (1992). *Digital Control Systems*. McGraw-Hill Higher Education.
- House, J.; Smith, T. & Arora, J. (1991). Optimal control of a thermal system. *ASHRAE Transactions* **97**(2), 991-1001.
- Hudson, G. & Underwood, C.P. (1999). A simple building modelling procedure for MATLAB/Simulink. In *Sixth International IBPSA Conference*, Kyoto, Japan. September 13-15.
- Hutcheon, N.B. & Handegord, G. (1983). *Building Science for a Cold Climate*. Institute for Research in Construction, NRC, Canada.
- IEA-SHC/ECBCS. (2008). Task 40/Annex 52 - Towards Net Zero Energy Solar Buildings. International Energy Agency, Solar Heating and Cooling Programme/Energy Conservation in Buildings and Community Systems Programme. URL: <http://www.iea-shc.org/task40/>.
- IEA. (2010). World Energy Outlook 2010: Executive Summary. Report: *International Energy Agency*. Paris.
- Incropera, F.P. & DeWitt, D.P. (2002). *Fundamentals of Heat and Mass Transfer*. John Wiley & Sons, New York, USA.
- IPCC. (2007). Climate Change 2007: Synthesis Report. Report: *Intergovernmental Panel on Climate Change*. Valencia, Spain.
- Jähnig, D.; Hausner, R.; Wagner, W. & Isaksson, C. (2006). Thermochemical storage for solar space heating in a single family house. *Proceedings of the Tenth International Conference on Thermal Energy Storage, Ecstock 2006*.
- Kämpf, J.H. & Robinson, D. (2007). A simplified thermal model to support analysis of urban resource flows. *Energy & Buildings* **39**(4), 445-453.
- Karlekar, B.V. (1983). *Thermodynamics for Engineers*. Prentice Hall, Inc., Englewood Cliffs, USA.
- Kintner-Meyer, M. & Emery, A. (1995). Optimal control of an HVAC system using cold storage and building thermal capacitance. *Energy & Buildings* **23**(1), 19-31.
- Kirk, D.E. (2004). *Optimal Control Theory: An Introduction*. Courier Dover Publications, Mineola, NY, US.
- KNX. (2011). KNX - The Worldwide Standard for Home and Building Control. <http://www.knx.org/>.
- Krarti, M.; Henze, G. & Bell, D. (1999). Planning horizon for a predictive optimal controller for thermal energy storage systems. *ASHRAE Annual Meeting, Seattle, WA (US)*, 06/18/1999-06/23/1999.
- Kuhn, T.E. (2006). Solar control: A general evaluation method for facades with venetian blinds or other solar control systems. *Energy & Buildings* **38**(6), 648-660.

- Kulacki, F.; Fellow, A.; Davidson, J.H. & Hebert, M. (2007). On the Effectiveness of Baffles in Indirect Solar Storage Systems. *Journal of Solar Energy Engineering* **129**, 494.
- Kummert, M. & André, P. (2005). Simulation of a Model-Based Optimal Controller for Heating Systems under Realistic Hypothesis. In *Ninth International IBPSA Conference*, Montréal, Canada.
- Kummert, M.; André, P. & Argiriou, A.A. (2006). Comparing control strategies using experimental and simulation results: Methodology and application to heating control of passive solar buildings. *HVAC&R Research* **12**(3a), 715-737.
- Kummert, M.; André, P. & Nicolas, J. (1996). Development of simplified models for solar buildings optimal control. In *Proceedings of ISES Eurosun 96 Congress*, 1055-1061., Freiburg, Germany. September 16-19.
- Kummert, M.; André, P. & Nicolas, J. (2001). Optimal heating control in a passive solar commercial building. *Solar Energy* **69**, 103-116.
- Kummert, M. & Bernier, M. (2008). Sub-hourly simulation of residential ground coupled heat pump systems. *Building Services Engineering Research and Technology* **29**(1), 27.
- LeBreux, M.; Lacroix, M. & Lachiver, G. (2006). Fuzzy and feedforward control of an hybrid thermal energy storage system. *Energy and Buildings* **38**, 1149-1155.
- Lee, K.-h. & Braun, J.E. (2004). Development and Application of an Inverse Building Model for Demand Response in Small Commercial Buildings. In *SimBuild 2004, IBPSA-USA National Conference*, Boulder, Colorado, USA. August 4-6.
- Lee, K.-h. & Braun, J.E. (2006). Evaluation of Methods for Determining Set-point Trajectories in Commercial Buildings Using Short-Term Data Analysis. In *SimBuild 2006, IBPSA-USA National Conference*, Cambridge, Massachusetts. August 2-4.
- Lee, K.-h. & Braun, J.E. (2008a). Development of methods for determining demand-limiting setpoint trajectories in buildings using short-term measurements. *Building and Environment* **43**, 1755-1768.
- Lee, K.-h. & Braun, J.E. (2008b). Model-based demand-limiting control of building thermal mass. *Building and Environment* **43**(10), 1633-1646.
- Lee, K.-h.; Braun, J.E.; Fredrickson, S.; Konis, K. & Arens, E. (2007). Testing of Peak Demand-Limiting Using Thermal Mass at a Small Commercial Building. Report: *Demand Response Research Center, California Energy Commission*. July.
- Lefebvre, G.; Bransier, J. & Neveu, A. (1987). Simulation du comportement thermique d'un local par des méthodes numériques d'ordre réduit. *Revue générale de thermique* **26**(302), 106-114.
- Levy, E. (1959). Complex curve fitting. *IRE Transactions on Automatic Control* **4**(3), 37-44.

- Liao, L.; Athienitis, A.; Candanedo, L.; Park, K.W.; Poissant, Y. & Collins, M. (2007). Numerical and experimental study of heat transfer in a BIPV/Thermal system. *Journal of Solar Energy Engineering* **129**, 423.
- Liu, S. (2005). *Analytical and experimental comparison of model-based, model-free and hybrid learning control of active and passive building thermal storage* Thesis. University of Nebraska - Lincoln, Lincoln, Nebraska, US.
- Liu, S. & Henze, G.P. (2007). Evaluation of reinforcement learning for optimal control of building active and passive thermal storage inventory. *Journal of Solar Energy Engineering* **129**, 215.
- Ljung, L. (1999). *System Identification: Theory for the User*. Second Edition. Prentice Hall, Upper Saddle River, New Jersey.
- Ljung, L. (2010). *System Identification Toolbox™ 7 User's Guide - MATLAB & Simulink*. The Mathworks, Inc., Natick, MA. URL: http://www.mathworks.com/help/pdf_doc/ident/ident.pdf
- Lund, H. & Kempton, W. (2008). Integration of renewable energy into the transport and electricity sectors through V2G. *Energy Policy* **36**(9), 3578-3587.
- Lute, P.J. & Paassen, A.H.C.v. (1989). Predictive Control of Indoor Temperatures in Office Buildings. Energy Consumption and Comfort. In *CLIMA 2000 II. Heating Components and Systems*, 290-295, Sarajevo, Yugoslavia. August 27-September 1.
- Lute, P.J. & Paassen, A.H.C.v. (1990). Integrated Control System for Low Energy Buildings. *ASHRAE Transactions* **96**(2), 889-895.
- Ma, Y.; Borrelli, F.; Hancey, B.; Coffey, B.; Bengesa, S. & Haves, P. (2010). Model Predictive Control for the Operation of Building Cooling Systems. In *American Control Conference*, Baltimore, Maryland, USA. June 30-July 2.
- Ma, Y.; Borrelli, F.; Hancey, B.; Packard, A. & Bortoff, S. (2009). Model Predictive Control of Thermal Energy Storage in Building Cooling Systems. In *48th IEEE Conference on Decision and Control and 28th Chinese Control Conference*, Shanghai, China.
- Mahdavi, A. (2003). Self-organizing models for sentient buildings. In *Advanced Building Simulation*, ed. Malkawi AM & Augenbroe G. Spon Press (Taylor & Francis Group), New York and London.
- Mahdavi, A. (2008). Predictive simulation-based lighting and shading systems control in buildings. *Building Simulation* **1**(1).
- Mahdavi, A. & Pröglhöf, C. (2005). A Model-Based Method for the Integration of Natural Ventilation in Indoor Climate Systems Operation. *Proceedings of the Ninth IBPSA Conference*, Montréal, Canada. August 15-18, 2005.

- Mahdavi, A.; Schuss, M.; Suter, G.; Metzger, S.; Camara, S. & Dervishi, S. (2009). Recent Advances in Simulation-Powered Building Systems Control. In *Eleventh International IBPSA Conference*, Glasgow, Scotland.
- Malys, L. (2007). Modélisation et contrôle d'une maison solaire. Report: *École Normale Supérieure de Cachan*. Cachan, France. August.
- Massie, D.D. (2002). Optimization of a building's cooling plant for operating cost and energy use. *International Journal of Thermal Sciences* **41**(12), 1121-1129.
- Mathsoft. (2001). Mathcad: User's Guide with Reference Manual. MathSoft. *Cambridge, Massachusetts*.
- MathWorks. (2010). *Simulink 7 User's Guide*. Natick, Massachusetts.
- Mathworld. (2008). Bilateral Z-Transform. *Mathworld website*.
- May-Ostendorp, P.; Henze, G.P.; Corbin, C.D.; Rajagopalan, B. & Felsmann, C. (2011). Model-predictive control of mixed-mode buildings with rule extraction. *Building and Environment* **46**, 428-437.
- McAdams, W.H. (1954). *Heat Transmission*. McGraw-Hill.
- McCausland, I. (1969). *Introduction to Optimal Control*. John Wiley & Sons.
- McKinley, T.L. & Alleyne, A.G. (2008). Identification of building model parameters and loads using on-site data logs. In *SimBuild 2008: Third National Conference IBPSA-USA*, Berkeley, California. July 30 - August 1.
- McQuiston, F.C.; Parker, J.D. & Spitler, J.D. (2005). *Heating, Ventilating, and Air Conditioning: Analysis and Design*. John Wiley & Sons.
- Mitalas, G. & Stephenson, D. (1967). Room thermal response factors. *ASHRAE Transactions* **73**(1), 1-15.
- Mo, Z. & Mahdavi, A. (2003). An Agent-Based Simulation-Assisted Approach to Bi-Lateral Building Systems Control. *Eight International IBPSA Conference*, Eindhoven, Netherlands. August 11-14.
- Moon, J.W.; Jung, S.K. & Kim, J.-J. (2009). Application of ANN (Artificial Neural Networks) in Residential Thermal Control. In *Building Simulation 2009*, Glasgow, Scotland. July 27-30, 2009.
- Morel, N.; Bauer, M.; El-Khoury, M. & Krauss, J. (2001). NEUROBAT, a predictive and adaptive control system using artificial neural networks. *International Journal of Sustainable Energy* **21**(2), 161-201.
- Morgan, S. & Krarti, M. (2010). Field Testing of Optimal Controls of Passive and Active Thermal Storage. *ASHRAE Transactions* **116**(1).

- Morosan, P.-D.; Bourdais, R.; Dumur, D. & Buisson, J. (2010a). Distributed Model Predictive Control for Building Temperature Regulation. In *2010 American Control Conference*, Baltimore, MD, USA. June 30-July 2.
- Morosan, P.-D.; Bourdais, R.; Dumur, D. & Buisson, J. (2010b). A dynamic horizon distributed predictive control approach for temperature regulation in multi-zone buildings. In *18th Mediterranean Conference on Control and Automation (MED)*, Marrakech, Morocco. 23-25 June 2010.
- Morris, F.; Braun, J. & Treado, S. (1994). Experimental and simulated performance of optimal control of building thermal storage. *ASHRAE Transactions* **100**(1), 402-414.
- Moudgalya, K.M. (2007). *Digital Control*. John Wiley & Sons, Chichester, UK.
- Mustafaraj, G.; Chen, J. & Lowry, G. (2009). Development of room temperature and relative humidity linear parametric models for an open office using BMS data. *Energy and Buildings*.
- Nagai, T. (1999). Dynamic optimization technique for control of HVAC system utilizing building thermal storage. In *Proceedings of the Sixth International IBPSA Conference*, Kyoto, Japan. September, 13-15.
- Negron, E. & Hayes, P.H. (2009). System and Method for Appliance Control via a Personal Communication or Entertainment Device. U.S.
- NIBE. (2010). *Air/Water Heat Pump NIBE F 2025-6, Technical Data (obtained by personal communication)*. NIBE Wärmetechnik AG 8247 Flurlingen, Switzerland.
- Nielsen, K. (2003). Thermal Energy Storage: A State-of-the-Art. A report within the research program Smart Energy-Efficient Buildings at NTNU and SINTEF 2002-2006. Report: *Department of Geology and Mineral Resources Engineering, Norwegian University of Science and Technology*. Trondheim, Norway.
- Noguchi, M.; Athienitis, A.K.; Delisle, V.; Ayoub, J. & Berneche, B. (2008). Net zero energy homes of the future: a case study of the EcoTerra House in Canada. In *Renewable Energy Congress* Glasgow, Scotland. July 19-25.
- NRC. (1997). *Model National Energy Code for Buildings*. Institute for Research in Construction, National Research Council, Ottawa, Ontario, Canada.
- NRCan-OEE. (2010a). Energy Use Data Handbook Tables - 1990 to 2007. Report: *Natural Resources Canada, Office of Energy Efficiency*.
- NRCan-OEE. (2010b). Survey of Household Energy Use - 2007. Report: *Natural Resources Canada, Office of Energy Efficiency*. Ottawa.
- NRCan. (2005a). NRCan-Heating and Cooling with a Heat Pump.
- NRCan. (2005b). R-2000 Standard.

- NRCan. (2006). Types of Solar Collectors. URL: http://www.canren.gc.ca/tech_appl/index.asp?CaID=5&PgID=282.
- NRCan. (2010). What is the R-2000 Standard? November 2010.
- NREL. (2009). Open Studio, Plugin for Google SketchUp 3D drawing program. URL: <http://sourceforge.net/projects/openstudio/>.
- NYB. (2007). *Technical Specifications*
- Nygård-Ferguson, M. (1990). *Predictive Thermal Control of Building Systems*, Ph.D. Thesis. École Polytechnique Fédérale de Lausanne, Lausanne, Switzerland.
- Nygård-Ferguson, M. & Scartezzini, J.-L. (1988). Performance of a Predictive Controller Applied to a Passive Solar Room. In *PLEA88 - Energy and Buildings for Temperate Climates: a Mediterranean Regional Approach*, 575-581, Porto, Portugal. July 27-31.
- Nygård-Ferguson, M. & Scartezzini, J.-L. (1989a). Computer simulation of an optimal stochastic controller applied to passive solar rooms. *Energy & Buildings* **14**, 1-7.
- Nygård-Ferguson, M. & Scartezzini, J.-L. (1989b). Experimental performance of a predictive controller designed for passive solar buildings. In *ISES Solar World Congress*, Kobe, Japan. Sept 4-8.
- Nygård-Ferguson, M. & Scartezzini, J.-L. (1992). Evaluation of an optimal stochastic controller in a full-scale experiment. *Energy & Buildings* **18**, 1-10.
- O'Neill, B. (2008). *Model-Based Control of Venetian Blinds*, Master's Thesis. Concordia University, Montréal, Canada.
- O'Neill, B. & Athienitis, A.K. (2007). Daylight and solar gain management using an automated venetian blind. In *Proceedings of the Joint 2nd Solar Buildings Research Network - 32nd Solar Energy Society of Canada Inc(SESOCI), 2007 Conference*, Calgary, AB, Canada.
- OCA. (2007). Air Quality Issues Fact Sheet #24: Reducing Peak Demand. Ontario Clean Air Alliance. URL: <http://www.cleanairalliance.org/files/active/0/fs24.pdf>
- Ogata, K. (1987). *Discrete-time control systems*. Prentice-Hall, Inc., Upper Saddle River, NJ, USA.
- Oldewurtel, F.; Parisio, A.; Jones, C.N.; Morari, M.; Gyalistras, D.; Gwerder, M.; Stauch, V.; Lehmann, B. & Wirth, K. (2010a). Energy Efficient Building Climate Control using Stochastic Model Predictive Control and Weather Predictions. In *American Control Conference*, Baltimore, Maryland. June 30 - July 2.
- Oldewurtel, F.; Ulbig, A.; Parisio, A.; Andersson, G. & Morari, M. (2010b). Reducing Peak Electricity Demand in Building Climate Control using Real-Time Pricing and Model Predictive Control. *49th IEEE Conference on Decision and Control*, Atlanta, Georgia, USA. December 15-17.

- Østergaard, S. (2003). Results from measurements on a roof integrated PV system with preheating of fresh air. Report: *Solar Energy Centre Denmark, Danish Technological Institute*. Denmark. apr.
- Owen, N.A.; Inderwildi, O.R. & King, D.A. (2010). The Status of Conventional World Oil Reserves -Hype or Cause for Concern? *Energy Policy* **38**, 4743-4749.
- Paassen, A.H.C.v. (1988). Passive Solar Energy in Intelligent Buildings. *ASHRAE Transactions* **94**, 1289-1296.
- Paassen, A.H.C.v. (1989). Passive Building Control. In *CLIMA 2000 II. Heating Components and Systems*, Sarajevo, Yugoslavia. August 27-September 1.
- Park, K.W. & Athienitis, A.K. (2003). Workplane illuminance prediction method for daylighting control systems. *Solar Energy* **75**(4), 277-284.
- Pasini, M. (2006). *Modeling and Design of an Independent Solar House*, Master's Thesis. Concordia University.
- Patankar, S. (1980). *Numerical Heat Transfer and Fluid Flow*. Hemisphere Publishing Corporation, Washington DC, USA.
- Pelland, S. & Abboud, I. (2007). Estimating the Capacity Value and Peak-Shaving Potential of Photovoltaics in Ontario: A Case-Study for the City of Toronto. *17th International Photovoltaic Science and Engineering Conference*, Fukuoka, Japan. December 2007.
- Perez, R.; Ineichen, P.; Seals, R.; Michalsky, J. & Stewart, R. (1990). Modeling daylight availability and irradiance components from direct and global irradiance. *Solar Energy* **44**(5), 271-289.
- Pipes, L. (1957). Matrix analysis of heat transfer problems. *Journal of the Franklin Institute* **263**(3), 195-206.
- Pogharian, S. (2007). Final Report: Team Montréal Zéro. Report: *Sevag Pogharian Design*. Montréal, Canada. January 10.
- Pogharian, S.; Ayoub, J.; Candanedo, J.A. & Athienitis, A.K. (2008). Getting to a net zero energy lifestyle: the Alstonvale Net Zero House. *23rd European Photovoltaic Solar Energy Conference and Exhibition*, Valencia, Spain. September 1-4, 2008.
- Poulin, L.; Yu, W. & Hodgson, J. (2006). Renewable energy forecasts for solar powered applications. *First SBRN Conference, Poster Session*.
- Prívará, S.; Siroký, J.; Ferkl, L. & Cigler, J. (2011). Model predictive control of a building heating system: the first experience. *Energy and Buildings* **43**, 564-572.
- Puren. (2007). Puren Bomatherm solar air collector roof insulating heat recovery system. *Puren gmbh website*. Retrieved on April, 2008.

<http://www.puren.eu/construction-products/steep-roof-diffusion-sealed/puren-bomatherm.html>.

Rabl, A. & Norford, L. (1991). Peak load reduction by preconditioning buildings at night. *International Journal of Energy Research* **15**(9), 781-798.

RDVE. (2010). Imaginons le Québec Sans Pétrole. Report: *Rendez-Vous de l'Énergie*. Montréal. October 2010.

Rees, S.; Spitler, J.; Davies, M. & Haves, P. (2000). Qualitative comparison of North American and UK cooling load calculation methods. *International Journal of Heating, Ventilating, Air-Conditioning and Refrigeration Research* **6**(1), 75-99.

Reginato, B.C.; Freire, R.Z.; Oliveira, G.H.C.; Mendes, N. & Abadie, M.O. (2009). Predicting the Temperature Profile of Indoor Buildings by Using Orthornormal Basis Functions. *Eleventh International IBPSA Conference*, Glasgow, Scotland.

Reinhart, C.F. (2006). *Tutorial on the Use of Daysim Simulations for Sustainable Design*. Ottawa, Canada.

Research Frontiers. (2010). SmartGlass. *Research Frontiers, Inc Website*. <http://www.refr-spd.com/>.

RETScreen. (2008). RETScreen International website.

Richardson, T.J.; Slack, J.L.; Armitage, R.D.; Kostecki, R.; Farangis, B. & Rubin, M.D. (2001). Switchable mirrors based on nickel-magnesium films. *Applied Physics Letters* **78**(20), 3.

Riederer, P. (2005). MATLAB/SIMULINK for building and HVAC simulation- state of the art. In *Ninth International IBPSA Conference*, Montréal, Canada. August 15-18.

Riverdale. (2008). Riverdale Net Zero Project. URL: <http://www.riverdalenetzero.ca/Home.html>.

Rossiter, J.A. (2003). *Model-based predictive control: a practical approach*. CRC Press.

Rowlands, I.; Poissant, Y. & Dignard-Bailey, L. (2004). Demand side management billing programs - a photovoltaic residential study. *20th European Photovoltaic Solar Energy Conference*, Paris, France.

Rowlands, I.H. (2005a). Envisaging feed-in tariffs for solar photovoltaic electricity: European lessons for Canada. *Renewable and Sustainable Energy Reviews* **9**(1), 51-68.

Rowlands, I.H. (2005b). Solar PV electricity and market characteristics: two Canadian case-studies. *Renewable Energy* **30**(6), 815-834.

Salom, J.; Widén, J.; Candanedo, J.A.; Sartori, I.; Voss, K.; Marszal, A. & Berggren, B. (2011). Understanding net-zero energy buildings: evaluation of load matching and grid interaction

- indicators. In *In Preparation for the Twelfth International IBPSA Conference*, Sydney, Australia. November 14-17.
- Seborg, D.E.; Edgar, T.F. & Mellichamp, D.A. (1989). *Process Dynamics and Control*. John Wiley & Sons, Hoboken, NJ, USA.
- Siroky, J.; Oldewurtel, F.; Cigler, J. & Prıvara, S. (2011). Experimental analysis of model predictive control for an energy efficient building heating system. *Applied Energy* **88**(9), 3079-3087.
- Siroky, J.; Prıvara, S. & Ferkl, L. (2010). Model Predictive Control of Building Heating System. In *CLIMA 2010 - 10th REHVA World Congress*, Antalya, Turkey.
- Solarbuzz. (2011). Module pricing. URL: <http://solarbuzz.com/facts-and-figures/retail-price-environment/module-prices>.
- Spitler, J.; Fisher, D. & Pedersen, C. (1997). The radiant time series cooling load calculation procedure. *ASHRAE Transactions* **103**, 503-518.
- Spitler, J.D. (2005). Ground source heat pump research: past, present and future. *HVAC&R Research* **11**(2).
- Stauch, V.; Hug, C.; Schubiger, F. & Steiner, P. (2010). Weather Forecasts, Observations and Algorithms for Building Simulation and Predictive Control. Report: *MeteoSwiss*. Zurich. July 30.
- Stene, J. (2005). Residential CO₂ heat pump system for combined space heating and hot water heating. *International Journal of Refrigeration* **28**(8), 1259-1265.
- Stephanopoulos, G. (1984). *Chemical Process Control: an Introduction to Theory and Practice*. Prentice-Hall, Englewood Cliffs, NJ, USA.
- Stephenson, D. & Mitalas, G. (1971). Calculation of heat conduction transfer functions for multi-layers slabs. *ASHRAE Transactions* **77**(2), 117-126.
- SunEarth Inc. (2005).
- TiNOX. (2010). *TiNOX Energy*. Munich, Germany. www.tinox.com.
- Todtli, J.; Gwerder, M.; Renggli, F.; Guntensperger, W.; Lehmann, B.; Dorer, V. & Hildebrand, K. (2009). Regelung und Steuerung von thermoaktiven Bauteilsystemen (TABS). *Bauphysik* **31**(5), 319-325.
- Tonkoski, R.; Lopes, L.A.C. & El-Fouly, T.H.M. (2010). Droop-based active power curtailment for overvoltage prevention in grid-connected PV inverters. In *IEEE International Symposium on Industrial Electronic (ISIE)*, Bari, Italy. July 4-7.

- Tonkoski, R.; Lopes, L.A.C. & El-Fouly, T.H.M. (2011). Coordinated active power curtailment of grid connected PV inverters for overvoltage prevention. *IEEE Transactions on Sustainable Energy* **2**(2), 139-147.
- Torcellini, P.; Deru, M.; Griffith, B.; Long, N.; Pless, S. & Judkoff, R. (2004). Lessons Learned from Field Evaluation of Six High-Performance Buildings. *ACEEE Summer Study*, Pacific Grove, California.
- Tzempelikos, A. (2005). *A Methodology for Integrated Daylighting and Thermal Analysis of Buildings* Thesis. Concordia University, Montréal, Canada.
- Tzempelikos, A. & Athienitis, A.K. (2003). Simulation for facade options and impact on HVAC system design. *Proceedings of the Eighth IBPSA Conference*, 1301-1308.
- Tzempelikos, A. & Athienitis, A.K. (2005). Integrated Thermal and Daylighting Analysis for Design of Office Buildings. *ASHRAE Transactions* **111**(1), 227-238.
- Underwood, C.P. (1999). *HVAC Control Systems: Modeling Analysis and Design*. Taylor & Francis, London.
- Underwood, C.P. & Yik, F.W.H. (2004). *Modelling Methods for Energy in Buildings*. Blackwell Publishing.
- van Schijndel, A.W.M.J. & Hensen, J. (2005). Integrated heat, air and moisture modeling toolkit in MATLAB. In *Ninth International IBPSA Conference*, Montréal, Canada. August 15-18.
- Vieira, B.B.S.; Wyant, R.S.; Oliveira, F.A.R.; Litz, L. & Bauchspiess, A. (2008). Building Identification for Energy-Saving Automation Using First-Principles Models. In *VIII Conferencia Internacional de Aplicações Industriais (Induscon)*, Poços de Caldas, Brazil. August 17-20
- Viessmann. (2010). Vitocal 300-A, Air/water heat pump. http://www.viessmann.com/com/en/products/Heat_pumps/Vitocal_300-A.html.
- Vinot, B. (1988). Combined Control of Direct Gains and Heating in Passive Solar Buildings. In *PLEA88 - Energy and Buildings for Temperate Climates: a Mediterranean Regional Approach*, 583-588, Porto, Portugal. July 27-31.
- Vinot, B. (1989). Energy Saving in Building by Optimization of Control Strategies Design Using Simulation Analysis. In *2nd European Conference on Architecture*, 511-513, Paris, France. December 4-8.
- Vlassis, N. (2007). *A Concise Introduction to Multiagent Systems and Distributed Artificial Intelligence*. Morgan Clay Pool.
- Voss, K.; Sartori, I.; Napolitano, A.; Geier, S.; Gonçalves, H.; Hall, M.; Heiselberg, P.; Widen, J.; Candanedo, J.A.; Musall, E.; Karlsson, B. & Torcellini, P. (2010). Load matching and grid interaction of net zero energy buildings. *EUROSUN 2010*, Graz, Austria. September 29th - October 1st.

- Wang, L. (2009). *Model Predictive Control System Design and Implementation using MATLAB*. Springer-Verlag, London, UK.
- Wang, S. & Ma, Z. (2008). Supervisory and Optimal Control of Building HVAC Systems: A Review. *HVAC & R Research* **14**(1), 3-32.
- Wang, Z.; Yang, R. & Want, L. (2010). Multi-agent Intelligent Controller Design for Smart and Sustainable Buildings. *Systems Conference, 2010 4th Annual IEEE*, 277-282, San Diego. April 4-8.
- Weiss, W. & Faninger, G. (2002). Solar Thermal Collector Markets in IEA Member Countries. Report: *IEA Solar Heating & Cooling Programme*. Klagenfurt, Austria.
- Wetter, M. (2009). Modelica-based Modelling and Simulation to Support Research and Development in Building Energy and Control Systems. *Journal of Building Performance Simulation* **2**(2), 143-161.
- Wetter, M. & Haves, P. (2008). A Modular Building Controls Virtual Test Bed for the Integration of Heterogeneous Systems. *Third National Conference of IBPSA - USA*, Berkeley, California. July 30 - August 1, 2008.
- Wilson, B.; Hagenström, H. & Dvorjetski, P. (2002). The Optical Properties of Gasochromic Glazing. *Proceedings of the 4th International Conference on Coatings on Glass*, 649-657.
- Winn, R. & Winn, C. (1985). Optimal control of auxiliary heating of passive-solar-heated buildings. *Solar Energy* **35**(5), 419-428.
- Wittchen, K.B.; Løgberg, E.; Pedersen, S.; Djurtoft, R. & Thiesen, J. (2005). Use of weather forecasts to control night cooling. *Proceedings of the Ninth International IBPSA Conference*, Montréal, Québec, Canada. August 15-18.
- Wong, J.K.W.; Li, H. & Wang, S.W. (2005). Intelligent Building Research: a Review. *Automation in Construction* **14**, 143-159.
- WordNet. (2008). Definition of Sorption. Retrieved on March, 2008.
<http://wordnet.princeton.edu/perl/webwn?s=sorption>.
- Xu, P.; Haves, P.; Braun, J.E. & Hope, L.t. (2004). Peak Demand Reduction from Pre-Cooling with a Zone Temperature Reset in an Office Building. Report: *Lawrence Berkeley National Laboratory*. Berkeley, California, USA.
- Xu, P.; Haves, P.; Piette, M. & Zagreus, L. (2006). Demand Shifting with Thermal Mass in Large Commercial Buildings: Field Tests, Simulations and Audits. Report: *Lawrence Berkeley National Laboratory*. Berkeley, California.
- Yager, A.J. (1980). *A Study of the La Macaza Solar House*, Master of Engineering Thesis. Concordia University, Montréal, Québec.

Yu, Z. & Dexter, A. (2009). Simulation based predictive control of low-energy building systems. In *Eleventh International IBPSA Conference*, Glasgow, Scotland. July 27-30.

ZENN. (2008). ZENN Motor Company. Retrieved on March, 2008.

www.zenncars.com.

Zhou, G.; Krarti, M. & Henze, G.P. (2005). Parametric analysis of active and passive building thermal storage utilization. *Journal of Solar Energy Engineering* **127**, 37.

Appendices

A. Alstonvale Net Zero House Schematics

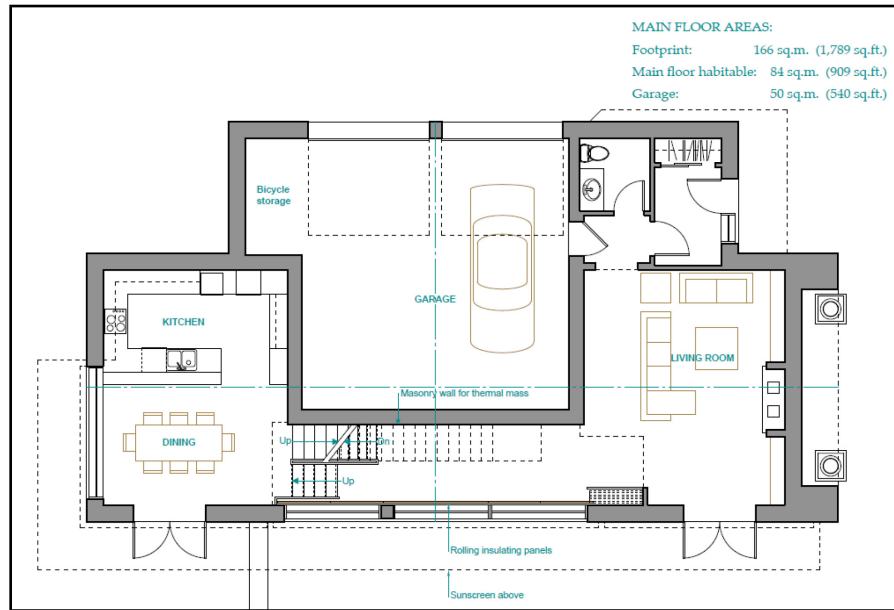


Figure A.1. Main floor plan.

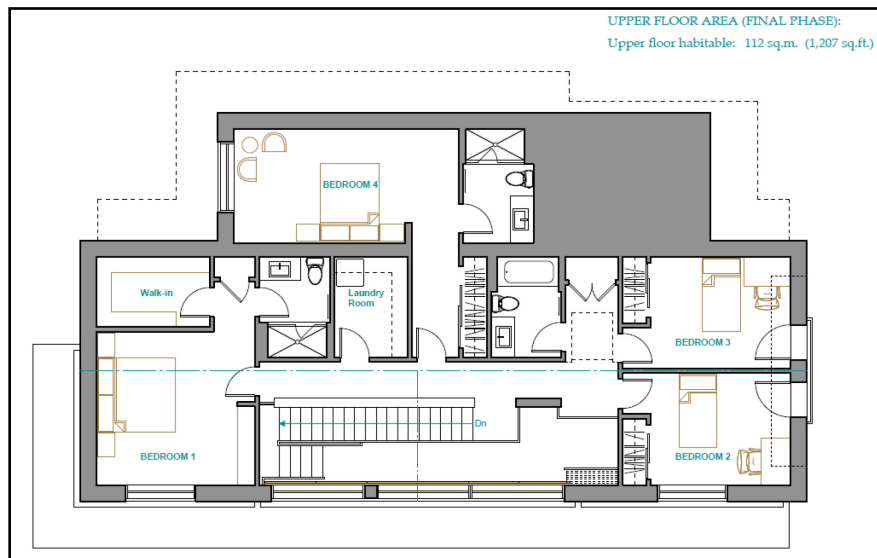


Figure A.2. Upper floor plan.

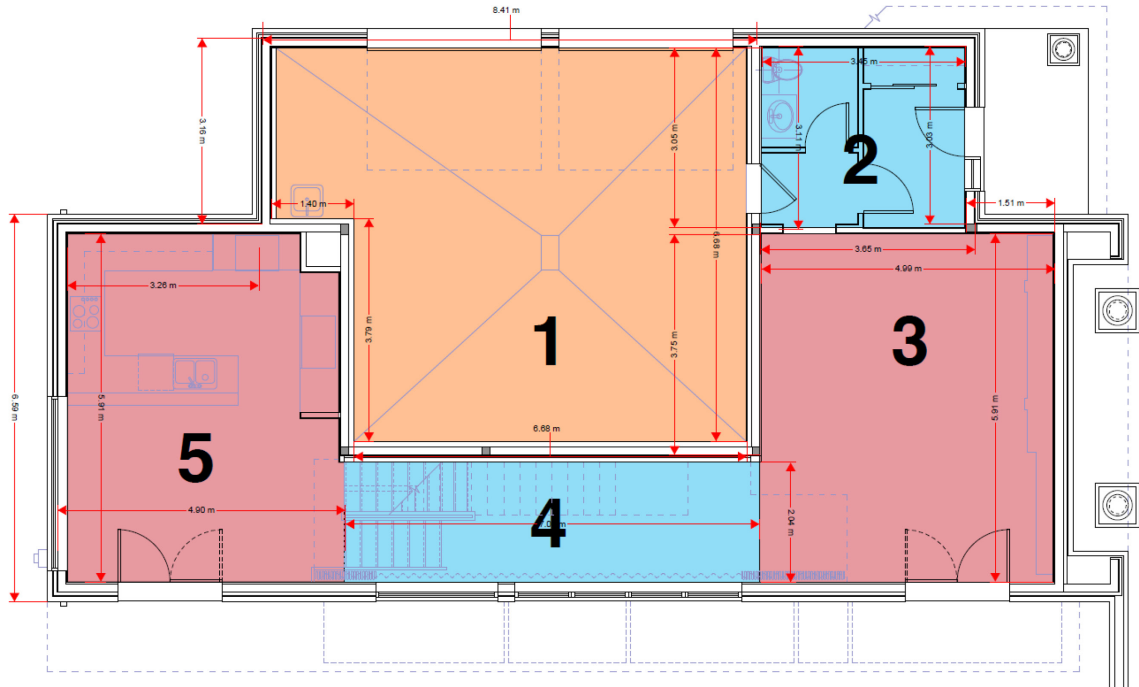


Figure A.3. Radiant floor heating zones, main floor.

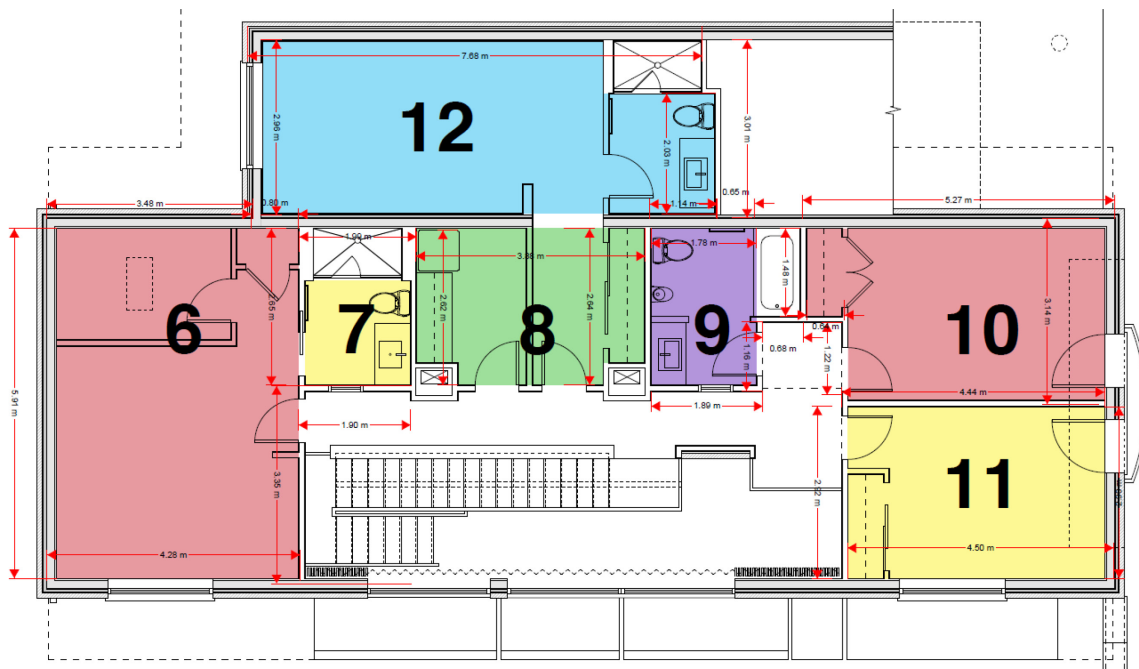


Figure A.4. Radiant floor heating zones, upper floor.

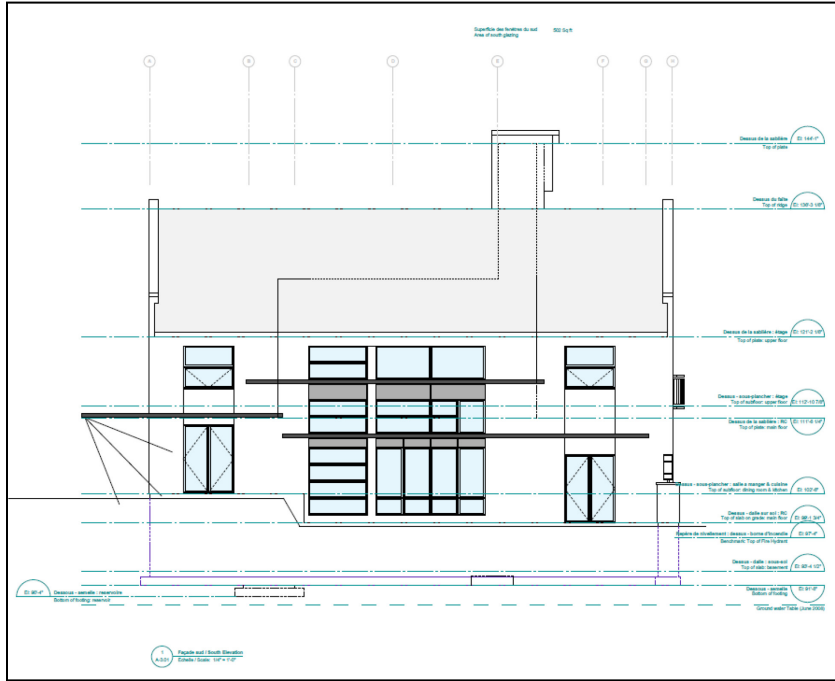


Figure A.5. South elevation view (Pogharian, 2007)

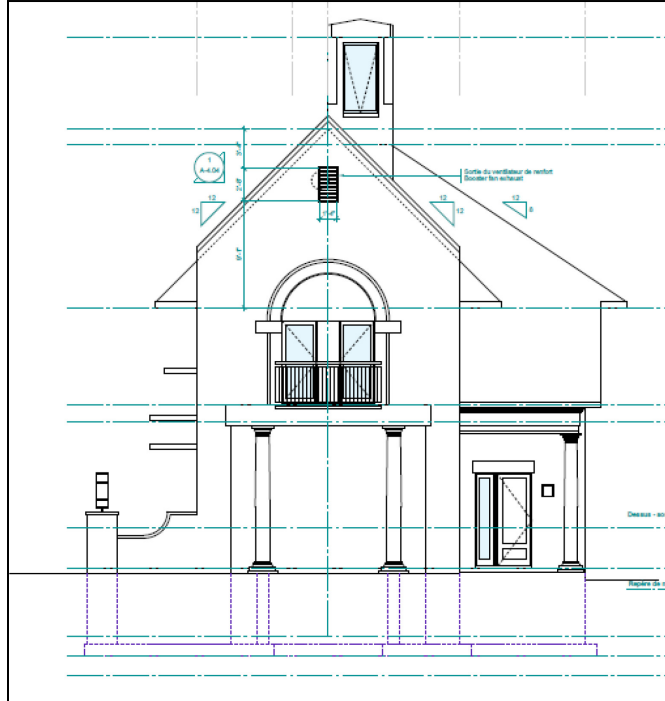


Figure A.6. East elevation view (Pogharian, 2007)

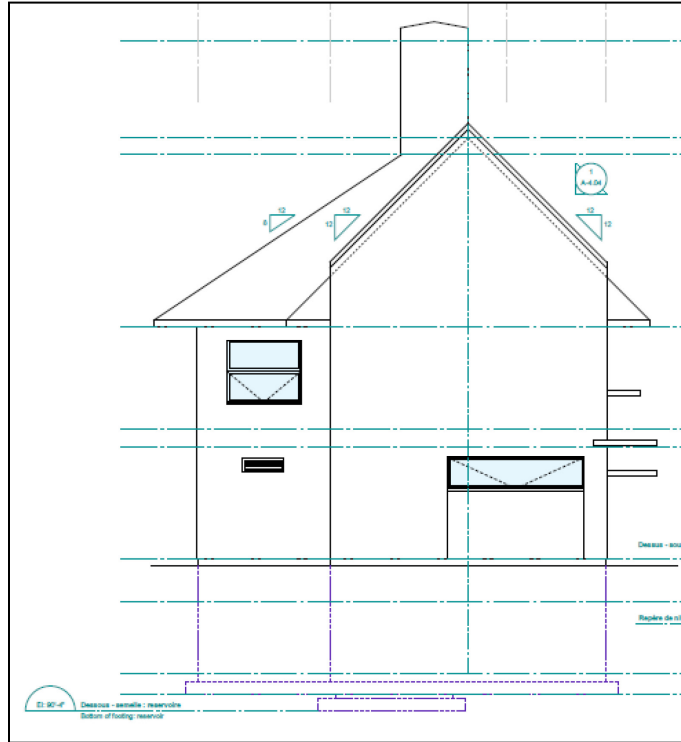


Figure A.7. West elevation view (Pogharian, 2007).

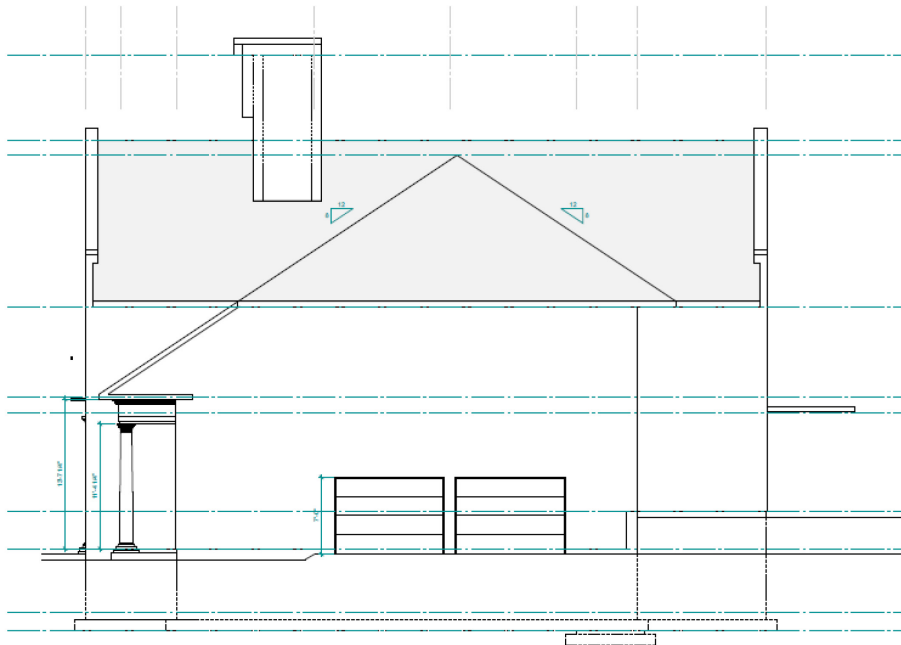


Figure A.8. North elevation view (Pogharian, 2007)

B. Equipment Technical Specification Sheets

"U"		Transmission %			Réf. lum. Visible %		Coefficient d'assombrissement	Coeff. gain de chaleur solaire	Gain relatif de chaleur Blu / h - PC
		Lumière visible	Solaire Total	UV T dw-K	Extérieur	Inérieur			
0.158	6.329	63.2	45.53	37.2	22.92	22.9	0.653	0.567	133

La description des verres est de l'extérieur vers l'intérieur

PERFORMANCES

Composition:

3mm Low-e pyro de LOF (#2)	9921
11.68mm d'argon	
3mm clair	887
11.68mm d'argon	
3mm Low-e pyro de LOF (#5)	9921

Performances des unités scellées selon le logiciel Window 5,2 de L.B.N.L

Figure B.1. Window details from manufacturer.

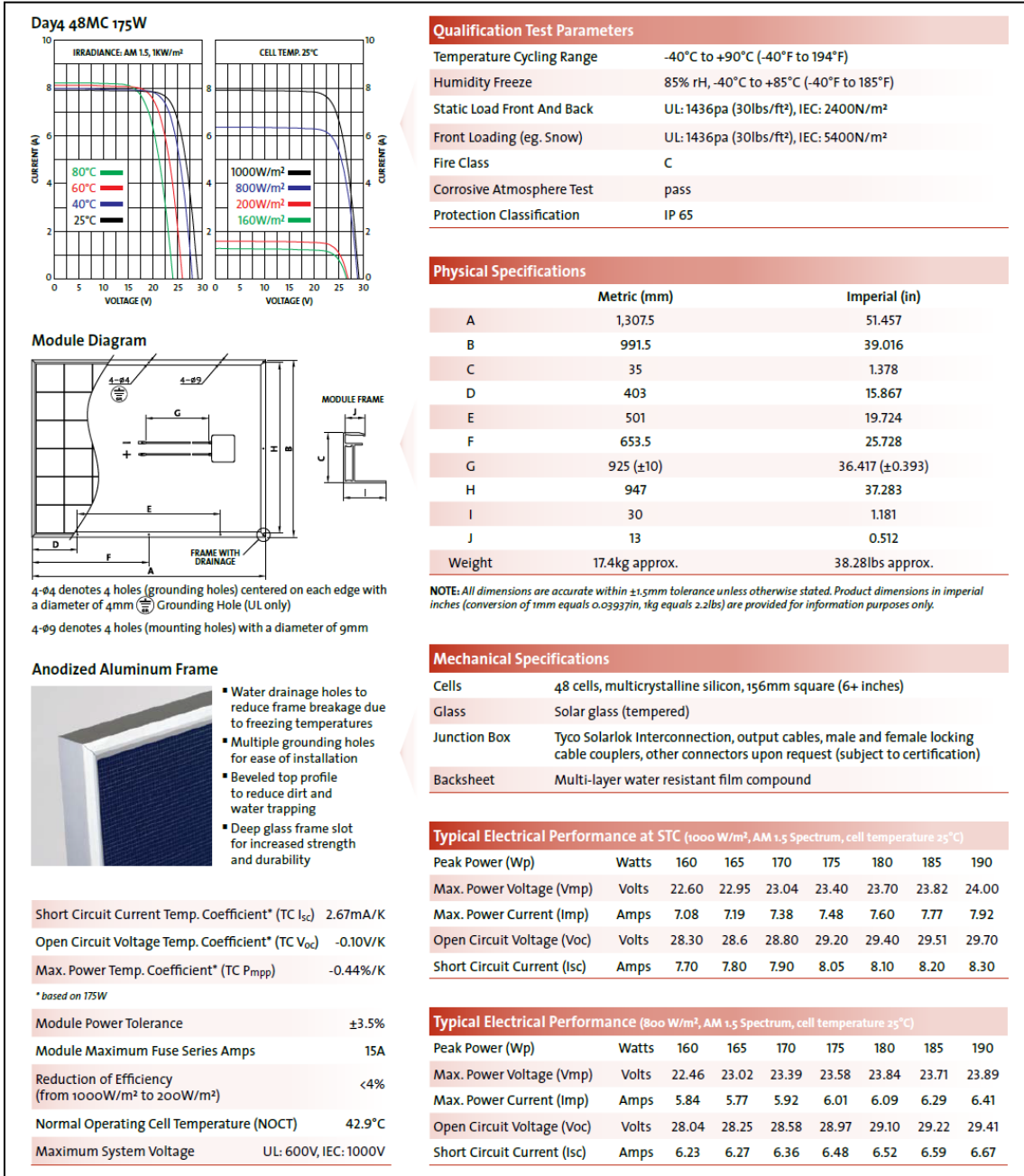


Figure B.2. Day-4 PV panels used on the Alstonvale Net Zero House.

COIL OPERATING CONDITIONS
(INCH-POUND UNITS)

Tube Mat'l. - 1, 2 or 3 (below)		1		
Type of Coil		Glycol Cooling		
		Scenario 1	Scenario 2	
Number of Coils		1		

When **MULTIPLE COILS** are selected, the following information is **PER COIL**

FPI/Feeds/Passes/Rows		14/12/16/8	14/12/16/8	
Size of Coil:	Finned Height (in.)	36.00	36.00	
	Finned Length (in.)	50.00	50.00	
	Face Area (sq. ft.)	12.50	12.50	
	Air Flow (cfm)	1,000	2,000	
	Face Velocity (fpm)	80	160	
	Air Pressure Drop (in. W.C.)	0.06	0.17	
Entering Air Temp:	Dry Bulb (deg. F.)	36.5	104.0	
Leaving Air Temp	Dry Bulb (deg. F.)	23.3	66.0	
Output:	Total Heat (BTUH)	14,200	82,100	
	Fluid Type	30% P.G.	30% P.G.	
Fluid Temp:	Entering (deg. F.)	23.0	64.8	
	Leaving (deg. F.)	26.3	74.4	
	Fluid Flow Rate (USgpm)	9.0	18.0	
	Fluid Pressure Drop (ft. W.C.)	5.1	8.5	

Material Specifications: Coil tube material - 1/2" O.D. x 0.018" wall copper
Fin material - 0.0060" thick aluminum
Header Material - Type "L" copper and copper adaptors
Casing Material - 18 gauge galvanized steel

PREPARED FOR: José Candanedo

COMPANY: Concordia University

REFERENCE/DATE: Alstonvale / September 18, 2007

Figure B.3. Air-to-water heat exchanger.

Performance Data
GSW036 Heating

SOURCE				LOAD																								
EWT	Flow			EWT	Flow 5.0 gpm								Flow 7.0 gpm								Flow 9.0 gpm							
	GPM	WPD			HC MBtuh	Power KW	HE MBtuh	LRT °F	COP		HC MBtuh	Power KW	HE MBtuh	LRT °F	COP		HC MBtuh	Power KW	HE MBtuh	LRT °F	COP							
		PSI	FT						PSI	FT					PSI	FT					PSI	FT						
20	9.0	9.9	22.9	80	24.1	1.41	19.3	89.8	5.00	2.0	4.5	24.2	1.37	19.5	89.9	5.19	3.4	7.8	24.2	1.34	19.8	85.4	5.29	5.1	11.7			
				80	23.5	1.78	17.5	89.4	3.87	1.5	3.5	23.8	1.72	17.8	86.7	4.03	2.8	6.4	23.7	1.88	17.9	85.2	4.12	4.3	10.0			
				100	23.0	2.29	15.2	109.2	2.94	1.1	2.4	23.1	2.21	15.6	106.8	3.07	2.2	5.2	23.2	2.18	15.8	105.1	3.14	3.8	8.2			
				120	22.8	2.94	12.5	129.0	2.24	0.9	2.1	22.6	2.84	12.9	128.4	2.33	2.0	4.8	22.7	2.78	13.2	125.0	2.39	3.3	7.6			
30	5.0	3.8	8.7	80	25.4	1.42	20.5	70.2	5.22	2.0	4.5	25.5	1.38	20.8	87.3	5.42	3.4	7.8	25.5	1.38	20.9	85.7	5.53	5.1	11.7			
				80	24.8	1.80	18.7	89.9	4.04	1.5	3.5	24.9	1.73	19.0	87.1	4.21	2.8	6.4	25.0	1.70	19.2	85.5	4.31	4.3	10.0			
				100	24.3	2.32	16.4	109.7	3.07	1.1	2.4	24.4	2.23	16.8	107.0	3.20	2.2	5.2	24.4	2.18	17.0	105.4	3.27	3.8	8.2			
					120	23.8	2.97	13.6	129.5	2.34	0.9	2.1	23.8	2.87	14.1	128.8	2.44	2.0	4.8	23.9	2.81	14.3	125.3	2.49	3.3	7.6		
	7.0	5.8	13.5	80	27.2	1.43	22.3	70.9	5.58	2.0	4.5	27.3	1.39	22.6	87.8	5.77	3.4	7.8	27.4	1.38	22.7	86.1	5.89	5.1	11.7			
				80	26.8	1.81	20.4	90.8	4.30	1.5	3.5	26.7	1.75	20.8	87.8	4.48	2.8	6.4	26.8	1.71	20.9	85.9	4.59	4.3	10.0			
				100	26.0	2.33	18.1	110.4	3.27	1.1	2.4	26.1	2.25	18.5	107.5	3.41	2.2	5.2	26.2	2.20	18.7	105.8	3.49	3.8	8.2			
					120	25.5	2.99	15.3	130.2	2.50	0.9	2.1	25.6	2.89	15.7	127.3	2.60	2.0	4.8	25.6	2.83	16.0	125.7	2.65	3.3	7.6		
	9.0	8.5	19.5	80	27.7	1.44	22.8	71.1	5.84	2.0	4.5	27.8	1.39	23.0	87.9	5.84	3.4	7.8	27.8	1.37	23.2	86.2	5.98	5.1	11.7			
80				27.1	1.82	20.9	90.8	4.38	1.5	3.5	27.2	1.75	21.2	87.8	4.54	2.8	6.4	27.2	1.72	21.4	86.0	4.65	4.3	10.0				
100				26.5	2.34	18.5	110.8	3.31	1.1	2.4	26.6	2.25	18.9	107.8	3.45	2.2	5.2	26.6	2.21	19.1	105.9	3.53	3.8	8.2				
				120	25.9	3.00	15.7	130.4	2.53	0.9	2.1	26.0	2.90	16.1	127.4	2.63	2.0	4.8	26.0	2.84	16.2	125.8	2.69	3.3	7.6			
40	5.0	3.2	7.4	80	28.2	1.45	23.2	71.3	5.89	2.0	4.5	28.3	1.39	23.5	88.1	5.97	3.4	7.8	28.4	1.38	23.7	86.3	6.12	5.1	11.7			
				80	27.5	1.88	21.8	91.0	4.81	1.5	3.5	27.7	1.80	22.2	87.9	5.07	2.8	6.4	27.7	1.88	22.4	86.2	5.21	4.3	10.0			
				100	26.8	2.16	19.4	110.7	3.64	1.1	2.4	26.9	2.06	19.9	107.7	3.84	2.2	5.2	27.0	2.00	20.2	106.0	3.95	3.8	8.2			
					120	26.0	2.78	16.6	130.4	2.77	0.9	2.1	26.2	2.64	17.2	127.5	2.91	2.0	4.8	26.3	2.57	17.5	125.8	2.99	3.3	7.6		
	7.0	5.0	11.5	80	30.2	1.46	25.2	72.1	6.08	2.0	4.5	30.4	1.40	25.6	88.7	6.35	3.4	7.8	30.4	1.37	25.8	86.8	6.52	5.1	11.7			
				80	29.5	1.89	23.8	91.8	5.12	1.5	3.5	29.7	1.81	24.2	88.5	5.39	2.8	6.4	29.7	1.87	24.4	86.8	5.55	4.3	10.0			
				100	28.8	2.17	21.3	111.5	3.88	1.1	2.4	28.9	2.07	21.8	108.3	4.09	2.2	5.2	29.0	2.02	22.1	106.4	4.21	3.8	8.2			
					120	27.9	2.78	18.5	131.2	2.95	0.9	2.1	28.1	2.66	19.0	128.0	3.10	2.0	4.8	28.2	2.59	19.3	126.3	3.18	3.3	7.6		
	9.0	7.2	16.7	80	30.7	1.47	25.7	72.3	6.14	2.0	4.5	30.9	1.41	26.1	88.8	6.44	3.4	7.8	30.9	1.37	26.3	86.9	6.60	5.1	11.7			
80				30.0	1.70	24.2	92.0	5.19	1.5	3.5	30.2	1.82	24.6	88.8	5.48	2.8	6.4	30.2	1.88	24.8	86.7	5.82	4.3	10.0				
100				29.2	2.18	21.8	111.7	3.93	1.1	2.4	29.4	2.08	22.3	108.4	4.14	2.2	5.2	29.5	2.03	22.3	106.5	4.26	3.8	8.2				
				120	28.4	2.79	18.9	131.4	2.99	0.9	2.1	28.5	2.67	19.4	128.2	3.14	2.0	4.8	28.6	2.60	19.6	126.4	3.23	3.3	7.6			
50	5.0	2.8	6.1	80	32.0	1.48	28.9	72.8	6.33	2.0	4.5	32.1	1.42	27.3	89.2	6.64	3.4	7.8	32.2	1.39	27.5	87.2	6.81	5.1	11.7			
				80	31.2	1.88	24.8	92.5	4.88	1.5	3.5	31.4	1.79	25.3	89.0	5.14	2.8	6.4	31.5	1.74	25.5	87.0	5.29	4.3	10.0			
				100	30.4	2.41	22.2	112.2	3.70	1.1	2.4	30.6	2.30	22.7	108.7	3.89	2.2	5.2	30.7	2.24	20.0	106.8	4.01	3.8	8.2			
					120	29.8	3.08	19.0	131.8	2.81	0.9	2.1	29.7	2.95	19.6	128.5	2.95	2.0	4.8	29.8	2.88	20.0	126.8	3.03	3.3	7.6		
	7.0	4.1	9.5	80	34.3	1.49	29.2	73.7	6.74	2.0	4.5	34.5	1.43	29.6	89.9	7.07	3.4	7.8	34.6	1.40	29.8	87.7	7.25	5.1	11.7			
				80	33.5	1.89	27.1	93.4	5.19	1.5	3.5	33.7	1.80	27.5	89.8	5.47	2.8	6.4	33.8	1.78	27.8	87.5	5.83	4.3	10.0			
				100	32.8	2.43	24.3	113.1	3.94	1.1	2.4	32.8	2.32	24.9	109.4	4.15	2.2	5.2	32.9	2.26	25.2	107.3	4.27	3.8	8.2			
					120	31.7	3.11	21.1	132.7	2.99	0.9	2.1	31.9	2.97	21.7	129.1	3.14	2.0	4.8	32.0	2.90	22.1	127.1	3.23	3.3	7.6		
	9.0	6.0	13.8	80	34.9	1.50	29.8	74.0	6.83	2.0	4.5	35.1	1.43	30.2	70.0	7.16	3.4	7.8	35.1	1.40	30.4	87.8	7.34	5.1	11.7			
80				34.1	1.90	27.8	93.8	5.26	1.5	3.5	34.2	1.81	28.1	89.8	5.54	2.8	6.4	34.3	1.78	28.4	87.6	5.71	4.3	10.0				
100				33.2	2.44	24.9	113.3	3.99	1.1	2.4	33.4	2.33	25.4	109.5	4.20	2.2	5.2	33.5	2.27	25.7	107.4	4.33	3.8	8.2				
				120	32.2	3.12	21.8	132.9	3.03	0.9	2.1	32.4	2.98	22.2	129.3	3.18	2.0	4.8	32.5	2.91	22.6	127.2	3.27	3.3	7.6			
60	5.0	2.9	6.8	80	35.5	1.50	30.4	74.2	6.94	2.0	4.5	35.7	1.44	30.8	70.2	7.27	3.4	7.8	35.8	1.40	31.0	87.9	7.48	5.1	11.7			
				80	34.7	1.88	28.9	93.9	5.08	1.5	3.5	34.8	1.80	29.4	90.0	6.38	2.8	6.4	34.9	1.88	29.6	87.8	6.57	4.3	10.0			
				100	33.8	2.16	26.4	113.5	4.59	1.1	2.4	33.9	2.06	26.9	109.7	4.84	2.2	5.2	34.0	2.00	27.2	107.8	4.98	3.8	8.2			
					120	32.8	2.78	23.4	133.1	3.49	0.9	2.1	33.0	2.64	24.0	129.4	3.68	2.0	4.8	33.1	2.57	24.3	127.4	3.77	3.3	7.6		
	7.0	3.9	8.9	80	38.1	1.51	32.9	75.2	7.39	2.0	4.5	38.3	1.45	33.3	70.9	7.74	3.4	7.8	38.4	1.41	33.5	88.5	7.94	5.1	11.7			
				80	37.2	1.89	31.4	94.9	6.45	1.5	3.5	37.4	1.81	31.9	90.7	6.80	2.8	6.4	37.5	1.87	32.1	88.3	7.00	4.3	10.0			
				100	36.2	2.17	28.8	114.5	4.89	1.1	2.4	36.4	2.07	29.3	110.4	5.15	2.2	5.2	36.5	2.02	29.6	108.1	5.30	3.8	8.2			
					120	35.2	2.78	25.7	134.1	3.71	0.9	2.1	35.4	2.66	26.3	130.1	3.90	2.0	4.8	35.5	2.69	26.6	127.9	4.01	3.3	7.6		
	9.0	5.0	11.4	80	38.7	1.52	33.8	75.5	7.48	2.0	4.5	38.9	1.45	33.9	71.1	7.84	3.4	7.8	39.0	1.42	34.1	88.7	8.08	5.1	11.7			
80				37.8	1.70	32.0	105.1	6.53	1.5	3.5	38.0	1.82	32.5	100.9	6.88	2.8	6.4	38.1	1.88	32.7	98.5	7.09	4.3					

Capacity Data

EW020 Heating

ELT °F	EST °F	Load Flow			Source Flow - 3 GPM						Source Flow - 6 GPM						Source Flow - 9 GPM											
		Flow GPM	PSI	PD FT HD	LLT °F	HC KBTUH	Power KW	HE KBTUH	COP	LST °F	PSI	PD FT HD	LLT °F	HC KBTUH	Power KW	HE KBTUH	COP	LST °F	PSI	PD FT HD	LLT °F	HC KBTUH	Power KW	HE KBTUH	COP	LST °F	PSI	PD FT HD
30	3	1.2	2.8									74	20.3	1.24	16.1	4.81	25	4.9	11.3	74	21.0	1.25	16.7	4.92	26	10.6	24.5	
		4.5	10.4									67	21.2	1.25	16.9	4.97	24	4.9	11.3	67	21.9	1.26	17.6	5.09	26	10.6	24.5	
		9.7	22.4									65	21.6	1.26	17.3	5.00	24	4.9	11.3	65	22.3	1.28	18.0	5.12	26	10.6	24.5	
	50	1.2	2.8	77	24.8	1.24	20.6	5.87	36	1.2	2.6	77	25.1	1.25	20.9	5.89	43	4.6	10.6	77	26.0	1.26	21.7	6.04	45	10.0	23.1	
		4.5	10.4	69	25.9	1.25	21.7	6.08	36	1.2	2.6	69	26.3	1.26	22.0	6.10	43	4.6	10.6	69	27.2	1.28	22.8	6.24	45	10.0	23.1	
		9.7	22.4	66	26.4	1.26	22.1	6.11	35	1.2	2.6	66	26.7	1.28	22.4	6.13	43	4.6	10.6	66	27.7	1.29	23.3	6.28	45	10.0	23.1	
	60	3	1.2	2.8	80	29.8	1.26	25.5	6.95	53	1.1	2.4	80	30.2	1.27	25.9	6.98	61	4.3	9.9	81	31.3	1.28	26.9	7.14	64	9.4	21.7
			4.5	10.4	70	31.2	1.27	26.9	7.19	52	1.1	2.4	71	31.6	1.28	27.2	7.22	61	4.3	9.9	71	32.7	1.30	28.3	7.39	64	9.4	21.7
			9.7	22.4	67	31.7	1.29	27.3	7.23	52	1.1	2.4	67	32.2	1.30	27.7	7.26	61	4.3	9.9	67	33.3	1.31	28.8	7.43	64	9.4	21.7
70	1.2	2.8	82	32.9	1.26	28.6	7.63	71	1.1	2.2	82	33.4	1.28	29.0	7.68	80	4.0	9.2	83	34.5	1.29	30.1	7.85	83	8.8	20.3		
	4.5	10.4	71	34.5	1.28	30.1	7.90	70	1.1	2.2	72	34.9	1.29	30.5	7.93	80	4.0	9.2	72	36.1	1.30	31.7	8.12	83	8.8	20.3		
	9.7	22.4	68	35.0	1.29	30.6	7.94	70	1.1	2.2	68	35.5	1.31	31.1	7.97	80	4.0	9.2	68	36.7	1.32	32.2	8.17	83	8.8	20.3		
90	1.2	2.8	86	38.6	1.33	34.1	8.49	87	1.0	2.1	86	39.2	1.35	34.6	8.52	98	3.8	8.8	87	40.5	1.36	35.9	8.73	102	8.2	18.9		
	4.5	10.4	73	40.4	1.35	35.8	8.79	86	1.0	2.1	74	41.0	1.36	36.3	8.82	98	3.8	8.8	74	42.4	1.38	37.7	9.03	102	8.2	18.9		
	9.7	22.4	69	41.1	1.36	36.4	8.84	86	1.0	2.1	69	41.7	1.38	37.0	8.87	98	3.8	8.8	70	43.1	1.39	38.3	9.08	101	8.2	18.9		
80	3	1.1	2.5									94	20.6	1.68	14.9	3.59	25	4.9	11.3	94	21.3	1.70	15.5	3.68	27	10.6	24.5	
		4.2	9.7									87	21.2	1.70	15.8	3.72	25	4.9	11.3	87	22.3	1.72	16.4	3.81	26	10.6	24.5	
		9.1	21.0									85	21.9	1.72	16.1	3.74	25	4.9	11.3	85	22.7	1.74	16.8	3.83	26	10.6	24.5	
	50	1.1	2.5	97	25.2	1.71	19.4	4.32	37	1.2	2.6	97	25.5	1.73	19.7	4.34	43	4.6	10.6	98	26.4	1.74	20.5	4.44	45	10.0	23.1	
		4.2	9.7	89	26.4	1.73	20.5	4.47	36	1.2	2.6	89	26.7	1.75	20.8	4.49	43	4.6	10.6	89	27.6	1.76	21.6	4.59	45	10.0	23.1	
		9.1	21.0	86	26.8	1.75	20.8	4.50	36	1.2	2.6	86	27.2	1.76	21.1	4.51	43	4.6	10.6	86	28.1	1.78	22.0	4.62	45	10.0	23.1	
	70	1.1	2.5	100	30.3	1.76	24.3	5.05	54	1.1	2.4	100	30.7	1.78	24.7	5.07	62	4.3	9.9	101	31.8	1.80	25.7	5.19	64	9.4	21.7	
		4.2	9.7	91	31.7	1.78	25.6	5.22	53	1.1	2.4	91	32.1	1.80	26.0	5.24	61	4.3	9.9	91	33.3	1.82	27.1	5.37	64	9.4	21.7	
		9.1	21.0	87	32.2	1.80	26.1	5.25	53	1.1	2.4	87	32.7	1.82	26.5	5.27	61	4.3	9.9	88	33.8	1.84	27.5	5.40	64	9.4	21.7	
90	1.1	2.5	102	33.5	1.79	27.4	5.47	72	1.1	2.2	103	33.9	1.81	27.8	5.49	81	4.0	9.2	103	35.1	1.83	28.9	5.62	84	8.8	20.3		
	4.2	9.7	92	35.0	1.81	28.8	5.68	71	1.1	2.2	92	35.5	1.83	29.2	5.68	80	4.0	9.2	92	36.7	1.85	30.4	5.81	83	8.8	20.3		
	9.1	21.0	88	35.6	1.83	29.4	5.69	70	1.1	2.2	88	36.1	1.85	29.8	5.71	80	4.0	9.2	88	37.3	1.87	31.0	5.85	83	8.8	20.3		
110	1.1	2.5	106	39.3	1.85	33.0	6.23	88	1.0	2.1	107	39.8	1.86	33.4	6.28	99	3.8	8.8	107	41.2	1.88	34.7	6.41	102	8.2	18.9		
	4.2	9.7	94	41.1	1.87	34.7	6.45	87	1.0	2.1	94	41.6	1.89	35.2	6.47	98	3.8	8.8	94	43.1	1.90	36.6	6.63	102	8.2	18.9		
	9.1	21.0	89	41.8	1.89	35.3	6.48	86	1.0	2.1	89	42.3	1.91	35.8	6.51	98	3.8	8.8	90	43.8	1.92	37.2	6.67	102	8.2	18.9		
100	3	1.0	2.3									114	20.9	2.12	13.7	2.90	25	4.9	11.3	114	21.7	2.14	14.4	2.97	27	10.6	24.5	
		3.9	9.0									107	21.9	2.14	14.6	3.00	25	4.9	11.3	108	22.7	2.16	15.3	3.07	27	10.6	24.5	
		8.5	19.6									105	22.3	2.16	14.9	3.02	25	4.9	11.3	105	23.0	2.19	15.6	3.09	27	10.6	24.5	
	50	1.0	2.3	117	25.6	2.13	18.3	3.52	38	1.2	2.6	117	26.0	2.15	18.6	3.54	44	4.6	10.6	118	26.8	2.17	19.4	3.62	46	10.0	23.1	
		3.9	9.0	109	26.8	2.15	19.4	3.65	37	1.2	2.6	109	27.1	2.17	19.7	3.66	43	4.6	10.6	109	28.1	2.20	20.6	3.75	45	10.0	23.1	
		8.5	19.6	106	27.2	2.18	19.6	3.67	37	1.2	2.6	106	27.6	2.20	20.1	3.68	43	4.6	10.6	106	28.6	2.22	21.0	3.77	45	10.0	23.1	
	70	1.0	2.3	121	36.1	2.18	23.4	4.18	54	1.1	2.4	121	31.2	2.18	23.8	4.20	62	4.3	9.9	122	32.3	2.20	24.8	4.30	64	9.4	21.7	
		3.9	9.0	111	32.2	2.18	24.8	4.33	53	1.1	2.4	111	32.7	2.20	25.1	4.35	62	4.3	9.9	111	33.8	2.22	26.2	4.45	64	9.4	21.7	
		8.5	19.6	107	32.8	2.20	25.2	4.36	53	1.1	2.4	107	33.2	2.23	25.6	4.37	61	4.3	9.9	108	34.4	2.25	26.7	4.48	64	9.4	21.7	
90	1.0	2.3	123	34.0	2.19	26.5	4.54	72	1.1	2.2	123	34.5	2.22	26.9	4.56	81	4.0	9.2	124	35.7	2.24	28.0	4.67	84	8.8	20.3		
	3.9	9.0	112	35.6	2.22	28.0	4.70	71	1.1	2.2	112	36.1	2.24	28.4	4.72	81	4.0	9.2	112	37.3	2.26	29.6	4.83	83	8.8	20.3		
	8.5	19.6	108	36.2	2.24	28.5	4.73	71	1.1	2.2	108	36.7	2.27	28.9	4.74	80	4.0	9.2	108	37.9	2.29	30.1	4.86	83	8.8	20.3		
110	1.0	2.3	127	36.6	2.23	32.3	5.25	88	1.0	2.1	127	40.4	2.25	32.8	5.27	99	3.8	8.8	128	41.8	2.27	34.1	5.40	102	8.2	18.9		
	3.9	9.0	114	41.7	2.25	34.0	5.44	87	1.0	2.1	114	42.3	2.27	34.5	5.45	98	3.8	8.8	115	43.8	2.30	35.9	5.59	102	8.2	18.9		
	8.5	19.6	109	42.4	2.27	34.7	5.47	87	1.0	2.1	110	43.0	2.30	35.2	5.49	98	3.8	8.8	110	44.5	2.32	36.6	5.62	102	8.2	18.9		
120	3	1.0	2.3									134	21.3	2.66	12.3	2.35	26	4.9	11.3	135	22.1	2.69	12.9	2.41	27	10.6	24.5	
		3.6	8.3									127	22.3	2.69	13.1	2.43	26	4.9	11.3	128	23.1	2.71	13.8	2.49	27	10.6	24.5	
		7.9	18.3									125	22.7	2.72	13.4	2.45	26	4.9	11.3	125	23.5	2.74	14.1	2.51	27	10.6	24.5	
	50	1.0	2.3																									
		3.6	8.3	129	27.3	2.78	17.8	2.88	38	1.2	2.6	129	27.7	2.80	18.1	2.89	44	4.6	10.6	130	28.6	2.83	19.0	2.96	46	10.0	23.1	
		7.9	18.3	126	27.8	2.81	18.2	2.90	38	1.2	2.6	126	28.1	2.83	18.5	2.91	44	4.6	10.6	126	29.1	2.86	19.3	2.98	46	10.0	23.1	
	70	1.0	2.3																									
		3.6	8.3	131	32.9	2.88	23.1	3.35	55	1.1	2.4	131	33.3	2.91	23.4	3.36	62	4.3	9.9	131	34.5	2.94	24.5	3.44	65	9.4	21.7	
		7.9	18.3	127	33.5	2.91	23.5	3.37	54	1.1	2.4	128	33.9	2.94	23.9	3.38	62	4.3	9.9	128	35.1	2.97	24.9	3.46	64	9.4		

Technische Daten

Luft	Vorlauf 35°C		Vorlauf 45°C		Vorlauf 55°C	
	Heizleistung	El. Aufnahme	Heizleistung	El. Aufnahme	Heizleistung	El. Aufnahme
-15	3.14	1.42	3.12	1.67	3.07	2.00
-7	4.34	1.56	4.25	1.77	3.94	2.16
2	5.90	1.55	5.56	1.81	5.23	2.26
7	6.78	1.53	6.44	1.84	6.07	2.26
15	8.11	1.56	7.78	1.87	7.35	2.30

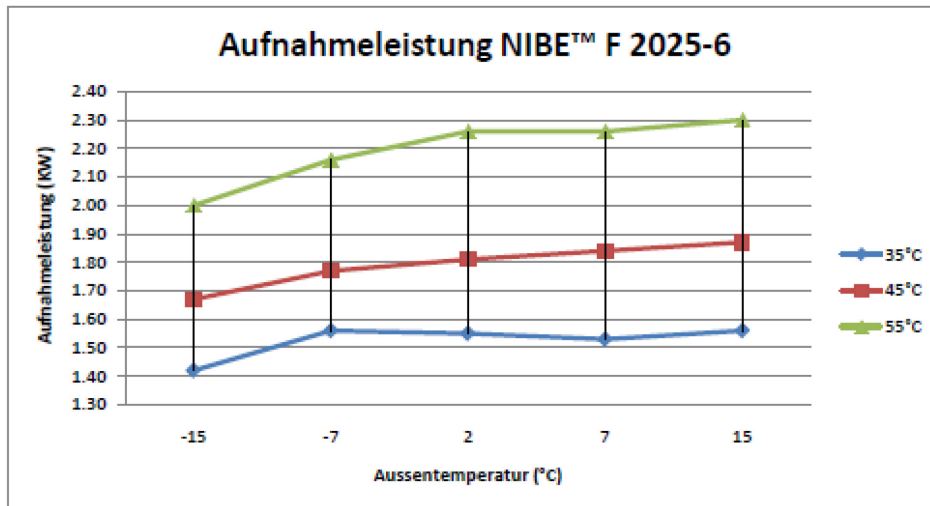
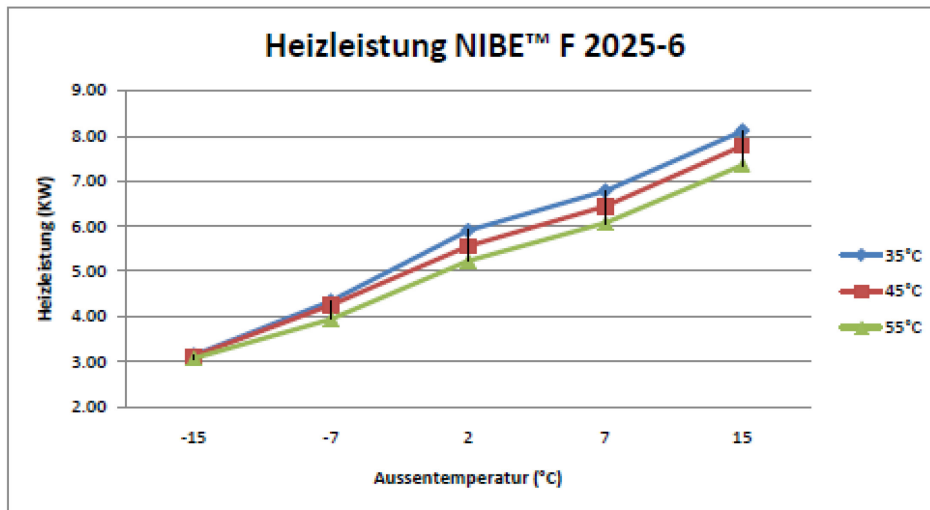
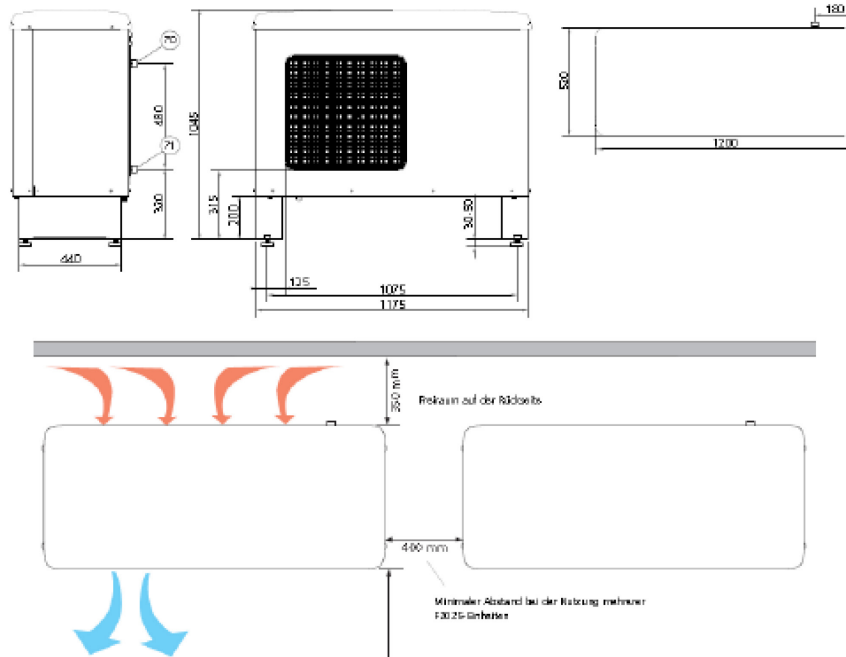


Figure B.6. Performance curves of NIBE F2025-6.

Kältekreis		Anschlüsse	
Kältemittel	R404A	Heizungs Vor- und Rücklauf	G 1" AG
Füllmenge	1.9 Kg		
Verdichter		Elektrische Daten	
Copeland	ZH15 K4E TFD	Anschlussspannung	3 x 400 V / 50 Hz
Verdichterart	Scroll	Absicherung	10 AT
Anschluss-Spannung	3 x 400V/50Hz	max. Betriebsstrom	5.0 A
max. Betriebsstrom	5.0 A	Anlaufstrom mit Softstarter	17 A
Blockierstrom	26 A	Heizkreis	
Öel - Inhalt	1.3 L	Nominelle Durchflussmenge	0.16 l/s
Ventilator 2-stufig			0.58 m ³ /h
Axialventilator	Rotomatika	Druckverlust am Kondensator	1.30 kPa
Spannung	1 x 230V/50Hz	Schalldruckpegel	
Aufnahmeleistung	70 W	Bei Abstand von 1 m	51 dB(A)
Luftvolumenstrom	1500 m ³ /h	Bei Abstand von 4 m	39 dB(A)
Abmessungen		Bei Abstand von 10 m	31 dB(A)
Anschluss 70	Vorlauf G1" AG	Breite x Tiefe x Höhe	1200 x 520 x 1045 mm
Anschluss 71	Rücklauf G1" AG	Gewicht	120 Kg



©NIBE Wärmetechnik AG 8247 Furlingen

Figure B.7. Technical specifications, NIBE F2025-6.

The New York Blower Company
 Fan-to-Size
 Fan Selection Data

Project:	
Location:	
Contact:	

Fan Design

Product:	Backward Inclined SWSI Square Fan	Arrangement:	4
Size/Model:	SQACF-13	Drive type:	Direct
Wheel Type:	Acoustafoil	AMCA Performance Class:	2
Wheel Material:	Aluminum		
Wheel Width:	100.0 %	Wheel Diameter:	100.0 %

Operating Conditions

Volume Flow Rate:	1 800 CFM	Fan Speed:	1750 rpm
Fan Static Pressure:	1.72 in wg	Fan Input Power:	0.727 bhp
Outlet Velocity:	1667 ft/min	VP/SP ratio:	0.1009
Altitude (above mean sea level):	0 ft	Operating Temperature:	70 Deg F
Operating Inlet Airstream Density:	0.0750 lb/ft3		
Static Efficiency:	66.88%	Mechanical Efficiency:	73.63%
Maximum Operating Temperature:	70 Deg F	Maximum Safe Operating Speed:	3600 rpm

Operating cost is 100.29 \$ for 2 080. hours with a 90% efficient motor when energy unit cost per kW-hr is 0.08

Sound Power Level Ratings Levels expressed in dB (power levels reference 10⁻¹² watts)

Center Frequency (Hz):	63	125	250	500	1000	2000	4000	8000	
Octave Bands:	1	2	3	4	5	6	7	8	Overall
Total Fan Power Levels*:	76.5	84.5	87.5	83.	78.	74.5	69.5	60.5	90.8
Inlet Power Levels**:	73.5	81.5	84.5	80.	75.	71.5	66.5	57.5	87.8
Outlet Power Levels**:	73.5	81.5	84.5	80.	75.	71.5	66.5	57.5	87.8

*As corrected for point of operation (location on fan curve)

**Unsilenced Inlet and Outlet power ratings are 3 dB lower than total fan power levels under the assumption that "half" of the sound power can be attributed to each opening. Silenced power ratings include this 3 dB reduction as well as the silencer attenuation.

Estimated Sound Pressure Levels Expressed in dB (pressure levels reference 2x10⁻⁷ microbar)

Directivity/Reflection Factor (Q) is 2, hemispherical radiation; Distance is 5 ft.; A-weighting is in use.

The estimated sound pressure level outside the fan due to an open inlet OR outlet is 70.3 dBA at 5.0 feet. The estimated sound pressure level outside the fan when BOTH inlet and outlet are ducted is 62.6 dBA at 5.0 feet (Housing Radiated Noise).

Your Representative:
 [Rep Info not available]

The New York Blower Company certifies that the Backward Inclined SWSI Square Fan is licensed to bear the AMCA Air Performance Seal. The ratings shown are based on tests and procedures performed in accordance with AMCA Publication 211 and comply with the requirements of the AMCA Certified Ratings program.

AMCA Licensed for Air Performance without Appurtenances (Accessories). Power (bhp) excludes drives.

Performance certified is for installation type: B - free inlet, ducted outlet.

Figure B.8. Details of BIPV/T fan used in the Alstonvale Net Zero House.

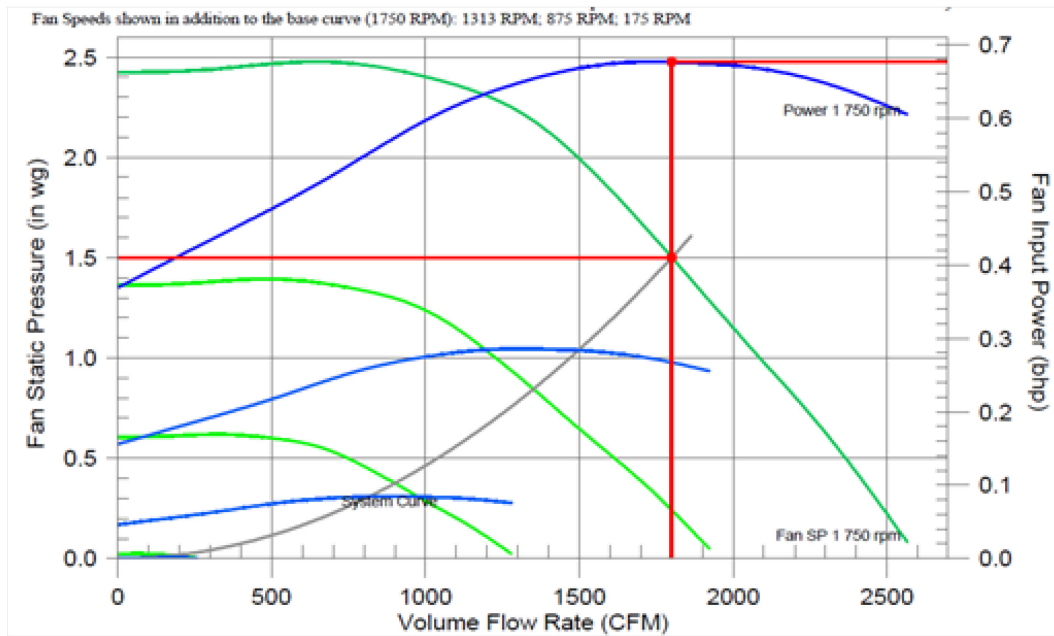


Figure B.9. Curve of BIPV/T fan used in the Alstonvale Net Zero House.

C. MATLAB M-FILE Model

```

%function TEMP = ALSTONVALE(slope,month)
% Alstonvale House model (introduce the slope of the PV roof
% and the month of the simulation (slope,month)
tic;
    month = 1;
    BACKUP = 0; %BACKUP ON = 1
    MET=load('C:\MATLAB7\PhD Research\Montréal_Data.txt');
    n = 8760;
    for i=1:n
        Month(i)=MET(i,1);
        Day(i)=MET(i,2);
        Julianday(i)=floor(i/24)+1;
        Hour_of_day(i)=MET(i,3);
        GlobRad(i)=MET(i,4);
        Direct(i)=MET(i,5);
        DifHor(i)=MET(i,6);
        Temp(i)=MET(i,7)/10;
        Windspeed(i)=MET(i,8)/10;
        hext(i) = 5.7 +3.8*Windspeed(i);
        East_V(i)=min(MET(i,9),1200);
        West_V(i)=min(MET(i,10),1200);
        North_V(i)=min(MET(i,11),1200);
        South_V(i)=min(MET(i,12),1200);
        % South_30(i)=min(MET(i,13),1200);
        % South_35(i)=min(MET(i,14),1200);
        % South_40(i)=min(MET(i,15),1200);
        South_45(i)=min(MET(i,16),1200);
        % South_50(i)=min(MET(i,17),1200);
        % South_55(i)=min(MET(i,18),1200);
        % South_60(i)=min(MET(i,19),1200);
        North_45(i)=min(MET(i,20),1200);
        %SOL-AIR TEMPERATURES
        TS_AIR_N(i) = Temp(i)+North_V(i)/hext(i);
        TS_AIR_S(i) = Temp(i)+South_V(i)/hext(i);
        TS_AIR_E(i) = Temp(i)+East_V(i)/hext(i);
        TS_AIR_W(i) = Temp(i)+West_V(i)/hext(i);
        %
        TS_AIR_S30(i) = Temp(i)+South_30(i)/hext(i);
        %
        TS_AIR_S35(i) = Temp(i)+South_35(i)/hext(i);
        %
        TS_AIR_S40(i) = Temp(i)+South_40(i)/hext(i);
        TS_AIR_S45(i) = Temp(i)+South_45(i)/hext(i);
        %
        TS_AIR_S50(i) = Temp(i)+South_50(i)/hext(i);
        %
        TS_AIR_S55(i) = Temp(i)+South_55(i)/hext(i);
        %
        TS_AIR_S60(i) = Temp(i)+South_60(i)/hext(i);
        TS_AIR_N45(i) = Temp(i)+North_45(i)/hext(i);
        Tground(i) = 5+5*sin((2*pi/8760)*(i-4128));
        x(i) = i;
    end
    %-----MONTREAL'S GEOGRAPHICAL DATA-----
    LAT = 45 + 30/60;
    LON = 73 + 40/60;
    LSM = 75;           % Local Standard Meridian
    %-----TIME STEP DEFINITION AND-----
    dt=150;           %Time step in seconds
    time_steps_ph = 3600/dt; %time steps per hour
    %-----INITIAL AND FINAL TIME-----
    % Initial and final hours of each month
    if (month==1)
        IT = 1;
    end

```

```

        FT = 744;
elseif(month==2)
        IT = 745;
        FT = 1416;
elseif(month==3)
        IT = 1417;
        FT = 2160;
elseif(month==4)
        IT = 2161;
        FT = 2880;
elseif(month==5)
        IT = 2881;
        FT = 3624;
elseif(month==6)
        IT = 3625;
        FT = 4344;
elseif(month==7)
        IT = 4345;
        FT = 5088;
elseif(month==8)
        IT = 5089;
        FT = 5832;
elseif(month==9)
        IT = 5833;
        FT = 6552;
elseif(month==10)
        IT = 6553;
        FT = 7296;
elseif(month==11)
        IT = 7297;
        FT = 8016;
elseif(month==12)
        IT = 8017;
        FT = 8760;
end
%-----SOLAR TIME-----
max_count = (FT-IT+1)*time_steps_ph;
%max_count = max_count - 2*time_steps_ph; %CORRECCION POR EL
PROBLEMA DE DICIEMBRE
tx=1:max_count;
for i=1:max_count
    Julian(i) = floor(i/(time_steps_ph*24))+IT/24;
    Equation_time(i) = ET(Julian(i)); %Minutes
    Time(i) = IT + (i-1)*dt/3600; %Time in hours with fractions
    AST(i) = (Equation_time(i)+4*(LSM-LON))/60 + Time(i);
end
%-----TIME PAST SOLAR NOON-----
for i=1:max_count;
    TPSN(i) = AST(i)-24*floor(AST(i)/24)-12;
end
%-----HOOR ANGLE-----
for i=1:max_count;
    HourAngle(i)=15*TPSN(i)*pi/180;
end
%-----DECLINATION ANGLE-----
for i=1:max_count;
    DEC(i)=23.45*pi/180*sin((360/365)*(284+Julian(i))*pi/180);
end
%-----ALTITUDE ANGLE-----
LAT = LAT*pi/180;
LON = LON*pi/180;
for i=1:max_count

```

```

alpha(i)=asin(cos(LAT)*cos(DEC(i))*cos(HourAngle(i))+sin(LAT)*sin(DEC(i)));
    if alpha(i)>= 0
        alpha(i)=alpha(i);
    else
        alpha(i)=0;
    end
end
%-----AZIMUTH ANGLE-----
for i=1:max_count;
    azim(i)=acos((sin(alpha(i))*sin(LAT)-
sin(DEC(i)))/(cos(alpha(i))*cos(LAT)))*HourAngle(i)/abs(HourAngle(i));
end
%-----
ngl = 3; %Number of glazings
kL = 0.11;%Extinction coefficient times thickness
for i=1:max_count
    %-----SOUTH VERTICAL INCIDENCE ANGLE-----
    SVIA(i) = inc_angle(0,alpha(i),azim(i),pi/2);
    %-----EAST VERTICAL INCIDENCE ANGLE-----
    EVIA(i) = inc_angle(-pi/2,alpha(i),azim(i),pi/2);
    %-----WEST VERTICAL INCIDENCE ANGLE-----
    WVIA(i) = inc_angle(pi/2,alpha(i),azim(i),pi/2);
end
%=====
%-----ALSTONVALE HOUSE-----
%=====
%-----SOUTH FACADE-----
hs = 6.30;
ws = 18.89;
Atotal_south=hs*ws;
Asouth_windows=50;
Asouth_walls=Atotal_south-Asouth_windows;
fr_south_windows = Asouth_windows/Atotal_south;
%-----EAST FACADE-----
%East Wall 1
he1 = 6.30;
we1 = 6.782;
Ae1 = he1*we1;
%East Wall 2
he2 = 3.86;
we2 = 3.17;
Ae2 = he2*we2;
%East Area
Aeast = Ae1 + Ae2;
%East Windows
WEW = 1.829;
HEW = 3.2;
WB23 = 0.9;
HB23 = 2.135;
Aeast_windows = WEW*HEW + 2*WB23*HB23;
%East Doors
WED = 0.864;
HED = 2.438;
Aeast_door = WED*HED;
Aeast_walls=Aeast-(Aeast_windows+Aeast_door);
%-----NORTH FACADE-----
%North wall 1
WNW1 = 1.59;
HNW1 = 3.86;
ANW1 = WNW1*HNW1;
%North wall 2

```

```

HNW2 = 3.86;
WNW2 = 4.26;
ANW2 = HNW2*WNW2;
%North wall 4
HNW4 = 2.79;
WNW4 = 5;
ANW4 = HNW4*WNW4;
Anorth_walls = ANW1+ANW2+ANW4;
%-----WEST FACADE-----
WWW2=6.782;
HWW2=2.791;
WWind=3.353;
HWind=0.747;
Awest_window=WWind*HWind;
Awest_wall = WWW2-Awest_window;
%-----MASONRY WALL-----
Amas = 45;           %Approximately
%-----CEILING/ROOF-----
%Acath = 64.03;
%Aflat = 40.36;
%Aceil = 2*Acath + Aflat;
Rooflength=6.5;
Roofwidth=18.5;
Aceil=0.9*2*Rooflength*Roofwidth;
%-----GARAGE-----
Pg = 7.112 + 3.1496;      %Exposed perimeter of garage
Pw = (156 + 280 + 156)*0.0254; %Perimeter in contact with house
hg = 3.66;              %Height of the wall
Agh = Pw*hg;           %Area in contact with house
Aexp = Pg*hg;          %Exposed area
%-----BASEMENT AND FLOOR-----
Ab_walls = (24.81)*(1.84); %Basement walls
Ab_floor = 28.3;         %Area of floor
Ab_house = Ab_floor;     %In contact with the house
Ab_ground = Ab_walls + Ab_floor; %In contact with the ground
Afloor = 100;           %Area of floor
Aupper = 90;            %Area of upper floor
%-----MATERIAL PROPERTIES-----
Rprime_walls=5.636;      %Walls
Rprime_exp=Rprime_walls; %Exposed garage wall
Rprime_floor=4.579;     %Floor insulation
Rprime_ceiling = 11.975; %Ceiling
Rprime_windows=1.233;   %Windows
Rprime_roof=Rprime_ceiling; %Roof
Rprime_hg=8.806;        %Masonry wall to garage
u_doors=1.533;          %Conductance of doors
kbrick=1;               %Conductivity of bricks
%-----THERMAL CAPACITANCES-----
%Inner layer (plywood)
Lw = 0.027;
cw = 1210;
rho_w = 540;
k_ply = 0.12;
Cw_pA = Lw*cw*rho_w;
%Slab on grade
Lf = 0.1524;
cf = 800;
rho_1 = 2200;
k_conc = 1.09;
Cf_pA = Lf*cf*rho_1;
%Floor on top of basement
Ltb = 0.0381;

```



```

R9_o = (Lw/2)/(k_ply*Anorth_walls) + Rprime_walls/Anorth_walls +
1/(ho*Anorth_walls);
R(9,10) = (Lw/2)/(k_ply*Anorth_walls);
CAP(9) = Cw_pA*Anorth_walls;
%-----8. EAST WALL MODELS-----
R(13,14) = (Lw/2)/(k_ply*Aeast_walls);
R13_o = (Lw/2)/(k_ply*Aeast_walls) + Rprime_walls/Aeast_walls +
1/(ho*Aeast_walls);
CAP(13) = Cw_pA*Aeast_walls;
%-----9. WEST WALL MODELS-----
R(11,12) = (Lw/2)/(k_ply*Awest_wall);
R11_o = (Lw/2)/(k_ply*Awest_wall) + Rprime_walls/Awest_wall +
1/(ho*Awest_wall);
CAP(11) = Cw_pA*Awest_wall;
%-----10. GARAGE AND MASONRY WALL MODELS-----
R(15,16) = 0.5*Lbv/(kbrick*Agh);
R15_o = 0.5*Lbv/(kbrick*Agh) + Rprime_hg/Agh + Rprime_exp/Aexp;
CAP(15) = Cmw_pA*Agh;
%-----11. WINDOWS AND DOORS-----
Rd = 1/u_doors*Aeast_door;
Awindows = Asouth_windows + Aeast_windows + Awest_window;
Rw = Rprime_windows/Awindows;
%-----12. INFILTRATION-----
Vol = 590 + 320;
ACH = 0.30;
Uinf = ACH*Vol*air_density*cp_air/3600;
%-----13. RESISTANCE DUE TO WINDOWS, DOOR AND INFILTRATION-----
Rl_o = (Uinf + 1/Rd + 1/Rw)^(-1);
Rprime_shutter = 1; %we had 1.32 before
Rw_sh = (Rprime_windows + Rprime_shutter)/Awindows;
Rl_o_sh = (Uinf + 1/Rd + 1/Rw_sh)^(-1);
%-----14. THERMAL CAPACITANCE OF THE INTERIOR AIR-----
CAP(1) = air_density*cp_air*Vol*30; %It is being multiplied by a factor
%-----15. RESISTANCES DUE TO THE INTERNAL FILM COEFFICIENT-----
R(1,10) = 1/(hwalls*Anorth_walls);
R(1,8) = 1/(hwalls*Asouth_walls);
R(1,6) = 1/(hceil*Aceil);
R(1,14) = 1/(hwalls*Aeast_walls);
R(1,12) = 1/(hwalls*Awest_wall);
R(1,2) = 1/(hfloor*Afloor);
R(1,16) = 1/(hwalls*Amas);
%-----16. RADIATIVE RESISTANCES-----
%16.1 APPROXIMATE VIEW FACTORS, BASED ON EDUCATED GUESSES
F = zeros(16,16);
%From the masonry wall to the other surfaces
F(16,8) = 0.7; %Masonry wall to south wall
F16_o = 0.1; %Masonry wall to windows
F(16,6) = 0.06;
F(16,2) = 0.06;
F(16,14) = 0.04;
F(16,12) = 0.04;
F(16,10) = 0;
%From the floor to the other surfaces
F(2,6) = 0.4;
F(2,10) = 0.25;
F(2,8) = 0.25;
F(2,12) = 0.035;
F(2,14) = 0.035;
F(2,16) = 0.03;
sigma = 5.67E-8;
Tm = (273.15 + 25); % Reasonable assumption for mean temperature
emissivity = 0.8;

```

```

%16.2 RADIATIVE HEAT TRANSFER COEFFICIENTS
hr = zeros(16,16);
%Between the masonry wall and other surfaces
hr(16,8) = (4*sigma*Tm^3)/(2/emissivity -1 +F(16,8));
hr(16,6) = (4*sigma*Tm^3)/(2/emissivity -1 +F(16,6));
hr(16,2) = (4*sigma*Tm^3)/(2/emissivity -1 +F(16,2));
hr(16,14) = (4*sigma*Tm^3)/(2/emissivity -1 +F(16,14));
hr(16,12) = (4*sigma*Tm^3)/(2/emissivity -1 +F(16,12));
hr16_o = (4*sigma*Tm^3)/(2/emissivity -1 +F16_o); %Masonry wall to the
exterior
%Between the floor and other surfaces
hr(2,6) = (4*sigma*Tm^3)/(2/emissivity -1 +F(2,6));
hr(2,10) = (4*sigma*Tm^3)/(2/emissivity -1 +F(2,10));
hr(2,8) = (4*sigma*Tm^3)/(2/emissivity -1 +F(2,8));
hr(2,14) = (4*sigma*Tm^3)/(2/emissivity -1 +F(2,14));
hr(2,12) = (4*sigma*Tm^3)/(2/emissivity -1 +F(2,12));
hr(2,16) = (4*sigma*Tm^3)/(2/emissivity -1 +F(2,16));
%16.3 RADIATIVE RESISTANCES
%Between the masonry wall and other surfaces
R(16,8) = 1/(Amas*hr(16,8));
R(16,6) = 1/(Amas*hr(16,6));
R(16,2) = 1/(Amas*hr(16,2));
R(16,14) = 1/(Amas*hr(16,14));
R(16,12) = 1/(Amas*hr(16,12));
R16_o = 2/(hwalls*Amas)+Rprime_windows/(Amas)+1/(hr16_o*Amas);
%Between the floor and other surfaces
R(2,6) = 1/(Afloor*hr(2,6));
R(2,10) = 1/(Afloor*hr(2,10));
R(2,8) = 1/(Afloor*hr(2,8));
R(2,14) = 1/(Afloor*hr(2,14));
R(2,12) = 1/(Afloor*hr(2,12));
R(2,16) = 1/(Afloor*hr(2,16));
%TANK - LARGE RESERVOIR - WITH 4 NODES
Vol_tank = 4.20; %m3 %TAMANO DEL TANQUE
utank = 0.2835; %W/m2*K
Atank = 13.4; %m2 %TAMANO DEL TANQUE
UTANK = utank*Atank; %W/K
density_water = 1000;
cp_water = 4186;
CTANK = Vol_tank*density_water*cp_water;
CNODE = CTANK/4;
UTANKNODE = UTANK/4; %heat loss per node
TTANK1(1)=45;
TTANK2(1)=40;
TTANK3(1)=35;
TTANK4(1)=30;
TAhp(1)=50;
TAtank(1)=30;
TBrf(1)=42;
TBtank(1)=45;
peA(1)=1;
peB(1)=2;
mdota_orig = (1.14E-3)*density_water;
mdotb_orig = (0.32E-3)*density_water;
Flow12(1)=mdota_orig-mdotb_orig;
Flow23(1)=mdota_orig;
Flow34(1)=mdota_orig;
%RESISTANCE MATRIX
R = R + transpose(R);
%TRANSMITTANCES
tauw = 0.6;
%-----INITIAL POWER VALUES-----

```

```

QHP(1)=0;
ELEC_POW_RF(1)=0;
ELEC_POW(1)=0;
FAN_OR_PUMP(1)=0;
VENT = 100;
COP_EF(1)= 0;
COP(1) = 0;
Power_gen(1) = 0;
%-----ENERGY-----
HEAT_ENERGY = 0;           %HEATING LOAD TIMES TIME
ELEC_ENERGY_RF = 0;       %RADIANT FLOOR HEATING SYSTEM
HP_EL_ENERGY_SPENT = 0;   %HEAT PUMP ENERGY CONSUMPTION
FAN_OR_PUMP_ENERGY = 0;   %FAN OR PUMP ENERGY SPENT (HX OR HP)
VENT_ENERGY = 0;         %VENTILATION
HEAT_HX = 0;             %HEAT FROM HEAT EXCHANGER
HEAT_BIPVT_ONEHP = 0;    %HEAT FROM BIPVT EXTRACTED WITH ONE HEAT PUMP
HEAT_BIPVT_TWOHP = 0;    %HEAT FROM BIPVT EXTRACTED WITH TWO HEAT PUMPS
HEAT_GROUND = 0;        %HEAT FROM THE GROUND
ELEC_ENERGY_GENERATED = 0; %ELECTRIC ENERGY GENERATED
%INITIAL VALUES-----
qauxTOTAL(1)=0;
qaux1(1)=0;
qaux2(1)=0;
qaux3(1)=0;
for k=1:30
    T(k,1)=21;
end
Toperative(1) = 21;
TexitBIPVT(1) = 0;
HORAS_OP_HX = 0;
HORAS_OP_2HP = 0;
HORAS_OP_1HP = 0;
HORAS_BACKUP = 0;
%-----
TOLERANCE = 2.5;
KP=2500;
QMAX = 13e3;
Tsetpoint = 21;
Tlower = Tsetpoint-TOLERANCE;
To(1)=Temp(IT);
SOLAR_RAD(1)= South_45(IT);
SOL_CURRDAY = 0;
SOL_DIA(1)=0;
Temp_at6am(1)=21;
hora6(1)= floor(24*3600/dt);
transcorr(1) = 1;
SOL_FOLLDAY = 0;           %SOLAR RADIATION NEXT DAY
SOL_CURRDAY = 0;          %SOLAR RADITION CURRENT DAY
SOL_DIASIG(1) = 0;
%-----EXTERIOR TEMPERATURE AND RADIATION (ADAPTED TO THE TIME SCALE)-----
for i=1:max_count-1
    j(i)= floor(Time(i));
    To(i+1)=Temp(j(i));
    SOLAR_RAD(i+1) = South_45(j(i));
end
%*****BEGINNING OF SIMULATION (BIG BIG MATRIX)*****
for i=1:max_count-1
    if (QHP(i)==0)
        mdota = 0.001;
    else
        mdota = mdota_orig;
    end
end

```

```

end

if (qauxTOTAL(i)==0)
    mdotb = 0.001;
else
    mdotb = mdotb_orig;
end
%%%%%%%%%%%%%%%%%%%%%%%%%%%%%%%%%%%%%%%%%%%%%%%%%%%%%%%%%%%%%%%%%%%%%%%%
HEAT_ENERGY = HEAT_ENERGY + qauxTOTAL(i)*dt;
HP_EL_ENERGY_SPENT = HP_EL_ENERGY_SPENT + ELEC_POW(i)*dt;
FAN_OR_PUMP_ENERGY = FAN_OR_PUMP_ENERGY + FAN_OR_PUMP(i)*dt;
VENT_ENERGY = VENT_ENERGY + VENT*dt;
ELEC_ENERGY_RF = ELEC_ENERGY_RF + ELEC_POW_RF(i)*dt;
ELEC_ENERGY_GENERATED = ELEC_ENERGY_GENERATED + Power_gen(i)*dt;
%%%%%%%%%%%%%%%%%%%%%%%%%%%%%%%%%%%%%%%%%%%%%%%%%%%%%%%%%%%%%%%%%%%%%%%%
j(i)= floor(Time(i)); %Time in discrete hours
%CALCULATION OF TEMPERATURES%
%IF IT IS GETTING UNBEARABLY HOT%%%%%%%%
if (Toperative(i) >= 27)
    ACH = 1.00;
    Uinf = ACH*Vol*air_density*cp_air/3600;
    R1_o = (Uinf + 1/Rd + 1/Rw)^(-1);
else
    ACH = 0.30;
    Uinf = ACH*Vol*air_density*cp_air/3600;
    R1_o = (Uinf + 1/Rd + 1/Rw)^(-1);
end
%SHUTTERS OPEN OR CLOSED
if(alpha(i)>0)
    R1_OUT = R1_o;
else
    R1_OUT = R1_o_sh;
end
%%%%%%%%%%%%%%%%%%%%%%%%%%%%%%%%%%%%%%%%%%%%%%%%%%%%%%%%%%%%%%%%%%%%%%%%
T(1,i+1)= T(1,i) + (dt/CAP(1))*((T(2,i)-T(1,i))/R(1,2) +...
    + (T(6,i)-T(1,i))/R(1,6) + (T(8,i)-T(1,i))/R(1,8) +...
    (T(10,i)-T(1,i))/R(1,10) + (T(12,i)-T(1,i))/R(1,12) +...
    (T(14,i)-T(1,i))/R(1,14) + (T(16,i) -T(1,i))/R(1,16) +...
    + (Temp(j(i))-T(1,i))/R1_OUT +...
    + (T(22,i)-T(1,i))/R(1,22) + qaux3(i)); %Node1 AIR
NUM2= T(1,i)/R(1,2)+T(3,i)/R(2,3)+T(6,i)/R(2,6)+...
    T(8,i)/R(2,8)+T(10,i)/R(2,10)+T(12,i)/R(2,12)+...
    T(14,i)/R(2,14)+T(16,i)/R(2,16)+ T(17,i)/R(2,17)+...

transcorr(i)*TRANS(SVIA(i),ngl,kL)*interp1(x,South_V,Time(i))*Asouth_windows*0.
3 +...

transcorr(i)*TRANS(WVIA(i),ngl,kL)*interp1(x,West_V,Time(i))*Awest_window*0.45
+...

transcorr(i)*TRANS(EVIA(i),ngl,kL)*interp1(x,East_V,Time(i))*Aeast_windows*0.45
;
DEN2 = 1/R(1,2)+1/R(2,3)+1/R(2,6)+...
    1/R(2,8)+1/R(2,10)+1/R(2,12)+...
    1/R(2,14)+1/R(2,16)+ 1/R(2,17);
T(2,i+1) = NUM2/DEN2; %Node2 FLOOR
T(3,i+1) = T(3,i) + (dt/CAP(3))*((T(2,i)-T(3,i))/R(2,3) +...
    (T(4,i)-T(3,i))/R(3,4) + qaux1(i) ); %Node3
T(4,i+1) = T(4,i) + (dt/CAP(4))*((T(3,i)-T(4,i))/R(3,4) +...
    (Tground(j(i))-T(4,i))/R4_ground ); %Node4
T(5,i+1) = T(5,i) + (dt/CAP(5))*((TS_AIR_S45(j(i))+10-T(5,i))/R5_south
+...

```

```

        (TS_AIR_N45(j(i))-T(5,i))/R5_north +...
        (T(6,i)-T(5,i))/R(5,6)); %Node5 CEILING
NUM6 = T(1,i)/R(1,6)+ T(2,i)/R(2,6) + T(5,i)/R(5,6) + T(16,i)/R(6,16);
DEN6 = 1/R(1,6)+1/R(2,6)+1/R(5,6)+1/R(6,16);
T(6,i+1) = NUM6/DEN6; %Node6
T(7,i+1) = T(7,i) + (dt/CAP(7))*((T(8,i)-T(7,i))/R(7,8)+...
        (TS_AIR_S(j(i))-T(7,i))/R7_o); %Node7 SOUTH WALL
NUM8 = T(2,i)/R(2,8)+T(1,i)/R(1,8)+T(16,i)/R(8,16)+T(7,i)/R(7,8);
DEN8 = 1/R(2,8)+1/R(1,8)+1/R(8,16)+1/R(7,8);
T(8,i+1) = NUM8/DEN8; %Node8
T(9,i+1) = T(9,i) + (dt/CAP(9))*((T(10,i)-T(9,i))/R(9,10)+...
        (TS_AIR_N(j(i))-T(9,i))/R9_o); %Node9 NORTH WALL
NUM10 = T(2,i)/R(2,10)+T(1,i)/R(1,10)+T(9,i)/R(9,10);
DEN10 = 1/R(2,10)+1/R(1,10)+1/R(9,10);
T(10,i+1)=NUM10/DEN10; %Node10
T(11,i+1) = T(11,i) + (dt/CAP(11))*((T(12,i)-T(11,i))/R(11,12)+...
        (TS_AIR_W(j(i))-T(11,i))/R11_o); %Node11 WEST WALL
NUM12 = T(2,i)/R(2,12)+T(1,i)/R(1,12)+T(16,i)/R(12,16)+T(11,i)/R(11,12);
DEN12 = 1/R(2,12)+1/R(1,12)+1/R(12,16)+1/R(11,12);
T(12,i+1) = NUM12/DEN12; %Node12
T(13,i+1) = T(13,i) + (dt/CAP(13))*((T(14,i)-T(13,i))/R(13,14)+...
        (TS_AIR_E(j(i))-T(13,i))/R13_o); %Node13 EAST WALL
NUM14 = T(2,i)/R(2,14)+T(1,i)/R(1,14)+T(16,i)/R(14,16)+T(13,i)/R(13,14);
DEN14 = 1/R(2,14)+1/R(1,14)+1/R(14,16)+1/R(13,14);
T(14,i+1) = NUM14/DEN14; %Node14
T(15,i+1) = T(15,i) + (dt/CAP(15))*((T(16,i)-T(15,i))/R(15,16)+...
        (TS_AIR_N(j(i))-T(15,i))/R15_o); %Node15 GARAGE
NUM16 = T(2,i)/R(2,16)+T(1,i)/R(1,16)+T(15,i)/R(15,16)+...
        T(6,i)/R(6,16)+T(8,i)/R(8,16)+T(12,i)/R(12,16)+...
        T(14,i)/R(14,16)+Temp(j(i))/R16_o+...

transcorr(i)*TRANS(SVIA(i),ngl,kL)*interp1(x, South_V,Time(i))*Asouth_windows*0.
5 +...

transcorr(i)*TRANS(WVIA(i),ngl,kL)*interp1(x, West_V,Time(i))*Awest_window*0.30
+...

transcorr(i)*TRANS(EVIA(i),ngl,kL)*interp1(x, East_V,Time(i))*Aeast_windows*0.30
;
DEN16 = 1/R(2,16)+1/R(1,16)+1/R(15,16)+...
        1/R(6,16)+1/R(8,16)+1/R(12,16)+...
        1/R(14,16)+1/R16_o;
T(16,i+1) = NUM16/DEN16; %Node 16 MASONRY WALL SURF
T(17,i+1) = T(17,i) + (dt/CAP(17))*((T(2,i)-T(17,i))/R(2,17) +...
        (T(18,i)-T(17,i))/R(17,18) ); %Node 17 BASEMENT
T(18,i+1) = T(18,i) + (dt/CAP(18))*((T(17,i)-T(18,i))/R(17,18) +...
        (T(19,i) - T(18,i))/R(18,19) ); %Node 18
T(19,i+1) = T(19,i) + (dt/CAP(19))*((T(18,i)-T(19,i))/R(18,19) +...
        (T(20,i)-T(19,i))/R(19,20) +
        (TTANK1(i)-
T(19,i))*UTANKNODE+...
        (TTANK2(i)-T(19,i))*UTANKNODE +
        (TTANK3(i)-
T(19,i))*UTANKNODE +...
        (TTANK4(i)-T(19,i))*UTANKNODE); %Node 19 BASEMENT AIR
T(20,i+1) = T(20,i) + (dt/CAP(20))*((T(19,i)-T(20,i))/R(19,20) +...
        (T(21,i)-T(20,i))/R(20,21) ); %Node 20
T(21,i+1) = T(21,i) + (dt/CAP(21))*((T(20,i)-T(21,i))/R(20,21) +...
        (Tground(j(i))-T(21,i))/R21_g + qaux2(i) ); %Node 21
        %BASEMENT CONNECTED TO THE GROUND
T(22,i+1) = T(22,i) + (dt/CAP(22))*((T(1,i)-T(22,i))/R(1,22) +...

transcorr(i)*TRANS(SVIA(i),ngl,kL)*interp1(x, South_V,Time(i))*Asouth_windows*0.
2 +...

```

```

transcorr(i)*TRANS(WVIA(i),ngl,kL)*interp1(x,West_V,Time(i))*Awest_window*0.25
+...

transcorr(i)*TRANS(WVIA(i),ngl,kL)*interp1(x,East_V,Time(i))*Aeast_windows*0.25
); %Node 22
%*****END OF NODES*****
%-----BIPVT-----
TexitBIPVT(i+1) =
BIPVT(South_45(j(i)),1600,Temp(j(i)),Temp(j(i)),T(1,i)-5,Windspeed(j(i)));
Power_gen(i+1) =
BIPVTgen(South_45(j(i)),1600,Temp(j(i)),Temp(j(i)),T(1,i)-5,Windspeed(j(i)));
%-----TANK SETPOINT-----
if (SOL_FOLLDAY > 10E6)
    if(SOL_CURRDAY > 10E6)
        ADJ = 6;
    elseif((SOL_CURRDAY > 6.5E6) & (SOL_CURRDAY <= 10E6))
        ADJ = 4;
    elseif((SOL_CURRDAY > 3.5E6) & (SOL_CURRDAY <= 6.5E6))
        ADJ = 2;
    elseif(SOL_CURRDAY <= 3.5E6)
        ADJ = 0;
    end
    Tank_setpoint = 34 + ADJ;

elseif ((SOL_FOLLDAY > 6.5E6) & (SOL_FOLLDAY <= 10E6))

    if(SOL_CURRDAY > 10E6)
        ADJ = 4;
    elseif((SOL_CURRDAY > 6.5E6) & (SOL_CURRDAY <= 10E6))
        ADJ = 2.5;
    elseif((SOL_CURRDAY > 3.5E6) & (SOL_CURRDAY <= 6.5E6))
        ADJ = 1.5;
    elseif(SOL_CURRDAY <= 3.5E6)
        ADJ = 0;
    end
    Tank_setpoint = 36 + ADJ;

elseif ((SOL_FOLLDAY > 3.5E6) & (SOL_FOLLDAY <= 6.5E6))
    if(SOL_CURRDAY > 6.5E6)
        ADJ = 2;
    elseif((SOL_CURRDAY > 3.5E6) & (SOL_CURRDAY <= 6.5E6))
        ADJ = 1;
    elseif(SOL_CURRDAY <= 3.5E6)
        ADJ = 0;
    end
    Tank_setpoint = 38 + ADJ;

elseif (SOL_FOLLDAY <= 3.5E6)
    Tank_setpoint = 40;
end

%*****
%-----HEAT EXCHANGER AND HEAT PUMP-----
%*****

if (TTANK4(i) <= Tank_setpoint)
%LEVEL 1

```

```

if ((TexitBIPVT(i+1)-TTANK4(i))>=3)
%LEVEL 2
    QHP(i+1)=0.8*0.569*1600*(TexitBIPVT(i+1)-TTANK4(i));
    ELEC_POW(i+1) = 0;
    FAN_OR_PUMP(i+1) = 500;
    COP_EF(i+1) = QHP(i+1)/(ELEC_POW(i+1)+FAN_OR_PUMP(i+1));
    HORAS_OP_HX = HORAS_OP_HX + dt/3600;
    COP(i+1)=0;
    HEAT_HX = HEAT_HX + dt*QHP(i+1);
elseif (TexitBIPVT(i+1)>=10 & TexitBIPVT(i+1) < 48.9)
%-----
if TTANK4(i)>15.6
%LEVEL 3
    RES=TWO_3TON_HP(TexitBIPVT(i+1),TTANK4(i),1600,9,9);
    QHP(i+1) = RES(5)*1000;
    ELEC_POW(i+1) = RES(4)*1000;
    FAN_OR_PUMP(i+1) = 500;
    COP_EF(i+1) = QHP(i+1)/(ELEC_POW(i+1)+FAN_OR_PUMP(i+1));
    HORAS_OP_2HP = HORAS_OP_2HP + dt/3600;
    HEAT_BIPVT_TWOHP = HEAT_BIPVT_TWOHP + dt*QHP(i+1);
    COP(i+1)=QHP(i+1)/(ELEC_POW(i+1));
else
    RES=TWO_3TON_HP(TexitBIPVT(i+1),15.6,1600,9,9);
    QHP(i+1) = RES(5)*1000;
    ELEC_POW(i+1) = RES(4)*1000;
    FAN_OR_PUMP(i+1) = 500;
    COP_EF(i+1) = QHP(i+1)/(ELEC_POW(i+1)+FAN_OR_PUMP(i+1));
    HORAS_OP_2HP = HORAS_OP_2HP + dt/3600;
    HEAT_BIPVT_TWOHP = HEAT_BIPVT_TWOHP + dt*QHP(i+1);
    COP(i+1)=QHP(i+1)/(ELEC_POW(i+1));
end
%CLOSE LEVEL 3
%-----
elseif (TexitBIPVT(i+1)>=3.5 & TexitBIPVT(i+1) < 10)
%-----
if TTANK4(i) > 15.6
%LEVEL 3
    RES=ONE_3TON_HP(TexitBIPVT(i+1),TTANK4(i),1600,9,9);
    QHP(i+1) = RES(5)*1000;
    ELEC_POW(i+1) = RES(4)*1000;
    FAN_OR_PUMP(i+1) = 500;
    COP_EF(i+1) = QHP(i+1)/(ELEC_POW(i+1)+FAN_OR_PUMP(i+1));
    HORAS_OP_1HP = HORAS_OP_1HP + dt/3600;
    HEAT_BIPVT_ONEHP = HEAT_BIPVT_ONEHP + dt*QHP(i+1);
    COP(i+1)=QHP(i+1)/(ELEC_POW(i+1));
else
    RES=ONE_3TON_HP(TexitBIPVT(i+1),15.6,1600,9,9);
    QHP(i+1) = RES(5)*1000;
    ELEC_POW(i+1) = RES(4)*1000;
    FAN_OR_PUMP(i+1) = 500;
    COP_EF(i+1) = QHP(i+1)/(ELEC_POW(i+1)+FAN_OR_PUMP(i+1));
    HORAS_OP_1HP = HORAS_OP_1HP + dt/3600;
    HEAT_BIPVT_ONEHP = HEAT_BIPVT_ONEHP + dt*QHP(i+1);
    COP(i+1)=QHP(i+1)/(ELEC_POW(i+1));
end
%CLOSE LEVEL 3
%-----
elseif (TexitBIPVT(i+1)<3.5)
if ((TTANK4(i) < 30) & (BACKUP ==1))
%LEVEL 3
    if TTANK4(i) > 15.6
%LEVEL 4

```

```

RES=GROUND_3TON_HP(Tground(j(i))-2,TTANK4(i),9,9);
QHP(i+1) = RES(5)*1000;
ELEC_POW(i+1) = RES(4)*1000;
FAN_OR_PUMP(i+1) = 150;
COP_EF(i+1) = QHP(i+1)/(ELEC_POW(i+1)+FAN_OR_PUMP(i+1));
HORAS_BACKUP = HORAS_BACKUP + (dt/3600);
COP(i+1)=QHP(i+1)/(ELEC_POW(i+1));
HEAT_GROUND = HEAT_GROUND + QHP(i+1)*dt;
else
RES=GROUND_3TON_HP(Tground(j(i))-2,TTANK4(i),9,9);
QHP(i+1) = RES(5)*1000;
ELEC_POW(i+1) = RES(4)*1000;
FAN_OR_PUMP(i+1) = 150;
COP_EF(i+1) = QHP(i+1)/(ELEC_POW(i+1)+FAN_OR_PUMP(i+1));
HORAS_BACKUP = HORAS_BACKUP + dt/3600;
COP(i+1)=QHP(i+1)/(ELEC_POW(i+1));
HEAT_GROUND = HEAT_GROUND + QHP(i+1)*dt;
end
%CLOSE LEVEL 4
else
QHP(i+1)=0;
ELEC_POW(i+1) = 0;
FAN_OR_PUMP(i+1)=0;
COP_EF(i+1)=0;
COP(i+1)=0;
end
%CLOSE LEVEL 3
end
%CLOSE LEVEL 2
else
QHP(i+1)=0;
ELEC_POW(i+1) = 0;
FAN_OR_PUMP(i+1)=0;
COP_EF(i+1)=0;
COP(i+1)=0;
end
%CLOSE LEVEL 1
%-----
%-----TANK-----
%-----
TAhp(i) = TTANK4(i)+QHP(i)/(mdota*cp_water); %RETURNING
WATER FROM HP
TBrf(i) = TTANK1(i)-qauxTOTAL(i)/(mdotb*cp_water); %RETURNING
WATER FROM RADIANT FLOOR
%---point of entry loop A-----
-
if (TAhp(i) >= TTANK1(i))
peA(i) = 1;
elseif ((TTANK2(i) <= TAhp(i)) & (TAhp(i) < TTANK1(i)))
peA(i) = 2;
elseif ((TTANK3(i) <= TAhp(i)) & (TAhp(i) < TTANK2(i)))
peA(i) = 3;
elseif (TAhp(i)<TTANK3(i))
peA(i) = 4;
end
%---point of entry loop B-----
if (TBrf(i) >= TTANK1(i))
peB(i) = 1;
elseif ((TTANK2(i) <= TBrf(i)) & (TBrf(i) < TTANK1(i)))
peB(i) = 2;
elseif ((TTANK3(i) <= TBrf(i)) & (TBrf(i) < TTANK2(i)))
peB(i) = 3;

```

```

elseif (TBrf(i)<TTANK3(i))
    peB(i) = 4;
end
%-----FLOW 1 TO 2-----
if ((peA(i) == 1) & (peB(i) ~= 1))
    Flow12(i) = mdota-mdotb; %OK
elseif ((peA(i) == 1) & (peB(i) == 1))
    Flow12(i) = mdota; %OK
elseif ((peA(i) ~= 1) & (peB(i) == 1))
    Flow12(i) = 0; %OK
elseif ((peA(i) ~= 1) & (peB(i) ~= 1))
    Flow12(i) = -mdotb;
%OK
end
%-----FLOW 3 TO 4-----
if ((peA(i) ~= 4) & (peB(i) ~= 4)) %OK
    Flow34(i) = mdota;
elseif ((peA(i) == 4) & (peB(i) ~= 4)) %OK
    Flow34(i) = 0;
elseif ((peA(i) == 4) & (peB(i) == 4)) %OK
    Flow34(i) = -mdotb;
elseif ((peA(i) ~= 4) & (peB(i) == 4)) %OK
    Flow34(i) = mdota - mdotb;
end
%-----FLOW 2 TO 3-----
if ((peA(i) == 2) & (peB(i) ~= 2))
    Flow23(i)=mdota+Flow12(i); %OK
elseif ((peA(i) ~= 2) & (peB(i) == 2))
    Flow23(i)=mdotb+Flow12(i); %OK
elseif ((peA(i) == 2) & (peB(i) == 2))
    Flow23(i)=mdota+mdotb+Flow12(i); %OK
elseif ((peA(i) ~= 2) & (peB(i) ~= 2))
    Flow23(i)=Flow12(i); %OK
end
%-----
%-----
TTANK1(i+1)=
TTANK1(i)+(dt/CNODE)*cp_water*(mdota*TAhp(i)*(peA(i)==1)+mdotb*TBrf(i)*(peB(i)=
=1)-mdotb*TTANK1(i) +...
-Flow12(i)*TTANK1(i)*(Flow12(i)>=0)-
Flow12(i)*TTANK2(i)*(Flow12(i)<0) - (UTANKNODE/cp_water)*(TTANK1(i)-T(19,i)));
TTANK2(i+1)=
TTANK2(i)+(dt/CNODE)*cp_water*(mdota*TAhp(i)*(peA(i)==2)+mdotb*TBrf(i)*(peB(i)=
=2)+...
+Flow12(i)*TTANK1(i)*(Flow12(i)>=0)+Flow12(i)*TTANK2(i)*(Flow12(i)<0) +...
-Flow23(i)*TTANK2(i)*(Flow23(i)>=0)-
Flow23(i)*TTANK3(i)*(Flow23(i)<0) - (UTANKNODE/cp_water)*(TTANK2(i)-T(19,i)));
TTANK3(i+1)=
TTANK3(i)+(dt/CNODE)*cp_water*(mdota*TAhp(i)*(peA(i)==3)+mdotb*TBrf(i)*(peB(i)=
=3)+...
+Flow23(i)*TTANK2(i)*(Flow23(i)>=0)+Flow23(i)*TTANK3(i)*(Flow23(i)<0) +...
-Flow34(i)*TTANK3(i)*(Flow34(i)>=0)-
Flow34(i)*TTANK4(i)*(Flow34(i)<0) - (UTANKNODE/cp_water)*(TTANK3(i)-T(19,i)));
TTANK4(i+1)=
TTANK4(i)+(dt/CNODE)*cp_water*(mdota*TAhp(i)*(peA(i)==4)+mdotb*TBrf(i)*(peB(i)=
=4)-mdota*TTANK4(i)+...
+Flow34(i)*TTANK3(i)*(Flow34(i)>=0)+Flow34(i)*TTANK4(i)*(Flow34(i)<0) -
(UTANKNODE/cp_water)*(TTANK4(i)-T(19,i)));
%-----TOPERATIVE-----

```

```

Toperative(i+1) = T(1,i)/3 + (2/3)*( T(6,i)+T(8,i)+T(10,i)+
T(12,i)+T(14,i)+T(16,i) )/6;
%-----
%-----TEMPERATURE AT 6:00 AM OF THAT DAY-----
if (i > 1)
    if (TPSN(i) > -6.05) & (TPSN(i) < -5.95)
        Temp_at6am(i) = Toperative(i);
        hora6(i) = i;
    else
        Temp_at6am(i) = Temp_at6am(i-1);
        hora6(i) = hora6(i-1);
    end
end
%-----
SOL_CURRDAY = 0;

%-----SOLAR RADIATION CURRENT DAY-----
if (i < max_count-1-12*3600/dt)
    for k = hora6(i):hora6(i)+12*3600/dt
        SOL_CURRDAY = SOL_CURRDAY + SOLAR_RAD(k)*dt;
        SOL_DIA(i)=SOL_CURRDAY;
    end
end
if (i >= max_count-1-12*3600/dt)
    SOL_CURRDAY = 10.2E6;
end

%-----SOLAR RADIATION FOLLOWING DAY-----
SOL_FOLLDAY = 0;
if (i < max_count-1-36*3600/dt)
    for k = hora6(i)+24*3600/dt:hora6(i)+36*3600/dt
        SOL_FOLLDAY = SOL_FOLLDAY + SOLAR_RAD(k)*dt;
        SOL_DIASIG(i+1)=SOL_FOLLDAY;
    end
end
if (i >= max_count-1-36*3600/dt)
    SOL_FOLLDAY = 10.2E6;
end

%%%%%%%%%%%%%%%%%%%%%%%%%%%%%%%%%%%%%%%%%%%%%%%%%%%%%%%%%%%%%%%%%%%%%%%%
%-----PREDICTIVE CONTROL-----%
%%%%%%%%%%%%%%%%%%%%%%%%%%%%%%%%%%%%%%%%%%%%%%%%%%%%%%%%%%%%%%%%%%%%%%%%
Tsetpoint = 21;
if SOL_CURRDAY > 10E6
    if (Temp_at6am(i) > 20)
        transcorr(i+1) = 0.400;
    else
        transcorr(i+1) = transcorr(i);
    end
elseif ((SOL_CURRDAY > 6.5E6) & (SOL_CURRDAY <= 10E6))
    if (Temp_at6am(i) > 20)
        transcorr(i+1) = 0.60;
    else
        transcorr(i+1) = transcorr(i);
    end
elseif ((SOL_CURRDAY > 3.5E6) & (SOL_CURRDAY <= 6.5E6))
    if (Temp_at6am(i) > 20)
        transcorr(i+1) = 0.80;

```

```

        else
            transcorr(i+1) = transcorr(i);
        end
    elseif (SOL_CURRDAY <= 3.5E6)
        if (Temp_at6am(i) > 20)
            transcorr(i+1) = 1.00;
        else
            transcorr(i+1) = transcorr(i);
        end
    end

%-----
if(( (Toperative(i)<(Tsetpoint-TOLERANCE)) | ( (qauxTOTAL(i)>0) &
(Toperative(i)<Tsetpoint) ) )
    qauxTOTAL(i+1) = (TTANK1(i)>28)*min(KP*(Tsetpoint-
Toperative(i)),QMAX);
    ELEC_POW_RF(i+1)=80;
else
    qauxTOTAL(i+1) = 0;
    ELEC_POW_RF(i+1)=0;
end
qaux1(i+1) = 0.70*qauxTOTAL(i);
qaux2(i+1) = 0.10*qauxTOTAL(i);
qaux3(i+1) = 0.20*qauxTOTAL(i);
PROGRESS = i/(max_count-1);
progressbar(PROGRESS,0);
end
%*****END OF LOOP*****
time_elapsed = toc;
display(time_elapsed);
%=====PLOTS=====
%plot(AST/24,azim*180/pi,'r',AST/24,alpha*180/pi,'b');
% title('TEST')
% xlabel('time')
% ylabel('angle')
%plot(x,Tground,'r');
%plot(Time,Julian,'r');
%plot(tx/(time_steps_ph*24)+IT/24,T(1,:), 'r',tx/(time_steps_ph*24)+IT/24,Top
erative,'b',...
%
tx/(time_steps_ph*24)+IT/24,To,'m',tx/(time_steps_ph*24)+IT/24,TextitBIPVT,'k');

hora6(max_count)=hora6(max_count-1);

txm = tx/(time_steps_ph*24)+IT/24;

plot(txm,TTANK1,'r',txm,TTANK2,'B',...
txm,TTANK3,'M',txm,TTANK4,'K',txm,To,'g',...
txm,Toperative,'c',txm,SOLAR_RAD/50,'g',...
txm,TextitBIPVT,'r');
% gtext('unnecessary labeling')
% axis([(IT-1)/24, FT/24, 0, 90])
% axis([37, 38, -90, 90])
% axis([0, 8760, -90, 90])
%-----

```

D. Overview of Simulink Model

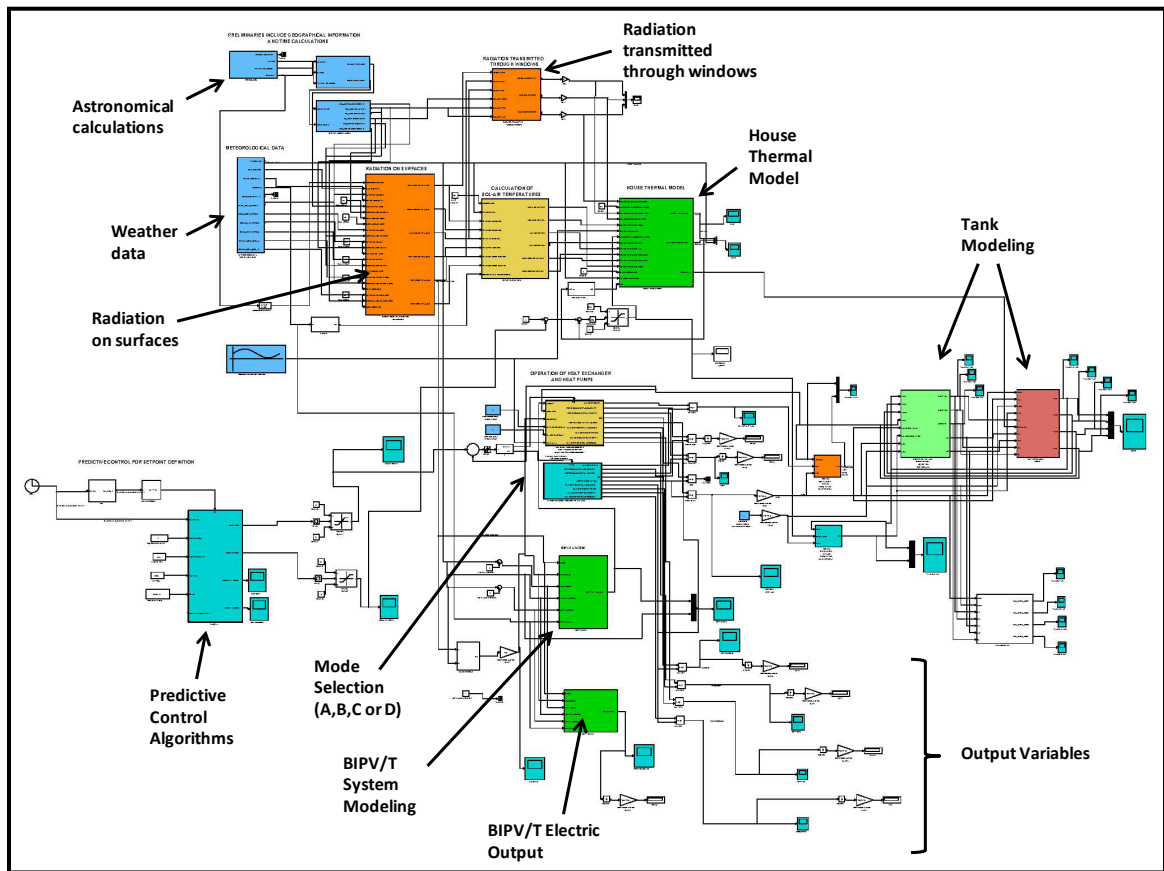


Figure D.1. Summary of Simulink Model.

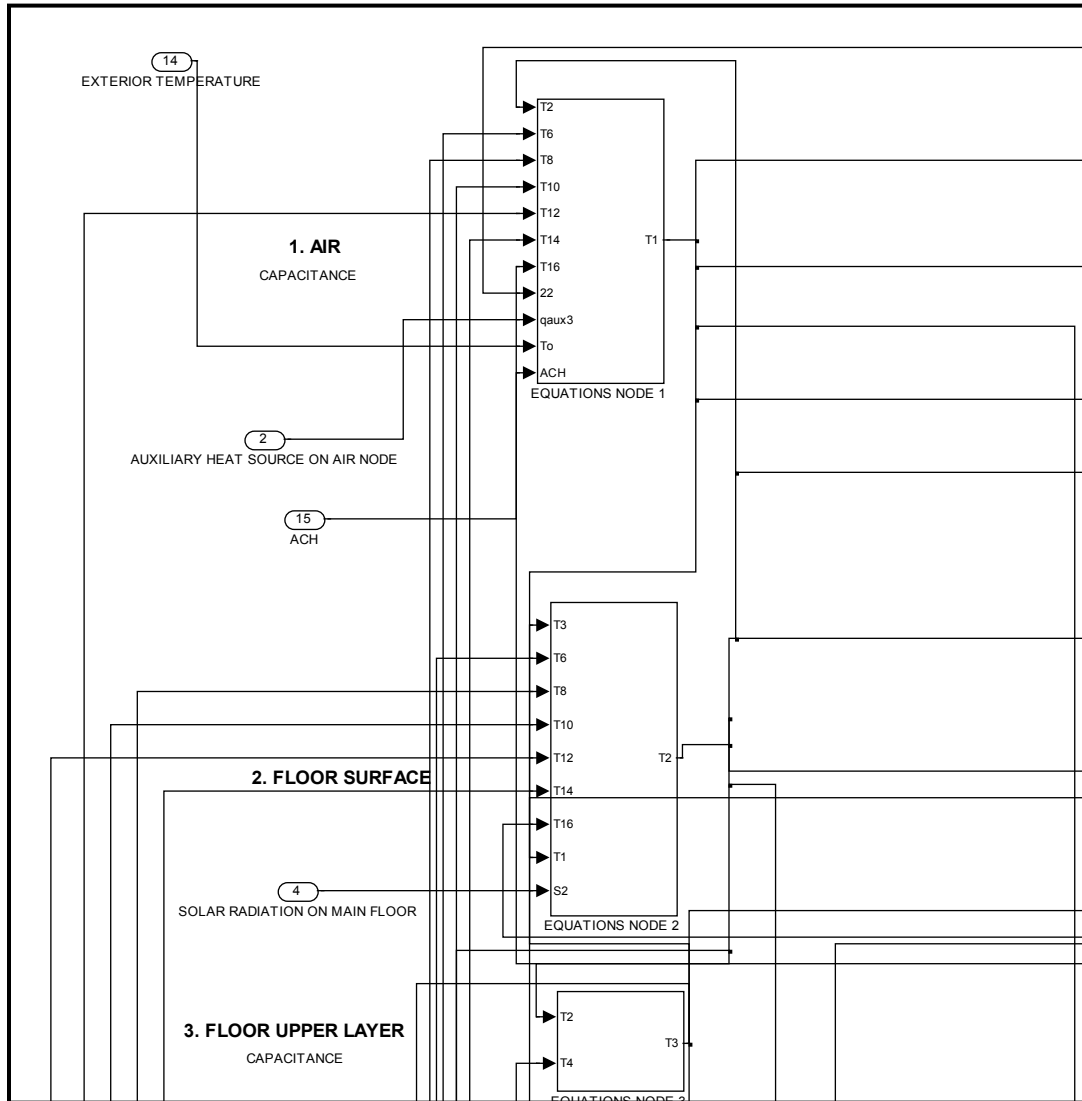


Figure D.2. House Thermal Model (Partial View).

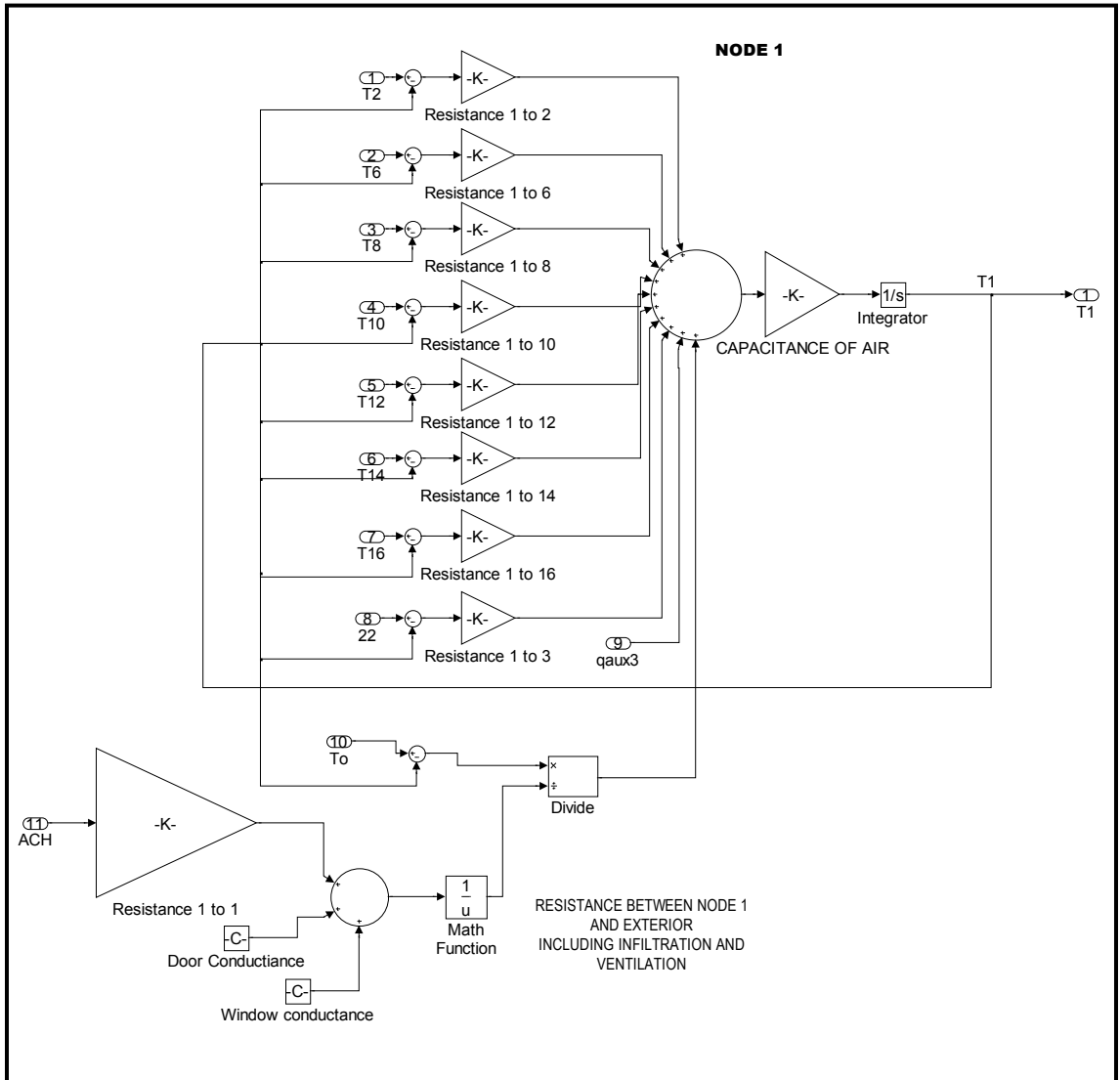


Figure D.3. Model for Node 1 (out of 22 nodes) within “House Thermal Model”.

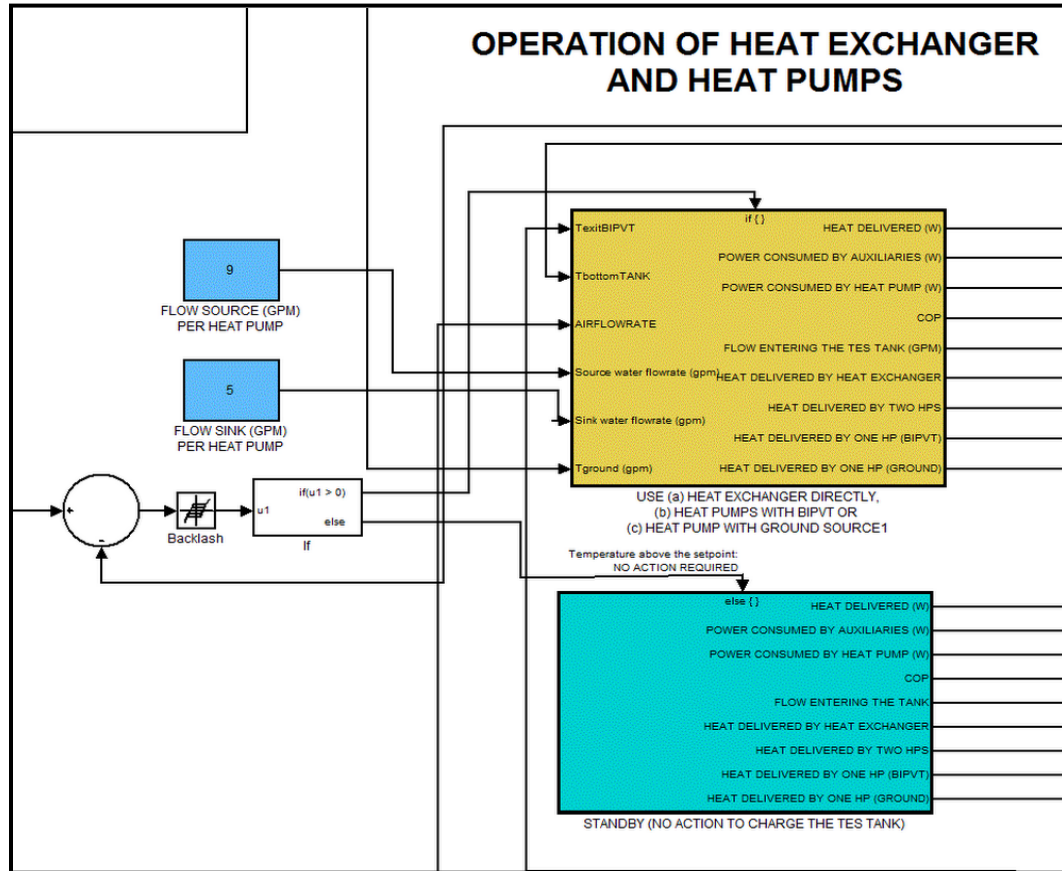


Figure D.4. Close-up of selection between modes of operation (higher level of several nested blocks).

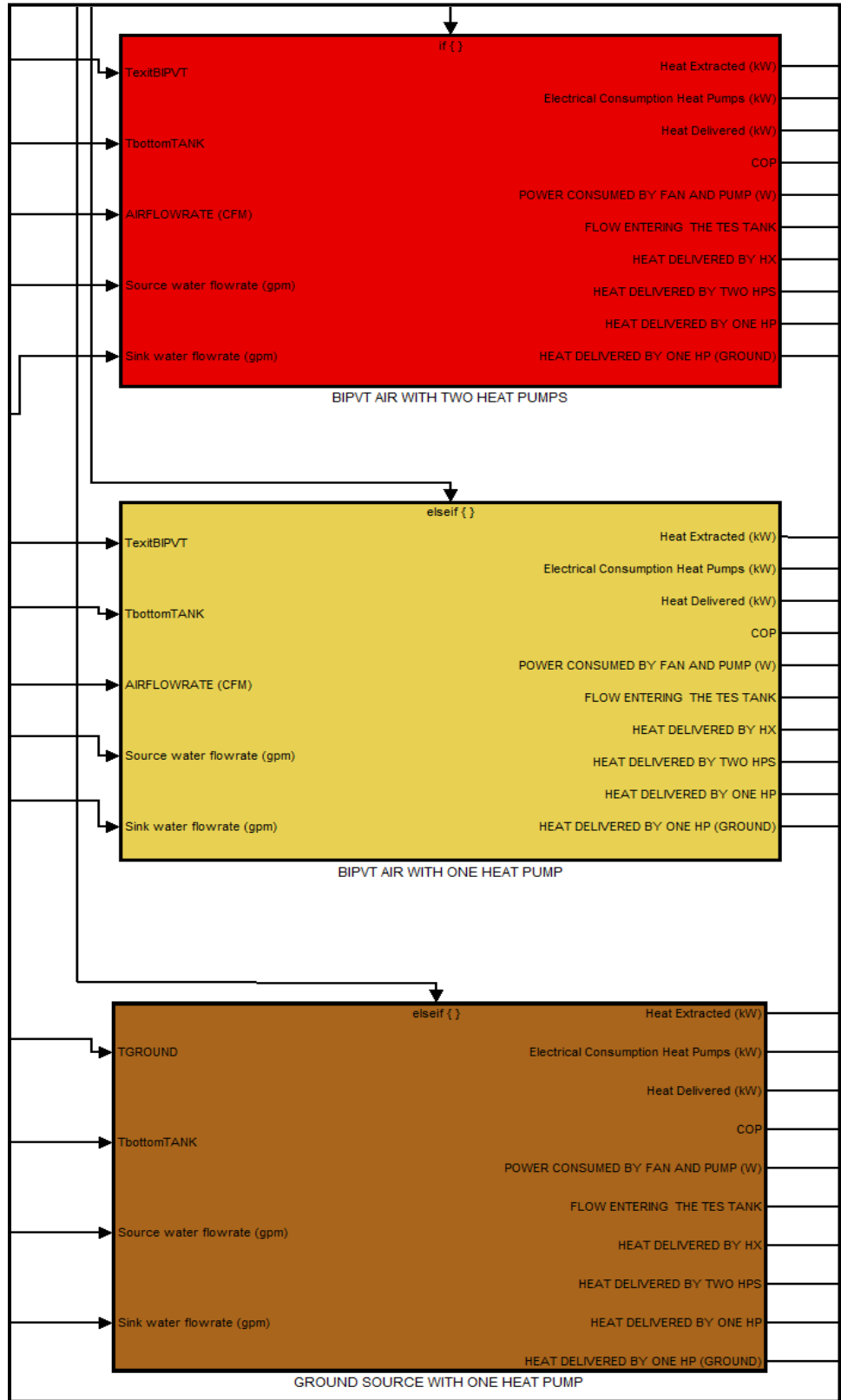


Figure D.5. Selection between modes B, C and D.

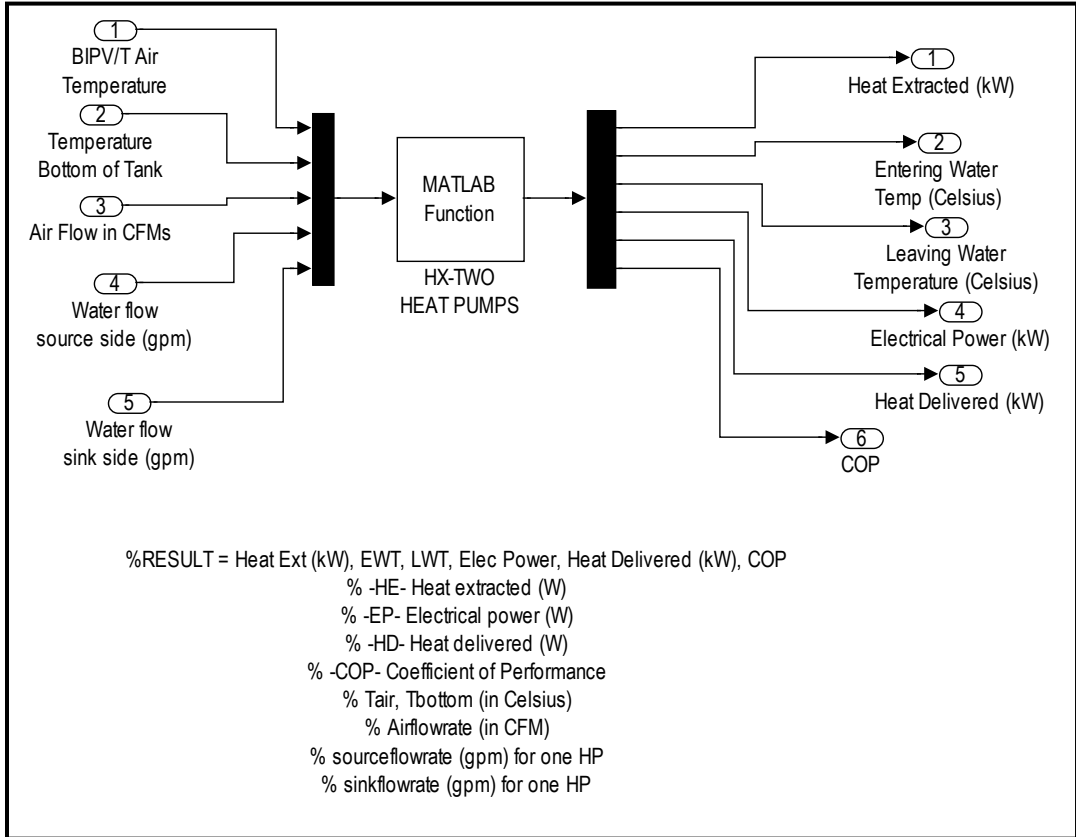


Figure D.6. Graphical implementation of a MATLAB M-function of multiple variables.

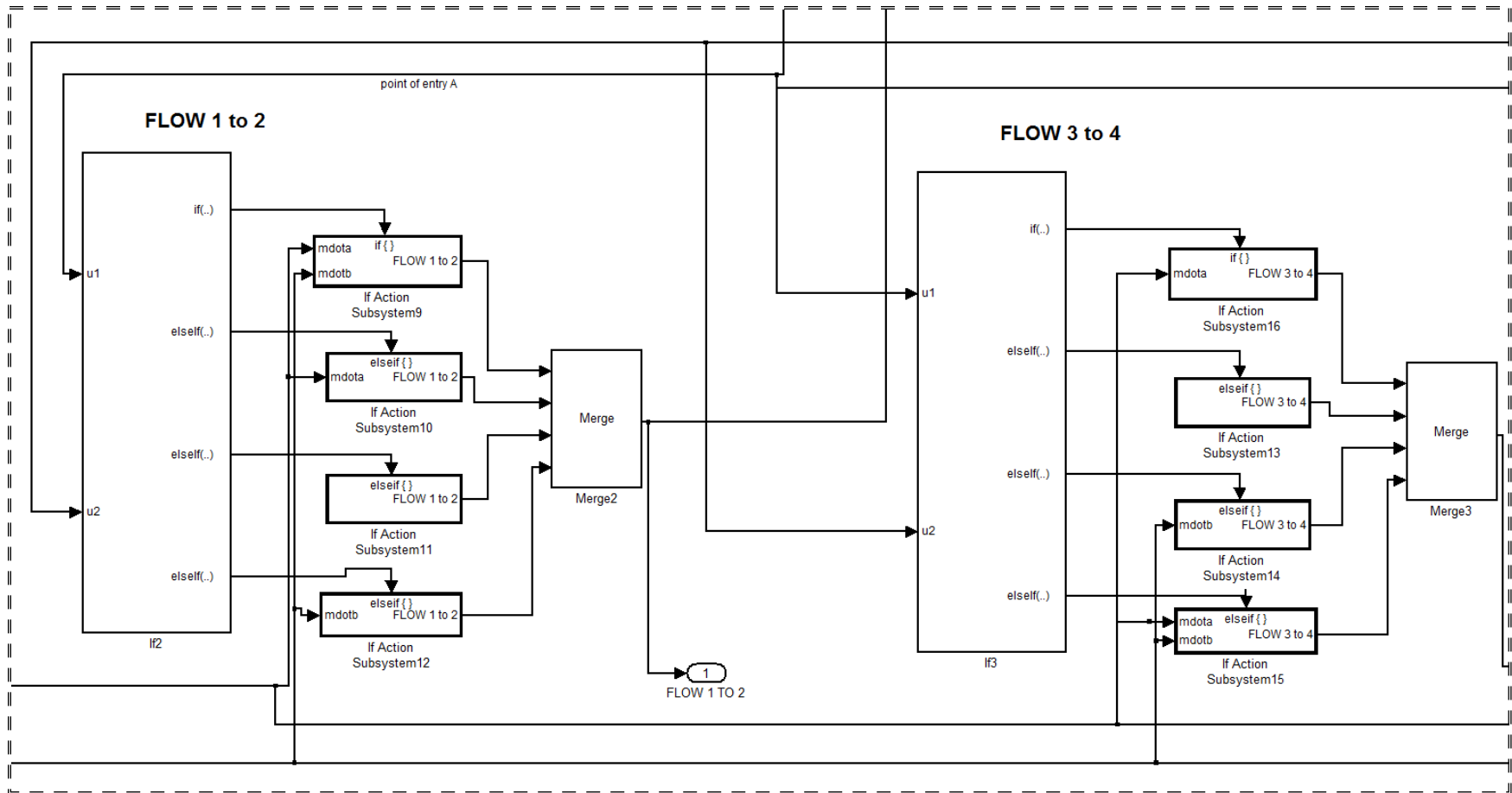


Figure D.7. Partial view of the TES tank model (4 nodes).

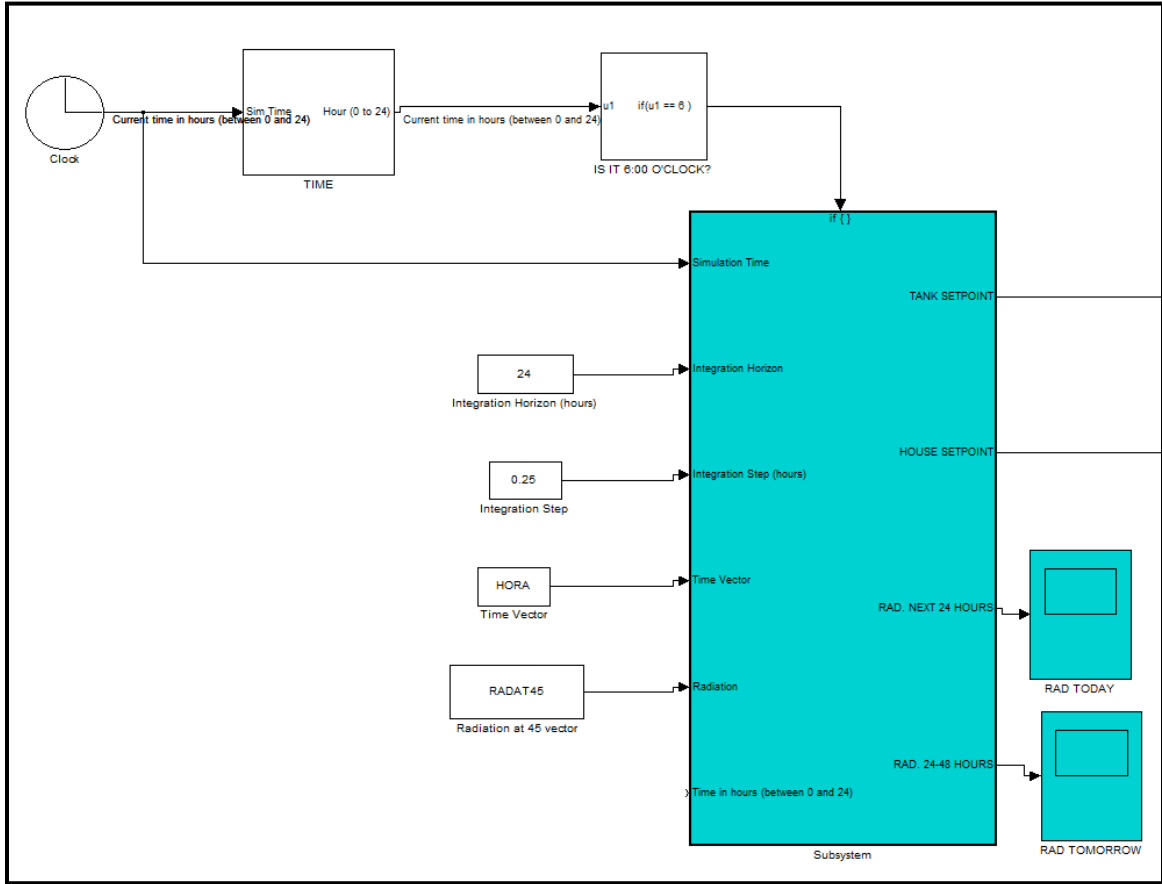


Figure D.8. Close-up: predictive control for set-point adjustments in the house and the TES tank.

E. BIPV/T Model and Heat Pumps

Filename: BIPVT_8kW.m

```
function Tfinal = BIPVT_8kW(RAD,Flowrate,Ti,To,Tattic,Wspeed)
% Final temperature of a BIPVT System
% Final_temp = BIPVT(RAD,Flowrate,Ti,To,Tattic,Wspeed)
% Temperatures in Celsius
% Flowrate in CFM
% Windspeed in m/s
%-----
-----
To = To + 273.15;
%Temperature in K
Ti = Ti + 273.15;
%Temperature in K
Tattic = Tattic + 273.15;
%Temperature in K
Flowrate = Flowrate/(2117.253);
%Flowrate in m3/s
%-----
-----
%-----GEOMETRY OF THE ROOF-----
-----
%WidthPV = 18.23; %Width of the
BIPV/T roof
WidthPV = 7.5;
Total_length_slope = 5.63; %Length of the system in the flow
direction (upwards)
%Total_length_slope = 3.53;
LengthPV = 3.5299; %Lenght of the PV in the flow
direction (upwards)
%LengthPV = 4.2;
%LengthPV = 3.00;
LengthGL = Total_length_slope - LengthPV; %Length of the glazing
section
Gapsize = 5.56E-2;
%Gap size
%-----SOME FLOW CALCULATIONS-----
-----
ACS = WidthPV*Gapsize; %Area
cross section
Per = 2*(WidthPV+Gapsize);
%Perimeter
Dh = 4*ACS/Per;
%Hydraulic diameter
sigma = 5.67E-8; %Stefan-
Boltzmann constant
%-----AIR PROPERTIES-----
-----
Pr = 0.71;
%Prandlt number
M_air = 0.0289; %Molecular mass of
air (kg/mol)
R = 8.314; %Ideal gas
constant (J/K-mol)
Pressure = 101300;
%Atmospheric pressure
air_density = Pressure*M_air/(R*Ti); %Air density
based on Ti
```

```

k_air = (0.002528*(Ti)^1.5)/(Ti+200);           %Thermal cond. of air based on
Ti
cp_air = 1000;
%cp of air
b = 1.458E-6;
Su = 110.4;
visc = (b*(Ti)^1.5)/(Ti+Su);           %Viscosity (Sutherland model)based on Ti
%-----MASS FLOW AND REYNOLDS-----
-----
Vel_gap = Flowrate/ACS;                 %Velocity
in the gap
MFR = Flowrate*air_density;
%Mass flow rate
Jones = 2/3 + (11/24)*(Gapsize/WidthPV)*(2-Gapsize/WidthPV);           %Jones'
correction
Rey = air_density*Vel_gap*Dh/visc;
%Reynolds number
Rey_corr = Rey*Jones;                   %Corrected
Reynolds number
%-----HEAT TRANSFER CONVECTIVE COEFFICIENT-----
-----
%f = 0.03;                             %Assumed friction factor (or equiv.
friction factor)
%Nu_turb = ((f/8)*(Rey_corr-1000)*Pr)/(1+12.7*(f/8)^0.5*(Pr^(2/3)-1));
hc = 6.5;                             %Assumed value of convective heat
transfer coefficient
%-----Exterior heat transfer coefficient-----
-----
hox = 5.7 + 3.8*Wspeed;
%-----SEGMENTS OF PV-----
-----
npv = 5;
DeltaPV=LengthPV/npv;
xPV(1) = 0;
for i=1:npv
    xPV(i+1)=i*DeltaPV-DeltaPV/2;           %Coordinates of central points
of PV panels
end
xPV(npv+2)=LengthPV;
%-----SEGMENTS OF GLAZING-----
-----
ngl = 4;
DeltaGL=LengthGL/ngl;
xGL(1) = 0;
for i=1:ngl
    xGL(i+1)=i*DeltaGL-DeltaGL/2;           %Coordinates of central points of
Glazing panels
end
xGL(ngl+2)=LengthGL;
%-----SEGMENTS OF VERTICAL GLAZING-----
-----
%*****
%*****
%*****MAIN
CALCULATIONS*****
%*****
%*****
%-----PV SECTION-----
-----
e1 = 0.9;                               %Emissivity of back of PV
e2 = 0.3;                               %Emissivity of absorber plate
aPV = 0.92;                             %Absorptance of PV panel

```

```

Afraction = 0.95; %Effective fraction of PV area actually
occupied by PV
uins = 0.15; %Conductance per unit area of insulation
below attic
%-----
%Guess temperatures
TPVguess = 50+273.15;
TABguess = 30+273.15;
Tmaguess = 40+273.15;
%convection coefficients in both sides
hcb = hc;
hcf = hc;
Tin = Ti; %Initial Temperature
for n=1:npv
    TPV = TPVguess;
    TAB = TABguess;
    Tma = Tmaguess;
    error_tol = 0.1;
    while abs(error_tol)>=0.001
        Tprevious = Tma;
        C1 = (hcf*TPV+hcb*TAB)/(hcf+hcb);
        C2 = (WidthPV*(hcf+hcb))/(MFR*cp_air);
        Tma = (1/(DeltaPV))*quad(@ (x) (C1 + (Tin-C1)*exp(-C2*x)),0,DeltaPV);
        Tmean = (TPV+TAB)/2;
        hrad = (4*sigma*Tmean^3)/(1/e1 + 1/e2 -1);
        eff = 0.126 - 0.00055*(TPV-(25+273.15));
        TPV = (hox*To+hcf*Tma+hrad*TAB+RAD*Afraction*(aPV-
eff))/(hox+hcf+hrad);
        TAB = (Tma*hcb+Tattic*uins+TPV*hrad)/(hcb+uins+hrad);
        error_tol = (Tma-Tprevious)/Tprevious;
    end
    PVMidpoints(n) = Tma;
    PVFinalpoints(n) = C1 + (Tin-C1)*exp(-C2*DeltaPV);
    Gen(n) = eff*WidthPV*DeltaPV*Afraction*RAD;
    Tin = PVFinalpoints(n);
end
%-----
%-----GLAZING SECTION-----
%-----
e1 = 0.9; %Emissivity of back of glazing (infrared)
e2 = 0.05; %Emissivity of absorber plate (infrared)
taupv = 0.9; %Transmittance of glazing
aAB = 0.95; %Absorptance of absorber plate (overall)
uins = 0.15; %Conductance per unit area of insulation below
attic
%-----
%Guess temperatures
TGLguess = 50+273.15;
TABguess = 30+273.15;
Tmaguess = 40+273.15;
%convection coefficients in both sides
hcb = hc;
hcf = 2.5*hc;
Tin = PVFinalpoints(npv); %Initial Temperature = final point of PV
for n=1:ngl
    TGL = TGLguess;
    TAB = TABguess;
    Tma = Tmaguess;
    error_tol = 0.1;

```

```

while abs(error_tol)>=0.001
    Tprevious = Tma;
    C1 = (hcf*TGL+hcb*TAB)/(hcf+hcb);
    C2 = (WidthPV*(hcf+hcb))/(MFR*cp_air);
    Tma = (1/(DeltaGL))*quad(@(x) (C1 + (Tin-C1)*exp(-C2*x)),0,DeltaGL);
    Tmean = (TGL+TAB)/2;
    hrad = (4*sigma*Tmean^3)/(1/e1 + 1/e2 -1);
    TGL = (hox*To+hcf*Tma+hrad*TAB)/(hox+hcf+hrad);
    TAB = (Tma*hcb+Tattic*uins+TGL*hrad+RAD*taupv*aAB)/(hcb+uins+hrad);
    error_tol = (Tma-Tprevious)/Tprevious;
end
GLMidpoints(n) = Tma;
GLFinalpoints(n) = C1 + (Tin-C1)*exp(-C2*DeltaGL);
Tin = GLFinalpoints(n);
end
%-----RESULTS-----
---
```

```
Tfinal = GLFinalpoints(ngl)-273.15;
```

Filename: TWO_3TON_HP.m

```

function RESULT =
TWO_3TON_HP(Tair,Tbottom,Airflowrate,sourceflowrate,sinkflowrate)
%function RESULT =
TWO_3TON_HP(Tair,Tbottom,Airflowrate,sourceflowrate,sinkflowrate)
%RESULT = Heat Ext (kW), EWT, LWT, Elec Power, Heat Delivered (kW), COP
% -HE- Heat extracted (W)
% -EP- Electrical power (W)
% -HD- Heat delivered (W)
% -COP- Coefficient of Performance
% Tair, Tbottom (in Celsius)
% Airflowrate (in CFM)
% sourceflowrate (gpm) for one HP
% sinkflowrate (gpm) for one HP

%-----UNIT CONVERSIONS-----
AirflowrateSI = Airflowrate/2117.25; %From CFM to m3/s
sourceflowrateSI = sourceflowrate/(15.873*1000); %water flow at source in m3/s
sinkflowrateSI = sinkflowrate/(15.873*1000); %water flow at sink in m3/s
%-----HEAT RATE CAPACITIES-----
CAIR = AirflowrateSI*1.2*1000; %Heat rate capacity of air
CWATER = sourceflowrateSI*1000*4180; %Heat rate capacity of water
Cmin = min(CAIR,CWATER);
Cmax = max(CAIR,CWATER);
Cr = Cmin/Cmax; %Heat capacity ratio
UA = 2000;
NTU = UA/Cmin;
eff = 1-exp((NTU^0.22/Cr)*(exp(-Cr*(NTU^0.78))-1));
%-----
Tsink =[15.6 26.7 37.8 48.9];
Tsource = [-6.1 -1.1 4.4 10 15.6 21.1];
% Table A is for 7.5 gal/min on the source side
% Table B is for 11.3 gal/min on the source side
% Table C is for 15.0 gal/min on the source side
%*****HEAT EXTRACTION RATES*****
%*****HEAT EXTRACTION RATES*****
%-----DATA FOR SINK FLOW RATE 5 GPM-----
GSW036A1 = [0 0 0 0; %SOURCE FLOW = 5.0
GPM
```

	20.5	18.7	16.4	13.6;	
	23.2	21.8	19.4	16.6;	
	26.9	24.8	22.2	19;	
	30.4	28.9	26.4	23.4;	
	35.0	32.9	30.1	0];	
GSW036B1 =	[0	0	0	0;	%SOURCE FLOW = 7.0
GPM					
	22.3	20.4	18.1	15.3;	
	25.2	23.8	21.3	18.5;	
	29.2	27.1	24.3	21.1;	
	32.9	31.4	28.8	25.7;	
	37.9	35.7	32.9	0];	
GSW036C1 =	[19.3	17.5	15.2	12.5;	%SOURCE FLOW = 9.0
GPM					
	22.8	20.9	18.5	15.7;	
	25.7	24.2	21.8	18.9;	
	29.8	27.6	24.9	21.6;	
	33.6	32.0	29.4	26.3;	
	38.6	36.4	33.5	0.0];	
%-----DATA FOR SINK FLOW RATE 7 GPM-----					
GSW036A2 =	[0	0	0	0;	%SOURCE FLOW = 5.0
GPM					
	20.8	19.0	16.8	14.1;	
	23.6	22.2	19.9	17.2;	
	27.3	25.3	22.7	19.6;	
	30.8	29.4	26.9	24.0;	
	37.1	35.1	32.5	29.1];	
GSW036B2 =	[0	0	0	0;	%SOURCE FLOW = 7.0
GPM					
	22.6	20.8	18.5	15.7;	
	25.6	24.2	21.8	19.0;	
	29.6	27.5	24.9	21.7;	
	33.3	31.9	29.3	26.3;	
	40.1	38.1	35.3	31.9];	
GSW036C2 =	[19.5	17.8	15.6	12.9;	%SOURCE FLOW = 9.0
GPM					
	23.0	21.2	18.9	16.1;	
	26.1	24.6	22.3	19.4;	
	30.2	28.1	25.4	22.2;	
	33.9	32.5	29.9	26.9;	
	40.8	38.8	36.0	32.6];	
%-----DATA FOR SINK FLOW RATE 9 GPM-----					
GSW036A3 =	[0	0	0	0;	%SOURCE FLOW = 5.0
GPM					
	20.9	19.2	17.0	14.3;	
	23.7	22.4	20.2	17.5;	
	27.5	25.5	23.0	20.0;	
	31.0	29.6	27.2	24.3;	
	37.3	35.4	32.9	29.6];	
GSW036B3 =	[0	0	0	0;	%SOURCE FLOW = 7.0
GPM					
	22.7	20.9	18.7	16.0;	
	25.8	24.4	22.1	19.3;	
	29.8	27.8	25.2	22.1;	
	33.5	32.1	29.6	26.6;	
	40.3	38.4	35.8	32.4];	
GSW036C3 =	[19.6	17.9	15.8	13.2;	%SOURCE FLOW = 9.0
GPM					
	23.2	21.4	19.1	16.4;	
	26.3	24.9	22.6	19.8;	
	30.4	28.3	25.7	22.6;	
	34.1	32.7	30.2	27.2;	

```

41.1      39.1      36.5      33.1];
%*****ELECTRICAL POWER CONSUMPTION*****
%-----DATA FOR SINK FLOW RATE 5 GPM-----
POWERA1 = [0      0      0      0;      %SOURCE FLOW = 5.0
GPM
1.42      1.80      2.32      2.97;
1.45      1.68      2.16      2.76;
1.48      1.88      2.41      3.08;
1.50      1.68      2.16      2.76;
1.56      1.97      2.53      0];
POWERB1 = [0      0      0      0;      %SOURCE FLOW = 7.0
GPM
1.43      1.81      2.33      2.99;
1.46      1.69      2.17      2.78;
1.49      1.89      2.43      3.11;
1.51      1.69      2.17      2.78;
1.57      1.98      2.54      0];
POWERC1 = [1.41      1.78      2.29      2.94;      %SOURCE FLOW = 9.0
GPM
1.44      1.82      2.34      3.00;
1.47      1.70      2.18      2.79;
1.50      1.90      2.44      3.12;
1.52      1.70      2.18      2.79;
1.57      1.99      2.55      0];
%-----DATA FOR SINK FLOW RATE 7 GPM-----
POWERA2 = [0      0      0      0;      %SOURCE FLOW = 5.0
GPM
1.38      1.73      2.23      2.87;
1.39      1.60      2.06      2.64;
1.42      1.79      2.30      2.95;
1.44      1.60      2.06      2.64;
1.49      1.87      2.39      3.07];
POWERB2 = [0      0      0      0;      %SOURCE FLOW = 7.0
GPM
1.39      1.75      2.25      2.89;
1.40      1.61      2.07      2.66;
1.43      1.80      2.32      2.97;
1.45      1.61      2.07      2.66;
1.50      1.88      2.41      3.09];
POWERC2 = [1.37      1.72      2.21      2.84;      %SOURCE FLOW = 9.0
GPM
1.39      1.75      2.25      2.90;
1.41      1.62      2.08      2.67;
1.43      1.81      2.33      2.98;
1.45      1.62      2.08      2.67;
1.50      1.89      2.42      3.10];
%-----DATA FOR SINK FLOW RATE 9 GPM-----
POWERA3 = [0      0      0      0;      %SOURCE FLOW = 5.0
GPM
1.35      1.70      2.18      2.81;
1.36      1.56      2.00      2.57;
1.39      1.74      2.24      2.88;
1.40      1.56      2.00      2.57;
1.44      1.80      2.31      2.97];
POWERB3 = [0      0      0      0;      %SOURCE FLOW = 7.0
GPM
1.36      1.71      2.20      2.83;
1.37      1.57      2.02      2.59;
1.40      1.76      2.26      2.90;
1.41      1.57      2.02      2.59;
1.45      1.82      2.33      2.99];

```

```

    POWERC3 = [1.34      1.68      2.16      2.78;   %SOURCE FLOW = 9.0
GPM          1.37      1.72      2.21      2.84;
             1.37      1.58      2.03      2.60;
             1.40      1.76      2.27      2.91;
             1.42      1.58      2.03      2.60;
             1.46      1.82      2.34      3.00];

%-----
%Which matrix to use??
%-----SINK FLOW RATE-----
AUX1 = abs(sinkflowrate-5);
AUX2 = abs(sinkflowrate-7);
AUX3 = abs(sinkflowrate-9);
VAUX = [AUX1 AUX2 AUX3];
MINIMO = min(VAUX);
if AUX1 == AUX2
    CSINKFR = 5;
elseif AUX2 == AUX3
    CSINKFR = 7;
elseif MINIMO == AUX1
    CSINKFR = 5;
elseif MINIMO == AUX2
    CSINKFR = 7;
elseif MINIMO == AUX3
    CSINKFR = 9;
end
%-----SOURCE FLOW RATE-----
AUX1 = abs(sourceflowrate-5);
AUX2 = abs(sourceflowrate-7);
AUX3 = abs(sourceflowrate-7);
VAUX = [AUX1 AUX2 AUX3];
MINIMO = min(VAUX);
if AUX1 == AUX2
    CSOURCEFR = 5;
elseif AUX2 == AUX3
    CSOURCEFR = 7;
elseif MINIMO == AUX1
    CSOURCEFR = 5;
elseif MINIMO == AUX2
    CSOURCEFR = 7;
elseif MINIMO == AUX3
    CSOURCEFR = 9;
end
%-----
if (CSINKFR == 5)
    if (CSOURCEFR == 5)
        MATRIX = GSW036A1;
        ELEC = POWERA1;
    elseif (CSOURCEFR == 7)
        MATRIX = GSW036B1;
        ELEC = POWERB1;
    elseif (CSOURCEFR == 9)
        MATRIX = GSW036C1;
        ELEC = POWERC1;
    end
elseif (CSINKFR == 7)
    if (CSOURCEFR == 5)
        MATRIX = GSW036A2;
        ELEC = POWERA2;
    elseif (CSOURCEFR == 7)
        MATRIX = GSW036B2;
        ELEC = POWERB2;

```

```

elseif (CSOURCEFR == 9)
MATRIX = GSW036C2;
ELEC = POWERC2;
end
elseif (CSINKFR == 9)
if (CSOURCEFR == 5)
MATRIX = GSW036A3;
ELEC = POWERA3;
elseif (CSOURCEFR == 7)
MATRIX = GSW036B3;
ELEC = POWERB3;
elseif (CSOURCEFR == 9)
MATRIX = GSW036C3;
ELEC = POWERC3;
end
end
%-----SOLVE CYCLE-----
%V(1) - HE
%V(2) - EWT
%V(3) - LWT
%-----
F = @(V) [V(1)*1000-CAIR*eff*(Tair-V(3));...
V(2)-V(3)-0.95*V(1)*1000/CWATER;...
0.95*V(1)-2*interp2(Tsink,Tsource,MATRIX,Tbottom,V(2))/3.4121];
InitialGuess = [18;10;5];
Options = optimset('Display','final');
SOLUTION = fsolve(F,InitialGuess);
%-----
RESULT(1) = SOLUTION(1);
RESULT(2) = SOLUTION(2);
RESULT(3) = SOLUTION(3);
EWT = SOLUTION(2);
if EWT < 21.1
RESULT(4) = 2*interp2(Tsink,Tsource,ELEC,Tbottom,EWT);
else
EWT = 21;
RESULT(4) = 2*interp2(Tsink,Tsource,ELEC,Tbottom,EWT);
end
RESULT(5) = 0.95*RESULT(1)+ RESULT(4);
RESULT(6) = RESULT(5)/RESULT(4);

if RESULT(1) < 32/3.4121
RESULT(1) = 0;
RESULT(2) = 0;
RESULT(3) = 0;
RESULT(4) = 0;
RESULT(5) = 0;
RESULT(6) = 0;
elseif RESULT(1) > 77.2/3.4121
RESULT(1) = 0;
RESULT(2) = 0;
RESULT(3) = 0;
RESULT(4) = 0;
RESULT(5) = 0;
RESULT(6) = 0;
end
end

```

F. System Identification and MPC Implementation

Filename: Prepare_model_Purdue.m

```
%Preliminaries
TS = 300;
NA = 3;
NB = 3;
NK = 1;

%-----
%1. Read Data corresponding to the response for each input and create data
% objects
EDATARFH = xlsread('C:\JOSE_CANDANEDO\CONFERENCES\CONFERENCE PURDUE\IO
DATA\IO_RFH.xls'); %Input = Radiant floor heating system
EDATAEXT = xlsread('C:\JOSE_CANDANEDO\CONFERENCES\CONFERENCE PURDUE\IO
DATA\IO_ET.xls'); %Input = Exterior temperature
EDATAGHR = xlsread('C:\JOSE_CANDANEDO\CONFERENCES\CONFERENCE PURDUE\IO
DATA\IO_SR.xls'); %Input = Solar radiation

%Radiant floor response
TIEMPO_RFH = EDATARFH(:,1);
RFH = EDATARFH(:,2);
TIN_RFH = EDATARFH(:,3);

%Exterior temperature response
TIEMPO_EXT = EDATAEXT(:,1);
EXT = EDATAEXT(:,2);
TIN_EXT = EDATAEXT(:,3);

%Solar radiation response
TIEMPO_GHR = EDATAGHR(:,1);
GHR = EDATAGHR(:,2);
TIN_GHR = EDATAGHR(:,3);

%Create data objects
Data_rfh = iddata(TIN_RFH,RFH,TS);
Data_ext = iddata(TIN_EXT,EXT,TS);
Data_ghr = iddata(TIN_GHR,GHR,TS);

%-----
%2. Identify z-transform models
%arx_rfh = arx(Data_rfh,[2 2 1], 'Focus', 'Stability'); %ARX for radiant
floor heating
P1_rfh = pem(Data_rfh,'P1'); %Already in Laplace domain
arx_ext = arx(Data_ext,[NA NB NK], 'Focus', 'Simulation'); %ARX for exterior
temperature
arx_ghr = arx(Data_ghr,[NA NB NK], 'Focus', 'Simulation'); %ARX for global
horizontal radiation

%-----
%3. Identify models in Laplace domain
%cont_arx_rfh = d2c(arx_rfh); %Laplace transfer function for radiant floor
heating system
```

```

cont_arx_ext = d2c(arx_ext); %Laplace transfer function for exterior
temperature
cont_arx_ghr = d2c(arx_ghr); %Laplace transfer function for global horizontal
radiation

%4. Identify numerators and denominators
[NUMRFH,DENRFH] = tfdata(cont_arx_rfh,'v');
[ARFH, BRFH, CRFH, DRFH] = tfdata(P1_rfh,'v');
[NUMEXT,DENEXT] = tfdata(cont_arx_ext,'v');
[AEXT, BEXT, CEXT, DEXT] = tfdata(P1_rfh,'v');
[UMGHR,DENGHR] = tfdata(cont_arx_ghr,'v');

%5. Space state models

[ARFH, BRFH, CRFH, DRFH] = tf2ss(NUMRFH,DENRFH);
[AEXT, BEXT, CEXT, DEXT] = tf2ss(NUMEXT,DENEXT);
[AGHR, BGHR, CGHR, DGHR] = tf2ss(UMGHR,DENGHR);

%6. Initial conditions
[YHext, FIText, X0_ext] = compare(Data_ext,arx_ext);
[YHghr, FITghr, X0_ghr] = compare(Data_ghr,arx_ghr);
[YHrfh, FITrfh, X0_rfh] = compare(Data_rfh,P1_rfh);

X0_ext = cell2mat(X0_ext);
X0_ghr = cell2mat(X0_ghr);
X0_rfh = cell2mat(X0_rfh);

%-----

```

Filename: CREATE_MPC_CONTROLLER.m

```

%Creation of the linear model for the room

GEXT = tf(NUMEXT,DENEXT);
GSRE = tf(UMGHR,DENGHR);
GRFH = tf(NUMRFH,DENRFH);

GEXT.InputName = 'Temp';
GSRE.InputName = 'Rad';
GRFH.InputName = 'Heat';

GEXT.OutputName = 'y1';
GSRE.OutputName = 'y2';
GRFH.OutputName = 'y3';

Suma = sumblk('Tin','y1','y2','y3');

SISTEMA = connect(GEXT,GSRE,GRFH,Suma,{'Temp' 'Rad' 'Heat'},'Tin');

%-----
%Creation of the MPC controller

TS = 900; %Time step in seconds
p = 192; %Prediction horizon in time steps
m = 16; %Control horizon in time steps

```

```
%Linear system with the definition of disturbances and manipulated
%variables

SISTEMA_CON_SENALES = setmpcsignals(SISTEMA, 'MD', [1 2], 'MV', [3]);

%Actual creation of the mpc controller

mpc_shed = mpc(SISTEMA_CON_SENALES, TS, p, m);
```

G. Cost Function and Dynamic Programming

Filename: NIBE_F20256_EP.m

```
function ELECTRIC_POWER = NIBE_F20256_EP(Tair,Twater)
%Tair in Celsius
%Twater in Celsius

Tref = 258.15;
factor = (Tair+273.15)/Tref;

if Tair<-15
    ELECTRIC_POWER = 1000;
else
    ORDER2 = Twater^2*4.00E-4;
    ORDER1 = Twater*7.00E-3;
    ORDERZERO = 1.18;
    ELECTRIC_POWER = factor*(ORDER2+ORDER1+ORDERZERO);
end
```

Filename: NIBE_F20256_HEAT.m

```
function HEAT = NIBE_F20256_HEAT(Tair)
%Tair in Celsius

ORDER1 = 0.1514*Tair;
ORDERZERO = 5.2701;

HEAT = ORDERZERO + ORDER1;
```

Filename: costfunction.m

```
function Cost =
costfunction(time1,state1,time2,state2,TS,TIMEVECTOR,HEATVECTOR,RADVECTOR,WSVEC
TOR,TEMPVECTOR)
%time1 - Time of initial state (seconds since the beginning of the year)
%state1 - Initial state (Celsius)
%time2 - Time of final state (seconds since the beginning of the year)
%state2 - Final state (Celsius)
%TS - Time step in hours
%TIMEVECTOR,
%LOADVECTOR,
%RADVECTOR,
%WSVECTOR,
%TEMPVECTOR,

mwater = 0.16;

%-----
%NECESSARY ENERGY to make the TES tank pass from one
%state to another
```

```

Vtank = 1000;           %Tank volume in L
cp = 4180;             %Water cp J/kg*K
rho = 1;               %Water density (kg/L)

DT = state2-state1;
Twater = (state2+state1)/2;           %Average water temperature
Energy_change = Vtank*cp*rho*DT/3.6E6; %Energy necessary for the T change in
kWhr

%-----
%LOADCALCULATION - The load is given in kW
LOAD1 = interp1 (TIMEVECTOR,HEATVECTOR,time1);
LOAD1 = LOAD1*(LOAD1>0)/1000;

LOAD2 = interp1 (TIMEVECTOR,HEATVECTOR,time2);
LOAD2 = LOAD2*(LOAD2>0)/1000;

AVG_LOAD = (LOAD1 + LOAD2)/2;
Energy_delivered = AVG_LOAD*TS; %Energy that will be delivered in kWhr
Energy_required = Energy_change + Energy_delivered;

%-----

if Energy_required <= 0
    %Cost = Energy_required;
    Cost = 0;
else
    Deltatime = TS*3600;
    n = 5; %Number of time intervals to evaluate within each TS
(minimum 2)
    ACCUM = 0;
    for k = 1:n
        currenttime = time1 + (k-1)*Deltatime;
        %-----Evaluate things-----
        RAD = interp1 (TIMEVECTOR,RADVECTOR,currenttime);
        RAD = RAD*(RAD>0);

        WSPEED = interp1 (TIMEVECTOR,WSVECTOR,currenttime);
        WSPEED = WSPEED*(WSPEED>0);

        TEMP = interp1 (TIMEVECTOR,TEMPVECTOR,currenttime);
        %-----Inputs for the BIPVT function-----
        RAD = RAD;
        Airflow = 750; %The flow is fixed at 750 CFM
        Ti = TEMP + 3;
        To = TEMP;
        Tattic = 21;
        Wspeed = WSPEED;
        %-----
        %-----BIPV Function-----
        Texit = BIPVT_SHED (RAD,Airflow,Ti,To,Tattic,Wspeed);
        %-----Accumulator for average value-----
        ACCUM = ACCUM + Texit;
    end
    %-----VERY IMPORTANT: FINAL BIPVT AIR TEMPERATURE IN THAT INTERVAL
    Texit_air = ACCUM/n;
    %-----

HeatfromHP = NIBE_F20256_HEAT(Texit_air); %Heat from HP in kW

```

```

    % Twater_sup = Twater + HeatfromHP*1000/(mwater*cp);
    Twater_sup = Twater;

    Power_HP = NIBE_F20256_EP(Texit_air,Twater_sup); %Power consumed
by the HP

    if HeatfromHP*TS >= Energy_required
        Cost = Power_HP*(Energy_required/(HeatfromHP*TS))*TS;
        %The cost is prorated
    else
        Cost = 10^18; %If the heat pump cannot deliver, the cost is
infinite!!
    end
end
end

```

Filename: Optimalpath.m

```

%DETERMINATION OF OPTIMAL TRAJECTORY

%%%%%%%%%%%%%%%%%%%%%%%%%%%%%%%%%%%%%%%%%%%%%%%%%%%%%%%%%%%%%%%%%%%%%%%%
%%-----PRELIMINARIES-----
%%%%%%%%%%%%%%%%%%%%%%%%%%%%%%%%%%%%%%%%%%%%%%%%%%%%%%%%%%%%%%%%%%%%%%%%

%-----
VALUES = xlsread('C:\JOSE_CANDANEDO\CONFERENCES\CONFERENCE
PURDUE\PURDUE_MATLAB\NEW_VALUES.xls');
TIME = VALUES(:,1);
TEMPERATURA = VALUES(:,2);
WINDSPEED = VALUES(:,3);
RAD_ROOF = VALUES(:,4);
HEAT = VALUES(:,5);

%costfunction(time1,state1,time2,state2,TS,TIMEVECTOR,LOADVECTOR,RADVECTOR,WSVE
CTOR,TEMPVECTOR);
%-----
Tinitial = 342*24*3600+0*3600; %Initial Time in Seconds

ntemps = 11; %Number of possible temperatures at each time state
ntimes = 17; %Number of time intimeservals (including the first one)
TS = 3; %Time step in hours

%POSSIBLE STATES

TMAX = 55;
TMIN = 30;

DTEMP = TMAX - TMIN;

for k=1:ntemps
    %Tem(k) = TMIN+(k-1)*DTEMP/ntemps;
    Tem(k) = TMIN+(k-1)*DTEMP/(ntemps-1); %Dividing by the number of intervals
end

%POSSIBLE TIMES
t(1) = 0; %Currenttimesimes time
for k=2:ntimes;

```

```

    t(k)=t(1) + TS*(k-1);    %Future times in hours
end

%INICIALIZATION OF LOCAL MINIMA
for counter1 = 1:ntimes-1
    for counter2 = 1:ntemps
        Localmin(counter1,counter2) = 10^20;
    end
end

%Initialization of global minima (until state ntimes-1)
for k=1:ntimes-1
    Globalmin(k) = 10^20;
end

#####
%-----END OF PRELIMINARIES-----
#####

%%%%%%%%%%%%%%%%%%%%%%%%%%%%%%%%%%%%%%%%%%%%%%%%%%%%%%%%%%%%%%%%%%%%%%%%%%
%-----1. ESTADO FINAL (ntimes). Se asume un valor
%%%%%%%%%%%%%%%%%%%%%%%%%%%%%%%%%%%%%%%%%%%%%%%%%%%%%%%%%%%%%%%%%%%%%%%%%%
guess = 1;
estado(17) = guess;
X(ntimes,:) = [t(ntimes)*3600+Tinitial Tem(guess)];    %DEFINICION DEL ULTIMO
ESTADO
Localmin(ntimes,:) = 0; %Minimo LOCAL en ULTIMO estado (ntimes).
Globalmin(ntimes,:)=0; %Minimo GLOBAL en ULTIMO estado (ntimes).

%%%%%%%%%%%%%%%%%%%%%%%%%%%%%%%%%%%%%%%%%%%%%%%%%%%%%%%%%%%%%%%%%%%%%%%%%%
%-----2. PENULTIMO ESTADO (ntimes-1).
%%%%%%%%%%%%%%%%%%%%%%%%%%%%%%%%%%%%%%%%%%%%%%%%%%%%%%%%%%%%%%%%%%%%%%%%%%

for count2 = 1:ntemps    %Temperature counter

    %The cost function will have 4 arguments (among others)
    ind_a = ntimes-1; %    (a) Initial time. Corresponding index:    ind_a
    ind_b = count2;   %    (b) Initial temperature. Corresponding index:    ind_b
    ind_c = ntimes;   %    (c) Final time. Corresponding index:    ind_c
    ind_d = guess;    %    (d) Final temperature. Corresponding index:    ind_d

    X(ntimes-1,:) = [t(ntimes-1)*3600+Tinitial Tem(count2)];    %Definicion del
penultimo estado

    %-----COST FUNCTION-----
    Costo = costfunction(X(ntimes-1,1),X(ntimes-
1,2),X(ntimes,1),X(ntimes,2),TS,TIME,HEAT,RAD_ROOF,WINDSPEED,TEMPERATURA);
    Localmin(ntimes-1,count2) = Costo;    %The cost is stored as LOCAL
MINIMUM OF EACH STATE
    Cost(ind_a,ind_b,ind_c,ind_d) = Costo;    %The calculated cost between states
is stored, USING INDICES
    NP(ntimes-1,count2) = guess;
    %-----
end
%-----

%%%%%%%%%%%%%%%%%%%%%%%%%%%%%%%%%%%%%%%%%%%%%%%%%%%%%%%%%%%%%%%%%%%%%%%%%%
%-----3. DYNAMIC PROGRAMMING for the rest of the states
%%%%%%%%%%%%%%%%%%%%%%%%%%%%%%%%%%%%%%%%%%%%%%%%%%%%%%%%%%%%%%%%%%%%%%%%%%

```

```

for count1 = ntimes-2:-1:1 %Beginning of scanning for "current times" (Cuenta
regresiva a partir de ntimes-2)
    for count2 = 1:ntemps %Beginning of scanning for "current temperatures"

        % (a) Initial time. Corresponding index: ind_a
        % (b) Initial temperature. Corresponding index: ind_b
        % (c) Final time. Corresponding index: ind_c
        % (d) Final temperature. Corresponding index: ind_d

        ind_a = count1;
        ind_b = count2;
        ind_c = count1+1;

        %%%%-----CURRENT STATE WITHIN THE CYCLE-----%%%%%%%%
        X(count1,:) = [t(count1)*3600+Tinitial Tem(count2)];
        %%%%%%%%%%%%%%%%%%%%%%%%%%%%%%%%%%%%%%%%%%%%%%%%%%%%%%%%%%%%%%%%%%%%%%%%%

        for count4 = 1:ntemps %Counter for future temperatures
            ind_d = count4; %Index of future state (for storage)

            %%%%-----FUTURE STATE WITHIN THE CYCLE-----%%%%%%%%
            X(count1+1,:) = [t(count1+1)*3600+Tinitial Tem(count4)];
            %%%%%%%%%%%%%%%%%%%%%%%%%%%%%%%%%%%%%%%%%%%%%%%%%%%%%%%%%%%%%%%%%%%%%%%%%

            %%%%COST BETWEEN CURRENT STATE AND FUTURE STATE%%%%%%%%
            Costo =
            costfunction(X(count1,1),X(count1,2),X(count1+1,1),X(count1+1,2),TS,TIME,HEAT,R
            AD_ROOF,WINDSPEED,TEMPERATURA);
            Cost(ind_a,ind_b,ind_c,ind_d) = Costo; %The calculated cost is
            stored, USING INDICES

            %%%%%%%%%%%%%%%%%%%%%%%%%%%%%%%%%%%%%%%%%%%%%%%%%%%%%%%%%%%%%%%%%%%%%%%%%
            %-----CALCULO DE MINIMOS-----
            TOTALCOST = Costo + Localmin(count1+1,count4);
            if TOTALCOST < Localmin(count1,count2)
                Localmin(count1,count2) = TOTALCOST;
                NP(count1,count2) = count4;
            end
        end %End of cycle for scanning differentimes "future states"
    end %End of cycle for scanning differentimes "currentimes states"
end %End of cycle for scanning differentimes "currentimes times"

%Calculation of trajectories

tiempo = 1;

Vtank = 1000; %Tank volume in L
cp = 4180; %Water cp J/kg*K
rho = 1; %Water density (kg/L)
COPASSUMED = 3;

for k=1:ntemps
    COSTOINICIAL(k) = Vtank*cp*rho*(Tem(k)-Tem(1))/(COPASSUMED*3.6E6);
end

for k=1:ntemps
    Localmin(1,k) = Localmin(1,k)+COSTOINICIAL(k);
end

```

```

for initialstate = 1:ntemps
    OIS = initialstate;
    secuencia = initialstate;
    for tiempo = 1:ntimes-1
        estado(tiempo,initialstate) = initialstate;
        nextstate = NP(tiempo,initialstate);
        secuencia = vertcat(secuencia,nextstate);
        initialstate = nextstate;
    end
    secuencia = vertcat(secuencia,guess);

    for k =1:ntimes
        sarray(k,OIS) = secuencia(k);
    end
end

SAR = [sarray(:,1) sarray(:,2) sarray(:,3) sarray(:,4) sarray(:,5)
sarray(:,6)];

```

Filename: COST_OF_PATH.m

```

function COST_OF_PATH = COST_OF_PATH(Ti,VPA)
%Ti = initial time
%VPA = Vector of arbitrary positions

VALUES = xlsread('C:\JOSE_CANDANEDO\CONFERENCES\CONFERENCE
PURDUE\PURDUE_MATLAB\VALUES.xls');
TIME = VALUES(:,1);
TEMPERATURA = VALUES(:,2);
WINDSPEED = VALUES(:,3);
RAD_ROOF = VALUES(:,4);
HEAT = VALUES(:,5);

ntemps = 11;           %Number of possible temperatures at each time state
ntimes = 17;          %Number of time intervals (including the first one)
TS = 3;               %Time step in hours

%POSSIBLE STATES

TMAX = 55;
TMIN = 30;

DTEMP = TMAX - TMIN;

for k=1:ntemps
    Tem(k) = TMIN+(k-1)*DTEMP/(ntemps-1); %Dividing by the number of intervals
end

COST_OF_PATH = 0;

for k=1:(ntimes-1)
    COST_OF_PATH = costfunction(Ti+(k-
1)*TS*3600,Tem(VPA(k)),Ti+k*TS*3600,Tem(VPA(k+1)),3,TIME,HEAT,RAD_ROOF,WINDSPEE
D,TEMPERATURA) + COST_OF_PATH;

```

end

H. Perez Model

Filename: PEREZ_Diffuse_Irradiance.m

```
function DIF_IR = PEREZ_Diffuse_Irradiance(Dh,I,Z,n,slope,incid)
% PEREZ MODEL
% DIFFUSE IRRADIANCE ON A GIVEN SURFACE
% Introduce Dh(W/m2),I(W/m2),Z(deg),n,slope(deg),incid(deg)

% ----- INITIAL VARIABLES -----
%--Angle transformations--
Z = Z*pi/180;
slope = slope*pi/180;
incid=incid*pi/180;
%-----
Isc = 1353;
Ion = Isc*(1+0.033*cos((360/365)*n*pi/180));
k = 1.041;
Ihd = I*cos(Z); % Horizontal direct radiation
G = Ihd+Dh; % Global horizontal radiation
epsilon = ((Dh+I)/(Dh+k*Z^3))/(1+k*Z^3); %Sky clearness definition
mo = (cos(Z)+0.50572*(96.07995-Z*(180/pi))^-1.6364)^(-1); %Optical air
mass
DeltaB = Dh*mo/Ion; % Sky brightness definition
%Water = exp(0.07*Td-0.075);
%----- DISCRETE SKY CLEARNESS CATEGORIES-----
if (epsilon < 1.065)
    bin = 1;
elseif ((1.065 <= epsilon) & (epsilon < 1.230))
    bin = 2;
elseif ((1.230 <= epsilon) & (epsilon < 1.500))
    bin = 3;
elseif ((1.500 <= epsilon) & (epsilon < 1.950))
    bin = 4;
elseif ((1.950 <= epsilon) & (epsilon < 2.800))
    bin = 5;
elseif ((2.800 <= epsilon) & (epsilon < 4.500))
    bin = 6;
elseif ((4.500 <= epsilon) & (epsilon < 6.200))
    bin = 7;
elseif (epsilon >= 6.200)
    bin = 8;
end
%-----GLOBAL LUMINOUS EFFICACY CONSTANTS-----
Agle = [96.8300; 107.5400; 98.7300; 92.7200; 86.7300; 88.3400;
78.6300; 99.6500];
Bgle = [-0.4700; 0.7900; 0.7000; 0.5600; 0.9800; 1.3900;
1.4700; 1.8600];
Cgle = [11.5000; 1.7900; 4.4000; 8.3600; 7.1000; 6.0600;
4.9300; -4.4600];
Dgle = [-9.1600; -1.1900; -6.9500; -8.3100; -10.9400; -7.6000; -
11.3700; -3.1500];
%-----DIRECT LUMINOUS EFFICACY CONSTANTS-----
Adle = [57.2000; 98.9900; 109.8300; 110.3400; 106.3600; 107.1900;
105.7500; 101.1800];
```

```

Bdle = [-4.5500;   -3.4600;   -4.9000;   -5.8400;   -3.9700;   -1.2500;
0.7700;    1.5800];
Cdle = [ -2.9800;  -1.2100;  -1.7100;  -1.9900;  -1.7500;  -1.5100;  -
1.2600;   -1.1000];
Ddle = [117.1200; 12.3800;  -8.8100;  -4.5600;  -6.1600;  -26.7300;  -
34.4400;   -8.2900];
%-----DIFFUSE LUMINOUS EFFICACY CONSTANTS-----
-----
Adifle=[97.2400; 107.2200; 104.9700; 102.3900; 100.7100; 106.4200;
141.8800; 152.2300];
Bdifle=[-0.4600;  1.1500;  2.9600;  5.5900;  5.9400;  3.8300;
1.9000;   0.3500];
Cdifle=[12.0000;  0.5900;  -5.5300; -13.9500; -22.7500; -36.1500;  -
53.2400;  -45.2700];
Ddifle=[-8.9100;  -3.9500;  -8.7700; -13.9000; -23.7400; -28.8300;  -
14.0300;   -7.9800];
%-----ZENITH LUMINANCE PREDICTION-----
-----
Azlp=[40.8600;  26.5800;  19.3400;  13.2500;  14.4700;  19.7600;
28.3900;  42.9100];
Bzlp=[26.7700;  14.7300;  2.2800;  -1.3900;  -5.0900;  -3.8800;  -
9.6700;  -19.6200];
Czlp=[-29.5900;  58.4600; 100.0000; 124.7900; 160.0900; 154.6100;
151.5800; 130.8800];
Dzlp=[-45.7500; -21.2500;  0.2500;  15.6600;  9.1300; -19.2100;  -
69.3900; -164.0800];
%-----IRRADIANCE COEFFICIENTS-----
-----
F11IR=[-0.0080;  0.1300;  0.3300;  0.5680;  0.8730;  1.1320;
1.0600;  0.6780];
F12IR=[0.5880;  0.6830;  0.4870;  0.1870;  -0.3920;  -1.2370;  -
1.6000;  -0.3270];
F13IR=[-0.0620; -0.1510; -0.2210; -0.2950; -0.3620; -0.4120;  -
0.3590;  -0.2500];
F21IR=[-0.0600; -0.0190;  0.0550;  0.1090;  0.2260;  0.2880;
0.2640;  0.1560];
F22IR=[0.0720;  0.0660;  -0.0640;  -0.1520;  -0.4620;  -0.8230;  -
1.1270;  -1.3770];
F23IR=[-0.0220; -0.0290; -0.0260; -0.0140;  0.0010;  0.0560;
0.1310;  0.2510];
%-----ILLUMINANCE COEFFICIENTS-----
-----
F11IL=[0.0110;  0.4290;  0.8090;  1.0140;  1.2820;  1.4260;
1.4850;  1.1700];
F12IL=[0.5700;  0.3630;  -0.0540;  -0.2520;  -0.4200;  -0.6530;  -
1.2140;  -0.3000];
F13IL=[-0.0810; -0.3070; -0.4420; -0.5310; -0.6890; -0.7790;  -
0.7840;  -0.6150];
F21IL=[-0.0950;  0.0500;  0.1810;  0.2750;  0.3800;  0.4250;
0.4110;  0.5180];
F22IL=[0.1580;  0.0080;  -0.1690;  -0.3500;  -0.5590;  -0.7850;  -
0.6290;  -1.8920];
F23IL=[-0.0180; -0.0650; -0.0920; -0.0960; -0.1140; -0.0970;  -
0.0820;  -0.0550];
%
-----
F1IR=F11IR(bin)+F12IR(bin)*DeltaB+F13IR(bin)*Z;
F2IR=F21IR(bin)+F22IR(bin)*DeltaB+F23IR(bin)*Z;
F1IL=F11IL(bin)+F12IL(bin)*DeltaB+F13IL(bin)*Z;
F2IL=F21IL(bin)+F22IL(bin)*DeltaB+F23IL(bin)*Z;
%-----ILLUMINANCE-----
-----

```

```

%g=G*(Agle(bin)+Bgle(bin)*Water+Cgle(bin)*cos(Z)+Dgle(bin)*log(DeltaB));
%global (horizontal)
%dh=G*(Adifle(bin)+Bdifle(bin)*Water+Cdifle(bin)*cos(Z)+Ddifle(bin)*log(DeltaB)
); %diffuse horizontal
%id=G*(Adle(bin)+Bdle(bin)*Water+Cdle(bin)*exp(5.73*Z-5)+Ddle*DeltaB); %direc
illumiance
%id=max(id,0);
%-----LUMINANCE AT ZENITH-----
-----
%Lvz=Dh*(Azlp(bin)+Bzlp(bin)*cos(Z)+Czlp(bin)*exp(-3*Z)+Dzlp(bin)*DeltaB);
%-----DIFFUSE IRRADIANCE AND ILLUMINANCE AT ANY GIVEN SURFACE-----
-----
a=max(0,cos(incid));
b=max(0.087,cos(Z));
if ((0<=Z) & (Z<(pi/2)))
    partA=0.5*(1-F1IR)*(1+cos(slope));
    partB=F1IR*a/b;
    partC=F2IR*sin(slope);
    DIF_IR=Dh*(partA+partB+partC);
else
    DIF_IR=0;
end
%-----
%if ((0<=Z) & (Z<(pi/2)))
%    partA=0.5*(1-F1IL)*(1+cos(slope));
%    partB=F1IL*a/b;
%    partC=F2IL*sin(slope);
%    DIF_IL=dh*(partA+partB+partC);
%else
%    DIF_IL=0;
%end

```